Development and Applications of Natural Orbital Functional Theory

Orbital Naturalen Funtzionalaren Garapena eta Aplikazioak

Ion Mitxelena Echeverria

eman ta zabal zazu

Universidad del País Vasco
Euskal Herriko Unibertsitatea

NAZIOARTEKO BIKAINTASUN CAMPUSA
CAMPUS DE EXCELENCIA INTERNACIONAL

Doctoral Thesis:

Development and Applications of Natural Orbital Functional Theory

Orbital Naturalen Funtzionalaren Garapena eta Aplikazioak

Ion Mitxelena Echeverria

2020

Doctoral Programme in Chemistry

Supervised by: Prof. Dr. Mario Piris Silvera

Tutor: Prof. Dr. Mario Piris Silvera

Presented in partial fulfillment of the requirements for a doctoral degree from the University of the Basque Country

ama eta aitari

Acknowledgements

Llegué al bachillerato con una gran motivación en la ciencia gracias a mi hermano, que probablemente sin saberlo inculcó en mi esta vocación. Fue ahí donde tuve la gozadera de tener a Estitxu como profesora de Física/Química. Ella me aclaró las ideas y me guió por la rama de ciencias básicas, convenciéndome así para estudiar Física. Por todo esto, además de ser dos personas importantes para mí, esta tesis está dedicada a Asier y Estitxu. Un abrazo de corazón desde aquí a mis abuelos y abuelas, allí donde estén, los cuales no tuvieron las cosas fáciles en cuanto al tema de educación académica respecta. Ellos y ellas estuvieron siempre orgullosos de vernos entre libros y apuntes tanto a mí como a mi hermano, de lo cual estoy agradecido.

Empecé Física y en cuanto pude me planté en el despacho de la profesora de "Física I" para preguntarle acerca de "Física Química", ya que Asier me lo había mencionado antes con gran interés. Caprichos del destino, ya que esta tesis trata exactamente acerca de "Física Química", o al menos se ha desarrollado en el grupo de "Kimika Teorikoa" de J. M. Ugalde.

Sin duda, todo esto se lo debo al Prof. Mario Piris, quien desde el momento en el que me planté en su despacho un caluroso día de Septiembre me inspiró confianza y todos los medios necesarios para llevar a cabo este trabajo. Mario ha estado allí en todo momento, discusiones infinitas y demás, gracias una vez más, Mario, a ti y a la gente de alrededor (compis de despacho ...) por aguantarnos! Gracias a Oihana también, cuyos consejos bajo el sol del Vedado fueron de gran ayuda para mí. Especial agradecimientos a Mauricio Rodríguez-Mayorga, ya que trabajar contigo me ha servido para empaparme de tu ilusión e ideas.

Eskerrik asko Kimika Teorikoko kideei, J. M. Ugalde, J. M. Matxain, E. Formoso, E. Rezabal, T. Mercero, X. Lopez, E. Ramos, E. Matito, D. Casanova, V. Postils, R. Grande, E. Jimenez, D. de Sancho, lankide ezinhobeak izatearren eta laguntza amaigabea eskaintzeagatik beti. Zuen eredua jarraitzen saiatuko naiz aurrerantzean.

Let me acknowledge the hospitality of Albert Eugene DePrince's group in the Florida State University (USA), you made my stay there very enriching. You are doing a great work as young research group leader! Also, thanks to Klaas J. Giesberts and Paola Gori Giorgi's group in VU

(Amsterdam) for your kindness during my short stay in the Netherlands.

Finalmente, un abrazo de gigante a todas y todos compañeras y compañeros que sois demasiado importantes para mí: Cris, Jorge, Sofia, Maru, Miri, Sergi, Uranga, Uriangato, Irene, Adrián, Montul, y los que me dejo por el camino. ¡Cuesta imaginar los meses que se avecinan sin estar a vuestro lado!

This thesis has been funded by the University of the Basque Country through the grant PIF//15/043. The authors thank for technical and human support provided by IZO-SGI SGIker of UPV/EHU and European funding (ERDF and ESF).

Full list of publications

Published and submitted articles included in the thesis :

1. Mitxelena I., Piris M.; **Molecular electric moments calculated by using natural orbital functional theory.** *J. Chem. Phys.* 144, 204108 (2016) doi:10.1063/1.4951685

2. Mitxelena I., Piris M.; **Analytic gradients for natural orbital functional theory.** *J. Chem. Phys.* 146, 014102 (2017) doi:10.1063/1.4973271

3. Mitxelena I., Piris M., Rodríguez-Mayorga M.; **On the performance of natural orbital functional approximations in hubbard model.** *J. Phys. Condens. Matter* 29, 425602 (2017) doi:10.1088/1361-648X/aa80ca

4. Mitxelena I., Piris M., Rodríguez-Mayorga M.; **Corrigendum: On the performance of natural orbital functional approximations in hubbard model (2017 J. Phys.: Condens. Matter 29 425602).** *J. Phys. Condens. Matter* 30, 089501 (2018) doi:10.1088/1361-648X/aaa659

5. Mitxelena I., Rodríguez-Mayorga M., Piris M.; **Phase dilemma in natural orbital functional theory from the N-representability perspective.** *Eur. Phys. J. B* (2018) 91: 109, doi:10.1140/epjb/e2018-90078-8

6. Mitxelena I., Piris M.; **Analytic second-order energy derivatives in natural orbital functional theory.** *J. Math. Chem.* 56, 1445 (2018) doi:10.1007/s10910-018-0870-0

7. Mitxelena I., Ugalde J. M., Piris M.; **Advances in approximate natural orbital functional theory.** in State of The Art of Molecular Electronic Structure Computations: Correlation Methods, Basis Sets and More, edited by Philip Hoggan and Ugo Ancarani, 2019

8. Mitxelena I., Piris M.; **An efficient method for strongly correlated electrons in one dimension.** *J. Phys. Condens. Matter* 32, 17LT01 (2020) doi:10.1088/1361-648X/ab6d11

9. Mitxelena I., Piris M.; **An efficient method for strongly correlated electrons in two-dimensions.** *J. Chem. Phys.* (Accepted Manuscript)

Other published articles not included in the thesis :

10. Quintero-Monsebaiz R., Mitxelena I., Rodríguez-Mayorga M., Vela A. and Piris M.; **Natural orbital functional for spin-polarized periodic systems.** *J. Phys. Condens. Matter* 91, 165501 (2019) doi:10.1088/1361-648X/ab0170

11. Vu N. H., Mitxelena I. and DePrince III A. E.; **An adiabatic connection for doubly-occupied configuration interaction wave functions.** *J. Chem. Phys.* 151, 244121 (2019) doi:10.1063/1.5130660

List of Abbreviations

Abbreviation	Description
N	Number of electrons
HF	Hartree-Fock
RHF	Restricted Hartree-Fock
CI	Configuration interaction
FCI	Full-Configuration interaction
CC	Coupled-cluster
CCSD	Coupled-cluster including only singles and doubles
CCSD(T)	Coupled-cluster including only singles and doubles and perturbative triples
MRSD-CI	Multi-reference single and double excitation CI
MP2	Second order Møller-Plesset perturbation theory
DFT	Density functional theory
DMRG	Density matrix renormalization group
vMPS	Variational matrix product state
AFQMC	Auxiliary field quantum Monte Carlo
ED	Exact diagonalization
OO-AP1roG	Orbital optimized antisymmetric product of 1-reference-orbital geminals
APSG	Antisymmetrized product of strongly orthogonal geminals
RDM	Reduced density matrix
1RDM	First-order reduced density matrix
Γ	First-order reduced density matrix
2RDM	Second-order reduced density matrix
D	Second-order reduced density matrix
pRDM	$p-$order reduced density matrix

RDMFT	Reduced density matrix functional theory
1RDMFT	First-order reduced density matrix functional theory
v2RDM	Variational second-order reduced density matrix
PQG	v2RDM enforcing P, Q and G conditions of the 2RDM
PQGT'	v2RDM enforcing P, Q, G, T1, and T2' conditions of the 2RDM
MBB	Müller and Barends-Buijse functional
MLSIC	Marques and Lathiotakis functional including self-interaction correction
CA	Csányi and Arias functional
CGA	Csányi, Goedecker and Arias functional
GU	Goedecker and Umrigar functional
F	Fermi level
NO	Natural orbital
NOF	Natural orbital functional
NOFT	Natural orbital functional theory
NOFA	Natural orbital functional approximation
PNOF	Piris natural orbital functional
AO	Atomic orbital
MO	Molecular orbital
ON	Occupation number
1D	One-dimensional
2D	Two-dimensional
GPC	Generalized Pauli constraints
V_{ee}	Electron-electron repulsive potential
PBC	Periodic boundary conditions

List of Figures

List of Tables

Contents

Abstract

In this dissertation, we address the attempt to treat many electrons within a one-electron picture. A 1RDM theory holds the promise to account for strong electron correlation with a minimal amount of effort. Chapter 1 is a summary written in Basque. Chapter 2 put us in the context of reduced density matrix as a tool to study quantum chemistry without wavefunctions. In practice, 1RDM theory is reduced to the diagonal representation of the 1RDM, given in terms of its eigenvectors (natural orbitals) and eigenvalues (occupation numbers). In chapter 3, we emphasize on the fundamental difference between Natural Orbital Functional (NOF) theory and approximations, in fact, theorems for the exact NOF are no longer valid for approximate expressions, so the dependence on the 2RDM remains in NOF approximations. In chapter 4, we briefly explain the objective of this thesis: establish NOF approximations as an electronic structure method able to compete with standard wavefunction and DFT approaches.

Chapters 5 through 8 cover the development and applications carried out along this thesis. We start with the geometry optimization procedure. Analytic derivative methods are developed and tested on molecular systems by using PNOF approximations against correlated wavefunction approaches. Secondly, model systems are employed for robust validation of mostly employed NOF approximations. Interestingly, these models turn out to be useful for the development of NOFs, and shine a light on the phase dilemma encountered in 1RDM theory. In this line, we propose PNOF7 as an efficient method to describe strongly correlated electrons in low dimensions. Finally, we analyze the most important molecular electric moments, namely, dipole, quadrupole, and octupole moments. The thesis is concluded in Chapter 9.

CHAPTER 1

Laburpena

Kapitulu honetan tesi osoaren euskarazko laburpen sakona egingo dugu. Ingelerazko laburdura batzuk erabiltzen diren arren, ondokoak bereziki kapitulu honetan erabiltzen dira:

DME	Dentsitate matrize erreduzitua
1DME	Lehenengo ordeneko dentsitate matrize erreduzitua
2DME	Bigarren ordeneko dentsitate matrize erreduzitua
ON	Orbital naturala (ez nahastu ingeleseko ON-rekin, okupazioei dagokio eta)
OA	Orbital atomikoa
OM	Orbital molekularra
ONF	Orbital naturalen funtzionala
ONFT	Orbital naturalen funtzionalaren teoria
ONFH	Orbital naturalen funtzionalaren hurbilketa

Kapitulua guztiz independentea da, beraz ez da beharrezkoa ingelerazko atalera jotzea azaldutako guztia ulertu ahal izateko. Dena den, aipatzekoa da ingelerazko atala osatutagoa dagoela, lagungarria izan daitekeelarik kasu batzuetan.

1.1 Dentsitate Matrize Erreduzituak

Lehenengo atalean dentsitate matrize erreduzituen (DME) inguruko oinarrizko kontzeptuak azalduko dira.

$\{\psi_m\}$ egoerei dagozkien dentsitate matrize operadorea ondoko moduan definitzen da

$$\widehat{\mathcal{D}} = \sum_m \omega_m |\psi_m\rangle\langle\psi_m| \tag{1}$$

non $0 \leq \omega_m \leq 1$; $\forall\, m$ eta $\sum\limits_m \omega_m = 1$. Orduan dentsitate matrizea (Γ^N) lortu daiteke operadore hau N-dimentsiotako basean proiektatuz

$$\begin{gathered}\Gamma^N\left(\mathbf{x_1'}\cdots\mathbf{x_N'}|\mathbf{x_1}\cdots\mathbf{x_N}\right) \equiv \langle\mathbf{x_1'}\cdots\mathbf{x_N'}|\widehat{\mathcal{D}}|\mathbf{x_1}\cdots\mathbf{x_N}\rangle = \\ \sum_m \omega_m\, \psi_m^*\left(\mathbf{x}_1'\cdots\mathbf{x}_N'\right)\psi_m\left(\mathbf{x}_1\cdots\mathbf{x}_N\right)\end{gathered} \tag{2}$$

non $\mathbf{x}_i$ bakoitzak koordinatu espazialak $\mathbf{r}_i$ eta spin koordinatuak s_i dituen. Orduan p ordeneko DME ondoko moduan definitzen da

$$\begin{gathered}\Gamma^p\left(\mathbf{x_1'}\cdots\mathbf{x_p'}|\mathbf{x_1}\cdots\mathbf{x_p}\right) = \\ \binom{N}{p}\sum_m \omega_m \int \psi_m^*\left(\mathbf{x}_1'\mathbf{x}_2'\cdots\mathbf{x}_p'\cdots\mathbf{x}_N\right)\psi_m\left(\mathbf{x}_1\mathbf{x}_2\cdots\mathbf{x}_p\cdots\mathbf{x}_N\right)dx_{p+1}\cdots dx_N\end{gathered} \tag{3}$$

Tesi honetan zehar bereziki lehenengo eta bigarren ordeneko DME-ak erabiliko ditugu, bigarren kuantizazioan erraz idatzi daitezkeenak

$$\Gamma_{ji} = \sum_m \omega_m \langle\psi_m|\widehat{a}_j^+\widehat{a}_i|\psi_m\rangle \tag{4}$$

eta

$$D_{kl,ij} = \frac{1}{2}\sum_m \omega_m \left\langle\psi_m|\widehat{a}_k^+\widehat{a}_l^+\widehat{a}_j\widehat{a}_i|\psi_m\right\rangle \tag{5}$$

non $\{\widehat{a}_k^+\}$ ($\{\widehat{a}_k\}$) adierazten ditu sorkuntza (deuseztapen) operadoreak. Esatekoa da $\{i,j,k,...\}$ indizeak spin orbitalak adierazteko erabiliko direla, orbital espazialentzako, berriz, $\{p,q,r,...\}$ erabiliko ditugu. Aipatzekoak dira ondoko propietateak

$$Tr(\Gamma^1) = N,\ Tr(\Gamma^2) = \binom{N}{2} = \frac{N\,(N-1)}{2} \tag{6}$$

$$\Gamma_{ji} = \Gamma_{ij}^*\ \left(\Gamma = \Gamma^+\right),\ D_{kl,ij} = D_{ij,kl}^*\ \left(D = D^*\right) \tag{7}$$

$$D_{kl,ij} = D_{lk,ji},\ D_{kl,ij} = -D_{lk,ij} = -D_{kl,ji} \tag{8}$$

$$\Gamma_{ii} \geq 0,\ D_{ij,ij} \geq 0 \tag{9}$$

Esatekoa da (9). propietatea interpretazio probabilistikoa duela, adibidez, 1DME-aren kasuan Γ_{ii}-k adierazten du elektroi bat ψ_i orbitalean aurkitzeko probabilitatea.
$\widehat{S}_z$-ren egoera propioen kasuan, bloke ez-nulu bakarrak $\Gamma_{p_\alpha q_\alpha}$ eta $\Gamma_{p_\beta q_\beta}$ dira, 2DME-rako $D_{p_\alpha q_\alpha, r_\alpha s_\alpha}$, $D_{p_\alpha q_\beta, r_\alpha s_\beta}$ eta $D_{p_\beta q_\beta, r_\beta s_\beta}$ ditugu [11].
Born-Oppenheimer hurbilketan, efektu erlatibistak kontutan hartu gabe, energia elektronikoa N-elektroidun sistemaren kasuan 1 eta 2 DME-en funtzional esplizitua da

$$E_{el}[\Gamma, D] = \sum_{ik} \Gamma_{ki} h_{ki} + \sum_{ijkl} D_{kl,ij} \langle kl|ij\rangle \tag{10}$$

h_{ik}-k adierazten du energia zinetikoaren eta nukleo (I. nukleoaren karga positiboa da Z_I)-elektroi indarraren gaiak

$$h_{ki} = \int d\mathbf{x}\, \psi_k^* (\mathbf{x}) \left[-\frac{1}{2}\nabla^2 - \sum_I \frac{Z_I}{|\mathbf{r} - \mathbf{r}_I|} \right] \psi_i (\mathbf{x}) \tag{11}$$

eta $\langle kl|ij\rangle$ elektroiren alderapenari dagozkien bi-elektroien integralak dira

$$\langle kl|ij\rangle = \int d\mathbf{x}_1 d\mathbf{x}_2\, \psi_k^* (\mathbf{x}_1)\, \psi_l^* (\mathbf{x}_2)\, \frac{1}{|\mathbf{r_1} - \mathbf{r_2}|} \psi_i (\mathbf{x}_1)\, \psi_j (\mathbf{x}_2) \tag{12}$$

Ohartu unitate atomikoak erabiltzen ari garela. Esatekoa da orden baxuko DME-ak ordeneko altuen funtzioak direla, adibidez

$$\Gamma \left(\mathbf{x_1'} | \mathbf{x_1} \right) = \frac{2}{N-1} \int d\mathbf{x}\, D \left(\mathbf{x_1'x} | \mathbf{x_1 x} \right) \tag{13}$$

Beraz, (13). ekuazioa dela eta, energia elektronikoa (10) berez 2DME-aren funtzionala da, hau da, $E_{el}[\Gamma, D] \to E_{el}[D]$.

1.1.1 N-adierazgarritasuna

Energia elektronikoa 2DME-aren funtzionala izan arren, Coleman [12] ohartu zen energia zentsu fisikoa izan dadin beharrezkoa dela bestelako baldintzak inposatzea matrize hauetan. Bestela esanda, N-adierazgarritasunaren problema ondokoa da: DME-aren eta uhin-funtzio baten arteko zuzeneko erlazioa dagoela ziurtatzea. Orduan soilik DME hura zentsu fisikoa izango du mekanika kuantikoaren testuinguruan.

Azpimarratzekoa da N-adierazgarritasuna puruaren eta multzoaren arteko diferentzia. Lehenengoak adierazten du uhin-funtzio puruarekin erlazioa, bigarrenak, berriz, N-ordeneko dentsitate matrizearekin erlazioari dagokio, non egoera fisiko ez-purua N-ordeneko dentsitate matrizearekin (2) deskribatu beharra dagoen. Orokorrean, tesi honetan zehar N-adierazgarritasunaren inguruan aritzen garenean multzoko baldintzei buruz ari gara, kontrakoa esaten ez bada behintzat.

1.1.1.1 1DME-aren N-adierazgarritasuna

Γ-ren kasuan beharrezko eta nahikoak diren N-adierazgarritasunaren baldintzak ezagunak dira [12, 13]

$$Tr(\Gamma) = \sum_i \Gamma_{ii} = N, \quad \Gamma \succeq 0, \quad 1 - \Gamma \succeq 0 \tag{14}$$

non $A \succeq 0$-k adierazten du A matrizearen positiboki definituaren baldintza, hortaz bere balore propioak positiboak edo zero izan behar dira. 1DME diagonala bada, aurreko baldintzak balore propioen menpe soilik idatzi daitezke: $0 \leq n_i \leq 1$; $\forall i$ non $\sum_i n_i = \mathrm{N}$. Orain dela urte gutxi [14, 15] 1DME-ari dagozkion N-adierazpen puruaren baldintzak ezagunak izan arren, ONFT-ren testuinguruan kasu oso berezietan bakarrik aplikatu dira [16–19], izan ere, baldintza kopurua basearen tamainarekin modu ez-praktikoan handitzen da.

1.1.1.2 2DME-aren N-adierazgarritasuna

2DME-aren kasuan N-adierazpen multzoaren baldintza nahikoak ezagunak badira ere [20], ez dira kalkuluetan aplikagarriak gastu konputazionala dela eta. Hori dela eta, 2DME-aren N-adierazgarritasuna ziurtatzeko nahikoak ez badira ere, N-adierazgarritasunarako beharrezkoak diren baldintzeetako batzuk inposatzen dira. Tesi honetan zehar bereziki garrantzitsuak izango dira bi-indizeko baldintzak, hau da,

$$P_{p_\sigma q_{\sigma'}, r_\sigma s_{\sigma'}} \succeq 0, \tag{15}$$

$$Q_{p_\sigma q_{\sigma'}, r_\sigma s_{\sigma'}} \succeq 0, \tag{16}$$

$$G_{p_\sigma q_\tau, r_\kappa s_\lambda} \succeq 0, \tag{17}$$

non eta matrizeak Ψ egoera batekiko definitzen diren

$$P_{p_\sigma q_{\sigma'}, r_\sigma s_{\sigma'}} = \langle \Psi | a^\dagger_{p_\sigma} a^\dagger_{q_{\sigma'}} a_{s_{\sigma'}} a_{r_\sigma} | \Psi \rangle \,, \tag{18}$$

$$Q_{p_\sigma q_{\sigma'}, r_\sigma s_{\sigma'}} = \langle \Psi | a_{p_\sigma} a_{q_{\sigma'}} a^\dagger_{s_{\sigma'}} a^\dagger_{r_\sigma} | \Psi \rangle \,, \tag{19}$$

$$G_{p_\sigma q_\tau, r_\kappa s_\lambda} = \langle \Psi | a^\dagger_{p_\sigma} a_{q_\tau} a^\dagger_{s_\lambda} a_{r_\kappa} | \Psi \rangle \,. \tag{20}$$

Ohiko moduan, $p, q, ...$ erabili dira orbital espazialak adierazteko, eta $\sigma, \sigma', \tau, \lambda, \kappa$ elektroi spin α edo β-rako. Interesgarria da esatea P, Q, eta G matrizeak bata bestearekin erlazionatuta dauden arren operadoreen propietateen bitartez, hauetako bakarra inposatzeak ez du ziurtatzen besteak betetzen direnik [21].

Konputazionalki, (15)-(17) inposatzeari dagokion gastua $\mathcal{O}\left(M^6\right)$-koa eta $\mathcal{O}\left(M^4\right)$-koa da, operazioei eta memoriari dagokienez, hurrenez hurren. Atal batzuetan oraindik garestiagoak diren T1 eta T2 (T2' bariantea barne) [21–23] baldintzak ere erabiliko dira.

1.2 1DME-aren funtzionalaren teoria

1975. urtean Gilbert-ek [13] 1DME-aren funtzionalaren existentzia frogatu zuen

$$E_{el}\left[\Gamma\right] = \sum_{ik} \Gamma_{ki} h_{ki} + V_{ee}\left[\Gamma\right] \tag{21}$$

non $V_{ee}\left[\Gamma\right]$ guztiz unibertsala da, hau da, kanpo eremuen independentea da. Gilbert-ek [13], Löwdin [24], Levy [25], Valone [26], eta Donelly eta Parr-ekin [27] batera, 1DME funtzionalaren teoria (1RDMFT) finkatu zuten. DFT-n gertatzen den bezala, erraza da 1DME-aren N-adierazgarritasunaren baldintzak aplikatzea. Aldiz, energia zinetikoaren funtzionalaren adierazpen zehatza dugu 1DME-aren menpe, horrek DFT-rekiko abantaila nabarmena suposatzen duelarik teoriaren ikuspuntutik. Hori dela eta, 1RDMFT DFT-aren erroreak zuzentzeko posibilitate baten moduan azaltzen da.

1967.urtean [28] Rosina-k oinarrizko egoerari dagokion 2DME-aren eta uhin-funtzioaren arteko erlazio zuzena frogatu zuen baldin eta Hamiltondarra bi-partikulako elkarrekintzak baditu gehienez. Hori dela eta, Gilbert-en teoremak aldi berean inplizituki frogatzen du oinarrizko egoeran $V_{ee}\left[\Gamma\right]$ existitzen dela, hau da, $E_{el}\left[\Gamma\right]$ eta $E_{el}\left[\mathrm{D}\right]$ baliokideak direla. Praktikan, 1DME-aren menpeko adierazpen zehatzak ezagunak ez direnez, hurbilpenak egitea nahitaezkoa da. Normalean $\mathrm{D}\left[\Gamma\right]$ onartzea nahikoa da hurbilpenak proposatzeko, HF da honen adibide errazena

$$\mathrm{D}\left(\mathbf{x_1'}\mathbf{x_2'}|\mathbf{x_1}\mathbf{x_2}\right) = \Gamma\left(\mathbf{x_1'}|\mathbf{x_1}\right)\Gamma\left(\mathbf{x_2'}|\mathbf{x_2}\right) - \Gamma\left(\mathbf{x_1'}|\mathbf{x_2}\right)\Gamma\left(\mathbf{x_2'}|\mathbf{x_1}\right) \tag{22}$$

non $\Gamma^2 = \Gamma$ (idenpotentzia) dugun kasu berezi honetan. 2DME 1DME-aren menpe adierazteak berriro ere 2DME-aren funtzionalarekin lan egitea suposatzen du [29]. Hori dela eta,

N-adierazgarritasunaren problema bai 1DME-ari bai 2DME-ari eragingo dio 1RDMFT-ren testuinguruan [30,31]. Beste era batera esanda, D [Γ]-ren hurbilketa 2DME-aren N-adierazgarritasunaren baldintzapetan egin behar da energiak zentsu fisikoa izan dadin.

1DME-aren N-adierazpen puruaren baldintzak aurkitzeak 1RDMFT-aren testuinguruan hurbilpen berriak proposatzeko erabili izan da [17, 18]. Hala ere, baldintza hauek ez dute D [Γ] hurbilpena hobetzen, ezta funtzionala ere. Izan ere, funtzionalaren adierazpena hurbildua den bitartean, beharrezkoa izango da 2DME-aren N-adierazgarritasunaren baldintzak kontuan izatea.

1.3 Metodologia

Spin simetria zuzena izan dadin, orbital espazial berberak erabiliko dira bai α-rako bai β-rako, hau da, $\varphi_p^\alpha(\mathbf{r}) = \varphi_p^\beta(\mathbf{r}) = \varphi_p(\mathbf{r})$. Aldi berean, spin blokeak paraleloak dituzten DME-en spin blokeak berdinak dira ere. Ezaugarri gehiago 1.5.1.2. atalean azalduko dira.

1.3.1 Orbital Naturalen Funtzionalaren Hurbilpenak

HF-ren kasu bereziaz aparte, praktikan 1DME-an oinarritutako hurbilpen gehienak 1DME-aren adierazpen diagonalaren menpe garatu dira, hau da, bektore propioen (orbital naturalak) eta balore propioen (okupazio zenbakiak) menpe

$$\Gamma_{ki} = n_i \delta_{ki} \tag{23}$$

edo, koordenatuen adierazpenean

$$\Gamma\left(\mathbf{x_1'}|\mathbf{x_1}\right) = \sum_i n_i \phi_i^*\left(\mathbf{x_1'}\right)\phi_i\left(\mathbf{x_1}\right) \tag{24}$$

Hori dela eta, 1RDMFT izan beharrean, egokiagoa da Orbital Naturalen Funtzionalaren inguruan aritzea, hau da

$$E_{el}[\{n_i,\phi_i\}] = \sum_i n_i \mathcal{H}_{ii} + \sum_{ijkl} D[n_i,n_j,n_k,n_l]\,\langle kl|ij\rangle \tag{25}$$

non $D[n_i,n_j,n_k,n_l]$-ren bitartez adierazten ari gara 2DME okupazioen funtzioa dela. Hortaz, kontsideratu dugu D-k ez duela orbitalekiko menpekotasunik, jada integralek orbitalekiko dituzten menpekotasuna handia baita. Ohartu ONF ez dela orbitalen transformazio unitarioekiko inbariantea, beraz ez da Fockianorik existitzen teoria honetan. Aurrean aipatutako ezaugarriak kontuan hartuz, 1DME-aren teoria izan ordez, praktikan 2DME-aren teoria bat dugu, non eta azken honek jokatzen duen errola nagusia. ONF hurbilketen (ONFH) inguruko informazio gehiago literaturan aurkitu daiteke [32–34].

1.3.1.1 $\mathcal{JK}$-motatako hurbilpenak

Modu laburrean, pena merezi du bi hurbilpen moten artean bereiztea. Batetik, $\mathcal{J}$ ($\mathcal{J}_{pq} = \langle pq|pq\rangle$) eta $\mathcal{K}$ ($\mathcal{K}_{pq} = \langle pq|qp\rangle$) moduko integralak soilik erabiltzen dituzten ONFH aurkitzen

dira. Orokorrean, hurbilpen hauetan HF spin paraleloko blokea ondoko moduan modifikatzen da

$$D^{\sigma\sigma}_{pq,rt} = \frac{n_p n_q}{2}\delta_{pr}\delta_{qt} - \frac{\mathcal{F}(n_p,n_q)}{2}\delta_{pt}\delta_{qr} \tag{26}$$

Table 1 – $\mathcal{F}(n_p,n_q)$ funtzioak 2DME eraikitzeko (26). ekuazioan.

ONFH	$\mathcal{F}(n_p,n_q)$	
MBB	$(n_p n_q)^{1/2}$	[35, 36]
Power	$(n_p n_q)^{0.53}$	[37]
CA	$n_p n_q + [n_p(1-n_p)n_q(1-n_q)]^{1/2}$	[38]
CGA	$\frac{1}{2}\left\{n_p n_q + [n_p(2-n_p)n_q(2-n_q)]^{1/2}\right\}$	[39]

$\mathcal{F}(n_p,n_q)$ funtzioak 1. taulan bildu dira. Ohartu HF-ri dagokion $\mathcal{F} = n_p n_q$ kasuan izan ezik, (26). ekuazioa antisimetriaren baldintzarekin ez duela betetzen, hortaz horrelako ONFH-ak ez dituzte inoiz N-adierazgarritasunaren baldintzak beteko [40, 41].

1.3.1.2 Piris Orbital Naturalen Funtzionala (PNOF)

Beste alde batetik, $\mathcal{L}$ ($\mathcal{L}_{pq} = \langle pp|qq\rangle$) motatako integralak [42] ere erabiltzen dituzten hurbilpenen artean aipatzekoak dira Piris-ek garatutako ONFH-ak, zehazki, PNOFi; i=$\overline{1,7}$ [43–47]. Izan ere, hauetako guztiak 2DME-aren N-adierazgarritasunaren baldintzak inposatuz garatu dira. Orokorrean, kumulantearen garapena [48, 49] erabiltzen da PNOF hurbilpenetan

$$D_{kl,ij} = \frac{1}{2}\left(\Gamma_{ki}\Gamma_{lj} - \Gamma_{li}\Gamma_{kj}\right) + \lambda_{kl,ij} \tag{27}$$

$\lambda_{kl,ij}$-k HF-rekiko diferentzia sortzen du, ondoko moduan adierazten delarik

$$\begin{aligned} \lambda^{\sigma\sigma}_{pq,rt} &= -\frac{\Delta_{pq}}{2}\left(\delta_{pr}\delta_{qt} - \delta_{pt}\delta_{qr}\right),\ \sigma = \alpha,\beta \\ \lambda^{\alpha\beta}_{pq,rt} &= -\frac{\Delta_{pq}}{2}\delta_{pr}\delta_{qt} + \frac{\Pi_{pr}}{2}\delta_{pq}\delta_{rt} \end{aligned} \tag{28}$$

(28). ekuazioan Δ matrize erreal simetrikoa da, eta Π spin-arekiko independentea den matrize hermitikoa. Spin simetriarekin betetzeko $\Delta_{pp} = n_p^2$ eta $\Pi_{pp} = n_p$ dugu [50]. Hortaz, balore ez-diagonalek PNOFi, i=$\overline{1,7}$ hurbilpen ezberdinak determinatzen dituzte. Lehen esan dugun bezala, (15)-(17) baldintzak kontuan hartuz, balore ez-diagonalak bete beharreko ekuazio berriak jasotzen ditugu. Funtzionalak garatzeko teknika honi *bottom-up* deritzogu [51]. Orain

arte esandakoa kontutan hartuz, PNOF energia ondoko moduan idatzi daiteke

$$E_{el} = 2\sum_{p} n_p \mathcal{H}_{pp} + \sum_{qp} \Pi_{qp} \mathcal{L}_{pq} + \sum_{qp} \left(n_q n_p - \Delta_{qp}\right) \left(2\mathcal{J}_{pq} - \mathcal{K}_{pq}\right) \tag{29}$$

non eta $\mathcal{H}_{pp}$-k energia zinetikoaren eta nukleo-elektroi alderapenaren gaiak dituen. Esatekoa da bestelako $\mathcal{JKL}$ motatako hurbilpenak agertu direla azken urteetan literaturan [52,53]. Hala ere, hauek ez dira bakarrik ON-en eta okupazioen menpeko funtzionalak, hortaz ez dira berez ONFH-ak eta ez ditugu tesi honetan zehar kontsideratuko.

PNOFi, i=$\overline{5,7}$ kasuetan elektroi pareen metodologia erabiltzen da. Honen bitartez, sistema osatzen duten orbitalak azpiespazioetan antolatzen dira. Orduan, elektroi pare ezberdinei dagozkien orbital taldeak disjuntoak dira, hauetako multzo bakoitzean (Ω_g; $g = 1, ..., N/2$) okupazioak guztira bi elektroi gehitzen dituztelarik

$$2\sum_{p\in\Omega_g} n_p = 2, \quad g = 1, 2, \ldots, \mathrm{N}/2 \tag{30}$$

Modu honetan, posiblea da [54]. erreferentzian garatutako bi elektroietarako funtzional zehatza erabiltzea N elektroietako sistemetan. Izan ere, elektroi pare berdinari dagozkien orbitalen arteko elkarrekintzak [54]-n definitutako funtzional forma izango dute. Bestalde, elektroi pare ezberdinei dagozkien orbitalen arteko elkarrekintzek determinatuko dituzte hurbilpen diferenteak, hau da, PNOFi, i=$\overline{5,7}$. Aipatzekoa da orbitalak optimizatzen dituguneanpareen eskema aldakorra dela [55]. Hemendik aurrera "intra-pair" eta "inter-pair" erabiliko ditugu "elektroi pareen barneko" edo/eta "elektroi pare ezberdinen arteko" adierazteko.

Lehenik eta behin, pareen arteko elkarrekintza HF modukoa baldin bada, elektroi pare independenteen modeloa definitzen dugu, PNOF5 [56, 57]

$$\begin{gathered}
\Delta_{qp} = n_p^2 \delta_{qp} + n_q n_p \left(1 - \delta_{qp}\right) \delta_{q\Omega_g} \delta_{p\Omega_g} \\
\Pi_{qp} = n_p \delta_{qp} + \Pi_{qp}^g \left(1 - \delta_{qp}\right) \delta_{q\Omega_g} \delta_{p\Omega_g} \\
\Pi_{qp}^g = \begin{cases} -\sqrt{n_q n_p}, & p = g \text{ or } q = g \\ +\sqrt{n_q n_p}, & p, q > \mathrm{N}/2 \end{cases}, \qquad \delta_{q\Omega_g} = \begin{cases} 1, & q \in \Omega_g \\ 0, & q \notin \Omega_g \end{cases}
\end{gathered} \tag{31}$$

Modu honetan, (29) energia ondokoa da PNOF5 kasuan

$$\begin{aligned}
E_{el}^{pnof5} &= \sum_{g=1}^{\mathrm{N}/2} E_g + \sum_{f\neq g}^{\mathrm{N}/2} E_{fg} \\
E_{fg} &= \sum_{p\in\Omega_f} \sum_{q\in\Omega_g} \left[n_q n_p \left(2\mathcal{J}_{pq} - \mathcal{K}_{pq}\right)\right] \\
E_g &= \sum_{p\in\Omega_g} n_p \left(2\mathcal{H}_{pp} + \mathcal{J}_{pp}\right) + \sum_{q,p\in\Omega_g, q\neq p} \Pi_{qp}^g \mathcal{L}_{pq}
\end{aligned} \tag{32}$$

Interesgarria da aipatzea PNOF5-k APSG moduko uhin-funtzioari dagokiola [57,58]. Hori dela eta, PNOF5 korrelazio elektronikoa kontutan hartuz, funtzionalaren N-adierazpen puruaren baldintza nahikoak betetzen dituen lehen ONF-a da.

Elektroi pareen artean korrelazio elektronikoa deskribatzeko asmoz, PNOF7-ri dagokion energia ondoko moduan idazten da

$$\begin{aligned} E_{el}^{pnof7} &= \sum_{g=1}^{\mathrm{N}/2} E_g + \sum_{f\neq g}^{\mathrm{N}/2} E_{fg} \\ E_g &= \sum_{p\in\Omega_g} n_p \left(2\mathcal{H}_{pp} + \mathcal{J}_{pp}\right) + \sum_{q,p\in\Omega_g, q\neq p} \Pi_{qp}^{g} \mathcal{L}_{pq} \\ E_{fg} &= \sum_{p\in\Omega_f} \sum_{q\in\Omega_g} \left[n_q n_p \left(2\mathcal{J}_{pq} - \mathcal{K}_{pq}\right) + \Pi_{qp}^{\Phi} \mathcal{L}_{pq}\right] \end{aligned} \tag{33}$$

edo, beste era batera

$$E_{el}^{pnof7} = E_{el}^{pnof5} + \sum_{f\neq g}^{\mathrm{N}/2} \sum_{p\in\Omega_f} \sum_{q\in\Omega_g} \Pi_{qp}^{\Phi} \mathcal{L}_{pq} \tag{34}$$

(17)-k definitutako G baldintza erabiliz, frogatu daiteke $|\Pi_{qp}| \leq \Phi_q \Phi_p$ non $\Phi_q = \sqrt{n_q h_q}$ eta $h_q = 1 - n_q$. Hortaz, berdintza hartzen badugu, soilik elkarrekintzaren zeinua edo fasea zehaztu beharra geratzen da. 1.6.2. atalean erakusten den bezala, $\Pi_{qp}^{\Phi} = -\Phi_q \Phi_p$ hautaketa egokiena da, azken hau PNOF7 edo PNOF7(-) bezala ezagutzen dugularik. Batzuetan, PNOF7(+) erabiliko dugu, zeinetan $\Pi_{qp}^{\Phi} = \Phi_q \Phi_p$ baldin eta $q, p > \mathrm{N}/2$, eta $\Pi_{qp}^{\Phi} = -\Phi_q \Phi_p$ beste edozein kasutan.

Azkenik, korrelazio dinamikoa eta ez-dinamikoa modu orekatuagoan deskribatzeko asmoz, PNOF6 [44] ondoko moduan definitzen den elektroi-pare korrelazionatuen modeloa da

$$E_{el}^{pnof6} = \sum_{g=1}^{N/2} E_g + \sum_{f\neq g}^{N/2} \sum_{p\in\Omega_f} \sum_{q\in\Omega_g} E_{pq}^{int} \tag{35}$$

elektroi pare diferenteen arteko elkarrekintzak ondoko gaiarekin deskribatzen direlarik

$$E_{pq}^{int} = \left(n_q n_p - \Delta_{qp}\right)\left(2\mathcal{J}_{pq} - \mathcal{K}_{pq}\right) + \Pi_{qp}\mathcal{L}_{pq} \tag{36}$$

non

Δ_{qp}	Π_{qp}	*Orbitalak*
$e^{-2S} h_q h_p$	$-e^{-S}\left(h_q h_p\right)^{\frac{1}{2}}$	$q \leq F, p \leq F$
$\frac{\gamma_q \gamma_p}{S_\gamma}$	$-\Pi_{qp}^{\gamma}$	$q \leq F, p > F$
		$q > F, p \leq F$
$e^{-2S} n_q n_p$	$e^{-S}\left(n_q n_p\right)^{\frac{1}{2}}$	$q > F, p > F$

(37)

Bestelako kantitateak ondoko moduan definitzen dira

$$\begin{gathered}\gamma_p = n_p h_p + \alpha_p^2 - \alpha_p S_\alpha \\ \alpha_p = \begin{cases} e^{-S} h_p\,, & p \leq F \\ e^{-S} n_p\,, & p > F \end{cases} \\ \Pi^\gamma_{qp} = \left(n_q h_p + \frac{\gamma_q \gamma_p}{S_\gamma} \right)^{\frac{1}{2}} \left(h_q n_p + \frac{\gamma_q \gamma_p}{S_\gamma} \right)^{\frac{1}{2}} \\ S = \sum_{q=F+1}^{F+FN_c} n_q, \quad S_\alpha = \textstyle\sum_{q=F+1}^{F+FN_c} \alpha_q, \quad S_\gamma = \textstyle\sum_{q=F+1}^{F+FN_c} \gamma_q \end{gathered} \tag{38}$$

N_c-k orbital subespazio bakoitzean gogor okupatutako orbital bakoitzarekin zenbat orbital (hauek Fermi mailaren gainekoak) aklopatzen diren zehazten du. Aipatzekoa da PNOF6-k PNOF5 baino korrelazio energia gutxiago berreskuratzen duela (eta ondorioz PNOF7 baino ere bai), elektroi-pare ezberdinen artean korrelazioa kontsideratu arren. Dena den, PNOF6 hurbilpen egokia da zenbait ikerketetarako [59–62].

1.3.2 Euler-en ekuazioak

(25). ekuazioa orbitalekiko eta okupazioekiko optimizatu beharra dugu sistemari dagokion oinarrizko energia lortu ahal izateko. Gainera, lehenengoetan ortonormalitatea inposatzen dugu, bigarrenetan normalizazioa inposatuko dugun bitartean, hortaz, lagrangiarra ondokoa da

$$\Lambda = E_{el} - \mu \left(\sum_i n_i - N \right) - \sum_{ki} \lambda_{ik} \left(\langle \phi_k | \phi_i \rangle - \delta_{ki} \right) \tag{39}$$

Ondoren, lagrangiarraren minimoa lortzeko hurrengo ekuazio sistema lortzen dugu

$$\frac{\partial E_{el}}{\partial n_i} = \mathcal{H}_{ii} + \frac{\partial V_{ee}}{\partial n_i} = \mu \tag{40}$$

$$\frac{\partial E_{el}}{\partial \phi_i^*} = n_i \hat{\mathcal{H}} \phi_i + \frac{\partial V_{ee}}{\partial \phi_i^*} = \sum_k \lambda_{ki} \phi_k \tag{41}$$

Ohartu (21). eta (25). ekuazioei erreparatuz V_{ee} hurbildu egiten dela (25). ekuazioaren bigarren gaiaren bitartez. Elektroi-pareen metodoa erabiltzen badugu, okupazioen normalizazioa automatikoki betetzen da, hortaz okupazioekiko optimizazioa *conjugate-gradient* edo LBFGS baldintza gabeko metodo numerikoak erabiliz egin dezakegu. Orbitalekiko, berriz, [55]-n garatutako diagonalizazio metodoa erabiltzen da (41). ekuazioa ebazteko. Izan ere, diagonalizazio prozesuan orbital ortogonalak sortzen dira, baldintzapeko optimizaziorik egitea saihesten dugularik. Diagonalizatzen den matrizearen eta metodoaren konbergentziaren inguruko informazio gehiago [55]. erreferentzian aurkitu daiteke.

1.3.3 DoNOF programa

Figure 1 – *Donostia Natural Orbital Functional* programaren logoa.

DoNOF (Donostia Natural Orbital Functional Software Program) Mario Piris-ek hainbat kolaboratzaileren laguntzarekin garatutako programa da. Programa ez-publikoa da eta bere erabilera egilearen baimenaren beharra du.

Tesi honetan zehar egindako ONFH-en kalkulu guztietarako DoNOF erabili da. Beraz, aipatzekoak dira kodean egindako ondoko hobekuntzak:

1) ONFH berriak inplementatu dira, besteak beste, Power [37], MBB [35], CA [38], eta CGA [39], Goedecker eta Umrigar (GU) [63], Marques eta Lathiotakis (MLSIC) [64], eta Gritsenko, Pernal eta Baerends (BBC2) [65].

2) Gradiente analitikoen konputazio efizientea programatu da, *on-the-fly* moduan kalkulatuz integralen deribatuak bakarrik benetan garrantzitsuenak direnak kalkulatu eta gorde ahal izateko.

3) Geometriaren optimizazioa egin ahal izateko prozedura inplementatu da, gradiente analitikoak erabiliz. Horretarako Eduard Matito-k programatutako MPI paralelizazioaren eskema orokortu egin da, geometriaren optimizazioak ere nodo bat baino gehiagotan kalkulatzeko asmoz.

4) Xabier Lopez-ekin batera, Hesiarraren eta propietate termokimikoen kalkulu numerikoa programatu da, batez ere bibrazio frekuentzia harmonikoak kalkulatu ahal izateko.

5) LBFGS [66] algoritmoa inplementatu da baldintza gabeko optimizazioak egiteko, zehatz mehatz, geometriaren optimizazioa eta energiaren optimizazioa okupazioekiko. Aurretik *conjugate-gradient* metodoa erabiltzen zen beti DoNOF programan, orain bi aukera ezberdinak daudelarik.

6) Hubbard Hamiltondarra programatu da, bat eta bi dimentsiotan. Mugako baldintza periodikoak erabili daitezke, korrelazio erregimenaren eta elektroi-betetzearen balio ezberdinak, eta kanpo eremu diferenteak, besteak beste.
7) Kuadrupoloaren eta oktupoloaren kalkuluak gehitu dira dipoloarenarekin batera, Buckinghamek proposatutako definizioak [67, 68] jarraituz.
Hobekuntza berri hauek guztiak eta Piris-ek egindako aurrerapen berriak [31,46,69] publikoa egingo den DoNOF programaren lehen bertsioan agertuko dira, ONFT-n oinarritutako lehen programa publikoa izango delarik. Egun, programaren argitalpenaren inguruko publikazio batean lan egiten ari gara.

1.4 Helburuak

Tesi honen helburu nagusia da ONFH-en garapena eta aplikazioak, egitura elektronikoan egunero erabiltzen diren DFT eta uhin-funtzio metodoetaz gain, DME-etan oinarritutako partikula bakarreko metodo eraginkorra finkatzeko asmoz. Puntuz puntu, ondoko helburuetan banatu dezakegu lanaren antolamendua:

1) Geometriaren optimizazioa prozedura garrantzitsuenetarikoa denez gero, ezinbestekoa da nukleoekiko deribatu analitikoak garatzea eta orekako geometriak kalkulatzea ONFH-ak erabiliz. Balioztatzeko, bai beste metodo teorikoekin bai datu esperimentalekin konparazioak egitea beharrezkoa izanen da.

2) ONF teoriaren eta hurbilpenen arteko oinarrizko diferentziak nabarmentzea ezinbestekoa da, honek praktikan dituen ondorioak azpimarratuz. 2DME-aren N-adierazgarritasuna da adibide garrantzitsuena. *Bottom-up* metodologiari esker baldintza hauek funtzionalak garatzeko erabili daitezke. Hala ere, kasu batzuetan ez dira nahikoak fasearen dilema ebazteko. Hori dela eta, funtzionalen garapenarako sistema modeloak erabiltzea da helburuetako bat.

3) Egun, korrelazio gogorra zehaztasunez deskribatzen duten metodoak gutxi eta erabiltzeko konplexuak dira. PNOF7 bat eta bi dimentsiotako sistemak deskribatzeko duen gaitasuna aztertuko dugu mota diferenteetako sistemak aztertuz. Modu honetan *black-box* bat bezala erabili daitekeen metodo baliogarria proposatzea da helburua.

4) Azkenik, egitura elektronikorako interesgarriak diren hainbat propietaterekin erlazionatutak egoteagatik, momentu elektriko dipolarra, kuadrupolarra eta oktupolarra inplementatzea garrantzitsua da ONFH-en testuinguruan. Ondoren, bai beste metodo teorikoekin bai datu esperimentalekin konparazioak egingo dira analisi estatistikoa egiteko asmoz.

1.5 Geometriaren optimizazioa

Puntu bakarreko energiaren ondoren, geometriaren optimizazioa kalkulurik hedatuena da egitura elektronikoaren teorian. Energiaren deribatuak (gradientea eta orden altuagokoak) minimoak eta puntu kritikoak identifikatzeko balio dute energia potentzialaren gainazalean. Honetaz aparte, beste hainbat aplikazio eta propietate batzuk zuzeneko erlazioa dute deribatu hauekin, momentu elektrikoak kasu [59].

1.5.1 Gradiente analitikoak ONFT-n

1.5.1.1 Sarrera

Energiaren gradienteak ezinbestekoak dira kimika eta fisikarentzako [70]. Kalkulu analitikoak numerikoa baino efizienteagoa da, hortaz, egitura elektronikoaren metodo ezberdinetarako gradienteen deribazio analitikoa garatu da urteetan zehar, besteak beste, configuration interaction (CI) [71, 72], density cumulant functional theory (DCFT) [73], Moller-Plesset perturbation theory (MP2) [74], edo coupled cluster kontuan hartuz kitzikapen bakarrak, dobleak, eta perturbatiboki tripleak (CCSD(T)) [75].
Kapitulu honetan, ONFT-rentzako gradiente analitikoen deribazioa egiten da, [76]-n proposatutako metodoa jarraituz. Hainbat molekulen kasuan PNOF hurbilpenak erabiliko ditugu orekako geometriak lortzeko, bai datu esperimentalekin bai maila altuko kalkulu teorikoekin alderatuz.

1.5.1.2 Gradiente analitikoen deribazioa

ON erreralak base batean garatuz, $\phi_i(\mathbf{x}) = \sum_\upsilon \mathcal{C}_{\upsilon i}\zeta_\upsilon(\mathbf{x})$, energia elektronikoa ondoko moduan idazten da

$$E_{el} = \sum_{\mu\upsilon} \Gamma_{\mu\upsilon}\mathcal{H}_{\mu\upsilon} + \sum_{\mu\upsilon\eta\delta} D_{\mu\eta\upsilon\delta}\langle\mu\eta|\upsilon\delta\rangle, \tag{42}$$

non eta $\Gamma_{\mu\upsilon}$ eta $D_{\mu\eta\upsilon\delta}$ 1 eta 2 DME-ak dira OA-etan, hurrenez hurren,

$$\begin{aligned} \Gamma_{\mu\upsilon} &= \sum_i n_i \mathcal{C}_{\mu i}\mathcal{C}_{\upsilon i}, \\ D_{\mu\eta\upsilon\delta} &= \sum_{klij} D_{klij}\mathcal{C}_{\mu k}\mathcal{C}_{\eta l}\mathcal{C}_{\upsilon i}\mathcal{C}_{\delta j}. \end{aligned} \tag{43}$$

Orduan, energia osoaren deribatua A nukleoaren x koordenatuarekiko

$$\frac{dE}{dx_A} = \frac{\partial E_{el}}{\partial x_A} + \frac{\partial E_{nuc}}{\partial x_A} + \sum_{\mu j} \frac{\partial E_{el}}{\partial \mathcal{C}_{\mu j}} \frac{\partial \mathcal{C}_{\mu j}}{\partial x_A} + \sum_i \frac{\partial E_{el}}{\partial n_i} \frac{\partial n_i}{\partial x_A}, \tag{44}$$

non eta $\partial E_{el}/\partial x_A$ eta $\partial E_{nuc}/\partial x_A$ gaiak menpekotasun esplizitua dute x_A-rekiko, eta beste gaiak (44). ekuazioan menpekotasun inplizitua dute orbitalen eta okupazioen bitartez. Lehenengoa, HF kasuan egiten den moduan, $\mathbf{C}^\dagger\mathbf{SC} = \mathbf{1}$ erlazioa erabiliz erraz lortu daiteke

$$\sum_{\mu j} \frac{\partial E_{el}}{\partial \mathcal{C}_{\mu j}} \frac{\partial \mathcal{C}_{\mu j}}{\partial x_A} = -\sum_{\mu\upsilon} \lambda_{\mu\upsilon} \frac{\partial \mathcal{S}_{\mu\upsilon}}{\partial x_A}, \tag{45}$$

non

$$\lambda_{\mu\upsilon} = \sum_{ij} \mathcal{C}_{\mu j} \lambda_{ji} \mathcal{C}_{\upsilon i}. \tag{46}$$

(44). ekuazioaren azken gaia nulua da, okupazioak optimizazio bariazionalaren bitartez lortu dira eta. Hori dela eta, ONF gradiente analitikoak lortzeko ondoko formula dugu

$$\frac{dE}{dx_A} = \sum_{\mu\upsilon} \Gamma_{\mu\upsilon} \frac{\partial \mathcal{H}_{\mu\upsilon}}{\partial x_A} + \sum_{\mu\upsilon\eta\delta} D_{\mu\eta\upsilon\delta} \frac{\partial \langle \mu\eta | \upsilon\delta \rangle}{\partial x_A} + \frac{\partial E_{nuc}}{\partial x_A} - \sum_{\mu\upsilon} \lambda_{\mu\upsilon} \frac{\partial \mathcal{S}_{\mu\upsilon}}{\partial x_A}. \tag{47}$$

Kapitulu honetan spin restricted teoria erabiltzen dugunez gero, orbital espazialak berdinak dira edozein spin baliorako, $\varphi_p^\alpha(\mathbf{r}) = \varphi_p^\beta(\mathbf{r}) = \varphi_p(\mathbf{r})$. Beraz, ON espazialak $\{\varphi_p\}$ OA-en konbinazio lineal moduan adieraziko ditugu, $\varphi_p(\mathbf{r}) = \sum_\upsilon \mathcal{C}_{\upsilon p}\chi_\upsilon(\mathbf{r})$. Orduan (47). ekuazioan agertzen diren gaiak ondoko moduan definitzen dira

$$\begin{aligned} \Gamma_{\mu\upsilon} &= 2\sum_p n_p \mathcal{C}_{\mu p}\mathcal{C}_{\upsilon p} \\ D_{\mu\eta\upsilon\delta} &= 2\sum_{pqrt} (D^{\alpha\alpha}_{pqrt} + D^{\alpha\beta}_{pqrt}) \mathcal{C}_{\mu p}\mathcal{C}_{\eta q}\mathcal{C}_{\upsilon r}\mathcal{C}_{\delta t} \\ \lambda_{\mu\upsilon} &= 2\sum_{pq} \mathcal{C}_{\mu q}\lambda_{qp}\mathcal{C}_{\upsilon p}. \end{aligned} \tag{48}$$

1.5.1.3 Alderdi konputazionalak

ONFT-n ez da sistemaren erantzuna kalkulatu behar energiaren gradienteak lortzeko, hortaz, (47). ekuazioa ebaluatzeko ez da prozesu iteratiborik behar, korrelazionatutak dauden metodo gehienetan gertatzen den ez bezala. Praktikan, lehendabizi $\Gamma_{\mu\upsilon}$, $D_{\mu\eta\upsilon\delta}$, eta $\lambda_{\mu\upsilon}$ kalkulatzen dira, jarraian integralen deribatuekin biderkatzeko energiaren gradienteari gehitzeko asmoz. Prozesu hau M^5-eko gastu konputazionala inplikatzen du M partikula bateko espazioaren dimentsioa delarik. Halere, $D_{\mu\eta\upsilon\delta}$ zehatz batzuetarako M^4-ra murriztu daiteke gastua, HF metodoan agertzen den gastu konputazionala lortzen dugularik. Gainera, Schwarz-en

metodoa [77] inplementatu dugu oso txikiak diren bi elektroien integralak kalkulatu behar ez izateko. Azkenik, esatekoa da *conjugate gradient* teknika erabili dugula oinarrizko egoeren geometriak lortzeko, izan ere, geometriaren optimizazioa inolako murrizketa edo baldintzapean egiten da.

1.5.1.4 Orekako geometriak

Atal honetan ondoko molekulen orekako geometriak aztertuko ditugu ONFT praktikan jartzeko: HF, H_2O, NH_3, CH_4, N_2, CO, HOF, HNO, H_2CO, HNNH, H_2CCH_2, HCCH, HCN, HNC, eta O_3. PNOF5, PNOF6, eta PNOF7 hurbilpenak aztertuko ditugu, CCSD-rekin [75] alderatuz, eta datu esperimentalak erreferentzia moduan erabiliz. Azken hauen kasuan, bibrazio korrekzioak aplikatu dira [78], hortaz, datu enpirikoak dira esperimentalak baino. cc-pVTZ basea erabili da kalkulu guztietan.
Taulak 2 eta 3 erakusten dute lotura distantzia eta angeluetarako lortutako erroreak PNOF5, PNOF6, eta CCSD erabilita datu enpirikoekiko. Orokorrean hiru metodoekin lortutako erroreak konparagarriak dira, esaterako, CCSD lotura distanzietarako onena den bitartean, PNOF6 errore txikiena erakutsi du lotura angeluetarako ($\overline{\Delta}_{abs} = 0.33$ degs). Ohartu PNOF5-ek PNOF6 baino lotura distantzia txikiagoak sortzen dituela, izan ere, korrelazio energia gehiago berreskuratzen du. Azpimarratzekoa da ozono molekularen kasua, honentzat bakarrik PNOF6 deskribatu baitu oinarrizko egoeraren geometria zehaztasunez. Coupled cluster teoriari dagokionez, beharrezkoa da CCSD(T) mailaraino joatea ozonoaren geometria enpirikoa zehaztasunez deskribatzeko [75].

1.5.1.5 PNOF7-ren orekako geometriak

Taulak 4 eta 5 erakusten dute lotura distantzia eta angeluetarako lortutako erroreak PNOF5, PNOF7, eta CCSD erabilita datu enpirikoekiko. PNOF7-k PNOF5 baino errore nabarmenagoak sortzen ditu. Izan ere, PNOF7-k korrelazio estatikoaren gehiengoa lortzen du, elektroi pareen arteko dinamika ez duelarik deskribatzen. Hori dela eta, PNOF7-ren orekako geometriak hobetu ahal izateko NOF-MP2 metodoa [45, 46] erabiltzea beharrezkoa da, pareen arteko korrelazio dinamikoa gehitzeko.

1.5.1.6 Ondorioak

Table 2 – Oreka loturetan lortutako erroreak (pm-tan) datu enpirikoekiko, PNOF5, PNOF6, eta CCSD erabiliz cc-pVTZ basearekin. $\overline{\Delta}$ eta $\overline{\Delta}_{abs}$ batez besteko erroreari eta batez besteko errore absolutoari dagozkie, hurrenez hurren.

Molekula	Lotura	PNOF5	PNOF6	CCSD [75]	ENP. [78]
HF	H—F	-0.2	-0.3	-0.3	91.7
H_2O	O—H	0.1	-0.5	-0.2	95.8
NH_3	N—H	0.6	-0.3	-0.3	101.2
CH_4	C—H	1.5	-0.5	-0.1	108.6
N_2	N—N	-0.7	-1.4	-0.4	109.8
CO	C—O	-1.1	-1.5	-0.3	112.8
HNO	N—O	0.0	-1.3	-0.9	120.9
	H—N	-0.7	-2.1	-0.3	105.2
H_2CO	C—O	0.2	-1.1	-0.5	120.5
	C—H	0.4	-1.1	-0.4	110.1
HNNH	N—N	-0.1	-1.2	-0.7	124.6
	N—H	0.1	-1.6	-0.4	102.9
H_2CCH_2	C—C	0.9	-0.3	-0.4	133.1
	C—H	1.1	-0.7	-0.4	108.1
HCCH	C—C	-0.1	-1.0	-0.4	120.4
	C—H	0.7	-0.7	-0.4	106.1
HCN	C—N	-0.5	-1.3	-0.4	115.3
	C—H	0.5	-0.8	-0.6	106.5
HNC	C—N	-2.3	-1.3	-0.4	116.9
	N—H	-1.3	-1.0	-0.4	99.5
HOF	O—F	3.6	2.4	-1.9	143.4
	H—O	-0.3	-1.9	-0.5	96.8
O_3	O—O	2.6	-3.5	-3.6	127.2*
$\overline{\Delta}$		0.2	-1.0	-0.6	
$\overline{\Delta}_{abs}$		0.8	1.2	0.6	

*Geometria [8] erreferentziatik.

Table 3 – Oreka angeluetan lortutako erroreak (deg-etan) datu enpirikoekiko, PNOF5, PNOF6, eta CCSD erabiliz cc-pVTZ basearekin. $\overline{\Delta}$ eta $\overline{\Delta}_{abs}$ batez besteko erroreari eta batez besteko errore absolutoari dagozkie, hurrenez hurren.

Molekula	Lotura angelua	PNOF5	PNOF6	CCSD [75]	ENP. [78]
H_2O	H—O—H	0.23	0.04	-0.47	104.51
NH_3	H—N—H	0.45	-0.89	-0.89	107.25
HOF	H—O—F	-0.27	-0.22	0.43	97.94
HNO	H—N—O	-0.53	0.21	0.00	108.27
H_2CO	H—C—O	-0.09	0.07	0.29	121.63
HNNH	H—N—N	0.82	1.07	-0.04	106.36
H_2CCH_2	H—C—C	-0.15	0.00	0.03	121.43
O_3	O—O—O	-3.44	0.09	1.57	116.70*
$\overline{\Delta}$		-0.37	0.05	0.12	
$\overline{\Delta}_{abs}$		0.75	0.33	0.47	

*Geometria [8] erreferentziatik.

Table 4 – Oreka loturetan lortutako erroreak (pm-tan) datu enpirikoekiko, PNOF5, PNOF7, eta CCSD erabiliz cc-pVTZ basearekin. $\overline{\Delta}$ eta $\overline{\Delta}_{abs}$ batez besteko erroreari eta batez besteko errore absolutoari dagozkie, hurrenez hurren.

Molekula	Lotura	PNOF5	PNOF7	CCSD [75]	ENP. [78]
HF	H—F	-0.2	0.2	-0.3	91.7
H_2O	O—H	0.1	0.5	-0.2	95.8
NH_3	N—H	0.6	0.9	-0.3	101.2
CH_4	C—H	1.5	1.7	-0.1	108.6
N_2	N—N	-0.7	0.2	-0.4	109.8
CO	C—O	-1.1	-0.6	-0.3	112.8
HNO	N—O	0.0	1.7	-0.9	120.9
	H—N	-0.7	-0.5	-0.3	105.2
H_2CO	C—O	0.2	1.1	-0.5	120.5
	C—H	0.4	0.4	-0.4	110.1
HNNH	N—N	-0.1	1.3	-0.7	124.6
	N—H	0.1	0.4	-0.4	102.9
H_2CCH_2	C—C	0.9	1.9	-0.4	133.1
	C—H	1.1	1.3	-0.4	108.1
HCCH	C—C	-0.1	0.7	-0.4	120.4
	C—H	0.7	0.9	-0.4	106.1
HCN	C—N	-0.5	0.4	-0.4	115.3
	C—H	0.5	0.7	-0.6	106.5
HNC	C—N	-2.3	-0.2	-0.4	116.9
	N—H	-1.3	0.4	-0.4	99.5
HOF	O—F	3.6	8.2	-1.9	143.4
	H—O	-0.3	0.3	-0.5	96.8
$\overline{\Delta}$		0.1	1.0	-0.5	
$\overline{\Delta}_{abs}$		0.8	1.1	0.5	

Table 5 – Oreka angeluetan lortutako erroreak (deg-etan) datu enpirikoekiko, PNOF5, PNOF7, eta CCSD erabiliz cc-pVTZ basearekin. $\overline{\Delta}$ eta $\overline{\Delta}_{abs}$ batez besteko erroreari eta batez besteko errore absolutoari dagozkie, hurrenez hurren.

Molekula	Lotura angelua	PNOF5	PNOF7	CCSD [75]	ENP. [78]
H_2O	H—O—H	0.23	-0.09	-0.47	104.51
NH_3	H—N—H	0.45	-0.92	-0.89	107.25
HOF	H—O—F	-0.27	-1.35	0.43	97.94
HNO	H—N—O	-0.53	-0.67	0.00	108.27
H_2CO	H—C—O	-0.09	-0.51	0.29	121.63
HNNH	H—N—N	0.82	0.44	-0.04	106.36
H_2CCH_2	H—C—C	-0.15	0.14	0.03	121.43
$\overline{\Delta}$		0.07	-0.42	-0.09	
$\overline{\Delta}_{abs}$		0.36	0.59	0.31	

Lehendabiziko aldiz ONFT-n oinarritutako metodoak erabiliz sistema molekularren orekako geometriak kalkulatu dira. Ez hori bakarrik, frogatu egin da gradiente energetikoen kalkulua efizientea eta zehaztasun altukoa dela PNOF hurbilpenak erabiliz. Izan ere, azken hauek CCSD metodoarekin bat datoz, kalkuluarin dagokion konputazio denbora nabarmenki murriztuz *one shot* izaerako kalkulua bakarrik beharrezkoa baita ONFT-n gradienteak lortzeko. Dena delakoan, argi dago kapitulu honetan zehar egindako ikerketa osatzeko bigarren deribatuaren inguruko eztabaida beharrezkoa dela. Hesiarrak energia potentzialaren inguruko ezinbesteko informazioa ematen du, hori dela eta, hurrengo atalean Hesiarraren kalkulua ONFT-ren testuinguruan aztertuko dugu deribatu analitikoen ikerketa osatzeko asmoz.

1.5.2 Bigarren ordeneko deribatu analitikoak ONFT-n

1.5.2.1 Sarrera

Hesiarraren (hau da, bigarren ordeneko nukleoen koordinatuekiko energiaren deribatuen) kalkulua interes handikoa da kimika eta fisika arloentzako [79–82]. Besteak beste, azpimarratzekoak dira espektroskopian duten aplikazioak [83]. Ondorioz, ezinbestekoa da egitura elektronikoaren edozein metodoarentzako Hesiarraren kalkulua modu efizientean garatzea. Kapitulu honetan ONFT-ren testuinguruan aztertuko dugu deribatu hauen inguruko teoria eta praktika, zenbait molekulen kasuan bibrazio frekuentziak kalkulatuko ditugularik.

1.5.2.2 Hesiarra

Lehenik eta behin, aurreko atalean lortutako gradientearen formula (47) ON-etan idatziko dugu

$$\frac{dE_{el}}{dx_A} = \sum_i n_i \frac{\partial \mathcal{H}_{ii}}{\partial x_A} + \sum_{ijkl} D_{kl,ij} \frac{\partial \langle ij|kl\rangle}{\partial x_A} - \sum_{ij} S_{ij}^{x_A} \lambda_{ij}, \quad S_{ij}^{x_A} = \sum_{\mu\upsilon} C_{\mu i} C_{\upsilon j} \frac{\partial \mathcal{S}_{\mu\upsilon}}{\partial x_A}. \tag{49}$$

Ohartu $\mathcal{S}$-k adierazten duela *overlap* matrizea OA-etan. Normalean, perturbatutako geometriari dagozkion orbitalak aurretiko orbital ez perturbatuen menpe adierazten dira. Orduan, ON batean nukleoaren perturbazioak ondoko aldaketa eragiten du

$$\phi_i + \delta x_A \left(\sum_j U_{ij}^{x_A} \phi_j + \sum_\mu C_{\mu i} \frac{\partial \zeta_\mu}{\partial x_A} \right) + \mathcal{O}\left(\delta x_A^2\right). \tag{50}$$

(50). ekuazioak OA-ak $\{\zeta_\mu\}$ erabiltzen ditu, ON-en koefizienteen aldaketak akoplatutako ekuazio perturbatuetatik lortutako koefizienteetatik ($\left\{U_{ij}^{x_A}\right\}$) lortzen direlarik. Posiblea da ON-en adierazpenean energiaren gradienteak ondoko moduan idaztea

$$\frac{dE_{el}}{dx_A} = \sum_i n_i \frac{\partial \mathcal{H}_{ii}}{\partial x_A} + \sum_{ijkl} D_{kl,ij} \frac{\partial \langle ij|kl\rangle}{\partial x_A} + 2 \sum_{ij} U_{ij}^{x_A} \lambda_{ij}. \tag{51}$$

Ondoren, bigarren ordeneko deribatuak (51). ekuazioa y nukleoaren B koordenatuarekiko deribatuz lortzen dira

$$\begin{aligned} \frac{d^2 E_{el}}{dx_A dy_B} &= \sum_i n_i \frac{\partial^2 \mathcal{H}_{ii}}{\partial x_A \partial y_B} + \sum_{ijkl} D_{kl,ij} \frac{\partial^2 \langle ij|kl\rangle}{\partial x_A \partial y_B} \\ &+ 2 \sum_{ij} U_{ij}^{y_B} \lambda_{ij}^{x_A} + 2 \sum_{ij} \frac{d}{dy_B}\left(U_{ij}^{x_A} \lambda_{ij}\right) + \sum_m n_m^{y_B} \frac{\partial}{\partial n_m} \left(\frac{dE_{el}}{dx_A} \right). \end{aligned} \tag{52}$$

Aurreko (52). ekuazioan lehenengo gaiak integralen deribatuak esplizituak adierazten dituzte, ondoko bi gaiak ON-en koefizienteen deribatuetatik agertzen dira, eta azkenik, $n_m^{y_B}$-k adierazten du m okupazioaren erantzuna y_B perturbazioarekiko. (52). ekuazioa modifikatu daiteke praktikan erabiltzen den formula lortuz, ON-etan adierazita

$$\frac{d^2E_{el}}{dx_A dy_B} = \sum_i n_i \frac{\partial^2 \mathcal{H}_{ii}}{\partial x_A \partial y_B} + \sum_{ijkl} D_{kl,ij} \frac{\partial^2 \langle ij|kl\rangle}{\partial x_A \partial y_B} + 2\sum_{ij} \left(U_{ij}^{y_B} \lambda_{ij}^{x_A} + U_{ij}^{x_A} \lambda_{ij}^{y_B} + U_{ij}^{x_A y_B} \lambda_{ij} \right)$$
$$+ 2\sum_{ijkl} U_{ij}^{x_A} U_{kl}^{y_B} Y_{ijkl} + \sum_m n_m^{y_B} \left(\frac{\partial \mathcal{H}_{mm}}{\partial x_A} + 2\sum_{ij} U_{ij}^{x_A} \frac{\partial \lambda_{ij}}{\partial n_m} + \sum_{ijkl} \frac{\partial D_{kl,ij}}{\partial n_m} \frac{\partial \langle ij|kl\rangle}{\partial x_A} \right). \tag{53}$$

Lehen ordeneko deribatuekin alderatuz, (53). ekuazioa erakusten du bai orbitalen bai okupazioen erantzuna perturbazioarekiko kalkulatzea beharrezkoa dela Hesiarra lortzeko. Lehenengoa U koefizienteen bitartez adierazita dago, bigarrena $n_m^{y_B}$ moduan idatzi delarik. Beraz, beharrezkoa da akoplatutako ekuazio perturbatuak kalkulatzea aurreko kantitateak lortu ahal izateko.

1.5.2.3 Akoplatutako ekuazio perturbatuak

Akoplatutako ekuazio perturbatuak 2006. urtean lortutak izan ziren ONFT-ren testuinguruan [84]. Oraingo honetan, berriz, kontsideratuko dugu ON-ak perturbazioarekiko menpekotasun esplizitua dutela. Gainera, *Fockian* baten existentzia eza kontsideratuko dugu, akoplatutako ekuazio perturbatuak Euler-en ekuazioetatik (hau da, 40-41) kalkulatzen direlarik. Izan ere, azken hauek baliogarriak ONF-aren edozein hurbilketarako, eta ez bakarrik teoria zehatzaren kasurako. Ondorioz, planteatu beharrezko ekuazioa ondokoa da

$$\frac{d}{dx_A}\left(\lambda_{ij} - \lambda_{ji}\right) = 0. \tag{54}$$

Hainbat modifikazioren ondoren, (54). ekuazioa ondoko ekuazio sistemetan bilakatzen da

$$\begin{aligned} \forall_{i>j} \quad & \sum_{k>l} A_{ij,kl} U_{kl}^{x_A} + \left(E_{ij}^k - E_{ji}^k\right) n_k^{x_A} = B_{ij}^{x_A} \\ \forall_i \quad & \sum_{k>l} \left(E_{kl}^i - E_{lk}^i\right) U_{kl}^{x_A} + W_{ik} n_k^{x_A} = F_i^{x_A} \end{aligned} \tag{55}$$

non eta

$$F_m^{x_A} = \mu^{x_A} - \left(\frac{\partial \mathcal{H}_{mm}}{\partial x_A} + \sum_{ijkl} \frac{\partial D_{kl,ij}}{\partial n_m} \frac{\partial \langle ij|kl\rangle}{\partial x_A} \right) + \sum_{i>j} S_{ij}^{x_A} E_{ji}^m + \tfrac{1}{2} \sum_i S_{ii}^{x_A} E_{ii}^m,$$
$$E_{ij}^m = 2\delta_{jm} \mathcal{H}_{ij} + 4\sum_{rkl} \frac{\partial D_{kl,jr}}{\partial n_m} \langle ir|kl\rangle, \qquad W_{mr} = \sum_{ijkl} \frac{\partial^2 D_{kl,ij}}{\partial n_m \partial n_r} \langle ij|kl\rangle,$$

$$A_{ij,kl} = \delta_{li}\lambda_{kj} - \delta_{ki}\lambda_{lj} - \delta_{lj}\lambda_{ki} + \delta_{kj}\lambda_{li} + \ Y_{ijkl} - Y_{ijlk} - Y_{jikl} + Y_{jilk},$$

$$B_{ij}^{x_A} = \sum_{k>l} S_{kl}^{x_A}\left(\delta_{ki}\lambda_{lj} - \delta_{kj}\lambda_{li} + Y_{ijkl} - Y_{jilk}\right) + \frac{1}{2}\sum_{k} S_{kk}^{x_A}\left(\delta_{ki}\lambda_{kj} - \delta_{kj}\lambda_{ki} + Y_{ijkk} - Y_{jikk}\right) - \lambda_{ij}^{x_A} + \lambda_{ji}^{x_A}.$$

Azpimarratzekoa da (55). ekuazioa guztiz orokorra dela, eta edozein hurbilketari dagokion $D\left[n_i, n_j, n_k, n_l\right]$ adierazpenaren beharra besterik ez duela inplemetatuta izateko.

1.5.2.4 Alderdi konputazionalak

Akoplatutako ekuazio perturbatuak kalkulatu behar izateak Hesiarraren kalkulu analitikoa konputazionalki garestia egiten du. Hori dela eta, efizienteak diren energiaren gradienteen deribatu numerikoak erabiliko ditugu Hesiarra lortzeko. Teknika honen baliogarritasuna aurretik finkatuta izan da [85], non eta lehen ordeneko deribatuekin gertatzen den ez bezala, Hesiarraren kalkulu analitikoaren eraginkortasuna zalantzan jarri izan den gastu konputazionala dela eta.

1.5.2.5 Bibrazio frekuentzia harmonikoak

Hesiarra kalkulatuko dugu gradiente analitikoen deribatu numerikoak erabiliz, [86] erreferentzian aipatutako prozesua jarraituz. Azken hauek erabiliz bibrazio frekuentzia harmonikoak lortu ditugu PNOF7, CCSD, eta MP2 metodoak erabiliz, aldi berean datu esperimentalekin konparatzen ditugularik. Bai balio esperimentalak, bai CCSD eta MP2 metodoei dagozkien balioak [8]-tik lortu dira ondoko molekulentzako: H_2O, NH_3, CH_4, N_2, CO, HNO, H_2CO, HNNH, H_2CCH_2, HNC, HCCH, HOF, LiH, HF, C_2H_2, H_2O_2, Li_2, LiH, HCN, F_2, CO_2, H_2, PH_3, SiH_4, H_2S, HCl, Na_2, P_2, Cl_2, NaCl, CS, SiO, ClF, eta HOCl. Kalkulu teoriko guztiak cc-pVTZ basearekin [87] lortu dira, eta PNOF7-ren kasuan, orbitalen arteko akoplamendu maximoa erabili da.

2. irudian datu esperimentalekiko lortutako erroreen banaketa azaltzen da, aurretik aipatutako molekulen talderako, CCSD, MP2, eta PNOF7 metodoak erabiliz. PNOF7 eta CCSD erakutsi dute emaitzarik zehatzenak, bi hauen arteko diferentzia nabarmenik ez dagoelarik. Bataz besteko balioei dagokienez, oso antzekoak dira balioak hiru metodoentzako: $\overline{\triangle}(PNOF7) = 104\,cm^{-1}$, $\overline{\triangle}(MP2) = 104\,cm^{-1}$ and $\overline{\triangle}(CCSD) = 100\,cm^{-1}$. Orokorrean datu esperimentalekiko erroreak oso handiak diruditen arren, errore hauek sistematikoak dira, hortaz, eskala faktoreak erabiliz efektu ez-harmonikoak zuzendu daitezke eta aurretik erakutsitako batez besteko balioak murriztu [88].

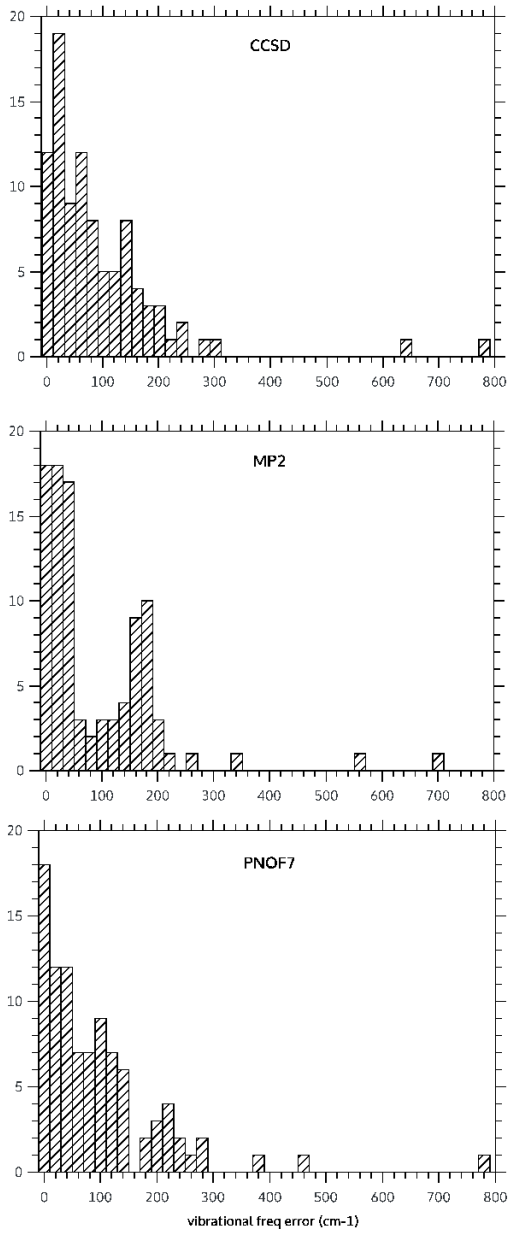

Figure 2 – 20 cm^{-1}-ko bin-a erabiliz eraikitako histogramak, datu esperimentalekiko erroreen banaketa adierazteko CCSD, MP2 eta PNOF7 metodoak erabilita cc-pVTZ basearekin batera.

1.5.2.6 Ondorioak

Nukleoen koordinatuekiko bigarren ordeneko energiaren deribatuak lortu dira ONFT-ren testuinguruan. Hauek lortzeko akoplatutako ekuazio perturbatuak ebaztea beharrezkoa da. Ekuazio hauek deribatu ditugu orbital eta okupazioen erantzun lineala kalkulatzeko, horretarako erabilitako prozedura edozein hurbilketarako baliogarria delarik. Energiaren gradienteen kalkulua Hesiarrarena baino askoz efizienteagoa denez, azken hauek erabili ditugu numerikoki lortzeko Hesiarra eta bibrazio frekuentzia harmonikoak. PNOF7-k ondo konparatzen du MP2 eta CCSD metodoekin mota eta tamaina ezberdinez osatutako molekula talde anitzaren kasuan, erreferentzia moduan datu esperimentalak erabili izan direlarik.

1.6 Sistema modeloak

Korrelazio elektronikoaren modelo sinpleak ONF hurbilpenen balioztatzerako egokiak dira. Atal honetan, dimentsio bakarreko Hubbard modeloa eta hidrogeno kateak erabiliko ditugu literaturan agertzen diren ONFH garrantzitsuenak aztertzeko.

1.6.1 Hubbard modeloan ONFH-en errendimendua

1.6.1.1 Sarrera

Hubbard modeloa korrelazio elektronikoa adierazteko modelo sinpleena dugu. Izan ere, energia zinetikoaren eta elektroien alderapenaren arteko proportzioa modifikatzen du, korrelazio gogorra adierazten duten sistemak simulatzeko baliogarria delarik. Hori dela eta, Hubbard Hamiltondarra gero eta erabiliagoa da ikerkuntzan [89–93]. Nukleo-elektroi erakarpen indarra ez dagoenez, korrelazio gogorra nabarmena da Hubbard modeloan, batez besteko eremuan oinarritutako metodoak ezegokiak direlarik. Kapitulu honetan, ONFH-ak dimentsio bakarreko Hubbard modeloan aplikatuko ditugu, informazio anitza lortu daiteke eta Hubbard Hamiltondarrean aldaketa txikiak eginez. Erreferentzia moduan kalkulu zehatzak erabiliko ditugu, FCI metodoarekin lortutak.

1.6.1.2 Hubbard modeloa

Hubbard Hamiltondarra ondoko moduan idatzi daiteke

$$H = -t \sum_{\langle \mu,\upsilon \rangle,\sigma} (c^{\dagger}_{\mu,\sigma} c_{\upsilon,\sigma} + c^{\dagger}_{\upsilon,\sigma} c_{\mu,\sigma}) + U \sum_{\mu} n_{\mu,\alpha} n_{\mu,\beta} + \sum_{\mu,\sigma} n_{\mu,\sigma} v_{\mu,\sigma} \tag{56}$$

non eta μ eta υ tokiak adierazten dituzten, $\langle \mu, \upsilon \rangle$ bakarrik hurrenez hurreneko tokien arteko elektroi jauziak soilik posibleak direla esan nahi du, $t > 0$ jauziekin erlazionatutako parametroa da, $\sigma = \alpha, \beta$, $n_{\mu,\sigma} = c^{\dagger}_{\mu,\sigma} c_{\mu,\sigma}$ non $c^{\dagger}_{\mu,\sigma}\,(c_{\mu,\sigma})$ fermioi sortzaile (deuseztapen) operadoreak dira, $v_{\mu,\sigma}$ tokiko potzentziala da, eta U elektroi-elektroi alderapenarekin erlazionatutako parametroa da. Kapitulu honetan zehar Hubbard homogeneoa deritzogu $v_{\mu,\sigma} = 0;\ \forall \{\mu, \sigma\}$ izateari, aldiz, Hubbard ez-homogeneoa izanen dugu baldin eta kanpoko potentziala modeloaren tokietan ez

nulua bada. Esate baterako, Hubbard dimeroaren kasuan $v_{S_A,\sigma} = -v_{S_B,\sigma}$ zehaztuko dugu, S_A eta S_B direlarik sistemaren toki posible bakarrak, eta Δv potentziala sortzen delarik. Aipatzekoa da Aubry-André modeloa [94] ere erabiliko dugula, orduan Hamiltondarra ondoko itxura hartuko du

$$H = -t \sum_{\langle \mu,\upsilon \rangle,\sigma} (c^{\dagger}_{\mu,\sigma} c_{\upsilon,\sigma} + c^{\dagger}_{\upsilon,\sigma} c_{\mu,\sigma}) + U \sum_{\mu} n_{\mu,\alpha} n_{\mu,\beta} + \sum_{\mu,\sigma} n_{\mu,\sigma} V \cos\left(2\pi\alpha\mu + \delta\right), \tag{57}$$

non eta V parametroak zehazten duen tokian tokiko kanpoko potentziala, α-k periodizitatea, eta δ-k modulazioaren fasea.

Bai (56) bai (57) ekuazioetan erakusten den moduan, elektroien arteko alderapena guztiz lokalizatuta dago. Interesgarria da U/t ratioa modifikatzea korrelazio elektronikoaren erregimen ezberdinak aztertzeko. Adibidez, $U/t \to 0$ limitean batez besteko eremuaren teoriak (HF, DFT, ...) ondo funtzionatzen dute, $U/t >> 1$ eremuan okupazio ez osoak deskribatzea beharrezkoa den bitartean. Are gehiago, U/t balio txikietatik handietarako trantsizioa okupazioen bitartez kuantifikatu daiteke, hauek baitira korrelazio elektronikoaren indikatzaileak [92]. Kapitulu honetan U/t-ren balio zabalak aztertuko ditugu, elektroi eta modeloaren toki kopurua berdinak direlarik kasu guztietan. Energia eta okupazioak ez gero, tokien okupazio bikoitza ere aztertuko dugu, hau da,

$$\frac{dE}{dU} = \sum_{\mu} \langle \Psi | n_{\mu,\alpha} n_{\mu,\beta} | \Psi \rangle. \tag{58}$$

1.6.1.3 Emaitzak eta eztabaida

Atal honetan ONFH erabilienak kolokan jarriko ditugu Hubbard modeloa erabiliz. Horretarako, energiaren, okupazioen, eta okupazio bikoitzaren (58) azterketa egingo ditugu, betiere FCI kalkulu zehatzekin alderatuz. Azken hauek lortzeko Knowles eta Handy [95, 96] idatzitako kodea erabiliko dugu, eta DME-ak lortzeko E. Matito eta F. Feixas-en DMN programa [97] erabiliko dugu. ONFH kalkuluak DoNOF kodearekin egingo dira. Okupazio bikoitza kalkulatzeko ondoko formula erabili dugu

$$\frac{dE}{dU} \approx \frac{E(U-2h) - 8E(U-h) + 8E(U+h) - E(U+2h)}{12h} \tag{59}$$

non eta $h = 0.001$.

Spin mugatua erabiliko dugu simetria zuzena mantentzeko, hau da, $\langle S^2 \rangle = 0$ eta $\langle S_z \rangle = 0$. Gainera, sistema bakoitzari dagokion simetriari egokitutako orbital basea erabiliko dugu

kalkuluetan. Azken hau ON-en basearen berdina da 2 eta 4 tokiko sistemen kasuan, edozein ONFH eta U/t baliorako.

3. irudiak $\Delta[E/t] = E^{NOFA}/t - E^{FCI}/t$ adierazten du U/t-ren menpe, non eta NOFA eta ONFH baliokideak diren. Behetik gorako grafikak aztertuz, bakarrik MBB, PNOF5, eta PNOF7(+) dimeroa zehatz mehatz deskribatzen dute, CA eta CGA portaera asintotiko zuzenak erakusten dituztelarik $U/t \to \infty$ limitean. HF eta Power dibergenteak dira U/t-rekin, eta beste hainbat hurbilpen ez dira grafikan sartu lortutako emaitza kaxkarrengatik, besteak beste, Goedecker eta Umrigar [63], Marques eta Lathiotakis [64], eta Gritsenko, Pernal eta Baerends [65]. Interesgarria da aipatzea MBB eta Power N-adierazgarritasunaren P, Q, eta G baldintzak hausten dituztela bi elektroien kasuan [41]. Hortaz, ez da harritzekoa ez konbergenteak izatea korrelazio altuko kasuetan, hau da, $U/t >> 1$.

4 tokiko sistema korrelazio gogorra adierazten du, hidrogeno atomoen kasuan ziurtatu den moduan [98]. Errore ez nulua lortu arren, PNOF7(+) eta CGA sistema zehaztasunez gai dira edozein U/t baliorako. HF eta Power berriro ere errore handiegiak sortzen dituzte, beraz hurrengo kasuetan ez dira kontutan izango. PNOF5, MBB eta CA kualitatiboki zuzenak dira, baina ezin dira ziurtasunez erabili sistema honetan. Emaitza antzekoa da 6 tokiko sistema handiagoan. Hortaz, PNOF5 eta PNOF7(+) alderatuz, argi dago elektroi pareen arteko elkarrekintzak ezinbestekoak direla Hubbard sistema sinpleenetan. Begi bistakoa da Hubbard Hamiltondarrak molekulen oso ezberdina diren sistemak sortzen dituela, izan ere, ezaguna da molekulen kasuan elektroi pare ez korrelazionatutak erabiltzen dituzten metodoak oso eraginkorrak direla, gure emaitzei erreparatuz, berriz, PNOF5-rekin lortutako erroreak nabarmenak dira.

FCI kalkuluak posibleak izan daitezen, sistema handienak 10, 12, eta 14 tokikoak ditugu. CGA eta PNOF7(+) gai izan dira errorea mantentzeko sistema handitzean, beraz, metodo hauek sistema periodikoetan erabiltzeko aproposak dira. Kasu guztietan errore handienak U/t-ren erdiko balioetan agertzen dira korrelazio dinamikoaren eta estatikoaren arteko lehia dela eta. Korrelazio gabeko eta gogorreko limiteak, berriz, zehaztasunez deskribatzen dira aztertutako ONFH-ekin.

Okupazio doblearen azterketa hurbilpen bakoitzak eraikitako 2DME-ren kalitatea neurtzen du. Emaitza esperimentalarekiko lortutako baloreak 4. grafikan adierazi dira. HF okupazio osoetara murrizten denez, konstante baten moduan agertzen da, hau da, errorea konstante batera (0.5 edo 1 spin-a kontutan hartuz) jotzen du. PNOF7(+) ezik, metodo guztiak kurba ez jarraiak sortu dituzte, hortaz, emaitzari dagokion energia zuzena bada ere, zentsu fisikoa duen emaitza batetik urrun egotearen seinalea da hura.

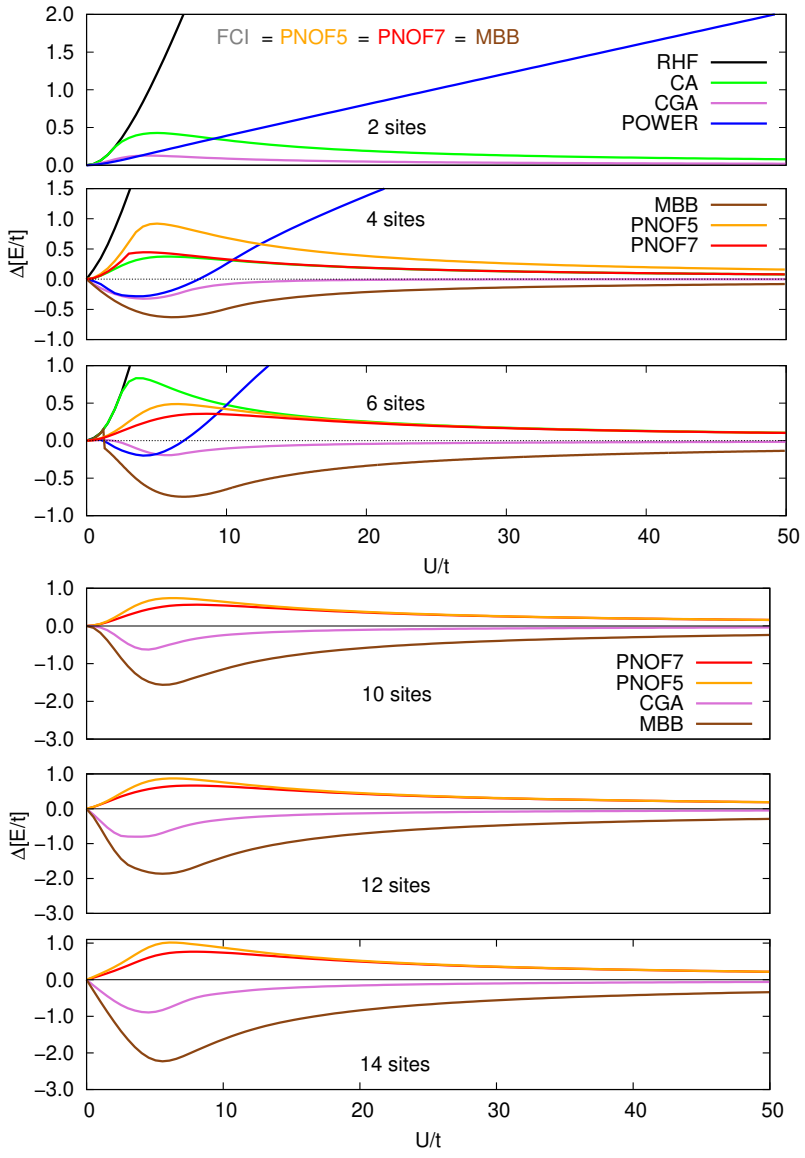

Figure 3 – FCI-rekiko diferentziak E/t balioetan dimentsio bakarreko Hubbard modeloan ONFH diferenteak erabiliz.

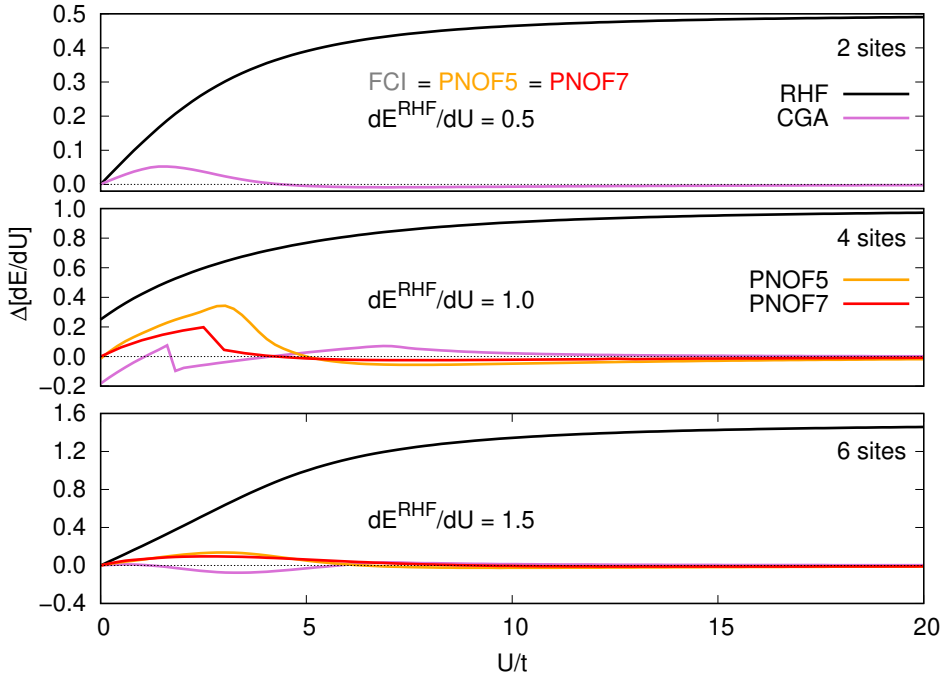

Figure 4 – FCI-rekiko lortutako dE/dU erroreak dimentsio bakarreko Hubbard modeloan ONFH diferenteak erabiliz.

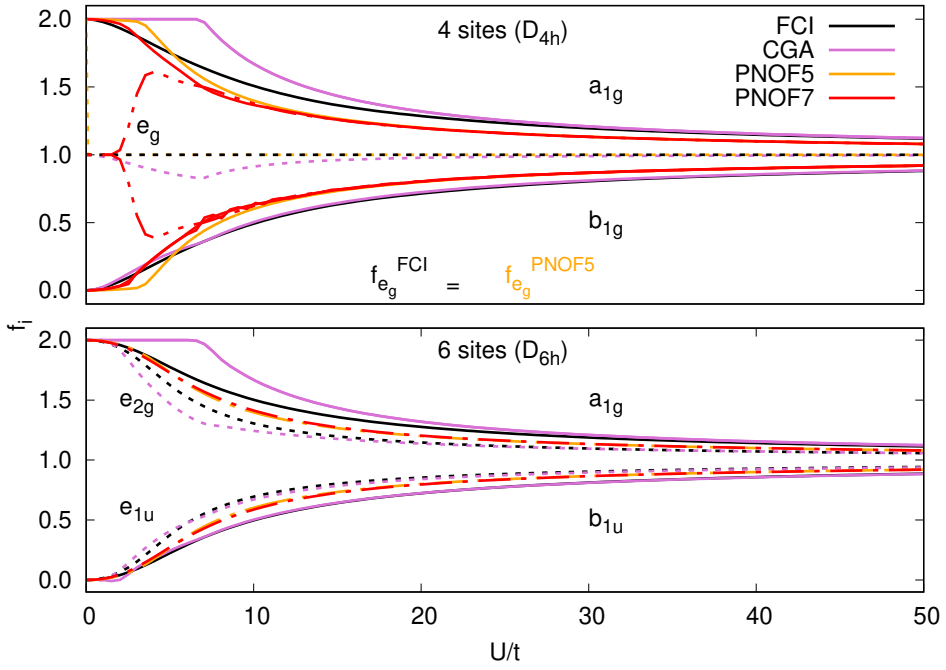

Figure 5 – ON-en okupazioak (spin-ak gehituta) 4 eta 6 tokiko Hubbard sistemetan FCI, CGA, PNOF5, eta PNOF7(+) metodoekin kalkulatutak. Lerro jarraiak erabili dira ez degeneratuta dauden okupazioentzako, puntuka eta marraka adierazitako kurbak okupazio degeneratuei dagozkie. Grafika honetan f erabili da ON-en okupazioak (n) adierazteko.

4 eta 6 tokiko sistemei dagozkien ON-en okupazioak 5. grafian marraztu dira. Lehenengoari dagokionez, CGA, MBB, eta PNOF5 nabarmenki huts egin dute, izan ere, $U/t \to 0$ limiteari dagokion minimo lokaletik ateratzeko ez dira gai U/t-k balio handiagoak hartzean. Finkatutako okupazioen fenomenoa okupazio doblearekin erlazio zuzena du, izan ere, (58). ekuazioa jarraituz ON-en okupazio zuzenak beharrezkoak dira kantitate hau ondo deskribatzeko. Egoera diferentea da 6 tokiko sistemaren kasuan, non eta PNOF5-k eta PNOF7(+)-k emandako ON-ak ez duten zerikusirik FCI-ren emaitzarekin. PNOF ON-ak degenerazioa hiru dute, ez daude beraz D_{6h} (6 tokiko sistemaren geometria hexagonoa da) simetriarekin erlazionaturik. Gertaera hau ezaguna da PNOF kasuan, eta orbitalen adierazpen ezberdin bati dagokio. Hau da, FCI-k emandako ON-ei dagozkien simetria lortu daiteke PNOF sortutakoei errotazio unitario zehatz bat aplikatzen bazaie. Xehetasunak ondoan aurkitu daitezke [99, 100].

Atal honekin bukatzeko pena merezi du Hubbard ez homogeneoa aztertzea. Batetik, kasurik sinpleena aztertuko dugu, dimero ez homogeneoa. Azken honetan $\Delta v = v_{S_B} - v_{S_A} = 2v$ potentzial diferentzia sortzen da bi tokien artean, hortaz, orbitalen optimizazioa ezinbestekoa da.

6. irudian energiak irudikatu ditugu U/t lau balio ezberdinentzako. $U = 0$ kasuan HF nahikoa da energia zuzena emateko, hau da, $E = -\sqrt{(2t)^2 + (\Delta v)^2}$. Halere, korrelazioa sartu adina, erroreak agertzen dira PNOF metodoarekin izan ezik.

Modelo hau aztertzeko ezinbestekoa da tokien arteko okupazioen diferentziari begiratzea, hau da, $|\Delta n| = |n_{S_B} - n_{S_A}|$ non eta n_{S_X}-k X tokiaren okupazioa adierazten duen. Esatekoa da bai MBB bai CGA-rekin energia onak lortu badira ere $U = 1$ kasuan, $|\Delta n|$-k erakusten du metodo hauen zehaztasun eza, 7. irudian ikusten den bezala. PNOF hurbilketak, berriz, guztiz zuzenak dira bi elektroiz osatutako edozein sistemaren kasuan.

Aubry-André modeloak potentzial oszilatzailea eragiten du Hubbard Hamiltondarrean, korrelazio elektronikoa konplexuagoa bilakatzen delarik. Erabilitako parametroak ondokoak dira: $\alpha = 1/10$, $V = 2.0$ eta $\delta = -2\pi/10$. 8. irudian agertzen den moduan, aurretik lortutako ondorioak baliogarriak dira ere kasu honetan. Hau da, MBB eta CGA errore negatiboak sortzen duten bitartean, horrek N-adierazgarritasunaren problemarekin duen erlazioa ezaguna delarik, PNOF5 eta PNOF7(+) kualitatiboki zuzena den emaitza sortzen dute. Halere, bakarrik PNOF7(+)-ren kasuan energia hurbildua zehatzaren paraleloa da, metodoaren fidagarritasuna handiagoa izanik.

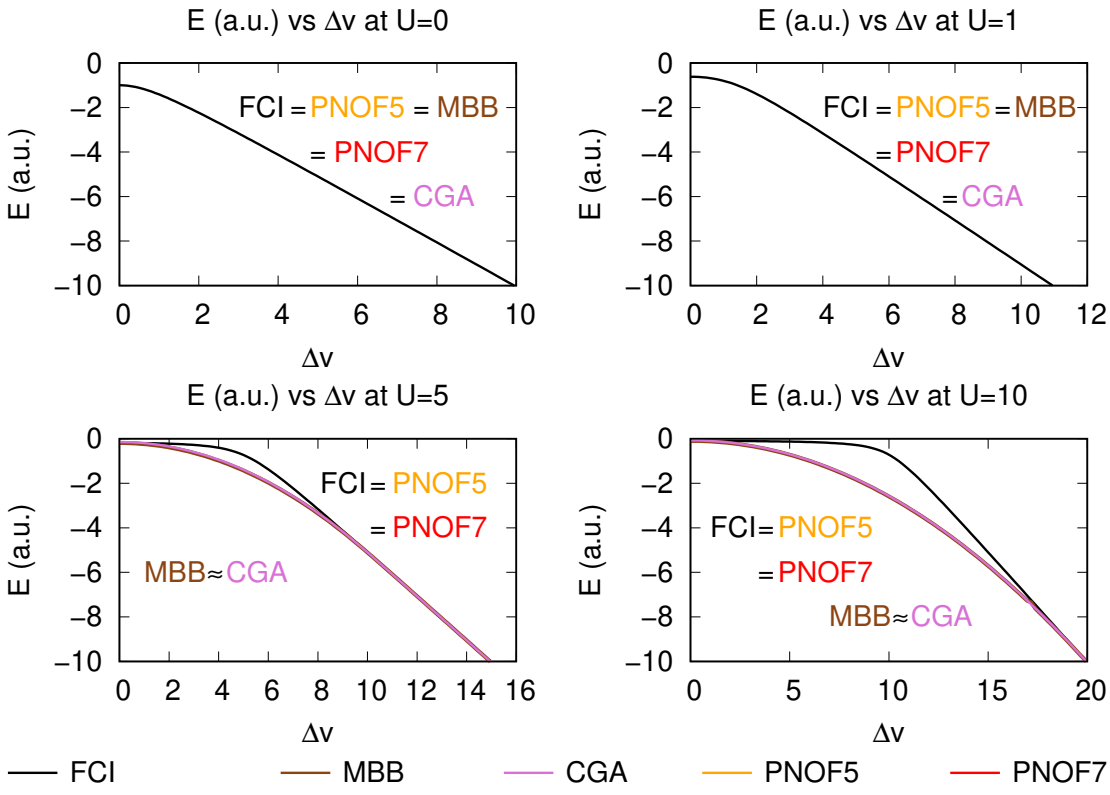

Figure 6 – Hubbard dimero ez homogenoaren energia zehatza eta hurbildua (MBB, CGA, PNOF) parametroen ondoko balioentzako: $U = 0$, 1, 5, 10 eta $t = 0.5$.

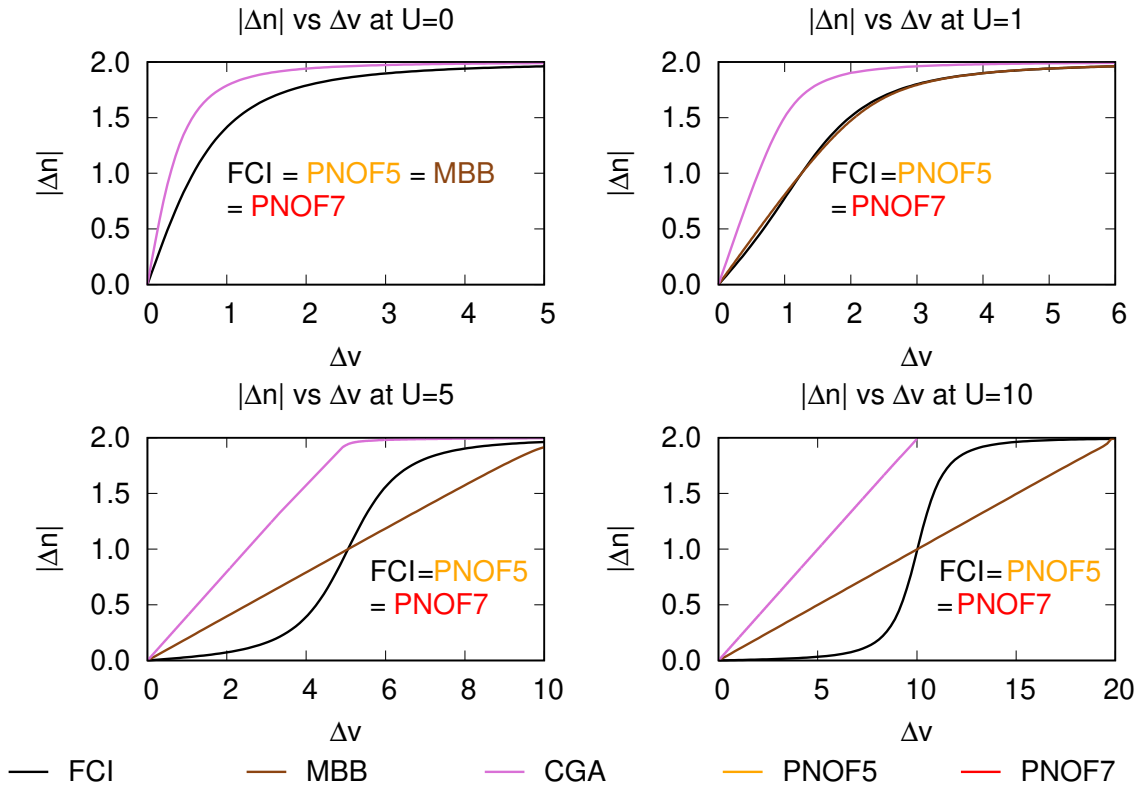

Figure 7 – Tokien okupazio diferentziak potentzial diferentziaren menpean, FCI, MBB, CGA eta PNOF erabiliz Hubbard dimero ez homogeneoan. $U = 0$, 1, 5, 10 eta $t = 0.5$.

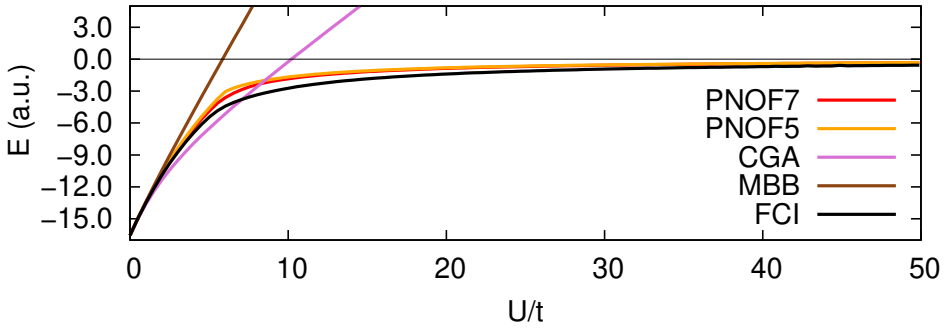

Figure 8 – Energia U/t-ren menpe 10 tokiko Hubbard modeloan Aubry-André kanpo potentzialarekin.

1.6.1.4 Ondorioak

Kapitulu honetan zehar ONFH esanguratsuenak [35–39, 44, 45, 56, 57, 63–65, 101] aztertu ditugu Hubbard modelo homogeneoaren eta ez homogeneoaren testuinguruan. 2 tokiko modelo sinplearen kasuan jada HF eta Power hurbilpenak ez konbergenteak dira U/t balio altuak deskribatzeko. Izan ere, erregimen honetan elektroien arteko alderapena gai zinetikoa baino gogorragoa da, beraz, elektroi kopuru eta sistemaren toki kopuru berdina finkatu dugunez gero, elektroi bakoitza toki batean lokalizatu egiten da. Ondorioz, Slater determinante bakarreko metodoak, eta honekin erlazionatutakoak, zailtasunez deskribatu dezakete Hubbard modeloa $U/t >> 1$ kasuan spin simetria apurtu gabe. Gure esperientzian, bakarrik MBB, CGA, PNOF5, eta PNOF7(+) kualitatiboki baliogarriak dira energia deskribatzeko edozein U/t ratioarentzako. Hala ere, ON-en okupazioak eta tokien okupazio bikoitza aztertuz gero, PNOF7(+) izan da sistema zehaztasunez deskribatzeko hurbilpen bakarra. Emaitzen balorazioa eginez gero, ondoko arrazoiak azpimarratu behar ditugu PNOF7(+)-ren emaitza ona justifikatzeko: (1) Ezinbestekoa da 2DME-ko N-adierazgarritasunaren baldintzak betetzea Hubbard Hamiltondarraren U/t balio posible guztiak deskribatzeko, eta (2) partikula-zulo simetria errespetatzeak Hubbard modeloan ezinbestekoa da. Izan ere, PNOF7(+) elektroi pareak modu zehatzean deskribatzen dituenez gero, hurbilpen bakarra pareen arteko elkarrekintzan egiten da. Elkarrekintza hura partikula-zulo simetria esplizituki duenez, emaitzaren zehaztasuna ez da korrelazio erregimenaren menpekoa.

Laburbilduz, lan honetan ziurtatu dugu ONFT-an N-adierazgarritasunaren problema ez duela bakarrik 1DME-ari eragiten, baizik eta zuzeneko erlazioa duela ere 2DME-aren N-adierazgarritasunarekin. Oinarrizko sistemak aztertu ondoren, argi geratu da ONFH erabilienen puntu ahulak eta gogorrak. Dena den, PNOF7(+)-rekin lortutako emaitza onak direla eta, Hubbard Hamiltondarra eta haratago joateko abiapuntu egokia aurkitu dugu.

1.6.2 Fasearen dilema N-adierazgarritasunaren ikuspuntutik

1DME-n oinarritutako funtzional teorian beti agertuko da fasearen dilema, hau da, elektroi-elektroi elkarrekintza deskribatzeko gaien zeinuen konbinazio kopuru askorekin lan egin behar izatea. Arazo hau hurbilpenak garatzeko *top-down* metodoan aurkitu zen [102], hau da, $E[\Gamma]$-ren bila gabiltzanean CI koefizienteen arteko konbinazio lineal kopurua handiegia da, baldintzarik ez dugularik prozesu hau arbitrarioa izan ez dadin. Espero bezala, fasearen dilema ere *bottom-up* metodoan agertzen da. Funtzionalak garatzeko *bottom-up* metodoa [30, 57] N-adierazgarritasunaren baldintzak inposatuz [20] eraikitako $D[\Gamma]$-an sortzen ditu hurbilpenak. Atal honetan zehar fasearen problema aztertuko dugu ONFT-ren testuinguruan, eta erakutsiko dugu nola fasearen hautaketa egokia hurbilpenen zehaztasunean eragin dezake.

1.6.2.1 Elektroi pareen arteko korrelazioa PNOF7-n

Lehen esan dugun bezala, PNOF7 hurbilketan (33) elektroi pareen arteko interakzioak zehazki deskribatzen dira, hortaz hurbilketa bakarra pare ezberdinen arteko elkarrekintza gaian datza, hau da, Π^{Φ}_{qp}. Hasiera batean, intra-pair kasuko faseak erabili dira PNOF7(+) sortzeko, hau da, $\Pi^{\Phi}_{qp} = \Phi_q\Phi_p$ baldin eta $q, p > \mathrm{N}/2$. Atal honetan, berriz, PNOF7(-) ere kontsideratuko dugu, non eta energiaren ikuspuntutik hobeagoa den fase guztiak negatiboak hartzea, hau da, $\Pi^{\Phi}_{qp} = -\Phi_q\Phi_p$. edozein p eta q indizeetarako. Hurrengo ataletan, fasearen egokitasuna aztertzeko korrelazio gogorra azaltzen duten sistemak erabiliko ditugu, izan ere, aurreko kapituluan jada frogatu dugu PNOF7 hurbilpenaren errendimendua Π^{Φ}_{qp}-rekin zerikusi handia duela, PNOF5-ek sortutako emaitzekin konparatu ondoren. Beraz, modelo hauek gai honen eraginkortasuna aztertzeko baliogarriak dira.

1.6.2.2 Pareen arteko korrelazio lokala

Zailtasunak urrun mantentzeko asmoz, aurreko kapituluan erabilitako Hubbard Hamiltondarra (56. ekuazioa) sinplifikatuko dugu, ondoko bi gaien menpe soilik utziko dugularik

$$H = -t \sum_{\langle r,r'\rangle,\sigma} (a^{\dagger}_{r,\sigma}a_{r',\sigma} + a^{\dagger}_{r',\sigma}a_{r,\sigma}) + U\sum_{r} n_{r,\alpha}n_{r,\beta} \tag{60}$$

non eta $\langle r, r'\rangle$ hurrenez-hurreneko tokien arteko elektroi saltoak soilik baimentzen dituen. $t > 0$

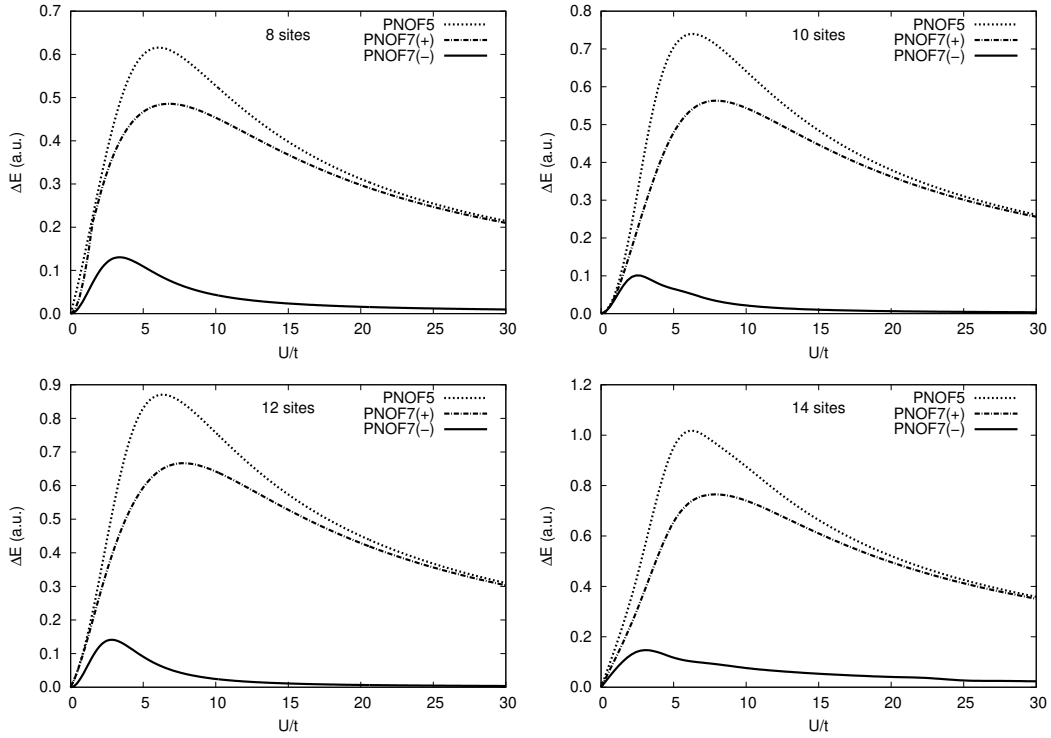

Figure 9 – Emaitza zehatzekiko energia E diferentziak U/t-ren menpe, 8, 10, 12, eta 14 tokiko dimentsio bakarreko Hubbard modeloarentzako. Elektroi kopurua toki kopuruen berdina finkatu da, baita mugako baldintza periodikoak ere.

eta U energia zinetikoaren eta elektroien arteko alderapenaren parametroak dira. $\sigma = \alpha, \beta$. $a^\dagger_{r,\sigma}$ ($a_{r,\sigma}$) sokuntza (deuseztapen) operadorea da, eta ondorioz $n_{r,\sigma} = a^\dagger_{r,\sigma} a_{r,\sigma}$ r tokian dagoen σ spin-eko elektroi kopurua bueltatzen du.

9. irudian PNOF5, PNOF7(+) eta PNOF7(-) hurbilpenekin lortutako erroreak agertzen dira, 8, 10, 12, eta 14 tokiko Hubbard sistementzat U/t-ren menpean. Emaitza zuzenak diagonalizazioaren bitartez kalkulatu dira Knowles eta Handy-ren kodea [95, 96] erabiliz, PNOF hurbilketen kasuan M. Piris eta kolaboratzaileak garatutako DoNOF programa erabili da.

9. irudiko emaitzei erreparatuz gero, argi geratzen da fasearen hautaketa eragin nabarmena duela PNOF7 hurbilketarekin lortutako emaitzetan. Izan ere, edozein U/t baliorako hurbilpenaren errorea murrizteaz aparte, errorearen magnitudea sistemaren toki kopuruarekiko duen menpekotasuna ere txikitzen du. Hortaz, elektroi pareen arteko elkarrekintzak partikula-zulo simetria erabiliz deskribatzea ezinbestekoa da, baina aldi berean Π^Φ_{qp} gaiaren faseak eragin zuzena du

Figure 10 – Bi dimentsiotako hidrogeno atomoen banaketa 2, 4, eta 16 nukleo kopuruarentzako. Kasu guztietan distantzia internuklearra $R_{H-H} = 2.0$ Å da.

korrelazio elektronikoa ondo deskribatzeko $U/t \gg 1$ den bitartean. Esatekoa da errore maximoa $0 < U/t < 10$ tartean aurkitzen bada ere, hemendik kanpo PNOF7(-)-k erakutsitako zehaztasuna errore numerikoarekin konparatu daitekeela.

1.6.2.3 Dimentsio bakarreko hidrogeno kateak

Orain arte ikusitako emaitzak kontuan hartuz, argi dago PNOF7(-) Hubbard modeloa ikasteko hurbilpen egokiena dela. Hala ere, modelo honetan korrelazioa guztiz lokala da, beraz, hurrengo pausoa da aztertzea PNOF7(-)-ren zehaztasuna mantentzen den edo ez korrelazio ez-lokala kontuan hartzen bada. Base minimoa erabiltzen bada, hidrogeno kate lineala dimentsio bakarreko Hubbard modeloaren antzekoa da, orain bai elektroien arteko urreneko elkarrekintzak kontutan hartzen direlarik, izan ere, bigarren kuantizazioan Hamiltondarra honako hau da

$$\begin{aligned} H = H_{nuc} + \sum_{\sigma} \sum_{ij} h_{ij} c^{\dagger}_{i\sigma} c_{j\sigma} \\ + \frac{1}{2} \sum_{\sigma\tau} \sum_{ijkl} < ij|kl > c^{\dagger}_{i\sigma} c^{\dagger}_{j\tau} c_{k\tau} c_{l\sigma}, \end{aligned} \tag{61}$$

non eta lehenengo gaiak nukleoen arteko alderapena deskribatzen duen, bigarren gaiak zinetika eta nukleo-elektroi indarra adierazten duen, eta azken gaiak elektroien arteko Coulomb indarrak deskribatzen dituen. Hamiltondarra (61) hidrogeno atomoekin erabilita dimentsio bakarrean korrelazio gogorra adierazten du baldin eta atomoen arteko distanzia $R_{H-H} = 2.0$ Å edo luzeagoa bada [103]. Sistema hauek 10. irudian marraztu dira 2, 4, eta 16 atomoen kasurako. Ohartu muga baldintza periodikoak simulatzeko eraztun moduko geometriak ditugula, hortaz, bi dimentsiotako fenomenoak agertu daitezke.

11. irudian PNOF7(-) eta PNOF7(+)-rekin lortutako energien erroreak marraztu dira, hidrogeno kateen tamaina 2 nukleotik 16 nukleoetara handituz. Hubbard modeloan nabarmena ez bada

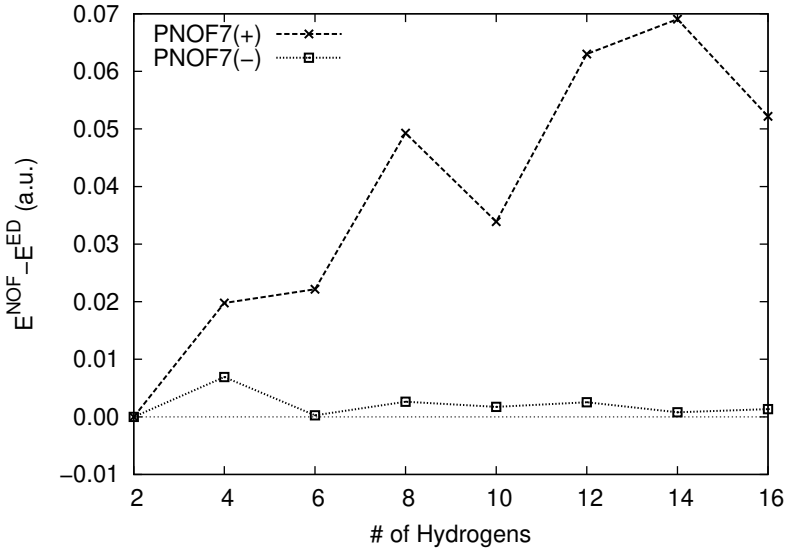

Figure 11 – Energia erroreak PNOF7(+) eta PNOF7(-)-rekin muga baldintza periodikopean eta $R_{H-H} = 2.0$ Å hartuz tamaina ezberdineko hidrogeno kateentzako. Kalkuluak base minimoarekin eginak daude.

ere, hidrogeno kateen kasuan argi dago PNOF7(+)-ren errorea sistemaren tamainarekin batera handitzen dela. PNOF7(-)-k, berriz, ez du arazo hau sufritzen, eta emaitzaren zehaztasuna mantentzeko gai da atomo kopurua handitu adina. Kuantitatiboki, 11. irudian lortutako emaitzarik kaxkarrena 0.007 hartree azpiko erroreari dagokio, ondorioz, zehaztasun handiz deskribatu da sistema.
12. irudian PNOF5 eta PNOF7(-) konparatzen ditugu, 11. irudian PNOF7(-) eta PNOF7(+)-rekin egin dugun moduan. Argi dago elektroi pareen arteko elkarrekintzak ezinbestekoak dira hidrogeno kateak deskribatzeko. Hala ere, PNOF7(+)-ren kasuan ikusi den bezala, fase egokiarekin egitekoa da ezinbestekoa da hurbilketaren zehaztasuna sistemaren tamainaren handitzearekin ez izorratzeko.

1.6.2.4 Ondorioak

Kapitulu honetan fasearen dilema aztertu dugu N-adierazgarritasunaren ikuspuntutik, ONFT-ren testuinguruan. Hurbilpenak garatzeko *bottom-up* metodoan fasearen jatorria azaldu dugu, PNOF7 adibide moduan erabiliz. Izan ere, azken honen kasuan G baldintzak pareen arteko

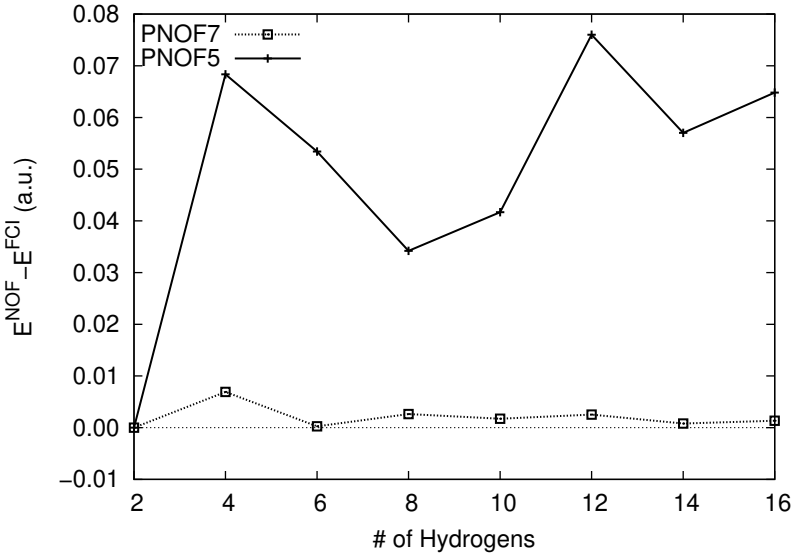

Figure 12 – Energia erroreak PNOF7(-) eta PNOF5-rekin muga baldintza periodikopean eta $R_{H-H} = 2.0$ Å hartuz tamaina ezberdineko hidrogeno kateentzako. Ohartu PNOF7 fase negatiboari dagokiol. Kalkuluak base minimoarekin eginak daude.

elkarrekintza zehazten du, baina ez honen fasea.

Hubbard modeloa eta hidrogeno kateak erabiliz, frogatu egin dugu korrelazio gogorra zuzeneko erlazioa duela pareen arteko korrelazioarekin. Gainera, fasearen hautaketa ezinbestekoa da PNOF7 erabiliz sistema hauen deskribapen zehatza egin ahal izateko. Ikerketa honi esker, PNOF7 hurbilpenaren arbitrarietatea konpontzea lortu dugu, eta sistema sinpleetan korrelazio gogorra zehaztasunez deskribatzen duen hurbilpena izatea.

1.7 Gogor korrelazionatutako elektroiak

1.7.1 Dimentsio bakarrean

Dimentsio bakarreko sistema elektronikoak problema konplexua izan daitezke egitura elektronikoaren metodoentzako. DFT ez da gai korrelazionatutako isolatzaileak deskribatzeko [91], CI ez da sistema oso handitan aplikagarria, eta CCSD(T) ez-egonkorra bilakatzen da hidrogeno atomoen arteko distantzia luzeentzako dimentsio bakarreko kateetan [1]. Dudarik gage, DMRG [104] da metodo efizienteena dimentsio bakarrean.

Uhin-funtzioan oinarritutako metodoetan, funtzio *geminal*-en arteko konbinazio linealak erabiltzen dira gastu konputazionala polinomiala izan dadin. Esaterako, variational Monte Carloren [105] edo OO-AP1roG [2] erabili izan dira dimentsio bakarreko sistema handiak deskribatzeko. ONFT [32, 33] korrelazio gogorra duten sistemak deskribatzeko alternatiba dugu. Izan ere, *geminal*-en egokitasuna sistema hauek aztertzeko ikusirik, ez da harritzekoa PNOF hurbilketak ere baliogarriak izatea. Azken finean, PNOF5-k APSG funtzioaren energiari dagokio. Ez hori bakarrik, PNOF7-k PNOF5-rekin erlazio zuzena izateaz gainera, aurreko kapituluan frogatu dugu elektroi pareen arteko elkarrekintza partika-zulo simetriaren bitartez deskribatzea bereziki egokia dela dimentsio baxuko korrelazio gogorra aztertzeko. Izan ere, gai hau aurretik erabilita izan da Bardeen, Cooper eta Schrieffer (BCS) [106] teorian elektroi pareen arteko elkarrekintza deskribatzeko, ondoren Hamiltondar ezberdinen kasuan aplikatuta izan delarik [10, 107]. Ondoko ataletan, PNOF7-ren gaitasuna korrelazio gogorreko limitea deskribatzeko aztertuko dugu.

1.7.1.1 Molekula luzeak

Lehendabizi, 50 hidrogeno atomoz osatutako katea erabiliz, lotura kimikoak apurtzeko PNOF7-k duen gaitasuna frogatuko dugu. Sistema hau dimentsio bakarreko korrelazio gogorreko eredua da, eta aurretik [1] erabili izan da korrelazio estatikoa aztertzeko. Kalkulu guztiak STO-6G [6] basearekin egin dira.

13. irudian H_{50} kate linealaren disoziazioari dagozkion energiak adierazi dira. Ikustekoa da PNOF7 eta DMRG arteko adostasuna kurba osoan zehar. Oreka egoeran PNOF7-k korre-

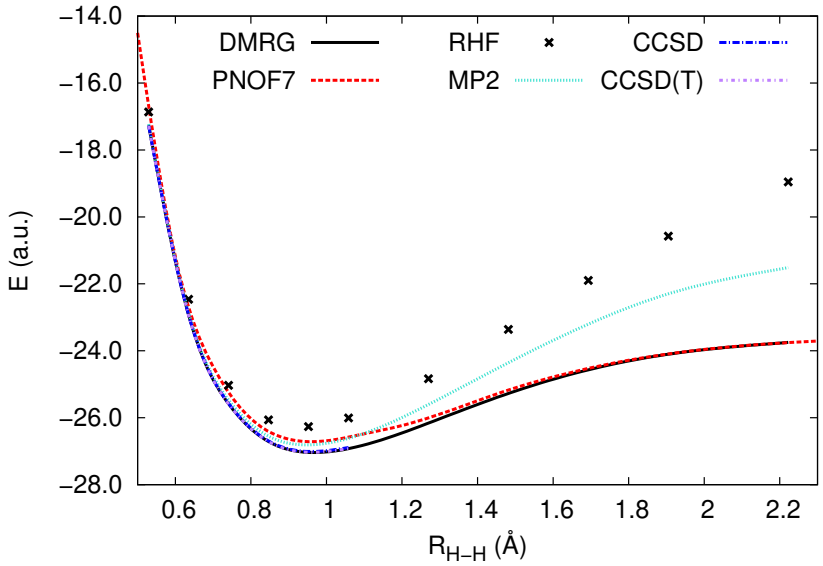

Figure 13 – H_{50} kate linealaren disoziazio simetrikoa STO-6G basearekin. RHF, MP2, CCSD, CCSD(T), eta DMRG balioak [1]-tik atera dira.

Table 6 – Oreka distantziak (R_e) eta disoziazio energiak (D_e) H_{50} kate linealaren disoziazio simetrikoan STO-6G basearekin. RHF, MP2, PBE, OO-AP1roG, eta DMRG datuak [2]-tik lortu dira.

	RHF	MP2	PBE	OO-AP1roG	PNOF7	DMRG
R_e (Å)	0.940	0.955	0.971	0.966	0.976	0.970
D_e (eV)	199.0	144.1	146.6	82.2	86.9	89.7

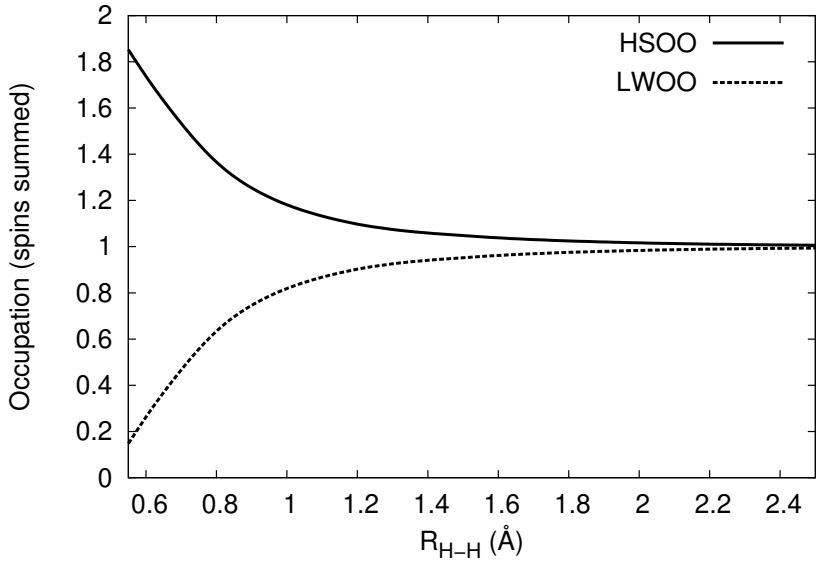

Figure 14 – Fermi mailako hurrenez hurreneko (goian (LWOO) eta behean (HSOO)) ON-en okupazioak H_{50} kate linealaren disoziazio simetrikoan PNOF7/STO-6G teoria mailan.

lazio guztia berreskuratzeko gai ez bada ere, balio espektroskopikoak (ikusi 6. taula) bat datoz DMRG-rekin, beste metodo batzuk baino zehatzago, i.e. RHF, MP2, edo Perdew-Burke-Ernzerhof (PBE). Beste hurbilketen artean, disoziazio limitearen deskribapena bakarrik OO-AP1roG metodoa erabiliz (ikusi 4. irudia [2] erreferentzian) lortu egin da. Izan ere, ezinbestekoa da okupazio ez osoekin lan egitea (ikusi 14. grafika) prozesu hau deskribatzeko, hori dela eta, CCSD eta CCSD(T) ez konbergenteak dira oreka ingurunetik urrun [1].
15. irudian H_{50}-aren disoziazio asimetrikoari dagozkion energiak azaltzen dira. Hurrenez hurreneko hidrogeno loturei dagozkionez, bata finkatuta egonen da bestea handitzen den bitartean. Orduan, disoziazio asimetrikoaren amaieran hidrogeno molekula independenteak lortuko ditugu. Ikustekoa da kasu honetan korrelazio gogorra guztiz dinamikoa dela, halere, PNOF7 eta DMRG paraleloak dira, eta distantzia txikietan PNOF7-ren emaitza hain zehatza ez bada ere, kurba osoa kualitatiboki zuzena da.

1.7.1.2 Dimentsio bakarreko Hubbard modeloa

Aurreko ataletan azaldu den moduan, base minimoa erabiltzen bada hidrogeno kateetan Hubbard modeloaren antzeko sistema dugu. Hubbard modeloa metodoak aztertzeko bereziki apro-

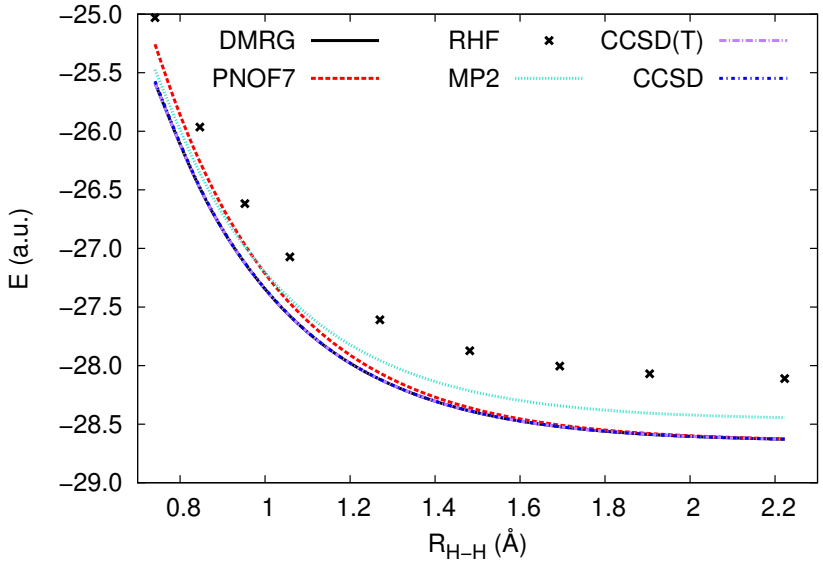

Figure 15 – H_{50} kate linealaren disoziazio asimetrikoa STO-6G basearekin. RHF, MP2, CCSD, CCSD(T), eta DMRG balioak [1]-tik lortu dira.

posa da [108], hortaz, ondoren (60). ekuazioan definitutako Hamiltondarra erabiliko dugu korrelazio gogorra aztertzeko dimentsio bakarrean Hubbard modeloaren testuinguruan.

16. grafikan PNOF7 eta OO-AP1roG-ren [3] energia erroreak marraztu dira dimentsio bakarreko Hubbard modeloan toki kopurua 14-tik 122-raino handituz, korrelazio ahula eta gogorra aztertuz. Aipatzekoa da OO-AP1roG-k sistema handien kasuan errore nabarmenak sortzen dituela, PNOF7-k, berriz, ez da sistemaren tamainaren menpekoa eta korrelazio gogorreko limitea zehaztasunez deskribatzen du.

PNOF7 ezplizituki erabiltzen du partikula-zulo simetria, beraz, ez da harritzekoa erdi-beteta dagoen (partikula eta toki kopurua berdina duen) Hubbard modeloa ondo deskribatzea. Erdi-betetzearen urrun simetria hau apurtu egiten da, eta fase ez-homogeneoak agertu daitezke [108]. 8. taulan korrelazio gogorreko limitea aztertzen dugu, hura baita zailtasuna *geminal*-ekin erlazionatutako metodoekin, OO-AP1roG kasu. Erreferentzia moduan v2RDM N-adierazgarritasunaren P, Q, eta G baldintzekin erabili dugu, vMPS balioekin batera [7].

8. taulan erakusten da PNOF7 v2RDM baino zehatzagoa dela, izan ere, [109, 110] erreferentzietan argitu da hiru-partikuletako baldintzak aplikatzea beharrezkoa dela korrelazio gogorraren limitea deskribatzeko Hubbard modeloan. Dena den, PNOF7 bereziki ona da elektroi kopuru batetik aurrera, zeren eta elektroi pare ezberdinen arteko elkarrekintzak eta pareetan gertatuko

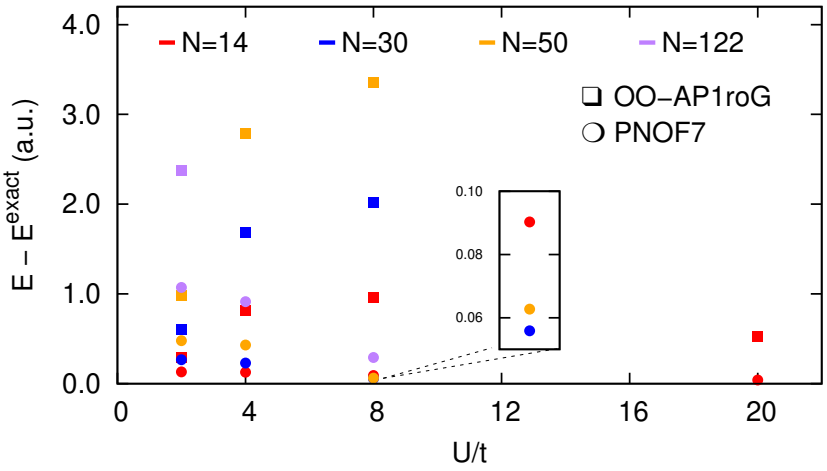

Figure 16 – Energiak (a.u.) dimentsio bakarreko Hubbard modeloan erdi-betetzean eta muga baldintza periodikoak erabiliz. OO-AP1roG eta emaitza zehatzak [2,3]-tik lortu dira. U/t = 20 kasurako N = 14 soilik aztertu da.

Table 7 – Energiak (a.u.) dimentsio bakarreko Hubbard modeloan erdi-betetzean eta muga baldintza periodikoak erabiliz. OO-AP1roG, RHF, eta emaitza zehatzak [2,3]-tik lortu dira.

N_{sites}	U/t	RHF	OO-AP1roG	PNOF7	EXACT
14	2	-10.9758	-11.6627	-11.8230	-11.9543
	4	-3.9758	-7.2701	-7.9610	-8.0883
	8	10.0242	-3.6471	-4.5228	-4.6131
	20	52.0242	-1.4132	-1.8932	-1.9340
30	2	-23.2671	-24.7779	-25.1161	-25.3835
	4	-8.2671	-15.5495	-17.0035	-17.2335
	8	21.7329	-7.8152	-9.78283	-9.8387
50	2	-38.7039	-41.2570	-41.7650	-42.2443
	4	-13.7039	-25.9154	-28.2696	-28.6993
	8	36.2961	-13.0253	-16.3215	-16.3842
122	2	-94.3524	-100.6497	-101.9499	-103.0211
	4	-33.3524	-63.2336	-69.0861	-70.0003
	8	88.6476	-31.7817	-39.6698	-39.9619

Table 8 – Tokiko energia (a.u.) dimentsio bakarreko Hubbard modeloan erdi-betetzearen urrun $U/t \to 100$ limitean. vMPS, v2RDM, eta emaitza zehatzak [7]-tik atera dira. N_{sites} eta N toki eta elektroi kopurua adierazten dituzte, hurrenez hurren.

N_{sites}	N	PNOF7	vMPS	v2RDM	Zehatza*
20	12	-0.6025	-1.0312	-1.2177	-1.0008
	16	-0.3820	-0.4951	-0.7860	-0.4639
50	20	-0.9081	-	-1.2191	-1.0008
	40	-0.4444	-	-0.7862	-0.4671

*$U/t \to \infty$-ri dagozkion emaitza zehatzak.

elkarrekintzak orekatu egiten dira.

1.7.1.3 Ondorioak

Atal honetan frogatu dugu PNOF7-ren aplikazioa dimentsio bakarreko korrelazio gogorra duten sistemetan. HF bezalako kostuarekin, PNOF7 gai da hidrogeno kate linealak aztertzeko [111], baita Hubbard modeloa edozein fasetan ere. Beraz, dagoeneko PNOF7 dimentsio baxuko sistemak aztertzeko eguneko metodoen artean sartu daiteke, besteak beste, DMRG edo quantum Monte Carlo-rekin batera.

1.7.2 Bi dimentsiotan

1.7.2.1 Sarrera

Bi dimentsiotan, Hubbard modeloa materialak simulatzeko erabiltzen da, esanak esan, grafenoa [112] edo tenperatura kritiko altuko superkonduktoreak [113]. Metodo numerikoak erabili beharra dago emaitza analitikoen faltan, eta soluzio orokorra oraindik ez badugu ere, baldintza zehatza batzuetan oso eraginkorrak diren metodoak ditugu. Zehatz mehatz, auxiliary-field quantum Monte Carlo (AFQMC) [10] tokien erdi-betzea badugu, density matrix embedding theory (DMET) [114] elkarrekintza gabeko eta limite atomikoetan, edo DMRG [115] baldin eta errenormalizatutako egoera kopuru nahikoa kontsideratzen badugu [5].
Kimika kuantikoan egunero erabiltzen diren metodoak bi dimentsiotako Hubbard modeloaren testuinguruan aztertu dira [108]-n egindako ikerketa zabalean, aldiz, azken urteetan garrantzitsuak bilakatzen ari diren DME-etan oinarritutako metodoak ez dira kontuan izan. Aurreko ataletan erakutsi dugu PNOF hurbilpenak gai direla dimentsio bakarreko korrelazio gogorra eta orokorrean Hubbard modeloa deskribatzeko batez besteko eremuko metodoen kostu konputazionala mantenduz. Atal honetan zehar, PNOF hurbilpenen aplikazioa bi dimentsiotako korrelazio gogorreko sistemetan aztertuko dugu. Horretarako, bai Hubbard modeloa bai hidrogeno atomoz osatutako sareak erabili ditugu, egun erabiltzen diren metodo zehatzekin alderatuz, hau da, DMRG, v2RDM, AFQMC eta diagonalizazio zehatza (ED).

1.7.2.2 Bi dimentsiotako Hubbard modeloa

Bi dimentsiotako Hubbard modeloa izanen dugu baldin eta (60). ekuazioan $\mathbf{r}$ bektoreek bi osagai badituzte. Ondoren, PNOF7 konparatzen dugu [108, 113] erreferentzietan erabilitako metodo ezagunekin. Horrez gain, DME-etan oinarritutako metodo guztiak aztertzeko, v2RDM-ri dagozkion emaitza ere azalduko ditugu, bai bi-partikulako (PQG) bai hiru-partikulako baldintzak (PQGT') kontutan hartuz.
17. grafikan 4x4 sistemaren kasurako energia erroreak azaltzen ditugu, PNOF7, PQG, eta PQGT' erabiliz. Kasu honetan, PNOF7 eta PQGT' bat datoz emaitza zehatzekin. Dena den, azpimarratzekoa da PQGT'-k $\mathcal{O}\left(M^9\right)$ gastu konputazionala duela, M partikula bakarreko espazioaren dimentsioa delarik. 17. irudian ikusi daiteke PQG erabiltzen bada, gastua $\mathcal{O}\left(M^6\right)$-

ra murriztu arren, jasotako emaitza ez dela fidagarria U/t balio altuentzako.

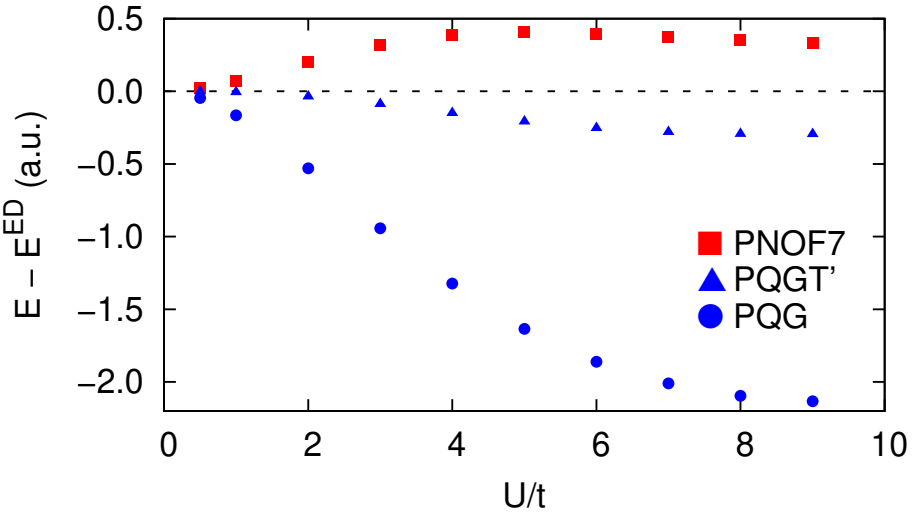

Figure 17 – PNOF7, PQG, eta PQGT' erabiliz kalkulatutako energia diferentziak kalkulu zehatzekiko erdi-betetako 4x4 Hubbard modeloan. PQG, PQGT', eta emaitza zehatzak [4]-tik lortu dira.

Partikula eta toki kopurua berdinak badira (hau da, erdi-betetzea), AFQMC numerikoki zehatza da [10], hortaz, sistema handien kasurako erreferentzia moduan erabili daiteke. 9. taulan 8x8, 10x10, eta 12x12 Hubbard sistema karratuentzako energiak azaltzen dira erdi-betetzean. Dimentsio bakarrean jasotako emaitza onak mantendu egin dira bi dimentsiotan: (1) Batetik, energien arteko adostasuna U/t balio guztientzako lortu da, eta (2) bestetik, PNOF7 gai da bi dimentsiotako sarearen tamaina handitzean errorea mantentzeko, magnitude honen independentea delarik. Kuantitatiboki, 9. taulan PNOF7-k energia totalaren %98-a berreskuratzen du $U/t = 2$ bada, aldiz, %96-a berreskuratzen du $U/t = 8$ bada.
4x4 Hubbard modeloari dagozkion emaitzak marraztu dira 18. grafikan. PNOF7-ren kasuan partikula-zulo simetria apurtzeak energiaren errorean nabarmenki azaltzen ez den bitartean, PQGT'-ren kasuan errorea gero eta handiagoa da U/t-ren handitzearekin batera.
Antzeko emaitza lortu dugu 6x6 sarearen kasuan, 19. irudian azaltzen den bezala. Erdi-betetzean (N=30 elektroi) PQGT'-k eta PNOF7-k DMRG-rekin bat datozen arren, elektroi kopurua murriztu ahala PQGT'-k sortutako kurbak DMRG-tik aldentzen dira, batez ere korrelazio gogorreko erregimenean. Beraz, PQGT'-k partikula-zulo simetria apurtutako sistemak

Table 9 – PNOF7 eta energi zehatzak 8x8, 10x10, eta 12x12 tokiko bi dimentsiotako Hubbard modeloan erdi-betetzean, U/t-ren menpe.

U/t	8x8		10x10		12x12	
	Zehatza	PNOF7	Exact	PNOF7	Exact	PNOF7
2	-74.47	-73.37	-116.91	-115.19	-168.75	-166.17
4	-55.05	-53.27	-86.12	-83.32	-123.95	-120.20
6	-42.16	-40.53	-64.80	-63.39	-94.66	-91.24
8	-33.68	-32.26	-52.54	-50.48	-75.54	-72.53

deskribatzeko gai ez den bitartean, PNOF7-k ez du erakusten arazo hura, korrelazio gogorraren limitea deskribatzeko gai delarik.

Izan ere, v2RDM kasuan problema ebazteko *semidefinite programming* erabili beharra dago, eta honako hau ez-egonkorra bilakatu daiteke egoera guztiak degeneratuta agertzen badira [4]. Bereziki konplexua izan daiteke problema hau bi dimentsiotan, izan ere, ez da horrelakorik gertatzen dimentsio bakarrean, non PQGT' erabilgarria den edozein elektroi eta toki kopuruarentzako [109, 110, 116]. Konbergentzia erroreak agertu dira beste metodo batzuk erabiliz aurretiko ikerketetan [108].

Bukatzeko, pena merezi du tokien okupazio bikoitzari begiratzea, izan ere, aurreko kapituluan erakutsi den bezala, 2DME-aren inguruko informazioa ematen du, zehazki

$$\frac{dE}{dU} = \sum_{\boldsymbol{r}} \langle \hat{n}_{\boldsymbol{r},\alpha} \hat{n}_{\boldsymbol{r},\beta} \rangle \tag{62}$$

(62). ekuazioarekin batera, dE/dU-k sortzen du tokien okupazio bikoitza. ONFH-en artean dE/dU kurba ez jarraiak jaso ditugu [99], hortaz, garrantzitsua izanen da kurben jarraitasuna eta limiteak aztertzea bi dimentsiotako eta dentsitate ezberdinen kasurako. Numerikoki ondoko moduan kalkulatuko dugu dE/dU

$$\frac{dE}{dU} \approx \frac{E(U-2h) - 8E(U-h) + 8E(U+h) - E(U+2h)}{12h} \tag{63}$$

non $h = 10^{-3}$.

20. grafikan tokien okupazio bikoitza azaltzen da U/t-ren menpean, 6x6 Hubbard modeloarentzako 30 eta 36 elektroirekin. Espero bezala, dE/dU maximoa da korrelazio gabeko limitean, txikitu egiten delarik elektroien arteko alderapen indarra handitu ahala. PNOF7-rekin lortutako kurbak jarraiak dira, eta forma zuzena erakusten dute elektroien kopurua modifikatu

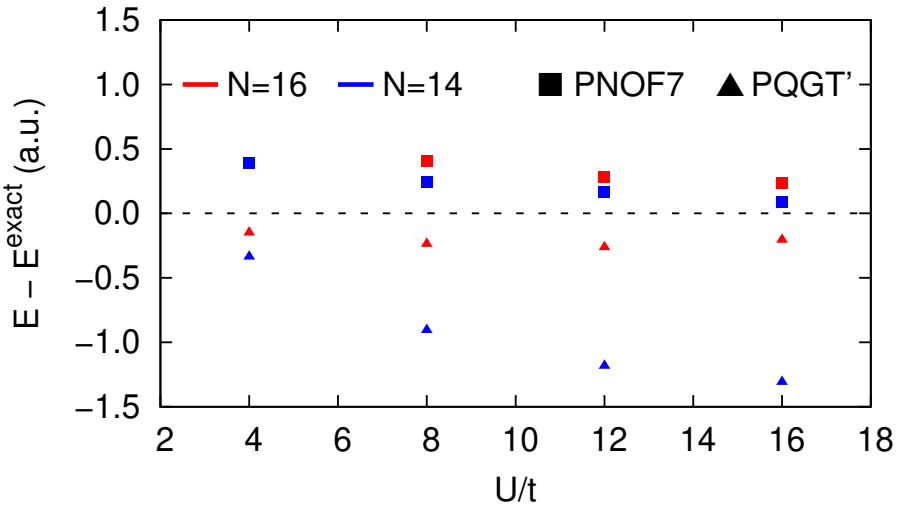

Figure 18 – PNOF7 eta PQGT' energien erroreak 4x4 Hubbard modeloan 14 eta 16 elektroiekin. PQGT' eta emaitza zehatzak [5]-tik atera dira.

arren. Ohartu korrelazio gogorreko limitean bi kurbak balio berdina hartzen dutela, izan ere, elektroien arteko alderapena handia dela eta, ezinezkoa izanen da bi elektroi toki berean aurkitzea.

1.7.2.3 Bi dimentsiotako hidrogeno sarea

Aurreko kapituluetan zehar erakutsi dugun moduan, garrantzitsua da hidrogeno atomoz osatutako sistemak aztertzea Hubbard modeloarekin lortutako ondorioak ziurtatzeko. Izan ere, bi dimentsiotan korrelazio elektroniko ez-lokalak efektu garratzitsuak izan ditzazke sareen disoziazio prozesuan.

21. irudian 4x4 hidrogeno sarearen disoziazion zehar lortutako energiak erakusten dira, PNOF7, CCSD(T), MP2, eta DMRG erabilita STO-6G basearekin [6]. Loturen bariazioa simetrikoa egin da bi dimentsioetan. CCSD(T) eta MP2 kalkuluak PSI4 [117] programarekin egin dira, DMRG kalkuluen kasuan CHEMPS2 [118] erabili delarik.

Espero bezala, MP2 eta CCSD(T) kalkuluak ez-konbergenteak dira lotura luzera handitan. Adibidez, CCSD(T)k energia dibergenteak sortzen ditu $R_{H-H} > 1.5$ Å loturetan, are gehiago, konbergentea ez da baldin eta $R_{H-H} > 1.9$ Å. Errore hau dagoeneko ezaguna zen dimentsio bakarrean [1], hemen bi dimentsiotako hidrogeno kateen kasurako frogatu dugularik. Aldiz,

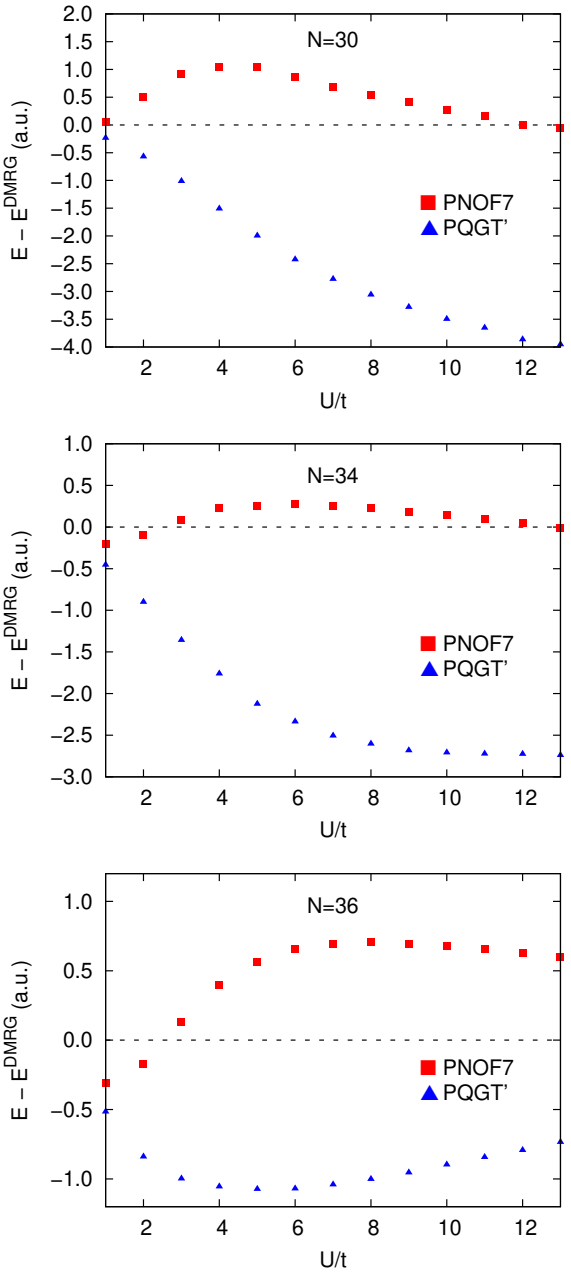

Figure 19 – PNOF7 eta PQGT' energia diferentziak DMRG-rekiko 6x6 Hubbard modeloan 30, 34, eta 36 elektroiekin. DMRG-ri eta PQGT'-ri dagozkien balioak [5]-tik lortu dira.

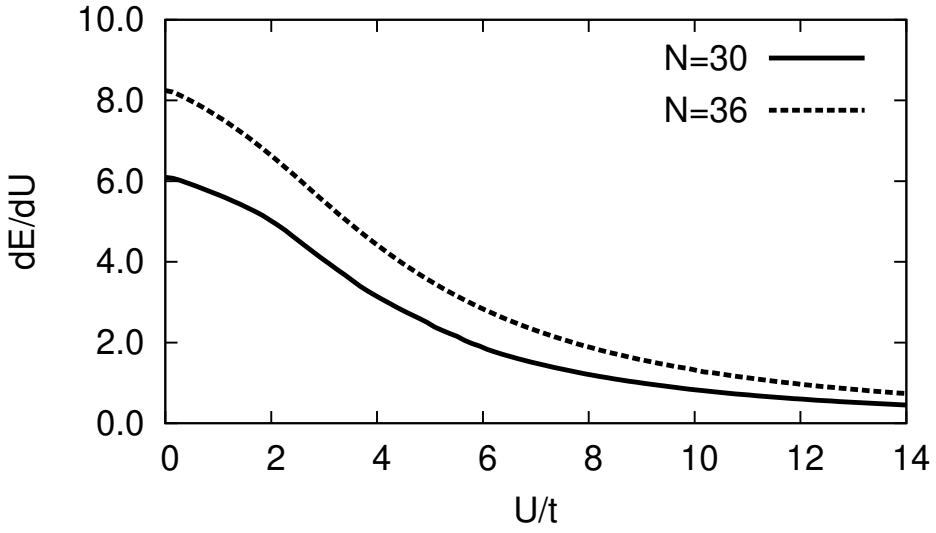

Figure 20 – Tokien okupazio bikoitza U/t-ren menpe 6x6 Hubbard modeloarentzat 30 eta 36 elektroiekin.

PNOF7 disoziazio prozesua bere osotasunean deskribatzeko gai da. Bereziki, azpimarratzekoa da DMRG eta PNOF7 arteko adostasuna baldin eta $R_{H-H} \geq 1.5$ Å. Oreka distantziaren inguruan PNOF7 MP2-rekin konparagarria da, beraz DMRG energien gainetik gelditzen da. Esatekoa da PNOF7-ren konbergentzia numerikoa antzekoa dela edozein lotura distantziarako.

1.7.2.4 Ondorioak

Atal honetan frogatu dugu PNOF7 metodo egokia dela korrelazio gogorra bi dimentsiotan deskribatzeko. PNOF7-ren energiak erreferentziazko AFQMC eta DMRG balioekin bat datoz bi dimentsioetako Hubbard modeloan, sistema txikietatik handietara, korrelazio ahuletatik gogorretara, eta tokien betetze baxuetatik handietara. Orokorrean, emaitzen zehaztasuna eta kalkuluetarako beharrezko denbora eta teknikak kontutan izanik, PNOF7 metodo efizientea da korrelazionatutako elektroiak bi dimentsiotan aztertzeko.

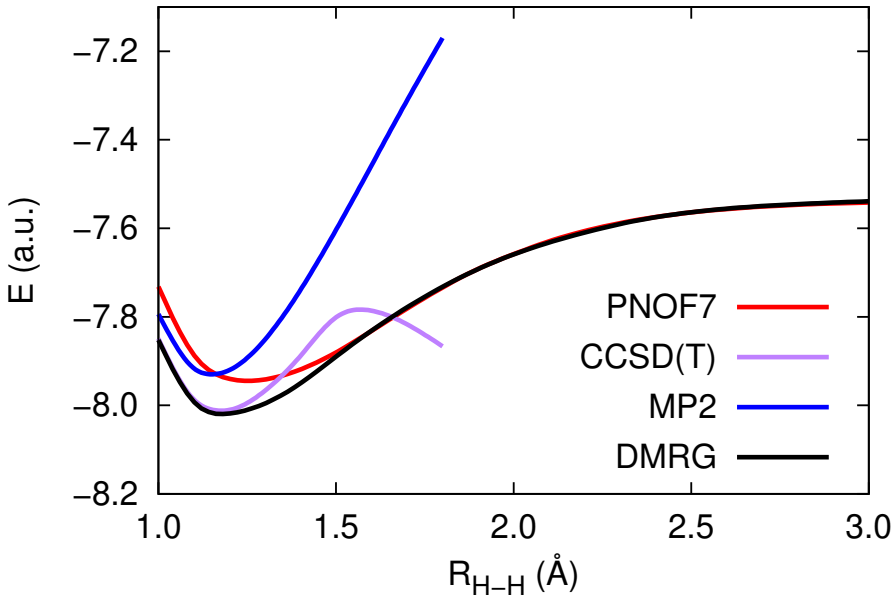

Figure 21 – Energia totalak (a.u.) 4x4 hidrogeno sarearen disoziazioan, PNOF7, CCSD(T), MP2, eta DMRG metodoak erabiliz STO-6G basearekin [6].

1.8 ONFT-rekin kalkulatuako momentu elektrikoak

1.8.1 Sarrera

Interakzio elektrostatikoa ezinbestekoa da molekulen arteko indarrak ulertzeko [67, 68]. Momentu elektrikoak molekula konplexuen eremu elektrikoaren inguruko informazioa ematen digute, beste hainbat propietateen artean (simetria...). Kalkulu teorikoak beharrezkoak dira hemen, izan ere, esperimentalki prozedura zailegiak eta ez guztiz ziurrak erabiltzea beharrezkoa da orden altuko momentuak neurtzeko, kuadrupoloa edo oktupoloa kasu [67, 119, 120]. Hortaz, teoria teknika esperimentalen osagarri bezala agertzen da.

Kapitulu honetan, PNOF6 erabiltzen dugu hainbat molekulen momentu elektrikoak kalkulatzeko. Izan ere, orekako geometrientzat lortutako emaitzak kontuan izanik, bai PNOF7 bai PNOF5 erabiliz kalkulatuko genituzkeen momentu elektrostatikoak ez litzateke izango PNOF6-

rekin lortutakoak baino hobeagoak. Aztertutako sistemak singleteak dira denak, zehazki, dipoloa eta kuadrupoloa lortuko dira ondoko sistementzako: H_2, HF, BH, HCl, H_2O, H_2CO, C_2H_2, C_2H_4, C_2H_6, C_6H_6, CH_3CCH, CH_3F, HCCF, ClF, CO, CO_2, O_3, N_2, NH_3, eta PH_3. Bestalde, CH_4 sistemaren oktupoloa ikasiko dugu, azken honek dipolo eta kuadrupolo nuluak ditu eta. Sadlej-ek [121, 122] garatutako Gaussian motatako base set-a erabiliko dugu, propietate elektrikoen kalkulurako egokiak baitira. PNOF6, CCSD, eta MRSD-CI balio esperimentalekiko aurkeztutako balioak aztertuko ditugu gure metodoaren zehaztasuna kuantifikatzeko.

1.8.2 Dipoloa, Kuadrupoloa, eta Oktupoloa

Karga elektrikoaren antolamendua momentu elektrikoen bitartez adierazi daiteke. Modu honetan, orden baxuko momentuak nahikoak izaten dira kargaren banaketa bereizteko. Dipoloa, kuadrupoloa, eta oktupoloa ditugu orden baxueneko momentu elektrostatikoak, eta ondorioz, garrantzitsuenak. Buckingham-ek [67, 68] garatutako definizioak erabiliko ditugu:

$$\mu_\alpha = -\frac{1}{2}\int \rho(\mathbf{r}) r_\alpha dV + \sum_{i=1}^{NUC} Z_i R_{i\alpha} \tag{64}$$

$$\Theta_{\alpha\beta} = -\frac{1}{2}\int \rho(\mathbf{r})(3r_\alpha r_\beta - \delta_{\alpha\beta} r^2) dV + \frac{1}{2}\sum_{i=1}^{NUC} Z_i (3R_{i\alpha}R_{i\beta} - \delta_{\alpha\beta}R_i^2) \tag{65}$$

$$\begin{aligned}\Omega_{\alpha\beta\gamma} = &-\frac{5}{2}\int \rho(\mathbf{r})\, r_\alpha r_\beta r_\gamma dV + \frac{1}{2}\int \rho(\mathbf{r}) r^2 \left(r_\alpha \delta_{\beta\gamma} + r_\beta \delta_{\alpha\gamma} + r_\gamma \delta_{\alpha\beta}\right) dV \\ &+\frac{5}{2}\sum_{i=1}^{NUC} Z_i\, R_{i\alpha} R_{i\beta} R_{i\gamma} - \frac{1}{2}\sum_{i=1}^{NUC} Z_i R_i^2 \left(R_{i\alpha}\delta_{\beta\gamma} + R_{i\beta}\delta_{\alpha\gamma} + R_{i\gamma}\delta_{\alpha\beta}\right)\end{aligned} \tag{66}$$

non eta azpiindize Grekoak ardatz kartesiarrak adierazten dituzte, hau da, x, y eta z. Nukleotako karga positiboa elektronikoaren aparte kontsideratzen da, izan ere, azken hau puntu zehatz batetara sinplifikatzen dugu, kargaren banaketa espaziala ez delarik kontuan hartzen. Ohartu (64)-(66). ekuazioetan tentsore simetrikoak definitzen direla.

1.8.3 Emaitzak eta eztabaida

Ondoan PNOF6(N_c), CCSD, HF, eta MRSD-CI metodoak erabiliz lortutako emaitzak eztabaidatuko ditugu, datu esperimentalekin batera. Kalkuluak egiteko geometria esperimentalak

Table 10 – H_2-ren kuadrupoloaren Θ_{zz} konponentea, kalkulatuta PNOF6(N_c) eta CCSD-rekin Sadlej-pVTZ basea erabiliz geometria esperimentalekin [8]. Datu esperimentalak gehitu dira [9].

PNOF6(1)	PNOF6(3)	PNOF6(5)	PNOF6(17)	CCSD	ESP.
0.3697	0.4030	0.3965	0.3935	0.3935	0.39 ± 0.01

[8, 123–125] eta DoNOF eta GAMESS [126, 127] programak erabili ditugu. Momentu elektrikoak masa zentroarekiko adierazita daude, unitate atomikoen menpe.

N_c-k zehazten du zenbat orbital akoplatzen dira Fermi mailaren azpiko orbital bakoitzarekin. Taula 10 erakusten duen bezala, intra-pair kasuan N_c maximoak ematen du emaitzarik zehatzena, hortaz, ondoko kalkuluetan Sadlej baseak lagatutako N_c balio maximoa erabiliko dugu PNOF6 kalkuluetan.

11. taulak erakusten du momentu dipolarraren μ_z konponentea HF, PNOF6(N_c), eta CCSD erabilita. Bataz besteko errore absolutuen (BEA) balioei begiratuz gero, argi geratzen da bai PNOF6(N_c) bai CCSD bat egiten dutela datu esperimentalekin, HF-ren errorea handiegia den bitartean. Ondorioz, korrelazio elektronikoa ezinbestekoa da momentu dipolarra zehaztasunez deskribatzeko.

12. eta 13. taulak erakusten dituzte momentu kuadrupolarrak HF, CCSD, MRSD-CI eta PNOF6(N_c) metodoekin kalkulatutak, datu esperimentalekin batera [9, 119, 123, 124, 128–131, 134–136]. Orokorrean, PNOF6(N_c)-rekin lortutako momentu kuadrupolarrak bat datoz datu esperimentalekin, eta diferentziak CCSD eta MRSD-CI metodoekin lortutakoen antzekoak dira. Are gehiago, balio esperimentalen errorea kontuan hartuz, PNOF6(N_c) datu esperimentalak erreproduzitzeko gai da H_2, HCl, CO, N_2, PH_3, ClF, CH_3F, C_2H_6, eta C_6H_6 molekulen kasuan. Azpimarratzekoa da Bentzenoaren adibidea, azken honetan momentu kuadrupolarrak molekulen arteko π motako indarrak deskribatzeko ezinbestekoa baita. 32. taulari dagokionez, PNOF6(N_c)-k MRSD-CI baino hobeto funtzionatzen du, eta korrelazio estatiko nabarmena duten molekulen kuadrupoloa ondo deskribatzen da, ozonoa kasu [129, 138].

Metanoaren kasuan oktupoloa garapen elektrostatikoaren lehenengo gai ez nulua da, hortaz, garrantzitsuena [125, 139, 140] ere bai. PNOF6(14) emandako balorea errorea erakusten du balio esperimentalarekin alderatuz, $\Omega_{xyz} = 2.1142 a.u.$, hala ere, CCSD-ren balioarekin ($\Omega_{xyz} = 2.1255\, a.u.$) ondo konparatzen du. Balio esperimentalaren fidagarritasuna ziurra ez denez gero [120], metanoaren oktupoloa ondo deskribatu dugula esan daiteke.

Table 11 – Momentu dipolar molekularraren μ_z osagaia unitate atomikoetan (ea_0) Sadlej-pVTZ basea eta geometria esperimentalak erabiliz [8].

Molekula	HF	PNOF6	(N_c)	CCSD	ESP.
HF	0.7565	0.7223	7	0.6994	0.7089 [123]
BH*	0.6854	0.5395	38	0.5551	0.4997 [123]
H_2O	0.7808	0.7458	9	0.7225	0.7268 [123]
H_2CO	1.1134	0.9872	10	0.9084	0.9175 [123]
HCl	0.4746	0.4598	8	0.4416	0.4301 [123]
HCCF	0.3535	0.3189	9	0.2733	0.2872 [119]
NH_3	0.6372	0.6153	12	0.5943	0.5789 [124]
PH_3	0.2780	0.2755	13	0.2340	0.2258 [128]
O_3	0.3033	0.1370	7	0.2276	0.2099 [129]
ClF	0.4453	0.3226	6	0.3451	0.3462 [130]
CH_3F	0.7706	0.7283	10	0.6919	0.7312 [131]
CH_3CCH	0.3203	0.3141	12	0.2866	0.3070 [132]
CO	−0.0987	0.0414	9	0.0725	0.0481 [123]
BEA	0.0843	0.0309		0.0177	

*aug-cc-pVTZ basearekin egindako kalkuluak.

Table 12 – Momentu kuadrupolarraren Θ_{zz} osagaia, unitate atomikoetan, Sadlej-pVTZ basea eta geometria esperimentalean kalkulatutak. C_{3v}, D_{6h}, eta D_{3d} simetria duten molekulak aztertzen dira.

Molekula	HF	PNOF6	(N_c)	CCSD	ESP.
H_2	0.4381	0.3935	17	0.3935	0.39 ± 0.01 [9]
HF	1.7422	1.6939	7	1.7156	1.75 ± 0.02 [124]
BH*	2.6772	2.3706	38	2.3388	2.3293† [133]
HCl	2.8572	2.7753	8	2.7233	2.78 ± 0.09 [123]
HCCF	3.3530	3.2482	9	2.9335	2.94 ± 0.10 [119]
CO	1.5366	1.4562	9	1.4889	1.44 ± 0.30 [124]
N_2	0.9397	1.0530	9	1.1712	1.09 ± 0.07 [124]
NH_3	2.1258	2.1080	12	2.1661	2.45 ± 0.30 [123]
PH_3	1.7217	1.6507	13	1.5695	1.56 ± 0.70 [128]
ClF	0.9413	1.1122	6	1.0514	1.14 ± 0.05 [130]
CH_3F	0.3482	0.3269	10	0.3002	0.30 ± 0.02 [131]
C_2H_2	5.3655	5.1531	12	4.6850	4.71 ± 0.14 [134]
C_2H_6	0.6329	0.6275	13	0.6234	0.59 ± 0.07 [135]
C_6H_6	6.6418	6.3571	12	5.6653	6.30 ± 0.27 [136]
CH_3CCH	4.2913	4.1146	12	3.6939	3.58 ± 0.01 [8]
CO_2	3.8087	3.6012	8	3.1966	3.19 ± 0.13 [124]
BEA	0.2646	0.1517		0.0902	

*aug-cc-pVTZ basearekin egindako kalkuluak.

† Halkier et al. [133] egindako FCI kalkulua.

Table 13 – Momentu kuadrupolarraren Θ_{zz} eta Θ_{xx} osagaiak, unitate atomikoetan, Sadlej-pVTZ basea eta geometria esperimentalean kalkulatutak.

Molekula	HF	PNOF6	(N_c)	MRSD-CI	ESP.
H_2O (xx)	1.7966	1.7808	9	1.8050	1.86 ± 0.02 [123]
H_2O (zz)	0.0981	0.0869	9	0.0950	0.10 ± 0.02 [123]
H_2CO (xx)	0.1019	0.0516	10	0.1100	0.04 ± 0.12 [137]
H_2CO (zz)	0.0921	0.1255	10	0.2230	0.20 ± 0.15 [137]
C_2H_4 (xx)	2.7819	2.5892	13	2.3700	2.45 ± 0.12 [123]
C_2H_4 (zz)	1.4942	1.3266	13	1.1700	1.49 ± 0.11 [123]
O_3 (xx)	1.1175	1.2426	7	1.2830	1.03 ± 0.12 [129]
O_3 (zz)	-0.2387	0.3606	7	0.1680	0.52 ± 0.08 [129]
BEA	0.1772	0.1066		0.1448	

1.8.4 Ondorioak

21 molekulen momentu elektrikoak aztertu ditugu, zehazki, dipoloa, kuadrupoloa, eta oktupoloa. PNOF6 bat dator CCSD eta MRSD-CI metodoekin. Orokorrean balio esperimentalak teorikoki lortzeko gai izan gara geometria esperimentalak eta Sadlej basea erabiliz. Laburbilduz, PNOF6 molekulen karga banaketaren deskribapen doia ematen du, korrelazio elektronikoaren izaera estatikoa edo dinamikoa delarik.

1.9 Ondorio orokorrak

N-elektroietako sistema atomiko eta molekularrentzako energia 2DME-aren funtzionala da. Hori dela eta, energia zuzenean 2DME-aren bitartez kalkulatu daiteke, uhin-funtzioaren beharrik gabe. Halere, 2DME zentsu fisikoa duela ziurtatzeko, beharrezkoa da N-adierazgarritasunaren baldintzak erabiltzea. Hauek inposatzeak gastu konputatzionala nabarmenki handitzen du, hortaz 2DME-n oinarritutako metodoa ez da nahi bezainbeste eraginkorra. Kontrako aldean dentsitate elektronikoaren funtzionalaren teoria (DFT) dugu. DFT kalkuluak oso efizienteak eta merkeak izan arren, korrelazio gogorra adierazten duten sistemak deskribatzea ezinezkoa da orain arteko garatutako DFT hurbilpenak erabiltzen badira. ONFT bi metodo hauen artean kokatzen da. Izan ere, 1DME-n oinarritzen denez gero, partikula bakarreko metodoa dugu eta beraz konputazionalki efizientea izatea posiblea da. Aldi berean, korrelazio gogorra deskribatzeko metodo eraginkorra da, zeren eta okupazio ez-osoak eta potentzial ez-lokalak erabiltzen dira ONFT-n.

Tesi hau DME-en oinarrizko definizio eta propietateekin hasi dugu. Bereziki 1 eta 2 DME-ak aztertu ditugu, izan ere, tesiarekin zuzeneko erlazioa dute. Azken hauetarako N-adierazgarritasunaren baldintzak azaldu ditugu, egungo praktikan erabiltzen direnak esplizituki adieraziz. ONFT lan askoren garapenari esker finkatutako teoria dugu [13, 24–27]. Azpimarratzekoa da Gilbert 1975.urtean 1DME-aren funtzionalaren existentzia frogatu egin zuela. Dena den, praktikan hurbilpenak 1DME-aren adierazpen diagonala erabiltzen dute, eta matrize honen bektore propiak orbital naturalak (ON) deritzogu, hortaz praktikan ONFT-rekin lan egiten dugu. Funtzionalaren hurbilpenak bakarrik ezagunak direnez gero, 1 eta 2 DME-rako N-adierazgarritasunaren baldintzak inposatzea ezinbestekoa da. Egungo literaturan, aipatzekoa da 2DME-aren baldintzak jarraituz garatutako hurbilpenak, zehatz mehatz, PNOFi (i=$\overline{5,7}$). PNOF5-ren kasuan, N-adierazgarritasunaren baldintzak bere osotasunean betetzen dira, izan ere, PNOF5-k APSG uhin-funtzioaren energiari dagokio. PNOF6 eta PNOF7 PNOF5-ren eskeletoaren gainean eraikitako hurbilpenak dira, eta elektroi pare independenteak baino haratago jotzen dute. Tesi osoan zehar egindako kalkuluak DoNOF programarekin egin dira. Programa hau Mario Piris-ek idatzitako kodea da, eta tesian zehar algoritmo berriak programatu dira kodearen erabilgarritasuna hobetzeko asmoz.

Orokorrean, tesiaren helburua ONFT garatzea da, normalean erabilitako egitura elektronikoaren metodoekin konparagarria izateko. Geometriaren optimizazioa energiaren kalkuluaren ondoko eragiketarik garratzitsuena da, beraz ezinbestekoa da edozein metodoarentzako prozedura hau modu efizientean egin ahal izatea. Hori dela eta, ONFT-ren testuinguruan lehenengo eta bigarren ordeneko deribatu analitikoak garatu ditugu. Frogatu dugu energiaren gradientea bereziki merkea dela, HF kasuaren antzekoa baita. Hesiarraren kalkulurako, berriz, beharrezkoa da akoplatutako ekuazio perturbatuak erabiltzea perturbazioarekiko erantzuna lortzeko, hortaz kalkulua nabarmenki garestiagoa da. Erakutsi dugu PNOFi (i=$\overline{5,7}$)-rekin lortutako orekako geometriak konparagarriak direla CCSD-rekin. Are gehiago, PNOF7-rekin lortutako bibrazio frekuentzia harmonikoak CCSD-rekin eta MP2-rekin bat datoz. Hori dela eta, propietate termokimikoen kalkulu zehatzak egitea posiblea da PNOF7 hurbilpena erabiliz, besteak beste, entalpia edo energia librearen kalkuluak.

Ondoko atalean sistema modeloak aztertu ditugu ONFT-ren testuinguruan. Alde batetik, Hubbard modeloa erabili dugu ONFH garrantzitsuenak oinarrizko ikuspuntu batetik aztertzeko. Frogatu dugu 2DME-aren N-adierazgarritasunaren baldintzak ezinbestekoak direla hurbilpen zehatzak garatzeko, bestela inolako zentsu fisikoak ez duten emaitzak lortzeko posibilitatea dago eta. Esate baterako, energia infinitoak edo okupazioen kurba ez-jarraiak U/t-aren menpe, Hubbard modeloaren testuinguruan. Beste aldetik, fasearen dilema N-adierazgarritasunaren ikuspuntutik aztertu dugu. Bereziki, PNOF7-ren kasuan N-adierazgarritasunaren G baldintzak zehazten du zein izan daitekeen elektroi pareak korrelazionatzeko gaia, baina ez du honetarako fase edo zeinurik zehazten. Aurreko atalean ikusi genuenez gai honen garrantzia korrelazio gogorreko sistemak deskribatzeko, azken hauek erabili ditugu fasearen azterketa egiteko. Dimentsio bakarreko Hubbard modeloa eta hidrogeno kateak erabiliz, frogatu dugu fase negatiboa hartzen badugu PNOF7-rekin elektroi pareak deskribatzeko, gure emaitzak oso zehatzak direla sistemaren edozein tamaina eta korrelazio erregimenerako. Ondorioz, PNOF7 hurbilpenaren forma matematikoa guztiz zehaztu dugu atal honetan egindako azterketari esker.

Aurreko atalean sistema modeloak ONFH-en garapenarako erabili badira ere, PNOF7-ren potentziala korrelazio gogorreko sistemak deskribatzeko begi bistan geratu da. Hortaz, potentzial hau ikertzeko asmoz, kapitulu honetan bat eta bi dimentsiotako korrelazio gogorreko sistemak aztertu ditugu PNOF7 erabiliz. Dimentsio bakarreko azterketaren kasuan azpimarratzekoa da H_{50} kate linealaren disoziazio simetriko eta asimetrikoetarako lortutako emaitza. Izan ere, bi kasuetan PNOF7-rekin eta DMRG-rekin lortutako kurbak bat datoz. Beraz, orekako distantzian CCSD(T) bezain zehatzak diren energiak ez baditugu ere, disoziazio prozesua bere

osotasunean deskribatu daiteke PNOF7 erabiliz. Bestalde, bi dimentsiotako azterketaren kasuan, aipatzekoa da Hubbard modeloarentzat lortutako emaitzak. Berriro ere DMRG-rekin alderagarriak diren kurbak lortu ditugu, korrelazio erregimenaren, sistemaren tamainaren, eta tokien betetzearen edozein balioetarako. Esatekoa da elektroien kopurua tokien kopurua baino txikiagoa denean metodo asko ez-egonkorrak bilakatzen direla, PNOF7-rekin, berriz, ez dugu horrelako arazorik topatu.

Azken lana ONFH-ekin kalkulatutako momentu elektrikoen inguruan datza. Momentu elektrikoak deskribatzea ezinbestekoa da egitura elektronikoaren metodoentzako, kargaren distribuzioarekin eta beste hainbat aplikazioekin zuzeneko erlazioa dute eta. Bai PNOF5-k bai PNOF6-k ondo konparatzen dute CCSD-rekin eta MRSD-CI-rekin sistema molekularren dipoloari, kuadrupoloari, eta oktupoloari begiratuz gero. Ondorioz, kanpo eremu elektrikoei ONFT-k emango dien erantzuna zehaztasunez deskribatzea espero da.

Laburbilduz, tesi honetan ONFT ikuspuntu diferenteetatik aztertu da. Teoriaren eta hurbilpenen arteko ezberdintasun garrantzitsuenak azpimarratu ditugu, eta literaturan eskura dauden hurbilpenen ikerketa sakona burutu dugu. Gainera, metodo hauen erabilgarritasuna nabarmenki hobetu dugu, dagoeneko posiblea baita egitura elektronikoan garrantzitsuenak diren prozedurak egitea DoNOF programa erabiliz. Dena den, ONFT garatu beharreko metodoa da oraindik. Partikularki inportantea izango da kalkuluak egiteko algoritmo numerikoak ikertzea eta hobetzea, benetan erabilgarria den metodo efizientea izateko. Honetaz aparte, garrantzitsua da 2DME-aren N-adierazgarritasunaren baldintzak inposatzen dituzten hurbilpenak gehiago aztertzea, hobetzea, eta garatzea. Beraz, PNOF hurbilpenak abiapuntu modu bezala egokiak badira ere, ezinbestekoa da eremu honetan ikerketa egitea hurbilpen zehatzagoak garatzeko helburuarekin.

CHAPTER 2

Introduction

In this section the basics of reduced density matrices (RDMs) are introduced, as well as the key concepts of 1RDM functional theory and Natural Orbital Functional (NOF) Theory (NOFT).

2.1 Reduced Density Matrices

The density matrix operator can be defined for a given set of states $\{\psi_m\}$ as

$$\widehat{\mathcal{D}} = \sum_m \omega_m |\psi_m\rangle\langle\psi_m| \tag{67}$$

where the weights satisfy the bounds and normalization conditions, i.e. $0 \leq \omega_m \leq 1;\ \forall\, m$ and $\sum_m \omega_m = 1$. Note that if there is only a single state in the set $\{\psi_m\}$ we obtain the pure state density operator $\widehat{\mathcal{D}} = |\psi\rangle\langle\psi|$. The density matrix Γ^N can be obtained by projecting $\widehat{\mathcal{D}}$ in some N-dimensional basis

$$\begin{gathered}\Gamma^N\left(\mathbf{x_1'}\cdots\mathbf{x_N'}|\mathbf{x_1}\cdots\mathbf{x_N}\right) \equiv \langle\mathbf{x_1'}\cdots\mathbf{x_N'}|\widehat{\mathcal{D}}|\mathbf{x_1}\cdots\mathbf{x_N}\rangle = \\ \sum_m \omega_m\, \psi_m^*\left(\mathbf{x}_1'\cdots\mathbf{x}_N'\right)\psi_m\left(\mathbf{x}_1\cdots\mathbf{x}_N\right)\end{gathered} \tag{68}$$

where each coordinate $\mathbf{x}_i$ is a combination of a space coordinate $\mathbf{r}_i$ and a spin coordinate s_i. Consequently, for any p such that $0 < p < N;\ p \in \mathbb{Z}$, the $p-$order reduced density matrix (pRDM) is defined as

$$\Gamma^p\left(\mathbf{x_1'}\cdots\mathbf{x_p'}|\mathbf{x_1}\cdots\mathbf{x_p}\right) = \binom{N}{p}\sum_m \omega_m \int \psi_m^*\left(\mathbf{x}_1'\mathbf{x}_2'\cdots\mathbf{x}_p'\cdots\mathbf{x}_N\right)\psi_m\left(\mathbf{x}_1\mathbf{x}_2\cdots\mathbf{x}_p\cdots\mathbf{x}_N\right)dx_{p+1}\cdots dx_N \tag{69}$$

Recall that Lowdin's normalization convention [24] has been used along this chapter, so the trace of the first-order RDM (1RDM) corresponding to $p = 1$ (and denoted hereafter by Γ) is equal to the number of electrons, $Tr(\Gamma^1) = N$, and the trace of the second-order RDM (2RDM) corresponding to $p = 2$ (and denoted hereafter by D) equals the number of electron pairs, i.e. $Tr(\Gamma^2) = \binom{N}{2} = \frac{N(N-1)}{2}$. In second quantization notation, the 1 and 2 RDMs can be expressed as

$$\Gamma_{ji} = \sum_m \omega_m \langle\psi_m|\widehat{a}_j^+\widehat{a}_i|\psi_m\rangle \tag{70}$$

and

$$D_{kl,ij} = \frac{1}{2}\sum_m \omega_m \left\langle\psi_m|\widehat{a}_k^+\widehat{a}_l^+\widehat{a}_j\widehat{a}_i|\psi_m\right\rangle \tag{71}$$

where $\{\widehat{a}_k^+\}$ ($\{\widehat{a}_k\}$) represents the set of creation (annihilation) operators. Hereafter, $\{i, j, k, ...\}$ indices will be employed to denote spin orbitals, whereas $\{p, q, r, ...\}$ indices will be used for spatial orbitals, unless stated otherwise. From the anticommutation relations of these operators is straightforward to derive the properties of RDMs. Just cite here the most important properties such as Hermiticity,

$$\Gamma_{ji} = \Gamma_{ij}^* \ \left(\Gamma = \Gamma^+\right),\ D_{kl,ij} = D_{ij,kl}^* \ (D = D^*) \tag{72}$$

symmetry and antisymmetry,

$$D_{kl,ij} = D_{lk,ji},\ D_{kl,ij} = -D_{lk,ij} = -D_{kl,ji} \tag{73}$$

and positivity of diagonal elements,

$$\Gamma_{ii} \geq 0,\ D_{ij,ij} \geq 0 \tag{74}$$

The last property is very interesting from the point of view of physical interpretations. The Γ_{ii} element represents the probability of finding a particle in an orbital ψ_i, while the other electrons occupy arbitrary spin orbitals. Similarly, $D_{ij,ij}$ is the probability of finding one particle in an orbital ψ_i and another in an orbital ψ_j, when all other particles occupy arbitrary orbitals. Thus, condition (74) arises from the fact that any probability must be positive or zero by definition.

Consequently, the trace of the 1RDM must sum up to the number of electrons, and the trace of the 2RDM to the number of electron pairs, as explained above.

For $\widehat{S}_z$ eigenstates, only density matrix blocks that conserve the number of each spin type are non-vanishing. Specifically, the 1RDM has two nonzero blocks $\Gamma_{p_\alpha q_\alpha}$ and $\Gamma_{p_\beta q_\beta}$, whereas the 2RDM has three independent nonzero blocks, $D_{p_\alpha q_\alpha, r_\alpha s_\alpha}$, $D_{p_\alpha q_\beta, r_\alpha s_\beta}$ and $D_{p_\beta q_\beta, r_\beta s_\beta}$. The parallel-spin components of the two-matrix must be antisymmetric, but $D_{p_\alpha q_\beta, r_\alpha s_\beta}$ (neither $D_{p_\beta q_\alpha, r_\beta s_\alpha}$) possesses no special symmetry [11].

So far, we have introduced the basic concepts and notation of RDMs, paying special attention to the 1RDM and 2RDM. In fact, in the Born-Oppenheimer approximation, neglecting relativistic effects, the Hamiltonian of a many-electron system contains at most two-particle interactions, so the electronic energy functional of N-electron systems is given explicitly in terms of the 1 and 2 RDMs

$$E_{el}[\Gamma, D] = \sum_{ik} \Gamma_{ki} h_{ki} + \sum_{ijkl} D_{kl,ij} \langle kl|ij\rangle \tag{75}$$

where h_{ik} corresponds to the one-electron matrix elements of the core-Hamiltonian, including the kinetic energy of the electrons and the attractive Coulomb potential between the nuclei (Z_I represents the positive charge of nucleus I) and the electrons,

$$h_{ki} = \int d\mathbf{x}\, \psi_k^* (\mathbf{x}) \left[-\frac{1}{2}\nabla^2 - \sum_I \frac{Z_I}{|\mathbf{r} - \mathbf{r}_I|} \right] \psi_i (\mathbf{x}) \tag{76}$$

and $\langle kl|ij\rangle$ are the two-electron integrals corresponding to the repulsive Coulomb potential between the electrons,

$$\langle kl|ij\rangle = \int d\mathbf{x}_1 d\mathbf{x}_2\, \psi_k^* (\mathbf{x}_1)\, \psi_l^* (\mathbf{x}_2)\, \frac{1}{|\mathbf{r_1} - \mathbf{r_2}|} \psi_i (\mathbf{x}_1)\, \psi_j (\mathbf{x}_2) \tag{77}$$

Note that atomic units are used. It is worth pointing out that any RDM can be calculated from RDMs of higher order according to the contraction relation, which is straightforward from the general definition (69). Therefore, the energy functional (75) is an exact functional of the 2RDM, i.e. $E_{el}[D]$, since the 1RDM can be expressed as a function of the 2RDM:

$$\Gamma \left(\mathbf{x_1'} | \mathbf{x_1} \right) = \frac{2}{N-1} \int d\mathbf{x}\, D \left(\mathbf{x_1'} \mathbf{x} | \mathbf{x_1} \mathbf{x} \right) \tag{78}$$

Note that the whole 2RDM is necessary to calculate the 1RDM according to Eq. (78), thus, although the electron-electron interaction term in Eq. (75) can be expressed as a function only

of diagonal terms of the 2RDM, the latter are not sufficient to determine completely the energy functional (75).

2.1.1 N-representability

The term N-representability was proposed by Coleman in 1963 [12]. To that time, it was already known that the 2RDM alone is sufficient to compute the ground-state energy of a Hamiltonian involving at most two-body interactions. Coleman realized, however, that it is necessary to impose some limitations on the allowed 2RDMs to ensure a physical value of ground-state energy. The N-representability problem is known as the necessity to assure that a given RDM derives from the integration of an N-particle wavefunction that is symmetric or antisymmetric with respect to the interchange of similar bosons or fermions,respectively.
It must be distinguished between pure and ensemble N-representability conditions. The former are related with the conditions to assure a one-to-one mapping with a pure N-particle density matrix, whereas the latter assure a mapping to a mixture of N-particle quantum states generally defined by an N-particle density matrix (68).
In the present thesis, we deal only with the 1 and 2 RDMs, so let us focus on the N-representability problem of the latter.

2.1.1.1 N-representability of the 1RDM

The necessary and sufficient conditions that guarantee the ensemble N-representability of Γ are already known [12,13]. These conditions apply to the eigenvalues of the 1RDM as $0 \leq n_i \leq 1;\ \forall\, i$ under the normalization condition $\sum_i n_i = \mathrm{N}$.
For a general representation of Γ, it can be expressed as the following normalization and positivity conditions

$$Tr(\Gamma) = \sum_i \Gamma_{ii} = N, \quad \Gamma \succeq 0, \quad 1 - \Gamma \succeq 0 \tag{79}$$

where $A \succeq 0$ represents a positive semidefinite condition for any matrix A, so its eigenvalues are greater than or equal to zero. Recently [14, 15], pure N-representability conditions of the 1RDM have been found, that is, those that are necessary for Γ to be representable by at least one pure N-particle density matrix. These conditions, named as Generalized Pauli constraints (GPC), read in the diagonal representation of the 1RDM as

$$\kappa_{0j} + \sum_{i=1}^{r} \kappa_{ij} n_i \leq 0 \tag{80}$$

where κ_{ij} are integer constants, r is the rank of the orbital space, and tdeprince2016variationalhe occupationi numbers (ONs) are decreasingly ordered. The GPC have been intensively investigated in the context of NOFT in last years [16, 19], and there have been many attempts to employ them in the development of NOF approximations (NOFAs) [17,18]. Nevertheless, it has been found that the number of conditions increases dramatically with the number of natural orbitals (NOs), so imposing GPC is not useful in practical implementations. This discussion is extended at the end of section 7.2.3.

2.1.1.2 N-representability of the 2RDM

The necessary and sufficient N-representability conditions for the 2RDM are already known, but they are of no practical use [20]. The most popular constraints are the p-positivity conditions, which derive from a class of positive semidefinite Hamiltonians of the form

$$\widehat{H} = \widehat{A}^\dagger \widehat{A} \tag{81}$$

where $\widehat{A}^\dagger$ is a p-particle operator. The expectation value of $\widehat{H}$ must be positive, since $\widehat{A}^\dagger \widehat{A}$ is Hermitian for a non-singular operator $\widehat{A}$. Therefore, its matrix representation must be positive semidefinite.

For two-particle operators, we obtain the well-known P, Q, and G two-positivity conditions

$$P_{p_\sigma q_{\sigma'}, r_\sigma s_{\sigma'}} \succeq 0, \tag{82}$$

$$Q_{p_\sigma q_{\sigma'}, r_\sigma s_{\sigma'}} \succeq 0, \tag{83}$$

$$G_{p_\sigma q_\tau, r_\kappa s_\lambda} \succeq 0, \tag{84}$$

where the matrices are defined for a given state Ψ as

$$P_{p_\sigma q_{\sigma'}, r_\sigma s_{\sigma'}} = \langle \Psi | a^\dagger_{p_\sigma} a^\dagger_{q_{\sigma'}} a_{s_{\sigma'}} a_{r_\sigma} | \Psi \rangle \,, \tag{85}$$

$$Q_{p_\sigma q_{\sigma'}, r_\sigma s_{\sigma'}} = \langle \Psi | a_{p_\sigma} a_{q_{\sigma'}} a^\dagger_{s_{\sigma'}} a^\dagger_{r_\sigma} | \Psi \rangle \,, \tag{86}$$

$$G_{p_\sigma q_\tau, r_\kappa s_\lambda} = \langle \Psi | a^\dagger_{p_\sigma} a_{q_\tau} a^\dagger_{s_\lambda} a_{r_\kappa} | \Psi \rangle \,. \tag{87}$$

As usual, $p, q, ...$ represents spatial orbital indices, whereas $\sigma, \sigma', \tau, \lambda, \kappa$ stands for spin coordinate α or β. Each of these matricese must be diagonalized in order to analyze their positive semidefinite character (by checking that all eigenvalues produced are greater or equal to zero). The first matrix coincides with the $\mathbf{D}$, then P condition is equivalent to prove that geminal

occupancies are non-negative. The **Q** matrix involves the positive semidefinite character of the holes while the **G** matrix involves the positive semidefinite character of particle-hole probabilities. Interestingly, these matrices are related each other by anticommutation relations of creation (annihilation) operators, but each one of them provide different N-representability constraints of the 2RDM [21].

Direct minimization of the electronic energy (75) with respect to the 2RDM imposing N-representability conditions of the 2RDM implies a computational scaling of $\mathcal{O}\left(M^6\right)$ for floating-point operations and $\mathcal{O}\left(M^4\right)$ for memory when using two-particle conditions. M represents the dimension of the single-particle space. The latter is referred to as variational 2RDM (v2RDM) calculation in the literature. When considering higher order N-representability conditions, the corresponding computational cost becomes prohibitively expensive; for instance, for the three- and four-positivity conditions, we have a scaling of $\mathcal{O}\left(M^9\right)$ and $\mathcal{O}\left(M^{12}\right)$, respectively, for floating-point operations. Further, they involve the computation of higher order RDMs, thus making the enforcement of the whole set of N-representability constraints non-effective. In this thesis, we restrict to the aforementioned P, Q, and G conditions, originally introduced by Garrod and Percus [141], but also to the T1 and T2 (and its T2' variant) conditions introduced by Erdahl [22] and firstly implemented by Zhao et al. [23]. The latter are three-particle conditions, but they are expressible in terms of the 2RDM because the terms with six creation and annihilation operators cancel upon addition due to opposite signs. More details about these constraints can be found elsewhere [21–23].

2.2 1RDM Functional Theory

In 1975, Gilbert [13] extended the Hohenberg-Kohn theorem to nonlocal external potentials, and he showed the existence of a universal functional of the 1RDM

$$E_{el}\left[\Gamma\right] = \sum_{ik} \Gamma_{ki} h_{ki} + V_{ee}\left[\Gamma\right] \tag{88}$$

where $V_{ee}\left[\Gamma\right]$ is universal in the sense that it is independent of the external field. This work together with those of Löwdin [24], Levy [25], Valone [26], and Donelly and Parr [27] laid the foundations of 1RDM functional theory (1RDMFT). The latter is usually referred to as NOFT, since any practical approach (see section 3.1) requires to employ the diagonal representation of the 1RDM, in terms of its eigenvalues (ONs) and eigenvectors (NOs). Thus, although in practice

it is more appropriate to speak of NOFAs, the general theory can be formulated, in principle, for a general representation of the 1RDM. The interest on this theory rely on the fact that the necessary and sufficient conditions that guarantee the ensemble N-representability of Γ are well established and are very easy to implement [142], in contrast with the N-representability of the 2RDM. In addition, the unknown functional in a Γ-based theory only needs to reconstruct the electron-electron potential energy [11], which is a notable advantage over DFT, where the kinetic energy functional needs also to be reconstructed. Thereby, Γ-functional theories seem a promising way of overcoming the drawbacks of density functional approximations currently in use.

Computational schemes based on the exact formulation[1] are several times more expensive than solving directly the Schrödinger equation [147], so practical applications require a different approach for $E_{el}[\Gamma]$. In 1967 [28], Rosina demonstrated that there is a one-to-one mapping from the ground-state 2RDM to the N-particle wavefunction in the case of a Hamiltonian with at most two-body interactions. Taking advantage of the Rosina's theorem, the existence theorem of Gilbert implicitly establishes a one-to-one correspondence between the ground-state D and Γ, therefore, the functional $E_{el}[\Gamma]$ must match the exact well-known functional $E_{el}[\mathrm{D}]$. Unfortunately, the exact reconstruction $V_{ee}[\Gamma]$ has been an unattainable goal so far, and we have to settle for making approximations. The typical approach is to employ the well-known 2RDM functional $E_{el}[\mathrm{D}]$ but using solely a reconstruction functional $\mathrm{D}[\Gamma]$. The existence of the exact reconstruction $\mathrm{D}[\Gamma]$ is not demonstrated, but it turns out to be of practical use, in contrast to $V_{ee}[\Gamma]$. An example of $\mathrm{D}[\Gamma]$ can be given for a system described by a single Slater determinant

$$\mathrm{D}\left(\mathbf{x_1'x_2'}|\mathbf{x_1x_2}\right) = \Gamma\left(\mathbf{x_1'}|\mathbf{x_1}\right)\Gamma\left(\mathbf{x_2'}|\mathbf{x_2}\right) - \Gamma\left(\mathbf{x_1'}|\mathbf{x_2}\right)\Gamma\left(\mathbf{x_2'}|\mathbf{x_1}\right) \tag{89}$$

where in this particular case Γ is idempotent, i.e. $\Gamma^2 = \Gamma$. Approximating 2RDMs in terms of 1RDMs lead to energy functionals that still depend on the 2RDM [29]. An undesired implication of such dependence is that the functional N-representability problem arises [30, 31]. That is, we have to observe the requirement that the 2RDM reconstructed in terms of 1RDM must satisfy the same N-representability conditions [20] as those imposed on unreconstructed 2RDMs. Otherwise, there might not exist an N-electron fermionic system compatible with the energy functional, therefore the energy can even drop below the exact value. In summary, we are no

[1] "Computational schemes based on the exact formulation" means to minimize the electronic energy (75) with respecto to all possible wavefunctions that reduce to a given 1RDM, and then minimize the energy with respect to the set of all N-representable 1RDMs (see [143–146]).

longer really dealing with the 1RDM functional theory but with an approximate one-particle theory, where the 2RDM continues to play a dominant, though hidden, role. It has been generally assumed that there is no N-representability problem for approximate functionals, as it is believed that the N-representability conditions of Coleman [12] on the 1RDM are sufficient on their own. Consequently, most of the approximate functionals currently in use are not N-representable [41].

Recall an essential difference between RDM theories based on the 1RDM and the 2RDM. In the former, we have assured that the 2RDM continues to play a dominant role. However, as no order relation between the exact and approximate functionals is available, the approximate energy can be either below or above the exact energy, i.e. $E_{el} \leq E_{el}^{exact}$ or $E_{el} \geq E_{el}^{exact}$. Obviously, imposing N-representability constraints on the 1 and 2 RDMs improves the quality of our result, but there is no any certainty about the relation between $E_{el}[\Gamma]$ and E_{el}^{exact}. On the contrary, if we employ the 2RDM (or any higher-order RDM) as our key variable the exact energy functional expression $E_{el}[D]$ is already known. Nevertheless, the minimization set is larger than the exact one, since non N-representable trial 2RDMs are included in the latter. Thus, we have a lower bound to the exact energy $E_{el}[D] \leq E_{el}^{exact}$. Enforcing N-representability conditions of the 2RDM reduces the minimization set until we reach the limit $E_{el}[D] = E_{el}^{exact}$, obtained if only N-representable 2RDMs are considered.

Recently, the discovery of a systematic way to derive pure-state N-representability conditions for the 1RDM has allowed to open a new way to develop functionals [17, 18]. The application of pure conditions restricts the 1RDM variational space that leads to improvements in energy but it is obvious that it does not improve the reconstruction of the approximate functional *per se*. In Refs. [31, 148], it has been discussed of whether GPC should be taken into account in the development of NOFAs. In both publications it is emphasized that the pairing conditions (see section 3.1.2.1) meet the requirements to be GPC, i.e. satisfy Eq. (80)[2]. So they claim on the use of additional pairing constraints in the reconstruction of the 2RDM and not in its later use to limit the domain of trial Γ matrices.

The application of GPC does not improve the reconstruction of the approximate functional *per se*. Indeed, as long as we are dealing with an approximate functional of Γ, having a 1RDM that represents a pure state does not guarantee that the reconstructed energy functional will be pure state N-representable, whereas if the approximate NOF is stricly pure state N-representable,

[2]For non-degenerate ground states the GPC are not crucial. On the contrary, they may have critical implications for open-shell systems or, more generally, if the ground state is degenerate [19].

then the 1RDM will also be automatically (by contraction) pure-state N-representable. Therefore, the pure-state N-representability problem for an approximate functional is related to the N-representability of the 2RDM which determines $V_{ee}[\Gamma]$. In addition, it has been recently demonstrated [148] that the energy functional $E_{el}[\Gamma]$, defined for ensemble or pure 1RDMs, coincide on the set of the v-representable 1RDMs, so the development of $E_{el}[\Gamma]$ restricting to the set of ensemble N-representable 1RDMs is formally correct.

CHAPTER 3

Methodology

This section is organized in three parts. In the first part, we review the most relevant NOFAs appeared in the literature in the last decades. We pay particular attention to the PNOF family, since among the NOFAs published so far, only the latter care about the N-representability of the energy functional, inherent to the N-representability of the 2RDM. The second part is dedicated to review the procedure for the minimization of the energy. Finally, the third section focus on the DoNOF program package, developed and employed in this thesis to carry out numerical calculations by means of NOFAs.

To avoid spin contamination effects, the spin restricted theory will be employed, in which a single set of orbitals is used for α and β spins: $\varphi_p^\alpha(\mathbf{r}) = \varphi_p^\beta(\mathbf{r}) = \varphi_p(\mathbf{r})$, and the parallel spin blocks of the RDMs are equal as well. In the case of non-singlet states, the spin-multiplet formulation of NOFT allows to employ spin restricted theory, as recently [69] shown by Piris, whereas for singlets this is the common use. The NOF for multiplets formulation is left out of this section, and it will be reviewed only in section 7.2.2. More details about how to employ the spin restricted theory can be found in section 5.1. In any case, in some parts spin orbitals will be employed for convenience.

3.1 Natural Orbital Functional Approximations

Apart from the special case of the Hartree-Fock (HF) approximation, none of the known approximate functionals are explicitly given in terms of the 1RDM, including the venerable functional that accurately describes two-electron closed-shell systems [54]. There are energy expressions [35, 37, 38, 64] that seem to depend properly on Γ, however, these functionals violate the functional N-representability [41] and that is why energy is often obtained far below true energy. One can obtain quite reasonable results for some systems using them but there is no N-particle density matrix (68) that supports their existence.

In most applications, the spectral decomposition of the 1RDM is used to express it in terms of the naturals orbitals (NOs) $\{|i\rangle\}$ ($\{\phi_i(\mathbf{x})\}$ in coordinate representation) and their occupation numbers (ONs) $\{n_i\}$

$$\Gamma_{ki} = n_i \delta_{ki} \tag{90}$$

or, in coordinate representation

$$\Gamma\left(\mathbf{x_1'}|\mathbf{x_1}\right) = \sum_i n_i \phi_i^*\left(\mathbf{x_1'}\right) \phi_i\left(\mathbf{x_1}\right) \tag{91}$$

Therefore, the energy expression is referred to as a natural orbital functional (NOF), and is written as

$$E_{el}[\{n_i, \phi_i\}] = \sum_i n_i \mathcal{H}_{ii} + \sum_{ijkl} D[n_i, n_j, n_k, n_l] \langle kl|ij\rangle \tag{92}$$

where $D[n_i, n_j, n_k, n_l]$ represents the 2RDM reconstructed from the ONs. We neglect any explicit dependence of D on the NOs themselves given that the energy functional already has a strong dependence on the NOs via the one- and two-electron integrals. Obviously, an exact reconstruction $E[\Gamma]$ is not linear in Γ, but this assumption would not lead us to any practical expression. It is worth noting that NOs are the orbitals that diagonalize the 1RDM corresponding to an approximate energy, such as those obtained from an approximate wavefunction. These energies are not invariant with respect to unitary transformations of the orbitals and the resulting functionals are only implicitly dependent on the 1RDM, through NOs and ONs. Consequently, there does not exist any extended Fockian matrix for the energy minimization by direct diagonalization, as is the case in HF or FCI. It is therefore misleading to talk about a functional of the 1RDM due to the existing dependence on the 2RDM, it is more appropriate to speak of a NOF. A more detailed discussion of the state of the art of NOF approximations (NOFAs) can be found elsewhere [32, 33].

3.1.1 $\mathcal{JK}$-only approximations

The HF like approximation for the 2RDM is defined as

$$\begin{aligned} D^{\sigma\sigma}_{pq,rt} &= \frac{n_p n_q}{2}(\delta_{pr}\delta_{qt} - \delta_{pt}\delta_{qr}),\ \sigma = \alpha, \beta \\ D^{\alpha\beta}_{pq,rt} &= \frac{n_p n_q}{2}\delta_{pr}\delta_{qt} \end{aligned} \tag{93}$$

Some approximations to the 2RDM are produced by replacing only the $\sigma\sigma$-elements of the HF like approximation, namely,

$$D^{\sigma\sigma}_{pq,rt} = \frac{n_p n_q}{2}\delta_{pr}\delta_{qt} - \frac{\mathcal{F}(n_p, n_q)}{2}\delta_{pt}\delta_{qr} \tag{94}$$

Table 14 – $\mathcal{F}(n_p, n_q)$ functions used for 2RDM reconstruction in Eq. (94)

Approximation	$\mathcal{F}(n_p, n_q)$	
MBB	$(n_p n_q)^{1/2}$	[35, 36]
Power	$(n_p n_q)^{0.53}$	[37]
CA	$n_p n_q + [n_p(1-n_p)n_q(1-n_q)]^{1/2}$	[38]
CGA	$\frac{1}{2}\left\{n_p n_q + [n_p(2-n_p)n_q(2-n_q)]^{1/2}\right\}$	[39]

The $\mathcal{F}(n_p, n_q)$ functions are collected in Table 14. These approximations lead to $\mathcal{JK}$-only NOFAs since the electronic energy involves only the Coulomb ($\mathcal{J}_{pq} = \langle pq|pq\rangle$) and exchange integrals ($\mathcal{K}_{pq} = \langle pq|qp\rangle$). Note that Eq. (94) violates the antisymmetric requirement unless $\mathcal{F} = n_p n_q$, consequently none of these functionals affords an N-representable 2RDM. Extensive N-representability violations for these NOFAs have been reported [40, 41].

3.1.2 Piris Natural Orbital Functional (PNOF)

In the last decade, a series of NOFAs has been proposed by Piris and collaborators (PNOFi, i=$\overline{1,7}$) [43–47]. In all cases the reconstruction functional is based on the cumulant expansion [48,49] of the 2RDM, and finding an approximation for the cumulant part. In detail, the 2RDM is expressed as an antisymmetrized product of the 1RDMs and a correction to it, namely

$$D_{kl,ij} = \frac{1}{2}\left(\Gamma_{ki}\Gamma_{lj} - \Gamma_{li}\Gamma_{kj}\right) + \lambda_{kl,ij} \tag{95}$$

Since the first two terms in (95) correspond to the HF approximation, the cumulant matrix, sometimes called the pair correlation matrix, must vanish for a single Slater determinant or,

equivalently, integer ONs. The HF term satisfies Eqs. (72, 73, 74), so the cumulant matrix should satisfy these relations too. In principle, $\lambda_{kl,ij}$ has a dependence on four indices but this implies a huge computational cost, therefore, it is approximated by two-particle matrices Δ and Π expressed in terms of the ONs. Following the $Bottom-Up$ method proposed by Piris [57,101] to generate improved reconstruction functionals, these matrices are built such that the (2,2)-positivity conditions (referred to as P, Q, and G conditions in section 2.1.1.2) defined by Eqs. (82, 83, 84) are enforced to ensure the N-representability of the energy functional (92) or, equivalently, of the 2RDM. The spin structure for the cumulant matrix is

$$\begin{aligned}\lambda^{\sigma\sigma}_{pq,rt} &= -\frac{\Delta_{pq}}{2}\left(\delta_{pr}\delta_{qt}-\delta_{pt}\delta_{qr}\right),\ \sigma=\alpha,\beta\\ \lambda^{\alpha\beta}_{pq,rt} &= -\frac{\Delta_{pq}}{2}\delta_{pr}\delta_{qt}+\frac{\Pi_{pr}}{2}\delta_{pq}\delta_{rt}\end{aligned} \tag{96}$$

where Δ is a real symmetric matrix and Π is a spin independent Hermitian matrix. The conservation of the total spin allows to determine the diagonal elements $\Delta_{pp}=n_p^2$ and $\Pi_{pp}=n_p$ [50], whereas known analytical necessary N-representability conditions provide bounds for the off-diagonal terms [51]. In detail, the P (Eq. 82) and Q (Eq. 83) conditions of the 2RDM impose the following inequalities on the off-diagonal elements of Δ:

$$\Delta_{qp}\leq n_q n_p,\ \Delta_{qp}\leq h_q h_p,\ q\neq p \tag{97}$$

and similarly, condition G (Eq. 84) imposes the next inequality on the Π-matrix:

$$\Pi^2_{qp}\leq\left(n_q h_p+\Delta_{qp}\right)\left(h_q n_p+\Delta_{qp}\right), \tag{98}$$

where $h_p=(1-n_p)$ is the hole in the spatial orbital p. Furthermore, due to the contraction rules of the 2RDM (Eq. 78), Δ must fulfill

$$\sum\nolimits_q{}' \Delta_{qp}=n_p h_p, \tag{99}$$

where the prime indicates hereafter that the $q=p$ term is omitted from the summation. So far, the $Bottom-Up$ method leads to the next energy expression for singlet state systems

$$E_{el}=2\sum_p n_p\mathcal{H}_{pp}+\sum_{qp}\Pi_{qp}\mathcal{L}_{pq}+\sum_{qp}\left(n_q n_p-\Delta_{qp}\right)\left(2\mathcal{J}_{pq}-\mathcal{K}_{pq}\right) \tag{100}$$

where $\mathcal{H}_{pp}$ is the matrix element of the kinetic energy and nuclear attraction terms in the NO representation, whereas $\mathcal{J}_{pp}=<pp|pp>$ is the Coulomb interaction between two electrons with opposite spins at the same spatial orbital p. $\mathcal{J}_{pq}=\langle pq|pq\rangle$ and $\mathcal{K}_{pq}=\langle pq|qp\rangle$ are the usual

direct and exchange integrals, respectively. $\mathcal{L}_{pq} = \langle pp|qq\rangle$ is the exchange and time-inversion integral [42], which reduces to $\mathcal{K}_{pq}$ for real orbitals. Note that the energy expression (100) belongs to the familiy of $\mathcal{JKL}$-only family of NOFAs. Different approximations to off-diagonal terms of matrices Δ and Π lead to the familiy of PNOFi, i=$\overline{1,7}$. It must be remarked that recently a few attempts to go beyond the $\mathcal{JKL}$-only NOFAs have been published in the last years [45, 46, 52, 53].

3.1.2.1 The electron pairing approach

We now focus on the simplest case of two electrons. An accurate NOF is well-known for this system from the exact wavefunction [54] assuming that all amplitudes, with the exception of the first one, are negative if the first amplitude is chosen to be positive [149]. The two-electron singlet energy reads as

$$E_{el}\left(2e^{-}\right) = 2\sum_{p=1}^{\infty} n_p \mathcal{H}_{pp} + n_1\mathcal{L}_{11} + \sum_{p,q=2}^{\infty}\sqrt{n_q n_p}\mathcal{L}_{pq} - 2\sum_{p=2}^{\infty}\sqrt{n_1 n_p}\mathcal{L}_{p1} \tag{101}$$

A recent study [41] on the two-electron Harmonium atom reveals that small contributions to energy may have opposite signs to those adopted in Eq. (101), specially in the high-correlation regime. Nevertheless, the convention of signs adopted in Eq. (101) provides very accurate results for almost all correlation regimes in two-electron systems, then it can be considered as a quasi-exact NOFA for two-electron systems.

The requirement that for any two-electron singlet system the NOF (100) yields the accurate expression (101) if $N = 2$, together with the cumulant sum rules (97), (98), and (99), and the N-representability conditions (82), (83) and (84), imply that $\Delta_{qp} = n_q n_p$ and $\Pi_{qp}^{max} = \sqrt{n_q n_p}$, respectively [51]. Furthermore, the phase factor of Π_{qp} is +1 if $q, p \in (1, \infty)$, and -1 otherwise.

3.1.2.2 PNOF5

The knowledge of the two-electron NOFA can be exploited by using an electron pairing approach, that is, dividing the system into pairs of electrons, so that the interactions within each pair are described according to Eq. (101). In other words, the orbital space Ω is divided into $N/2$ mutually disjoint subspaces Ω_g, so each orbital belongs only to one subspace. Consider each subspace contains one orbital g below the level $F = N/2$, and N_g orbitals above it, which

is reflected in additional sum rules for the ONs:

$$\sum_{p\in\Omega_g} n_p = 1, \quad g = 1, 2, \ldots, \mathrm{N}/2 \tag{102}$$

Taking into account the spin, each subspace contains only an electron pair, and the normalization condition for the 1RDM is automatically fulfilled:

$$2\sum_{p\in\Omega} n_p = 2\sum_{g=1}^{\mathrm{N}/2}\sum_{p\in\Omega_g} n_p = \mathrm{N} \tag{103}$$

Therefore, optimizing the NOF with respect to ONs can be done without restrictions if electron-pairing conditions are employed (see more details and the resulting Lagrangian in section 5.1.2.2). Coupling each orbital g below the $N/2$ level with only one orbital above it ($\mathrm{N}_g = 1$) leads to the perfect orbital pairing. It is important to note that orbitals satisfying the pairing conditions (102) are not required to remain fixed throughout the orbital optimization process [55]. For $N > 2$, the generalization of Eq. (101) according to the electron-pairing constraints described above leads to PNOF5 [56, 57]

$$\begin{gathered}
\Delta_{qp} = n_p^2\delta_{qp} + n_q n_p\left(1-\delta_{qp}\right)\delta_{q\Omega_g}\delta_{p\Omega_g} \\
\Pi_{qp} = n_p\delta_{qp} + \Pi_{qp}^g\left(1-\delta_{qp}\right)\delta_{q\Omega_g}\delta_{p\Omega_g} \\
\Pi_{qp}^g = \begin{cases} -\sqrt{n_q n_p}, & p = g \text{ or } q = g \\ +\sqrt{n_q n_p}, & p, q > \mathrm{N}/2 \end{cases}, \qquad \delta_{q\Omega_g} = \begin{cases} 1, & q \in \Omega_g \\ 0, & q \notin \Omega_g \end{cases}
\end{gathered} \tag{104}$$

It is worth noting that Δ_{qp} and Π_{qp} are zero between orbitals belonging to different subspaces, therefore the 2RDM reconstruction of PNOF5 corresponds to an independent-pair model. Given this functional form of the auxiliary matrices $\triangle$ and Π, the energy (100) of the PNOF5 can be conveniently written as

$$\begin{aligned}
E_{el}^{pnof5} &= \sum_{g=1}^{\mathrm{N}/2} E_g + \sum_{f\neq g}^{\mathrm{N}/2} E_{fg} \\
E_{fg} &= \sum_{p\in\Omega_f}\sum_{q\in\Omega_g}\left[n_q n_p\left(2\mathcal{J}_{pq} - \mathcal{K}_{pq}\right)\right] \\
E_g &= \sum_{p\in\Omega_g} n_p\left(2\mathcal{H}_{pp} + \mathcal{J}_{pp}\right) + \sum_{q,p\in\Omega_g, q\neq p}\Pi_{qp}^g\mathcal{L}_{pq}
\end{aligned} \tag{105}$$

The first term of E_{el}^{pnof5} is the sum of the $N/2$ electron-pair E_g energies corresponding to the two-electron NOFA (101), whereas the second term contains the contribution to the HF mean-field of the electrons belonging to different pairs. Several performance tests have shown that PNOF5 yields remarkably accurate descriptions of systems with near-degenerate one-particle

states and dissociation processes [150]. In this sense, the results obtained with PNOF5 for the electronic structure of transition metal complexes are probably the most relevant [151].

Pernal showed [58] that this NOFA corresponds to the energy obtained from a wavefunction of an antisymmetrized product of strongly orthogonal geminals (APSG) if the expansion of the $N/2$ geminals is limited to two-dimensional subspaces with fixed signs for the expansion coefficients of the corresponding geminals. This is a proof that PNOF5 is strictly a pure-state N-representable functional. Consequently, Piris demonstrated [57] that approximations for $E_{el}[\Gamma]$ can be obtained essentially using two methods, namely, the *top-down* and *bottom-up* methods [30, 152]. The *top-down* method consists in the reduction of an N-particle ground-state energy generated from an approximate wavefunction into a functional of Γ, whereas, in the *bottom-up* method $E_{el}[\Gamma]$ is generated by progressive inclusion of N-representability conditions [20, 40] on the reconstructed $D[\Gamma]$.

Looking closely at the constraints imposed on the ONs during the reconstruction of the PNOF5, one realizes that the resulting ONs meet the requirements for pure-state N-representability conditions [31] to hold, described by Eq. (80). Since the N-representability conditions of the 1RDM are embedded in the PNOF5 reconstruction of the 2RDM, the resulting 1RDM by contraction (see Eq. 78) of the so constructed 2RDM will necessarily be pure-state N-representable. Consequently, one needs to impose only ensemble N-representability constraints to the 1RDM in order to generate the variational Euler equations for the energy minimization. This is a great advantage with respect to imposing externally the 1RDM pure-state N-representability conditions as constraints on bounds of the domain of trial 1RDMs during the variational procedure, because the number of the latter increases drastically with the number of NOs. A more detailed of this discussion can be found in Refs. [31, 148]. From the practical point of view, only those NOFAs that enforce electron-pairing constraints are able to yield the correct number of electrons in the fragments after a homolytic dissociation [150]. The latter is a well-known problem in RDM theories, either based on the 1RDM or the 2RDM, and is related to the N-representability problem. Therefore, keeping pairing restrictions improve the obtained 1 and 2 RDMs.

Since the energy (92) is not invariant with respect to a unitary transformation of the orbitals, an approximate NOF provides two complementary representations of the one-electron picture. The latter was investigated for the case of PNOF5 in Ref. [100]. In summary, the NO and canonical orbital representations can be obtained, by diagonalization of the 1RDM or Lagrangian matrix (112), respectively. Both sets of orbitals represent unique correlated one-electron pictures of the same energy minimization problem, *ergo*, they complement each other in the analysis of the

molecular electronic structure. The orbitals obtained in both representations have shown [153] that the electron pairs with opposite spins continue to be a suitable language for the chemical bond theory.

3.1.2.3 PNOF7

PNOF5 takes into account the important part of the electron correlation corresponding to the intra-pair interactions. However, no inter-pair electron correlation is accounted for. To go beyond the independent-pair approximation, let us maintain $\Delta_{qp} = 0$ in order to satisfy the sum rule (99) and consider nonzero the Π-elements between orbitals belonging to different subspaces [45]. The resulting energy is

$$\begin{aligned} E_{el}^{pnof7} &= \sum_{g=1}^{\mathrm{N}/2} E_g + \sum_{f\neq g}^{\mathrm{N}/2} E_{fg} \\ E_g &= \sum_{p\in\Omega_g} n_p \left(2\mathcal{H}_{pp} + \mathcal{J}_{pp}\right) + \sum_{q,p\in\Omega_g, q\neq p} \Pi_{qp}^{g} \mathcal{L}_{pq} \\ E_{fg} &= \sum_{p\in\Omega_f} \sum_{q\in\Omega_g} \left[n_q n_p \left(2\mathcal{J}_{pq} - \mathcal{K}_{pq}\right) + \Pi_{qp}^{\Phi} \mathcal{L}_{pq}\right] \end{aligned} \tag{106}$$

which can be conveniently written as

$$E_{el}^{pnof7} = E_{el}^{pnof5} + \sum_{f\neq g}^{\mathrm{N}/2} \sum_{p\in\Omega_f} \sum_{q\in\Omega_g} \Pi_{qp}^{\Phi} \mathcal{L}_{pq} \tag{107}$$

From Eq. (98), note that provided the Δ_{qp} vanishes, we obtain that $|\Pi_{qp}| \leq \Phi_q \Phi_p$ with $\Phi_q = \sqrt{n_q h_q}$. Assuming equality, it only remains to determine the sign of Π_{qp}. For the intra-pair interactions Eq. (101) determines the sign of Π_{qp}, as already seen for PNOF5 (105). However, there is no hint to determine the sign of Π_{qp}^{Φ}, so a large number of possible combinations of these signs looms up for those terms correlating electron pairs. Making an adequate choice of the Π_{qp}^{Φ} signs is known as the phase dilemma [47].

In the original formulation of PNOF7 [45], the generalization of the sign convention adopted for Π_{qp}^{g} in Eq. (105), namely $\Pi_{qp}^{\Phi} = \Phi_q \Phi_p$ if $q, p > \mathrm{N}/2$, and $\Pi_{qp}^{\Phi} = -\Phi_q \Phi_p$ otherwise, was employed to define the PNOF7 (106) approximation. The latter is referred to as PNOF7(+) along this thesis to emphasize the signs adopted for Π_{qp}^{Φ}. However, in Ref. [47] it was proven that considering the PNOF7 (106) with the Π_{qp}^{Φ} phases equal to -1 for any p, q; i.e. $\Pi_{qp}^{\Phi} = -\Phi_q \Phi_p$ provides very accurate description of strong correlation effects in model systems such as hydrogen chains and the Hubbard model. Further, it is obvious that this election favors

decreasing of the energy (106). Therefore, in this thesis PNOF7 refers to the Eq. (106) with $\Pi^{\Phi}_{qp} = -\Phi_q\Phi_p$. In section 6.2, the phase dilemma is studied and the phase of the term Π^{Φ}_{qp} is investigated. Accordingly, along chapters 6.1 and 6.2 the PNOF7 is also referred to as PNOF7(-) in order make clear the difference with respect to PNOF7(+).

It is clear that the main weaknesses of PNOF7 is the absence of the inter-pair dynamic electron correlation since Π^{Φ}_{qp} has significant values only when the ONs differ substantially from 1 and 0. Consequently, PNOF7 is expected to be able to recover the complete intra-pair, but only the nondynamic inter-pair correlation. To remedy this situation and provide a global method for electron correlation, Piris proposed [45, 46] an alternative method in which using the solution of the NOF, together with MP2 methods, a single-reference method for capturing at the same time the static and dynamic correlation is obtained. The latter is known in the literature as the NOF-MP2 method [45, 46]. Another option is to propose different cumulant matrices (96), i.e. a different NOFA. This is the case of PNOF6, which is reviewed in the next section.

3.1.2.4 PNOF6

PNOF6 was presented [44] after the publication of PNOF5 [56], but the latter is more similar to PNOF7 according to Eq. (107). The idea behind PNOF6 is to propose the same electron-electron interactions regardless of belonging to one or another orbital subspace. In fact, from the physical point of view the Coulomb interaction is the same for all the electrons regardless of orbital subspaces. The electron-pairing approach is conserved in PNOF6, since the latter is of essential importance as aforementioned.

The PNOF6 energy for a singlet state of an N-electron molecule can be cast as

$$E_{el}^{pnof6} = \sum_{g=1}^{N/2} E_g + \sum_{f\neq g}^{N/2} \sum_{p\in\Omega_f} \sum_{q\in\Omega_g} E_{pq}^{int} \tag{108}$$

The first term of the energy (108) draws the system as independent $N/2$ electron pairs described by the accurate NOFA for two-electron systems (101), whereas the interaction energy is equal for electrons belonging to the same subspace Ω_g or two different subspaces $\Omega_g \neq \Omega_f$. Therefore, the intra-pair and inter-pair electron correlations are equally balanced in PNOF6. Then, E_{pq}^{int} is given by

$$E_{pq}^{int} = (n_q n_p - \Delta_{qp})\,(2\mathcal{J}_{pq} - \mathcal{K}_{pq}) + \Pi_{qp}\mathcal{L}_{pq} \tag{109}$$

where

$$\begin{array}{c|c|c} \Delta_{qp} & \Pi_{qp} & Orbitals \\ \hline e^{-2S}h_q h_p & -e^{-S}\left(h_q h_p\right)^{\frac{1}{2}} & q \leq F, p \leq F \\ \frac{\gamma_q \gamma_p}{S_\gamma} & -\Pi^{\gamma}_{qp} & \begin{array}{l} q \leq F, p > F \\ q > F, p \leq F \end{array} \\ e^{-2S}n_q n_p & e^{-S}\left(n_q n_p\right)^{\frac{1}{2}} & q > F, p > F \end{array} \tag{110}$$

The other magnitudes are defined as

$$\begin{aligned} \gamma_p &= n_p h_p + \alpha_p^2 - \alpha_p S_\alpha \\ \alpha_p &= \begin{cases} e^{-S}h_p\,, & p \leq F \\ e^{-S}n_p\,, & p > F \end{cases} \\ \Pi^{\gamma}_{qp} &= \left(n_q h_p + \frac{\gamma_q \gamma_p}{S_\gamma}\right)^{\frac{1}{2}} \left(h_q n_p + \frac{\gamma_q \gamma_p}{S_\gamma}\right)^{\frac{1}{2}} \\ S = \sum_{q=F+1}^{F+FN_c} n_q, \quad S_\alpha &= \textstyle\sum_{q=F+1}^{F+FN_c} \alpha_q, \quad S_\gamma = \sum_{q=F+1}^{F+FN_c} \gamma_q \end{aligned} \tag{111}$$

Interestingly, PNOF6 yields energies above the independent-pair model PNOF5. This reveals the subtle interplay between inter- and intra-pair correlation in electron-pairing approaches, so that more inter-pair correlation does not necessarily mean lower correlation energies. In any case, PNOF6 has proven to be an accurate NOFA in many situations [59–62].

3.2 Euler equations

The procedure for the minimization of the energy (92) requires optimizing with respect to the ONs and the NOs, separately. The method of Lagrange multipliers is used to ensure the orthonormality requirement for the NOs, and the normalization condition for the ONs. The latter can additionally be expressed by means of auxiliary variables in order to automatically enforce the N-representability bounds of the 1RDM. Hence, the auxiliary functional $\Lambda\left[N, \{n_i\}, \{\phi_i\}\right]$ is given by

$$\Lambda = E_{el} - \mu\left(\sum_i n_i - N\right) - \sum_{ki} \lambda_{ik}\left(\langle\phi_k|\phi_i\rangle - \delta_{ki}\right) \tag{112}$$

E_{el} is defined by Eq. (92). By making (112) stationary with respect to the NOs and ONs, we obtain the following system of Eqs.:

$$\frac{\partial E_{el}}{\partial n_i} = \mathcal{H}_{ii} + \frac{\partial V_{ee}}{\partial n_i} = \mu \tag{113}$$

$$\frac{\partial E_{el}}{\partial \phi_i^*} = n_i \hat{\mathcal{H}} \phi_i + \frac{\partial V_{ee}}{\partial \phi_i^*} = \sum_k \lambda_{ki} \phi_k \tag{114}$$

Note that according to Eqs. (88) and (92) V_{ee} is approximated by the second summation in Eq. (92). Eq. (113) is obtained holding the orbitals fixed, whereas the set of the orbital Euler Eqs. (114) is satisfied for a fixed set of occupancies. Unfortunately, since the energy functional (92) is not invariant with respect to a unitary transformation of the orbitals, solving Eq. (114) cannot be reduced to a pseudo-eigenvalue problem wherein diagonalizing λ brings us to the solution of the problem. This particularity makes NOFT far different from single-determinant approaches such as HF or Kohn-Sham DFT, in which Γ is idempotent, i.e. $\Gamma^2 = \Gamma$.

At present, the procedure of solving simultaneously Eqs. (113) and (114) is carried out by the iterative diagonalization method developed by Piris and Ugalde [55]. More in detail, at the extremum the 1RDM is completely diagonal, so the matrix of the Lagrange multipliers λ must be Hermitian. Consequently, we have that $\left[\lambda - \lambda^\dagger, \Gamma\right] = 0$ (where super-index $\dagger$ is used to express the conjugate transpose). In this vein, one can define an Hermitian matrix $\mathbf{F}$ containing $\lambda - \lambda^\dagger$ as off-diagonal elements

$$F_{ki} = \theta(i-k)\left[\lambda_{ki} - \lambda_{ik}^*\right] + \theta(k-i)\left[\lambda_{ik}^* - \lambda_{ki}\right] \tag{115}$$

where $\theta(x)$ is the unit-step Heaviside function, and λ is easily obtained from Eq. (114) (see section 5.2.2). Then, iterative diagonalization of (115) automatically solves the $\lambda - \lambda^\dagger = 0$ equation and thereby leads us to the NOs of the quantum system. Although diagonal elements of matrix $\mathbf{F}$ are not determined, so that the latter is not properly a generalized Fock matrix, an *aufbau* principle guarantees the convergency of this procedure. More details about the performance of the algorithm can be found in Ref. [55].

3.3 DoNOF program package

DoNOF (Donostia Natural Orbital Functional Software Program) is a program mainly written in Fortran 90 for electronic structure calculations by means of NOFAs. The code is mainly developed and owned by Prof. Mario Piris. Some additional contributions have been made by Prof. Xabier Lopez, Prof. Pedro Salvador, and Dr. Eduard Matito. The use of this software is restricted solely to academic institutions and for academic purposes.

All the NOF calculations carried out along this thesis have been done by using DoNOF, so **I have implemented new capabilities in the program**:

Figure 22 – Logo of *Donostia Natural Orbital Functional* Software Program.

1) Many of the NOFAs commonly used in the literature have been implemented, namely, the Power functional [37], MBB [35], CA [38], and CGA [39], GU from Goedecker and Umrigar [63], MLSIC from Marques and Lathiotakis [64], and BBC2 from Gritsenko, Pernal and Baerends [65].

2) The computation of analytic energy gradients has been coded following the Ref. [76]. The latter is done by the on-the-fly calculation of derivate integrals, in order to apply effectively the Schwarz integral screening and reduce substantially the number of integrals to be computed and stored.

3) By using analytic energy gradients the geometry optimization procedure has been implemented. The latter has been adapted to exploit the MPI parallelization scheme coded by Dr. Eduard Matito that deals with two-electron integrals.

4) Together with Prof. Xabier Lopez, the calculation of the numerical Hessian from the analytic gradients has been coded, and consecutively the computation of harmonic vibrational frequencies and thermodynamical properties.

5) The LBFGS method has been implemented according to Ref. [66] for the optimization of the ONs, as well as for the computation of equilibrium geometries, as an alternative to the mostly used conjugated gradient method.

6) We have implemented the Hubbard Hamiltonian as an alternative to the usually employed non-relativistic many-electron Hamiltonian. Thus, the energy and many properties of this model system can be obtained in 1D and 2D, by using periodic boundary conditions, varying the filling of the system and the correlation regime (quantified by the U/t ratio), and adding (or not) external potentials to make the Hubbard model inhomogeneous (or homogeneous).

7) Second and third order molecular electric moments have been implemented, namely, the quadrupole and octupole moments, following the Buckingham convention [67, 68].

All these advances, together with other advances obtained by Piris (see mainly [31, 46, 69] and references therein) will be made public in the first release of DoNOF as an open-source implementation of NOFAs for ab initio quantum chemistry, and thereby put NOFT in the list of electronic structure methods publicly available. A publication containing a summary of the program is now under construction.

CHAPTER 4

Objectives

The main objective of this thesis is the development and application of NOFAs, in order to establish them as an electronic structure method able to compete with standard wavefunction and DFT approaches. In this process, the next points have been specially considered:

1) Apart from single-point energy calculations, the most popular procedure in electronic structure simulations is the computation of energy gradients. Therefore, the first objective of this thesis is to develop an efficient method for the calculation of analytic energy derivatives in NOFT, and carry out a test by using many molecules to study the accuracy of some NOFAs, specifically, those satisfying at least some necessary N-representability conditions of the 2RDM; e.g. PNOFi (i=5,6,7).

2) We emphasize on the implications of doing approximations in the context of NOFT, so in practice we are dealing with an approximate theory of the 2RDM in terms of the 1RDM. Consequently, N-representability constraints of the 2RDM must be taken into account to get consistent and reliable results. Our aim is to show the importance of the latter by using model systems, such as the Hubbard model, since they are more adequate for benchmarking purposes. Also, there exists situations in which the N-representability conditions alone are not sufficient to determine the form of a given NOFA in the *bottom-up* method employed by Piris to build reconstructions for the 2RDM. Our aim is then to use model systems in order to shine a light on this problem, such as the phase-dilemma encountered for the inter-pair correlation term in

PNOF7.

3) In view of the accurate results obtained for simple systems involving strong correlation effects, the potential of the PNOF7 approximation for the description of strongly correlated electrons is more extensively investigated. In fact, understanding the physics of strongly correlated systems constitutes a very important theoretical issue, and an efficient, cheap, accurate, and simple approximation is still missing. The objective of this chapter is thus to study the ability of PNOF7 to describe strong correlation effects in 1D and 2D systems.

4) Finally, particular atenttion is paid to the calculation of molecular electric moments, namely, dipolar, quadrupolar, and octupolar moments. The latter are of fundamental interest for many disciplines; e.g. biomolecular simulations. Nevertheless, we are especially interested on their use for benchmarking NOFAs. In fact, molecular electric moments give information about charge distribution, so it is of essential importance for any electronic structure method to give an accurate description of electric moments for many *a-posteriori* studies, such as those related with electric fields or electrostatic interactions.

CHAPTER 5

Geometry optimization

It is essential for any electronic structure method to efficiently compute the energy derivatives with respect to nuclear coordinates. The latter are indeed necessary in order to get cheap and accurate equilibrium geometries, as well as related quantities (thermochemistry...).

5.1 Analytic gradients for NOFT

5.1.1 Introduction

Since in 1958 Bratoz [154] derived for first time the analytic gradient for the restricted Hartree-Fock (HF) case, the development and applications of analytical gradients has been of great interest for chemistry and physics [70]. Energy gradients are primarily employed to locate and characterize critical points on the energy surface in electronic structure theory, especially minima and saddle points, and calculate rovibrational spectroscopic constants and energy levels. The direct analytical calculation of energy derivatives from the wavefunction is computationally more complex than the numerical calculation, but offers greater speed and accuracy. In fact, that is why it has been invested much effort in the development of analytic energy derivatives for many well-known electronic structure methods, such as configuration interaction (CI) [71, 72], density cumulant functional theory (DCFT) [73], Moller-Plesset perturbation theory (MP2)

[74], or coupled cluster (CC) theory including different number of excitations, as recently Gauss and Stanton did for the full singles, doubles and triples (CCSDT) method [75].

From the very beginning there have been many attempts to use the Hellmann-Feynman theorem for calculating energy gradients [155–157], since this approach allows to compute them by using exclusively one-electron operators. It is important to note that the theorem is only valid if all parameters entering the involved density matrices are invariant with respect to nuclear distortion. Unfortunately, this condition is met solely in the complete basis set limit because the location of atomic orbitals (AO) is not important. To achieve accurate results, calculations require the contribution from two-electron terms, which are in turn the bottleneck of the analytic energy gradient computation. In this chapter, the method proposed in Ref. [76] has been followed to compute efficiently derivatives of the two-electron integrals.

Along this chapter we develop the analytic energy gradients for the NOFT. To our knowledge, this is the first direct analytical calculation of the energy derivatives with respect to nuclear motion in NOFT. Perhaps the only precedent is the derivation of analytical gradients in the IBCS theory, which can be considered as a NOFT [158]. No iterative procedure is needed in order to evaluate the derivative expressions, therefore, the presented here theory is analogous to the gradient computation at the HF level of theory. Our methodology allows the calculation of analytic energy gradients corresponding to a correlated method at low computational cost, in comparison with standard wavefunction based methods that must resort to linear-response theory in order to evaluate the energy derivatives with respect to nuclear distortions.

This chapter is organized as follows. The development of general expressions for the energy gradients with respect to nuclear motion in section 5.1.2, and analytic gradients for PNOF in section 5.1.2.1 Section 5.1.2.2 is dedicated to the special case of electron pairing approaches. The next section 5.1.3 is dedicated to discuss the computational aspects related to energy gradient calculations. In section 5.1.4, we compare the optimized structures of 15 spin-compensated systems at the PNOF5 and PNOF6 levels of theory with respect to the corresponding coupled cluster singles and doubles [CCSD] results, by using the correlation consistent triple-zeta (cc-pVTZ) basis set developed by Dunning and coworkers [87]. Accurate empirical geometries [78] are included in order to carry out a statistical analysis. In section 5.1.4.1, PNOF7 equilibrium geometries are also reported and compared with PNOF5 and reference CCSD and empirical results. The chapter 5.1 is concluded in section 5.1.5.

5.1.2 Derivation of analytic gradients

Assume all NOs are real and expand them in a fixed basis set, $\phi_i(\mathbf{x}) = \sum_\upsilon \mathcal{C}_{\upsilon i}\zeta_\upsilon(\mathbf{x})$, then, the electronic energy can be written as

$$E_{el} = \sum_{\mu\upsilon}\Gamma_{\mu\upsilon}\mathcal{H}_{\mu\upsilon} + \sum_{\mu\upsilon\eta\delta} D_{\mu\eta\upsilon\delta}\langle\mu\eta|\upsilon\delta\rangle, \tag{116}$$

where $\Gamma_{\mu\upsilon}$ and $D_{\mu\eta\upsilon\delta}$ are respectively the 1 and 2 RDM given in the atomic orbital (AO) representation,

$$\begin{aligned}\Gamma_{\mu\upsilon} &= \sum_i n_i \mathcal{C}_{\mu i}\mathcal{C}_{\upsilon i},\\ D_{\mu\eta\upsilon\delta} &= \sum_{klij} D_{klij}\mathcal{C}_{\mu k}\mathcal{C}_{\eta l}\mathcal{C}_{\upsilon i}\mathcal{C}_{\delta j}.\end{aligned} \tag{117}$$

Then, the derivative of the total energy with respect to the coordinate x of nucleus A is given by

$$\frac{dE}{dx_A} = \frac{\partial E_{el}}{\partial x_A} + \frac{\partial E_{nuc}}{\partial x_A} + \sum_{\mu j}\frac{\partial E_{el}}{\partial \mathcal{C}_{\mu j}}\frac{\partial \mathcal{C}_{\mu j}}{\partial x_A} + \sum_i \frac{\partial E_{el}}{\partial n_i}\frac{\partial n_i}{\partial x_A}, \tag{118}$$

where $\partial E_{el}/\partial x_A$ and $\partial E_{nuc}/\partial x_A$ represents the derivative of all terms with explicit dependence on the nuclear coordinate x_A, whereas the last two terms in Eq. (118) arise from the implicit dependence of the orbital coefficients and ONs on geometry, respectively.

The electronic energy (116) presents explicit dependence on the nuclear motion via one- and two-electron integrals, due to the dependence of the AOs on the geometry, namely,

$$\frac{\partial E_{el}}{\partial x_A} = \sum_{\mu\upsilon}\Gamma_{\mu\upsilon}\frac{\partial \mathcal{H}_{\mu\upsilon}}{\partial x_A} + \sum_{\mu\upsilon\eta\delta} D_{\mu\eta\upsilon\delta}\frac{\partial\langle\mu\eta|\upsilon\delta\rangle}{\partial x_A}. \tag{119}$$

The first term in Eq. (119) is the negative *Hellmann-Feynman force* [159,160]. The second term, which contains the derivatives of the two-electron integrals, is the bottleneck for calculating the analytical gradient.

Regarding the contribution from the NO coefficients, combining Eq. (114) with the chain rule, is not difficult to obtain the next formula:

$$\frac{\partial E_{elec}}{\partial \mathcal{C}_{\mu j}} = 2\sum_{\upsilon i}\mathcal{S}_{\mu\upsilon}\mathcal{C}_{\upsilon i}\lambda_{ij}, \tag{120}$$

where $\mathcal{S}_{\mu\upsilon}$ is the overlap matrix $\langle\mu|\upsilon\rangle$. At the same time, the response of NO coefficients to nuclear motion can be computed from the orthonormality relation in the AO representation ($\mathbf{C}^\dagger\mathbf{S}\mathbf{C} = \mathbf{1}$) [161], indeed,

$$2\sum_{\mu\upsilon}\frac{\partial \mathcal{C}_{\mu j}}{\partial x_A}\mathcal{S}_{\mu\upsilon}\mathcal{C}_{\upsilon i} = -\sum_{\mu\upsilon}\mathcal{C}_{\mu j}\frac{\partial \mathcal{S}_{\mu\upsilon}}{\partial x_A}\mathcal{C}_{\upsilon i}. \tag{121}$$

Combining then Eqs. (120) and (121), and taking into account the contribution from different indexes, we obtain the total contribution from the NO coefficients to the gradient, which is known as the *density force*:

$$\sum_{\mu j} \frac{\partial E_{el}}{\partial \mathcal{C}_{\mu j}} \frac{\partial \mathcal{C}_{\mu j}}{\partial x_A} = -\sum_{\mu \upsilon} \lambda_{\mu \upsilon} \frac{\partial \mathcal{S}_{\mu \upsilon}}{\partial x_A}, \tag{122}$$

where

$$\lambda_{\mu \upsilon} = \sum_{ij} \mathcal{C}_{\mu j} \lambda_{ji} \mathcal{C}_{\upsilon i}. \tag{123}$$

The last term of Eq. (118) does not bring any contribution to the gradient, since deriving the normalization condition ($\sum_i n_i = N$) of the ONs, one obtains

$$\sum_i \frac{\partial n_i}{\partial x_A} = 0. \tag{124}$$

Hence, combining (124) and (113), brings about a contribution to the gradient equal to zero:

$$\sum_i \frac{\partial E_{el}}{\partial n_i} \frac{\partial n_i}{\partial x_A} = \mu \sum_i \frac{\partial n_i}{\partial x_A} = 0. \tag{125}$$

Finally, bringing together Eqs. (119) and (122) with the nuclear contribution $\partial E_{nuc}/\partial x_A$, we obtain the expression for NOF analytic gradients, namely,

$$\frac{dE}{dx_A} = \sum_{\mu \upsilon} \Gamma_{\mu \upsilon} \frac{\partial \mathcal{H}_{\mu \upsilon}}{\partial x_A} + \sum_{\mu \upsilon \eta \delta} D_{\mu \eta \upsilon \delta} \frac{\partial \langle \mu \eta | \upsilon \delta \rangle}{\partial x_A} + \frac{\partial E_{nuc}}{\partial x_A} - \sum_{\mu \upsilon} \lambda_{\mu \upsilon} \frac{\partial \mathcal{S}_{\mu \upsilon}}{\partial x_A}. \tag{126}$$

The spin orbitals are direct products $|\phi_i\rangle = |\varphi_p\rangle \otimes |\sigma\rangle$, so $\{\phi_i(\mathbf{x})\}$ may be split into two subsets: $\left\{\varphi_p^\alpha(\mathbf{r})\,\alpha(\mathbf{s})\right\}$ and $\left\{\varphi_p^\beta(\mathbf{r})\,\beta(\mathbf{s})\right\}$. Given a set of $2R$ spin-orbitals $\{\phi_i | i = 1, ..., 2R\}$, we have two sets of R orthonormal spatial functions, $\left\{\varphi_p^\alpha(\mathbf{r})\right\}$ and $\left\{\varphi_p^\beta(\mathbf{r})\right\}$, such that in general the first set is not orthogonal to the second one. Nevertheless, the original set

$$\begin{aligned} \phi_{2p-1}(\mathbf{x}) &= \varphi_p^\alpha(\mathbf{r})\,\alpha(\mathbf{s}), \qquad p = 1, ..., R \\ \phi_{2p}(\mathbf{x}) &= \varphi_p^\beta(\mathbf{r})\,\beta(\mathbf{s}), \qquad p = 1, ..., R \end{aligned}$$

continues being orthonormal via the orthogonality of the spin functions

$$\int d\mathbf{s} \alpha^*(\mathbf{s})\,\beta(\mathbf{s}) = \int d\mathbf{s} \beta^*(\mathbf{s})\,\alpha(\mathbf{s}) = 0. \tag{127}$$

Since we deal herein only with singlet states, the spin restricted formulation is employed, in which a single set of orbitals is used for α and β spins: $\varphi_p^\alpha(\mathbf{r}) = \varphi_p^\beta(\mathbf{r}) = \varphi_p(\mathbf{r})$. Similarly as we did above for the spin NOs, let us expand the spatial NOs $\{\varphi_p\}$ as a linear combination

of atomic orbitals: $\varphi_p(\mathbf{r}) = \sum_\upsilon \mathcal{C}_{\upsilon p}\chi_\upsilon(\mathbf{r})$. Consequently, in Eq. (126), entering magnitudes become

$$\begin{aligned} \Gamma_{\mu\upsilon} &= 2\sum_p n_p \mathcal{C}_{\mu p}\mathcal{C}_{\upsilon p} \\ D_{\mu\eta\upsilon\delta} &= 2\sum_{pqrt}(D^{\alpha\alpha}_{pqrt} + D^{\alpha\beta}_{pqrt})\mathcal{C}_{\mu p}\mathcal{C}_{\eta q}\mathcal{C}_{\upsilon r}\mathcal{C}_{\delta t} \\ \lambda_{\mu\upsilon} &= 2\sum_{pq}\mathcal{C}_{\mu q}\lambda_{qp}\mathcal{C}_{\upsilon p}. \end{aligned} \tag{128}$$

5.1.2.1 Analytic gradients for PNOF

In this chapter, we use the aforementioned reconstruction of the 2RDM in terms of the 1RDM [101]. Thus, the electronic energy for a system with an even number N of electrons is given by the Eq. (100). For real orbitals, $\mathcal{L}_{pq}$ reduces to $\mathcal{K}_{pq}$, so the energy functional (100) becomes a $\mathcal{JK}$-only NOF, which for the present chapter is conveniently rewritten as

$$E_{el} = 2\sum_p n_p \mathcal{H}_{pp} + 2\sum_{pq}(n_q n_p - \Delta_{qp})\mathcal{J}_{pq} - \sum_{pq}(n_q n_p - \Delta_{qp} - \Pi_{qp})\mathcal{K}_{pq}. \tag{129}$$

Accordingly, the analytical gradients for PNOF are given by Eq. (126) together with the 1 and 2RDM defined in (128), where the latter is now expressed as

$$D_{\mu\eta\upsilon\delta} = \sum_{pq}[2(n_q n_p - \Delta_{qp})\mathcal{C}_{\mu p}\mathcal{C}_{\upsilon p}\mathcal{C}_{\eta q}\mathcal{C}_{\delta q} - (n_q n_p - \Delta_{qp} - \Pi_{qp})\mathcal{C}_{\mu p}\mathcal{C}_{\delta p}\mathcal{C}_{\eta q}\mathcal{C}_{\upsilon q}]. \tag{130}$$

Note that the four-index summation appearing in Eq. (128) for the 2RDM is reduced to only two in Eq. (130), due to the two-index nature of the PNOF reconstruction that leads to a $\mathcal{JKL}$-only NOF [101].

5.1.2.2 Electron pairing approaches

In accordance to electron-pairing constraints (Eq. 102) satisfied by these approximations, we may associate new Lagrange multipliers $\{\mu_g\}$ with the F pairing conditions (102), instead of the chemical potential μ. It has been suggested [162] that the smallest μ_g can be then identified as the chemical potential of an open system. The auxiliary functional Λ (112) may be in turn redefined by the formula

$$\Lambda = E_{el} - 2\sum_{g=1}^{F}\mu_g\Big(\sum_{p\in\Omega_g} n_p - 1\Big) - 2\sum_{qp}\lambda_{pq}\left(\langle\varphi_q|\varphi_p\rangle - \delta_{qp}\right). \tag{131}$$

The partial derivative $(\partial E/\partial n_p)$, holding the spatial NOs $\{\varphi_g\}$ fixed, are now given by the expressions

$$\frac{\partial E_{el}}{\partial n_p} = 2\mathcal{H}_{pp} + \frac{\partial V_{ee}}{\partial n_p} = 2\mu_g,\ \forall p \in \Omega_g. \tag{132}$$

Regarding the analytical gradient equation for orbital pairing approaches, the Eq. (124) fulfills independently for each orbital subspace g due to relation (102),

$$\sum_{p\in\Omega_g} \frac{\partial n_p}{\partial x_A} = 0, \tag{133}$$

thereby the contribution to the gradient becomes zero for each subspace

$$\sum_g \sum_{p\in\Omega_g} \frac{\partial E_{el}}{\partial n_p}\frac{\partial n_p}{\partial x_A} = 2\sum_g \mu_g \sum_{p\in\Omega_g} \frac{\partial n_p}{\partial x_A} = 0. \tag{134}$$

In consequence, the analytical energy gradients (126) remain unmodified for orbital pairing approaches.

5.1.3 Computational aspects

Eq. (126) implies that we do not require an iterative procedure for evaluating the derivative of the total energy with respect to the coordinate x_A. The gradient can be efficiently computed by first calculating the quantities $\Gamma_{\mu\upsilon}$, $D_{\mu\eta\upsilon\delta}$, and $\lambda_{\mu\upsilon}$, subsequently contracting by derivatives of the integrals.

In contrast to what happens in other post-HF theories, our methodology allows the calculation of analytic energy gradients by the simple evaluation without resorting to the linear-response theory. Our gradient computation is therefore analogous to that which is performed at the HF level of theory with the corresponding savings of computational time. Indeed, the PNOF analytic gradient reduces to the HF expression after removing Δ and Π matrices in Eq. (130), i.e., the two-electron cumulant matrix [101]. Consequently, as it happens in the HF case, the bottleneck of gradient evaluation is the computation of the two-electron contribution, since 12 gradient components arise from each two-electron integral [76]. In this sense, our approach is similar to the projected Hartree-Fock method that recovers a significant portion of static correlation too [163].

Overall, the calculation scales nominally as M^5 (M being the number of basis set functions) due to the pq-linkage in the auxiliary matrices of the PNOF $D_{\mu\eta\upsilon\delta}$, given by Eq. (130). However, in case of pairing approximations, the auxiliary matrices could contain a lot of zeros corresponding to neglecting ONs of the higher NOs in energy. For instance, in case of simplest pairing, PNOF5

or PNOF6, the number of involved NOs with non-zero occupancies is equal to the the number of electrons N, therefore, the summations by p and q, in Eq.(130), are up to N instead of M, and the scaling reduces from M^5 to $N \cdot M^4$. Obviously, factorized PNOF auxiliary matrices Δ and Π, i.e., $\Delta_{qp} = \Delta_q \Delta_p$ and $\Pi_{qp} = \Pi_q \Pi_p$, could reduce the scaling to M^4. In this case, we could make the summations by p and q before contracting by derivatives of the integrals, in a similar way to what one does in the HF approximation.

In practice, the scaling is also reduced by applying a previous screening of two-electron integrals based on Schwarz' inequality [77], especially in the case of large systems where the smallness of most two-electron integrals allows to skip their evaluation. In any case, the basis set employed determines the computational time instead of the number of geometrical degrees of freedom.

In the present implementation, as there is no constrain regarding the nuclear coordinates of the system, we use the well-known nonlinear conjugate gradient (CG) method [164] to locate ground state equilibrium geometries. This algorithm associates conjugacy properties with the steepest descent method, so that both efficiency and reliability are achieved, as reflected in the results reported in the next section. The main advantage is that the method requires only gradient evaluations and does not use much storage, because the search direction is acquired from linear combinations of the gradient obtained in the previous iteration. Its main drawback is that the search direction is not necessarily down. Herein, the studied systems are simple molecules with starting configurations close to the optimized geometries, therefore we have no doubt that they are equilibrium geometries. For diatomic molecules herein studied, the harmonic frequency analyses have already been done in previous works [44, 57, 165]. Nevertheless, to be sure of having reached a minimum in the other systems, it is required to compute the Hessian (matrix of second derivatives) in addition to the gradient. Note that it is possible to avoid the problems inherent to the analytic calculation of the Hessian, such as storage issues, solving coupled-perturbed equations, or computing the large amount of two-electron integral second derivatives, by a numerical differentiation of analytic gradients [85].

5.1.3.1 Separability

According to Eq. (126), the bottleneck of computing NOF gradients is due to $D_{\mu\eta,\upsilon\delta}$, which involves [62] a formal scaling of M^5 being M the number of functions present in the given basis set. In the following, we show that for some approximations it is possible to reduce the computational cost by summing over molecular orbital (MO) indices separately. Indeed, it is

known that for the HF approximation Eq. (126) scales as M^4. When electron correlation is considered, the same technique can be used whenever the cumulant matrices are factorized. The latter is best explained with an example. To this end we use the cumulant matrix corresponding to PNOF5 (Eq. 104). First, let us focus on the transformation of the Δ matrix to the AO representation, such that the term accompanying the Coulomb integrals $\mathcal{J}_{pq}$ reads as

$$\begin{aligned}
&\sum_{p,q}\left(n_p n_q-\Delta_{pq}\right)C_{\mu p}C_{\upsilon p}C_{\eta q}C_{\delta q}=\sum_{g=1}^{F}\sum_{p,q\epsilon\Omega_g}\left[n_p n_q-n_p^2\delta_{pq}-\left(1-\delta_{pq}\right)n_p n_q\right]C_{\mu p}C_{\upsilon p}C_{\eta q}C_{\delta q}\\
&+\sum_{g\neq f}^{F}\sum_{p\epsilon\Omega_g}\sum_{q\epsilon\Omega_f}n_p n_q C_{\mu p}C_{\upsilon p}C_{\eta q}C_{\delta q}=\sum_{g\neq f}^{F}\left[\sum_{p\epsilon\Omega_g}n_p C_{\mu p}C_{\upsilon p}\right]\left[\sum_{q\epsilon\Omega_f}n_q C_{\eta q}C_{\delta q}\right]=\sum_{g\neq f}^{F}D^g_{\mu\upsilon}D^f_{\eta\delta}\\
&=\left(\sum_{g=1}^{F}D^g_{\mu\upsilon}\right)\left(\sum_{f=1}^{F}D^f_{\eta\delta}\right)-\sum_{g=1}^{F}D^g_{\mu\upsilon}D^g_{\eta\delta}=D_{\mu\upsilon}D_{\eta\delta}-\sum_{g=1}^{F}D^g_{\mu\upsilon}D^g_{\eta\delta}.
\end{aligned}\tag{135}$$

where $D^g_{\mu\upsilon}=\sum_{p\epsilon\Omega_g}n_p C_{\mu p}C_{\upsilon p}$ and $D_{\mu\upsilon}=\sum_{g=1}^{\mathrm{N}/2}D^g_{\mu\upsilon}$. Eq. (135) scales as $L\cdot M^4$, where L is a prefactor equal to the number of orbitals up to the N/2 level. The remaining cumulant part is given by the Π matrix as

$$\begin{aligned}
&\sum_{p,q}\Pi_{pq}C_{\mu p}C_{\upsilon p}C_{\eta q}C_{\delta q}=\sum_{g=1}^{F}\sum_{p,q\epsilon\Omega_g}\left[n_p\delta_{pq}+\left(1-\delta_{pq}\right)\Pi^g_{pq}\right]C_{\mu p}C_{\upsilon p}C_{\eta q}C_{\delta q}=\\
&\sum_{g=1}^{F}\sum_{p\epsilon\Omega_g}n_p C_{\mu p}C_{\upsilon p}C_{\eta p}C_{\delta p}+\sum_{g=1}^{F}{\sum_{p,q\epsilon\Omega_g}}'\Pi^g_{pq}C_{\mu p}C_{\upsilon p}C_{\eta q}C_{\delta q}=\\
&\sum_{g=1}^{F}\sum_{p\epsilon\Omega_g}n_p C_{\mu p}C_{\upsilon p}C_{\eta p}C_{\delta p}+\sum_{g=1}^{F}\Bigg\{-\sum_{q\epsilon\Omega'_g}\sqrt{n_g n_q}C_{\mu g}C_{\upsilon g}C_{\eta q}C_{\delta q}\\
&-\sum_{p\epsilon\Omega'_g}\sqrt{n_g n_p}C_{\mu p}C_{\upsilon p}C_{\eta g}C_{\delta g}+{\sum_{p,q\epsilon\Omega'_g}}'\sqrt{n_q n_p}C_{\mu p}C_{\upsilon p}C_{\eta q}C_{\delta q}\Bigg\}=\\
&\sum_{g=1}^{F}\Bigg\{\sum_{p\epsilon\Omega_g}n_p C_{\mu p}C_{\upsilon p}C_{\eta p}C_{\delta p}-\sqrt{n_g}C_{\mu g}C_{\upsilon g}\sum_{q\epsilon\Omega'_g}\sqrt{n_q}C_{\eta q}C_{\delta q}\\
&-\sqrt{n_g}C_{\eta g}C_{\delta g}\sum_{p\epsilon\Omega'_g}\sqrt{n_p}C_{\mu p}C_{\upsilon p}+\widetilde{D}^g_{\mu\upsilon}\widetilde{D}^g_{\eta\delta}-\sum_{p\epsilon\Omega'_g}n_p C_{\mu p}C_{\upsilon p}C_{\eta p}C_{\delta p}\Bigg\},
\end{aligned}\tag{136}$$

where $\widetilde{D}^g_{\mu\upsilon} = \sum_{p\epsilon\Omega'_g}{}' \sqrt{n_p} C_{\mu p} C_{\upsilon p}$. Rearranging some terms in Eq. (136) we arrive to

$$\begin{aligned}\sum_{p,q} \Pi_{pq} C_{\mu p} C_{\upsilon p} C_{\eta q} C_{\delta q} &= \sum_{g=1}^{F} \Big\{ n_g C_{\mu g} C_{\upsilon g} C_{\eta g} C_{\delta g} - \sqrt{n_g} C_{\mu g} C_{\upsilon g} \widetilde{D}^g_{\eta\delta} \\ -\sqrt{n_g} \widetilde{D}^g_{\mu\upsilon} C_{\eta g} C_{\delta g} + \widetilde{D}^g_{\mu\upsilon} \widetilde{D}^g_{\eta\delta} \Big\} &= \sum_{g=1}^{F} \left[\widetilde{D}^g_{\mu\upsilon} - \sqrt{n_g} C_{\mu g} C_{\upsilon g} \right] \left[\widetilde{D}^g_{\eta\delta} - \sqrt{n_g} C_{\eta g} C_{\delta g} \right] \\ &= \sum_{g=1}^{F} \left[D^g_{\mu\upsilon} \right]^{\frac{1}{2}} \left[D^g_{\eta\delta} \right]^{\frac{1}{2}}.\end{aligned} \tag{137}$$

Note that Eq. (137) has the same computational cost as Eq. (135), so overall the cost corresponding to $D_{\mu\eta,\upsilon\delta}$ is reduced considerably by using separability of MO indexes. The factorization of PNOF5 described above can be easily extended to PNOF7. To this end we have to consider the inter-pair correlation terms

$$\begin{aligned}-\sum_{g\neq f}^{F} \left[\sum_{p\epsilon\Omega_g} \sqrt{n_p \left(1-n_p\right)} C_{\mu p} C_{\upsilon p} \right] \left[\sum_{q\epsilon\Omega_f} \sqrt{n_q \left(1-n_q\right)} C_{\eta q} C_{\delta q} \right] = \\ -\sum_{g\neq f}^{F} \phi^g_{\mu\upsilon} \phi^f_{\eta\delta} = -\left(\sum_g \phi^g_{\mu\upsilon} \right) \left(\sum_f \phi^f_{\eta\delta} \right) + \sum_g \phi^g_{\mu\upsilon} \phi^g_{\eta\delta}.\end{aligned} \tag{138}$$

where $\phi^g_{\mu\upsilon} = \sum_{p\epsilon\Omega_g} \sqrt{n_p \left(1-n_p\right)} C_{\mu p} C_{\upsilon p}$. Thus, the term accompanying the exchange integrals $\mathcal{K}_{pq}$ reads as

$$\sum_{p,q} \Pi_{pq} C_{\mu p} C_{\upsilon p} C_{\eta q} C_{\delta q} = \sum_{g=1}^{F} \left[D^g_{\mu\upsilon} \right]^{\frac{1}{2}} \left[D^g_{\eta\delta} \right]^{\frac{1}{2}} - \left(\sum_g \phi^g_{\mu\upsilon} \right) \left(\sum_f \phi^f_{\eta\delta} \right) + \sum_g \phi^g_{\mu\upsilon} \phi^g_{\eta\delta}. \tag{139}$$

Recall that formally the computational cost corresponding to PNOF5 and PNOF7 is the same, so a more complex functional form does not necessarily imply higher computation time.

Let us give an example to illustrate the gain when computing energy gradients. As it is shown in Table 1, the computation time is significantly reduced if separability is employed for both PNOF5 and PNOF7, independently of the number of orbitals considered in the calculation (determined by M and N_g).

5.1.4 Equilibrium geometries

In this section, we carry out a NOF study of the ground-state equilibrium geometries for a selected set of spin-compensated molecules. This set includes the following 15 systems: HF, H_2O, NH_3, CH_4, N_2, CO, HOF, HNO, H_2CO, HNNH, H_2CCH_2, HCCH, HCN, HNC, and O_3. As

Table 15 – Computation time (sec) obtained using the cc-pVTZ basis set for the energy gradient of C_2H_4. N_g determines the number of weak orbitals coupled with each strongly occupied orbital in each subspace.

	without separability	with separability
PNOF5 ($N_g = 1$)	14	8
PNOF7 ($N_g = 20$)	37	28

functionals, orbital-pairing approaches were used, namely, PNOF5, PNOF7 and PNOF6. These functionals, including their extended versions, take into account most of the non-dynamical effects, but also the important part of dynamical electron correlation corresponding to the intra-pair interactions [44, 56, 60, 61, 151, 166, 167]. PNOF5 does not describe correlation between electron pairs at all, while PNOF6 includes mostly non-dynamic inter-pair correlation. In order to include a non-separable functional such as PNOF6, separability is not considered in the present section.

We use HF geometries as starting points to PNOF optimizations. For comparison, we have included high-quality empirical equilibrium structures obtained from least-squares fits involving experimental rotational constants and theoretical vibrational corrections [78]. Furthermore, the corresponding CCSD [75] values are included. All calculations are carried out using the correlation-consistent polarized triple-zeta (cc-pVTZ) basis set developed by Dunning and coworkers [87], which are suitable in correlated calculations [78].

Tables 16 and 17 show respectively the errors in bond lengths and bond angles obtained for the selected set of molecules at PNOF5, PNOF6 and CCSD levels of theory, along with the empirical equilibrium structures. Note that reported NOF results involve the simplest coupling ($N_g = 1$) in our calculations, so each orbital below the Fermi level is coupled with a single orbital above it.

A survey of both tables 16 and 17 reveals that both NOFs employed here, PNOF5 and PNOF6, provide ground-state equilibrium structures comparable to those of the CCSD. For PNOF5, the corresponding mean absolute errors $\overline{\Delta}_{abs}$ are 0.75 degs and 0.8 pm for bond angles and bond lengths, respectively, which are slightly above 0.47 degs and 0.6 pm obtained by using the CCSD method. PNOF6 performs relatively worse for bond distances ($\overline{\Delta}_{abs} = 1.2$ pm), but it provides the best bond angles ($\overline{\Delta}_{abs} = 0.33$ degs), even better than the behavior of CCSD. The

Table 16 – Errors in the equilibrium bonds (in pm) at PNOF5, PNOF6, and CCSD levels of theory calculated by using the cc-pVTZ basis set with respect to empirical structural data. $\overline{\Delta}$ and $\overline{\Delta}_{abs}$ correspond to the mean signed error and mean absolute error, respectively.

Molecule	Bond	PNOF5	PNOF6	CCSD [75]	EMP. [78]
HF	H—F	-0.2	-0.3	-0.3	91.7
H_2O	O—H	0.1	-0.5	-0.2	95.8
NH_3	N—H	0.6	-0.3	-0.3	101.2
CH_4	C—H	1.5	-0.5	-0.1	108.6
N_2	N—N	-0.7	-1.4	-0.4	109.8
CO	C—O	-1.1	-1.5	-0.3	112.8
HNO	N—O	0.0	-1.3	-0.9	120.9
	H—N	-0.7	-2.1	-0.3	105.2
H_2CO	C—O	0.2	-1.1	-0.5	120.5
	C—H	0.4	-1.1	-0.4	110.1
HNNH	N—N	-0.1	-1.2	-0.7	124.6
	N—H	0.1	-1.6	-0.4	102.9
H_2CCH_2	C—C	0.9	-0.3	-0.4	133.1
	C—H	1.1	-0.7	-0.4	108.1
HCCH	C—C	-0.1	-1.0	-0.4	120.4
	C—H	0.7	-0.7	-0.4	106.1
HCN	C—N	-0.5	-1.3	-0.4	115.3
	C—H	0.5	-0.8	-0.6	106.5
HNC	C—N	-2.3	-1.3	-0.4	116.9
	N—H	-1.3	-1.0	-0.4	99.5
HOF	O—F	3.6	2.4	-1.9	143.4
	H—O	-0.3	-1.9	-0.5	96.8
O_3	O—O	2.6	-3.5	-3.6	127.2*
$\overline{\Delta}$		0.2	-1.0	-0.6	
$\overline{\Delta}_{abs}$		0.8	1.2	0.6	

*Geometry extracted from Ref. [8].

Table 17 – Errors in the equilibrium bond angles (in degs) at PNOF5, PNOF6, and CCSD levels of theory calculated by using the cc-pVTZ basis set with respect to empirical structural data. $\overline{\Delta}$ and $\overline{\Delta}_{abs}$ correspond to the mean signed error and mean absolute error, respectively.

Molecule	Bond angle	PNOF5	PNOF6	CCSD [75]	EMP. [78]
H_2O	H—O—H	0.23	0.04	-0.47	104.51
NH_3	H—N—H	0.45	-0.89	-0.89	107.25
HOF	H—O—F	-0.27	-0.22	0.43	97.94
HNO	H—N—O	-0.53	0.21	0.00	108.27
H_2CO	H—C—O	-0.09	0.07	0.29	121.63
HNNH	H—N—N	0.82	1.07	-0.04	106.36
H_2CCH_2	H—C—C	-0.15	0.00	0.03	121.43
O_3	O—O—O	-3.44	0.09	1.57	116.70*
$\overline{\Delta}$		-0.37	0.05	0.12	
$\overline{\Delta}_{abs}$		0.75	0.33	0.47	

*Geometry extracted from Ref. [8].

slight differences with respect to CCSD are mainly due to the HNC, HOF and O_3 molecules, for which the largest errors are observed.

It is worth noting that the systems studied in the current chapter can be well described by independent-pair approximations since they do not present delocalized electrons. For the latter, it is well-known that approaches like PNOF5 predict symmetry-breaking artifacts [44, 61]. On the other hand, the $\mathcal{JKL}$-only functional PNOF6 includes interactions between the electron pairs, but to the detriment of the correlation energy that recovers, which is smaller than that obtained with PNOF5 in the presented herein systems [44, 56]. That is why calculated bond distances decreases when going from PNOF5 to PNOF6, as happens when going to a lower-energy correlation method in wavefunction-based theories.

We note that the independent-pair approximation (PNOF5) underestimates some inter-atomic distances, while overestimates in other cases, with a slight tendency to the latter as evidenced by the mean signed value $\overline{\Delta}$ given in Table 16. It is worth to note that this trend has been observed when perturbative triples are included in CC theory [78] for the used basis set. On the other hand, the inclusion of the interactions between electron pairs by PNOF6, underestimates the bond distances in all studied cases, as CCSD consistently does, with the exception of the O—F length in the HOF molecule. In the case of bond angles, PNOF5 behaves similarly, but here the trend is slightly to underestimate, whereas PNOF6 reports practically equal values to experimental data ($\overline{\Delta} = 0.05$ degs), according to the results reported in Table 17. Obviously, more sample molecules are needed in order to come to a conclusion.

The case of ozone is remarkable, since none of the methods used in this chapter give a satisfactory result for the O—O bond length in comparison with the experimental value. Although, we should note that PNOF6 corrects the O—O—O bond angle obtained by using PNOF5, so the interactions between electron pairs seem to play an important role in O_3. Interestingly, for the employed cc-pVTZ basis set, CCSD(T) is able to correct the CCSD value and yield a bond distance of 127.6 pm [75] with an error of 0.4 pm, despite O_3 being a typical two-configuration system.

One of the possible ways to improve the results obtained herein is the inclusion of more orbitals in the description of the electron pairs. For simplicity, consider each orbital g is coupled to a fixed number of orbitals ($N_g = N_c$), which gives rise to the functionals PNOF5(N_c) or PNOF6(N_c) as appropriate. Taking into account that molecules studied here only comprise atoms of the first and second rows of the periodic table, the inclusion of 5 more orbitals in each subspace [PNOF5(5)] is suitable to improve our results. Our results for bond lengths and

Table 18 – Errors in the equilibrium bonds (in pm) at PNOF5, PNOF5(5), PNOF6, and PNOF6(5) levels of theory calculated by using the cc-pVTZ basis set with respect to empirical structural data. $\overline{\Delta}$ and $\overline{\Delta}_{abs}$ correspond to the mean signed error and mean absolute error, respectively.

Molecule	Bond	PNOF5	PNOF5(5)	PNOF6	PNOF6(5)
HF	H—F	-0.2	-0.5	-0.3	-1.2
H_2O	O—H	0.1	-0.3	-0.5	-0.9
NH_3	N—H	0.6	0.1	-0.3	-1.3
CH_4	C—H	1.5	-0.4	-0.5	-0.2
N_2	N—N	-0.7	-0.9	-1.4	-2.2
CO	C—O	-1.1	-1.4	-1.5	-1.8
HNO	N—O	0.0	-0.5	-1.3	-1.8
	H—N	-0.7	-1.4	-2.1	-2.1
H_2CO	C—O	0.2	-0.1	-1.1	-1.4
	C—H	0.4	-0.3	-1.1	-0.8
HNNH	N—N	-0.1	-0.4	-1.2	-1.7
	N—H	0.1	0.5	-1.6	-1.4
H_2CCH_2	C—C	0.9	0.6	-0.3	-0.8
	C—H	1.1	0.4	-0.7	-0.5
HCCH	C—C	-0.1	-0.8	-1.0	-1.7
	C—H	0.7	0.1	-0.7	-0.6
HCN	C—N	-0.5	-0.8	-1.3	-2.0
	C—H	0.5	-0.1	-0.8	-0.7
HNC	C—N	-2.3	-1.3	-1.3	-1.7
	N—H	-1.3	-0.6	-1.0	-0.9
HOF	O—F	3.6	3.3	2.4	-0.1
	H—O	-0.3	-0.9	-1.9	-1.9
O_3	O—O	2.6	1.4	-3.5	-3.8*
$\overline{\Delta}$		0.2	-0.2	-1.0	-1.4
$\overline{\Delta}_{abs}$		0.8	0.7	1.2	1.4

*For this molecule 3 orbitals are considered in each subspace.

Table 19 – Errors in the equilibrium bond angles (in degs) at PNOF5, PNOF5(5), PNOF6, and PNOF6(5) levels of theory calculated by using the cc-pVTZ basis set with respect to empirical structural data. $\overline{\Delta}$ and $\overline{\Delta}_{abs}$ correspond to the mean signed error and mean absolute error, respectively.

Molecule	Bond angle	PNOF5	PNOF5(5)	PNOF6	PNOF6(5)
H_2O	H—O—H	0.23	0.43	0.04	0.76
NH_3	H—N—H	0.45	-0.54	-0.89	0.46
HOF	H—O—F	-0.27	-0.25	-0.22	0.58
HNO	H—N—O	-0.53	0.07	0.21	0.31
H_2CO	H—C—O	-0.09	0.21	0.07	0.15
HNNH	H—N—N	0.82	1.01	1.07	1.01
H_2CCH_2	H—C—C	-0.15	0.02	0.00	0.21
O_3	O—O—O	-3.44	-2.99	0.09	0.38*
$\overline{\Delta}$		-0.37	-0.26	0.05	0.48
$\overline{\Delta}_{abs}$		0.75	0.69	0.33	0.48

* For this molecule 3 orbitals are considered in each subspace.

angles are reported in Tables 18 and 19, respectively.

By inspection of Table 18 one concludes that better description of the intra-pair electron correlation shortens calculated bond lengths. Accordingly, the performance of PNOF5 improves when the extended approach is employed, whereas in the case of PNOF6, which tends to underestimate bond distances, calculated geometries are slightly worse if more orbitals are included in the description of electron pairs. Table 19 shows that the mean absolute errors differ approximately in 0.1 degs for bond angles, so the use of extended versions of both functionals does not affect systematically our results.

Let us highlight some molecules for which the better description of the intra-pair correlation yields better geometrical parameters. In the case of methane, the C—H distance shortens from 110.1 pm to 108.2 pm, which closely compares to the experimental value of 108.6 pm. Similarly, the error in HNC bond lengths reduces from 2.3 pm and 1.3 pm to 1.3 pm and 0.6 pm, respectively, for the C—N and N—H bonds. It is worth noting that the only case for which PNOF6 overestimates a bond distance, the O—F bond in HOF molecule, is corrected using PNOF6(5), namely, this bond distance shortens from 145.9 pm to 143.4 pm, in outstanding agreement with the empirical value reported in Table 16.

5.1.4.1 PNOF7 equilibrium geometries

According to Tables 20 and 21, PNOF7 produces larger errors than PNOF5 for the studied equilibrium geometries. Indeed, PNOF7 retrieves most of static correlation effects but it lacks inter-pair dynamic correlation that are important in equilibrium region (*vide supra*). Hence, we expect that including gradients corresponding to second-order Møller-Plesset perturbative (MP2) corrections in the NOF-MP2 method [45, 46], the bond distances and angles will be corrected. A work in this direction is underway.

5.1.5 Conclusion

For first time, we have developed the direct analytical calculation of the energy derivatives with respect to nuclear motion in NOFT. Since the energy gradients give much information on potential energy surfaces and other properties, the study carried out in this work significantly extends the usefulness of NOFT.

It is well known that analytical gradients allow to speed up calculations and avoid numerical er-

Table 20 – Errors in the equilibrium bonds (in pm) at PNOF5, PNOF7, and CCSD levels of theory calculated by using the cc-pVTZ basis set with respect to empirical structural data. $\overline{\Delta}$ and $\overline{\Delta}_{abs}$ correspond to the mean signed error and mean absolute error, respectively.

Molecule	Bond	PNOF5	PNOF7	CCSD [75]	EMP. [78]
HF	H—F	-0.2	0.2	-0.3	91.7
H_2O	O—H	0.1	0.5	-0.2	95.8
NH_3	N—H	0.6	0.9	-0.3	101.2
CH_4	C—H	1.5	1.7	-0.1	108.6
N_2	N—N	-0.7	0.2	-0.4	109.8
CO	C—O	-1.1	-0.6	-0.3	112.8
HNO	N—O	0.0	1.7	-0.9	120.9
	H—N	-0.7	-0.5	-0.3	105.2
H_2CO	C—O	0.2	1.1	-0.5	120.5
	C—H	0.4	0.4	-0.4	110.1
HNNH	N—N	-0.1	1.3	-0.7	124.6
	N—H	0.1	0.4	-0.4	102.9
H_2CCH_2	C—C	0.9	1.9	-0.4	133.1
	C—H	1.1	1.3	-0.4	108.1
HCCH	C—C	-0.1	0.7	-0.4	120.4
	C—H	0.7	0.9	-0.4	106.1
HCN	C—N	-0.5	0.4	-0.4	115.3
	C—H	0.5	0.7	-0.6	106.5
HNC	C—N	-2.3	-0.2	-0.4	116.9
	N—H	-1.3	0.4	-0.4	99.5
HOF	O—F	3.6	8.2	-1.9	143.4
	H—O	-0.3	0.3	-0.5	96.8
$\overline{\Delta}$		0.1	1.0	-0.5	
$\overline{\Delta}_{abs}$		0.8	1.1	0.5	

Table 21 – Errors in the equilibrium bond angles (in degs) at PNOF5, PNOF7, and CCSD levels of theory calculated by using the cc-pVTZ basis set with respect to empirical structural data. $\overline{\Delta}$ and $\overline{\Delta}_{abs}$ correspond to the mean signed error and mean absolute error, respectively.

Molecule	Bond angle	PNOF5	PNOF7	CCSD [75]	EMP. [78]
H_2O	H—O—H	0.23	-0.09	-0.47	104.51
NH_3	H—N—H	0.45	-0.92	-0.89	107.25
HOF	H—O—F	-0.27	-1.35	0.43	97.94
HNO	H—N—O	-0.53	-0.67	0.00	108.27
H_2CO	H—C—O	-0.09	-0.51	0.29	121.63
HNNH	H—N—N	0.82	0.44	-0.04	106.36
H_2CCH_2	H—C—C	-0.15	0.14	0.03	121.43
$\overline{\Delta}$		0.07	-0.42	-0.09	
$\overline{\Delta}_{abs}$		0.36	0.59	0.31	

rors. The equations obtained herein allow computing analytic gradients of a correlated method without solving coupled equations as is the case in most post-HF methods, for example, in coupled cluster theories, so there is no need for iterative process to calculate the energy gradient in NOFT.

By using the nonlinear conjugate gradient method, we have optimized the structures of 15 spin-compensated molecules at the PNOF5 and PNOF6 levels of theory, employing the cc-pVTZ basis set of Dunning. In comparison with the CCSD method, the mean absolute error in bond distances obtained with PNOF5 differs only in 0.2 pm, although the difference increases to 0.6 pm when PNOF6 is employed. Bond angles calculated by using PNOF6 are the most accurate with mean signed error and mean absolute error equal to 0.05 and 0.33 degs, respectively. The present chapter proves the ability of both PNOF5 and PNOF6 to yield geometrical structures at lower computational cost than other post-HF methods.

The present study demonstrates the efficiency of computing energy gradients in NOFT, therefore its calculation in periodic solids is now affordable. The extension of NOFT to periodic systems has been done in the past [168–170], so we expect to achieve a computational efficiency close to that obtained in HF methodologies [171].

Finally, a comment about the optimization algorithm is mandatory. The nonlinear conjugate gradient method is often used to solve unconstrained optimization problems such as the energy minimization studied in this article. Its main advantage is that it requires only gradient evaluations and does not use much storage. Its main drawback is that the search direction is not necessarily down. To be sure of having reached a minimum or a transition state, or to improve our implementation with a Newton-like algorithm, we require computing the Hessian (matrix of second derivatives) in addition to the gradient. Then, the next section is dedicated to this task.

5.2 Analytic second-order derivatives in NOFT

5.2.1 Introduction

The matrix of second-order energy derivatives with respect to nuclear displacements, or just the Hessian, is directly related to many properties of great interest to chemists [79–82]. Derivative methods are widely used to characterize the stationary points on the potential energy surface, but are also essential for the study of high-resolution molecular spectroscopy [83], or geometry dependent molecular properties such as electrostatic moments [59]. Analytic first-order derivatives for RDM methods are well-established, e.g. for the parametric second-order RDM method [172], as well as analytical expressions of second-order energy derivatives are well-known for standard electronic structure methods. Nevertheless, the latter are still missing for methods that have been appeared in the last few decades, such as those derived directly from RDMs [32, 73, 173–176] without using the wavefunction.

In the last two decades, much effort has been put into making NOFT able to compete with well-established electronic structure methods [32,33]. In this vein, the analytic energy gradients in the atomic orbital representation for NOFT were obtained recently [62]. In the present chapter, an alternative expression for them in terms of the NOs is given. On the other hand, the analytical calculation of second-order derivatives is also desirable over numerical treatment when high accuracy is required. Here, for the first time in the context of NOFT, the second-order analytic energy derivatives with respect to nuclear displacements are given.

5.2.2 The Hessian

As it is shown in Ref. [62], the first-order derivative of the electronic energy with respect to Cartesian coordinate x of nucleus A, written in the atomic orbital representation, reads as

$$\frac{dE_{el}}{dx_A} = \sum_{\mu\upsilon}\Gamma_{\mu\upsilon}\frac{\partial\mathcal{H}_{\mu\upsilon}}{\partial x_A} + \sum_{\mu\upsilon\eta\delta}D_{\eta\delta,\mu\upsilon}\frac{\partial\left\langle\mu\upsilon|\eta\delta\right\rangle}{\partial x_A} - \sum_{\mu\upsilon}\lambda_{\mu\upsilon}\frac{\partial\mathcal{S}_{\mu\upsilon}}{\partial x_A}, \tag{140}$$

so the energy gradient depends only on the explicit derivatives of one- and two-electron integrals and the overlap matrix. Therefore, there is no contribution from ONs, and the resulting Eq. (140) does not require obtaining the NOs and ONs at the perturbed geometry. One could differentiate Eq. (140) to achieve an expression for the Hessian, nevertheless, perturbation of both NOs and ONs must be considered. For that purpose it is more convenient to work in the

NO representation $\{\phi_i\}$, so that Eq. (140) transforms into

$$\frac{dE_{el}}{dx_A} = \sum_i n_i \frac{\partial \mathcal{H}_{ii}}{\partial x_A} + \sum_{ijkl} D_{kl,ij} \frac{\partial \langle ij|kl\rangle}{\partial x_A} - \sum_{ij} S_{ij}^{x_A} \lambda_{ij}, \quad S_{ij}^{x_A} = \sum_{\mu\upsilon} C_{\mu i} C_{\upsilon j} \frac{\partial \mathcal{S}_{\mu\upsilon}}{\partial x_A}. \tag{141}$$

The NOs associated to the perturbed geometry are usually expressed as a linear combination of those NOs corresponding to the reference state, so a perturbation of x_A up to first order will carry out the next change in the ϕ_i

$$\phi_i + \delta x_A \left(\sum_j U_{ij}^{x_A} \phi_j + \sum_\mu C_{\mu i} \frac{\partial \zeta_\mu}{\partial x_A} \right) + \mathcal{O}\left(\delta x_A^2\right). \tag{142}$$

In Eq. (142), $\{\zeta_\mu\}$ are the atomic orbitals, whereas changes in NO coefficients are accounted by standard coupled-perturbed coefficients $\left\{U_{ij}^{x_A}\right\}$.

The orthonormality relation of the perturbed NOs provides the relationship [83]

$$\frac{\partial S_{ij}}{\partial x_A} = U_{ij}^{x_A} + U_{ji}^{x_A} + S_{ij}^{x_A} = 0, \tag{143}$$

which can be used to derive the relation

$$\sum_{ij} S_{ij}^{x_A} \lambda_{ij} = -2 \sum_{ij} U_{ij}^{x_A} \lambda_{ij}, \tag{144}$$

so the electronic energy gradients with respect to Cartesian coordinate x of nucleus A in the NO representation reads as

$$\frac{dE_{el}}{dx_A} = \sum_i n_i \frac{\partial \mathcal{H}_{ii}}{\partial x_A} + \sum_{ijkl} D_{kl,ij} \frac{\partial \langle ij|kl\rangle}{\partial x_A} + 2 \sum_{ij} U_{ij}^{x_A} \lambda_{ij}. \tag{145}$$

We may obtain second derivatives of the NOF energy by differentiating Eq. (145) with respect to coordinate y of nucleus B, namely,

$$\begin{aligned} \frac{d^2 E_{el}}{dx_A dy_B} = \sum_i n_i \frac{\partial^2 \mathcal{H}_{ii}}{\partial x_A \partial y_B} + \sum_{ijkl} D_{kl,ij} \frac{\partial^2 \langle ij|kl\rangle}{\partial x_A \partial y_B} + 2 \sum_{ij} U_{ij}^{y_B} \lambda_{ij}^{x_A} + 2 \sum_{ij} \frac{d}{dy_B} \left(U_{ij}^{x_A} \lambda_{ij} \right) \\ + \sum_m n_m^{y_B} \frac{\partial}{\partial n_m} \left(\frac{dE_{el}}{dx_A} \right). \end{aligned} \tag{146}$$

The first two terms in Eq. (146) contain the explicit derivatives of the core Hamiltonian and the two-electron integrals, respectively. The next two terms arise from the derivatives of NO coefficients with respect to the nuclear perturbation. Finally, $n_m^{y_B}$ represents the change in ON m due to perturbation y_B, so the last term in Eq. (146) accounts for the contribution from the perturbation of the ONs.

Taking into account Eq. (114), the matrix of Lagrange multipliers can be written as

$$\lambda_{ij} = n_j \mathcal{H}_{ij} + 2 \sum_{mkl} D_{kl,jm} \langle im|kl\rangle \,, \tag{147}$$

so explicit derivatives read as

$$\lambda_{ij}^{x_A} = n_j \frac{\partial \mathcal{H}_{ij}}{\partial x_A} + 2 \sum_{mkl} D_{kl,jm} \frac{\partial \langle im|kl\rangle}{\partial x_A}. \tag{148}$$

Regarding the fourth summation of Eq. (146), a more comprehensive expression can be obtained, namely,

$$\sum_{ij} \frac{d}{dy_B} \left(U_{ij}^{x_A} \lambda_{ij} \right) = \sum_{ij} \left\{ \frac{dU_{ij}^{x_A}}{dy_B} \lambda_{ij} + U_{ij}^{x_A} \frac{d\lambda_{ij}}{dy_B} \right\} \,, \tag{149}$$

where the first term in Eq. (149) is given by [83]

$$\frac{dU_{ij}^{x_A}}{dy_B} = U_{ij}^{x_A y_B} - \sum_k U_{ik}^{y_B} U_{kj}^{x_A}. \tag{150}$$

By using Eq. (143) together with the orthonormality relation of the NOs we arrive at [83]

$$\begin{aligned} \frac{\partial^2 S_{ij}}{\partial x_A \partial y_B} = U_{ij}^{x_A y_B} + U_{ji}^{x_A y_B} - \sum_m \{ S_{im}^{y_B} S_{jm}^{x_A} + S_{jm}^{y_B} S_{im}^{x_A} \\ - U_{im}^{y_B} U_{jm}^{x_A} - U_{jm}^{y_B} U_{im}^{x_A} \} + \sum_{\mu\upsilon} C_{\mu i} C_{\upsilon j} \frac{\partial^2 \mathcal{S}_{\mu\upsilon}}{\partial x_A \partial y_B} = 0, \end{aligned} \tag{151}$$

then

$$\begin{aligned} 2 \sum_{ij} U_{ij}^{x_A y_B} \lambda_{ij} = \sum_{ij} \lambda_{ij} \left(\sum_m \{ S_{im}^{y_B} S_{jm}^{x_A} + S_{jm}^{y_B} S_{im}^{x_A} \right. \\ \left. - U_{im}^{y_B} U_{jm}^{x_A} - U_{jm}^{y_B} U_{im}^{x_A} \} - \sum_{\mu\upsilon} C_{\mu i} C_{\upsilon j} \frac{\partial^2 \mathcal{S}_{\mu\upsilon}}{\partial x_A \partial y_B} \right). \end{aligned} \tag{152}$$

The derivative of Lagrange multipliers is obtained differentiating Eq. (147)

$$\frac{d\lambda_{ij}}{dy_B} = \lambda_{ij}^{y_B} + \sum_k U_{ki}^{y_B} \lambda_{kj} + \sum_{kl} U_{kl}^{y_B} Y_{ijkl}, \tag{153}$$

where

$$Y_{ijkl} = n_j \delta_{jl} \mathcal{H}_{ik} + 2 \sum_{mn} D_{ln,jm} \langle im|kn\rangle + 4 \sum_{mn} D_{mn,jl} \langle ik|mn\rangle \,.$$

In Eq. (153), the response from ONs has been omitted since it is included later. Overall the fourth summation in Eq. (146) is given by

$$\sum_{ij} \frac{d}{dy_B} \left(U_{ij}^{x_A} \lambda_{ij} \right) = \sum_{ij} \left\{ U_{ij}^{x_A y_B} \lambda_{ij} + U_{ij}^{x_A} \lambda_{ij}^{y_B} + \sum_{kl} U_{ij}^{x_A} U_{kl}^{y_B} Y_{ijkl} \right\} \,. \tag{154}$$

In the last summation of Eq. (146), the derivatives with respect to the occupancies read as

$$\frac{\partial}{\partial n_m}\left(\frac{\partial E_{el}}{\partial x_A}\right) = \frac{\partial \mathcal{H}_{mm}}{\partial x_A} + 2\sum_{ij} U_{ij}^{x_A}\frac{\partial \lambda_{ij}}{\partial n_m} + \sum_{ijkl}\frac{\partial D_{kl,ij}}{\partial n_m}\frac{\partial \langle ij|kl\rangle}{\partial x_A}, \tag{155}$$

where

$$\frac{\partial \lambda_{ij}}{\partial n_m} = \delta_{mj}\mathcal{H}_{ij} + 2\sum_{rkl}\frac{\partial D_{kl,jr}}{\partial n_m}\langle ir|kl\rangle \ . \tag{156}$$

Note that $\partial D_{kl,jr}/\partial n_m$ is determined by the given two-particle RDM reconstruction $D\left[n_i, n_j, n_k, n_l\right]$. Substituting Eqs. (154) and (155) into Eq. (146), we obtain the general expression for the Hessian in the NO representation, namely,

$$\begin{aligned}\frac{d^2 E_{el}}{dx_A dy_B} = &\sum_i n_i \frac{\partial^2 \mathcal{H}_{ii}}{\partial x_A \partial y_B} + \sum_{ijkl} D_{kl,ij}\frac{\partial^2 \langle ij|kl\rangle}{\partial x_A \partial y_B} + 2\sum_{ij}\left(U_{ij}^{y_B}\lambda_{ij}^{x_A} + U_{ij}^{x_A}\lambda_{ij}^{y_B} + U_{ij}^{x_A y_B}\lambda_{ij}\right) \\ &+2\sum_{ijkl} U_{ij}^{x_A}U_{kl}^{y_B}Y_{ijkl} + \sum_m n_m^{y_B}\left(\frac{\partial \mathcal{H}_{mm}}{\partial x_A} + 2\sum_{ij}U_{ij}^{x_A}\frac{\partial \lambda_{ij}}{\partial n_m} + \sum_{ijkl}\frac{\partial D_{kl,ij}}{\partial n_m}\frac{\partial \langle ij|kl\rangle}{\partial x_A}\right).\end{aligned} \tag{157}$$

In contrast to first-order energy derivatives, the calculation of the analytic Hessian requires the knowledge of NOs and ONs at the perturbed geometry, expressed in Eq. (157) by coefficients U and $n_m^{y_B}$, respectively. Both magnitudes are obtained from the solution of coupled-perturbed equations which are the result of deriving the variational conditions (113-114). It is worth noting that in the case of Eq. (114), it is more convenient to use its combination with its Hermitian conjugate equation that gives us the variational condition on the Hermiticity of Lagrange multipliers ($\lambda - \lambda^\dagger = 0$).

5.2.3 Coupled-perturbed equations

Coupled-perturbed equations for NOs and ONs were derived by Pernal and Baerends [84] to obtain the linear response of Γ in a problem with a one-electron static perturbation in the Hamiltonian. In particular, these equations were employed in the calculation of the static polarizabilities of atoms and molecules. The formalism was later extended by Giesbertz [177] to deal with pinned ONs.

Here we present the coupled-perturbed equations for NOs and ONs considering from the beginning that NOs have an explicit dependence on the perturbation (Eq. 142) through the position dependence of the basis functions. Therefore, instead of considering an anti-Hermitian U matrix as done in Refs. [84,177], standard coupled-perturbed coefficients are related with the overlap matrix S by Eq. (143). In addition, the existence of a generalized Fock matrix has not

been assumed in the present derivation. Our coupled-perturbed equations are obtained from the Euler equations (113-114), which are valid for any approximate NOF.

For real orbitals, at the extremum, the total derivatives of the variational condition on the Hermiticity of Lagrange multipliers vanishes,

$$\frac{d}{dx_A}\left(\lambda_{ij}-\lambda_{ji}\right)=0. \tag{158}$$

Taking into account Eqs. (153) and (156), Eq. (158) can be rewritten as

$$\begin{aligned}\lambda_{ij}^{x_A}-\lambda_{ji}^{x_A}+\sum_k\left(U_{ki}^{x_A}\lambda_{kj}-U_{kj}^{x_A}\lambda_{ki}\right)+\sum_{kl}(U_{kl}^{x_A}\\ Y_{ijkl}-U_{kl}^{x_A}Y_{jikl})+\sum_k\left(\frac{\partial\lambda_{ij}}{\partial n_k}-\frac{\partial\lambda_{ji}}{\partial n_k}\right)n_k^{x_A}=0.\end{aligned} \tag{159}$$

Eq. (143) can be used to simplify first and second summations in Eq. (159), namely,

$$\sum_k U_{ki}^{x_A}\lambda_{kj}=\sum_{k>l}[U_{kl}^{x_A}\left(\lambda_{kj}\delta_{li}-\lambda_{lj}\delta_{ki}\right)-S_{kl}^{x_A}\lambda_{lj}\delta_{ki}]-\frac{1}{2}\sum_k S_{kk}^{x_A}\lambda_{kj}\delta_{ki}, \tag{160}$$

$$\sum_{kl}U_{kl}^{x_A}Y_{ijkl}=\sum_{k>l}[U_{kl}^{x_A}\left(Y_{ijkl}-Y_{ijlk}\right)\ -S_{kl}^{x_A}Y_{ijlk}]-\frac{1}{2}\sum_k S_{kk}^{x_A}Y_{ijkk}. \tag{161}$$

Accordingly, Eq. (159) can be rewritten as

$$\begin{aligned}\lambda_{ij}^{x_A}-\lambda_{ji}^{x_A}+\sum_k\left(\frac{\partial\lambda_{ij}}{\partial n_k}-\frac{\partial\lambda_{ji}}{\partial n_k}\right)n_k^{x_A}-\frac{1}{2}\sum_k S_{kk}^{x_A}\left(\delta_{ki}\lambda_{kj}-\delta_{kj}\lambda_{ki}+Y_{ijkk}-Y_{jikk}\right)\\ +\sum_{k>l}U_{kl}^{x_A}\left(\delta_{li}\lambda_{kj}-\delta_{ki}\lambda_{lj}-\delta_{lj}\lambda_{ki}+\delta_{kj}\lambda_{li}+Y_{ijkl}-Y_{ijlk}-Y_{jikl}+Y_{jilk}\right)\\ -\sum_{k>l}S_{kl}^{x_A}\left(\delta_{ki}\lambda_{lj}-\delta_{kj}\lambda_{li}+Y_{ijlk}-Y_{jilk}\right)=0\end{aligned} \tag{162}$$

Let us now consider the Eq. (113) involving derivatives with respect to ONs. A perturbation up to first order transforms it into

$$\begin{aligned}\frac{\partial\mathcal{H}_{mm}}{\partial x_A}+\sum_{ijkl}\frac{\partial D_{kl,ij}}{\partial n_m}\frac{\partial\left\langle ij|kl\right\rangle}{\partial x_A}+\sum_{rijkl}\frac{\partial^2 D_{kl,ij}}{\partial n_m\partial n_r}\left\langle ij|kl\right\rangle n_r^{x_A}\\ +2\sum_{ij}\left[U_{ij}^{x_A}\left(\delta_{jm}\mathcal{H}_{ij}+2\sum_{rkl}\frac{\partial D_{kl,jr}}{\partial n_m}\left\langle ir|kl\right\rangle\right)\right]=\mu^{x_A}.\end{aligned} \tag{163}$$

Taking into account Eq. (143), Eq. (163) can be rewritten in compact form as

$$\sum_r W_{mr}n_r^{x_A}+\sum_{i>j}U_{ij}^{x_A}\left(E_{ij}^m-E_{ji}^m\right)=F_m^{x_A}, \tag{164}$$

where

$$F_m^{x_A} = \mu^{x_A} - \left(\frac{\partial \mathcal{H}_{mm}}{\partial x_A} + \sum_{ijkl} \frac{\partial D_{kl,ij}}{\partial n_m} \frac{\partial \langle ij|kl\rangle}{\partial x_A} \right) + \sum_{i>j} S_{ij}^{x_A} E_{ji}^m + \tfrac{1}{2} \sum_i S_{ii}^{x_A} E_{ii}^m,$$

$$E_{ij}^m = 2\delta_{jm}\mathcal{H}_{ij} + 4\sum_{rkl} \frac{\partial D_{kl,jr}}{\partial n_m} \langle ir|kl\rangle ,$$

$$W_{mr} = \sum_{ijkl} \frac{\partial^2 D_{kl,ij}}{\partial n_m \partial n_r} \langle ij|kl\rangle .$$

Note that E_{ij}^m relates to $\partial\lambda_{ij}/\partial n_m$ by a factor 1/2 according to Eq. (156), so Eqs. (162) and (164) can bring together to obtain the complete expression for the coupled-perturbed NOF equations

$$\begin{aligned} \forall_{i>j} \ \sum_{k>l} A_{ij,kl} U_{kl}^{x_A} + \left(E_{ij}^k - E_{ji}^k\right) n_k^{x_A} &= B_{ij}^{x_A} \\ \forall_i \quad \sum_{k>l} \left(E_{kl}^i - E_{lk}^i\right) U_{kl}^{x_A} + W_{ik} n_k^{x_A} &= F_i^{x_A} \end{aligned} \tag{165}$$

where

$$A_{ij,kl} = \delta_{li}\lambda_{kj} - \delta_{ki}\lambda_{lj} - \delta_{lj}\lambda_{ki} + \delta_{kj}\lambda_{li} + Y_{ijkl} - Y_{ijlk} - Y_{jikl} + Y_{jilk},$$

$$B_{ij}^{x_A} = \sum_{k>l} S_{kl}^{x_A} \left(\delta_{ki}\lambda_{lj} - \delta_{kj}\lambda_{li} + Y_{ijkl} - Y_{jilk}\right) + \frac{1}{2}\sum_k S_{kk}^{x_A} \left(\delta_{ki}\lambda_{kj} - \delta_{kj}\lambda_{ki} + Y_{ijkk} - Y_{jikk}\right) + \lambda_{ij}^{x_A} + \lambda_{ji}^{x_A}.$$

It is worth noting that the coupled-perturbed equations given by Eq. (165) are totally general, so that an expression for the reconstructed $D\left[n_i, n_j, n_k, n_l\right]$ is only required. The here presented formulation of such equations exploits Eq. (143) to calculate only necessary U coefficients, namely, the lower (or upper) block of matrix U.

The matricial form of Eq. (165) is

$$\begin{pmatrix} A & E - E^\dagger \\ E - E^\dagger & W \end{pmatrix} \begin{pmatrix} U^{x_A} \\ n^{x_A} \end{pmatrix} = \begin{pmatrix} B^{x_A} \\ F^{x_A} \end{pmatrix}, \tag{166}$$

where $E^\dagger$ represents conjugate transpose operation only acting on the subindexes, and it makes clear the symmetric nature of the square matrix. The latter has to be computed and inverted only once, since it is independent of the perturbation δx_A, and presents only dependence on non-perturbed NOs and ONs.

5.2.4 Computational aspects

In contrast to first-order derivatives (126), coupled-perturbed equations must be solved to evaluate the Hessian expression (157), so the corresponding computational cost increases dramatically. In fact, previous calculations involving coupled-perturbed equations in NOFAs have been

applied only to very small systems [178], e.g, single atoms or molecular dimers. Second-order energy derivatives are computationally much more demanding in terms of storage capacity than the evaluation of the total electronic energy or gradients. Indeed, derivative of two-electron integrals are 45 times greater in number than usual four-index integrals [85]. In order to overcome these drawbacks, in the following we use the numerical differentiation procedure to obtain the Hessian, specifically the $6N_a$ point formula (N_a being the number of atoms). The use of analytic gradients to compute the second derivatives has been developed efficiently before [85], where it has been assured that an analytic evaluation of the second derivatives is not necessarily much more efficient than a numerical differentiation of analytic gradients.

5.2.5 Harmonic vibrational frequencies

Second-order energy derivatives make the calculation of harmonic vibrational frequencies commonplace. Analogous to the procedure described in Ref. [86], the Hessian is obtained by numerical differentiation of analytic gradients and immediately after it is converted to mass weighted cartesian coordinates (MWC), i.e.

$$\left(\frac{\partial^2 E}{\partial x_A \partial y_B}\right)_{MWC} = \frac{1}{m_A m_B}\frac{\partial^2 E}{\partial x_A \partial y_B}. \tag{167}$$

We obtain a set of $3N_a$ eigenvectors corresponding to normal modes, and $3N_a$ eigenvalues corresponding to the harmonic vibrational frequencies of the molecule. Unfortunately, there are 6 eigenvalues corresponding to overall translation and rotation that are not exactly zero at a general point of the energy surface [179]. In fact, for displacements that are not rigorously orthogonal in the $3N_a$ dimensional vector space to the gradient vector, the potential is not quadratic, so rotational and translational contaminant modes may arise. The Eckart-Sayvetz conditions are an indicator of this contamination [180], thereby they can be employed to ensure separation of the vibrational motions via projection techniques. Thus, the Hessian is projected in order to restrict the displacements to be orthogonal to the $3N_a$ dimensional vectors corresponding to the rotations and translations of the system, i.e. displacements satisfying the Eckart-Sayvetz conditions are the only ones allowed.

We have made a comparison between harmonic vibrational frequencies obtained by using CCSD, MP2 and PNOF7, with respect to experimental fundamentals. CCSD, MP2 and experimental values are obtained from Ref. [8]. Harmonic vibrational frequencies correspond to the set of molecules H_2O, NH_3, CH_4, N_2, CO, HNO, H_2CO, HNNH, H_2CCH_2, HNC, HCCH, HOF, LiH, HF, C_2H_2, H_2O_2, Li_2, LiH, HCN, F_2, CO_2, H_2, PH_3, SiH_4, H_2S, HCl, Na_2, P_2, Cl_2, NaCl, CS,

SiO, ClF, and HOCl. All calculations are carried out by using the cc-pVTZ basis set [87] and the maximum N_g value allowed by the basis set.

Fig. 23 shows the distribution of the errors for the above mentioned set of molecules. According to these plots, PNOF7 shows good agreement with CCSD and MP2. The latter has several errors between 150 and 200 cm^{-1}, whereas the distributions corresponding to both CCSD and PNOF7 show most of the results with errors below 100 cm^{-1}. Regarding the average values, there are no significance differences between the three methods: $\overline{\triangle}(PNOF7) = 104 cm^{-1}$ over, $\overline{\triangle}(MP2) = 104 cm^{-1}$ and $\overline{\triangle}(CCSD) = 100 cm^{-1}$. It is worth noting that the large differences between experimental fundamental frequencies and theoretically determined harmonic vibrational frequencies are systematic, so scaling factors can be used to correct anharmonic effects in the determination of those values [88].

5.2.6 Closing remarks

Simple analytic expressions have been derived for computation of the second-order energy derivatives with respect to nuclear displacements in the context of NOFT. An alternative expression for analytic gradients in terms of the NOs is given as well. In contrast to first-order energy derivatives, the calculation of the analytic Hessian requires the knowledge at the perturbed geometry of NOs and ONs, which are obtained from the solution of coupled-perturbed equations.

The coupled-perturbed equations have been obtained from the corresponding variational Euler equations considering that also basis functions have explicit dependence on the geometry perturbations. Consequently, the linear response of both NOs and ONs to non-external perturbations of the Hamiltonian, as in the case of nuclear geometry displacements, are obtained by solving a set of equations that need to specify the reconstruction of the second-order RDM in terms of the ONs.

Since the energy gradients can be computed at a computational scaling near to the HF approximation, the latter have been employed to compute harmonic vibrational frequencies, which turns out to agree with MP2 and CCSD when PNOF7 is employed.

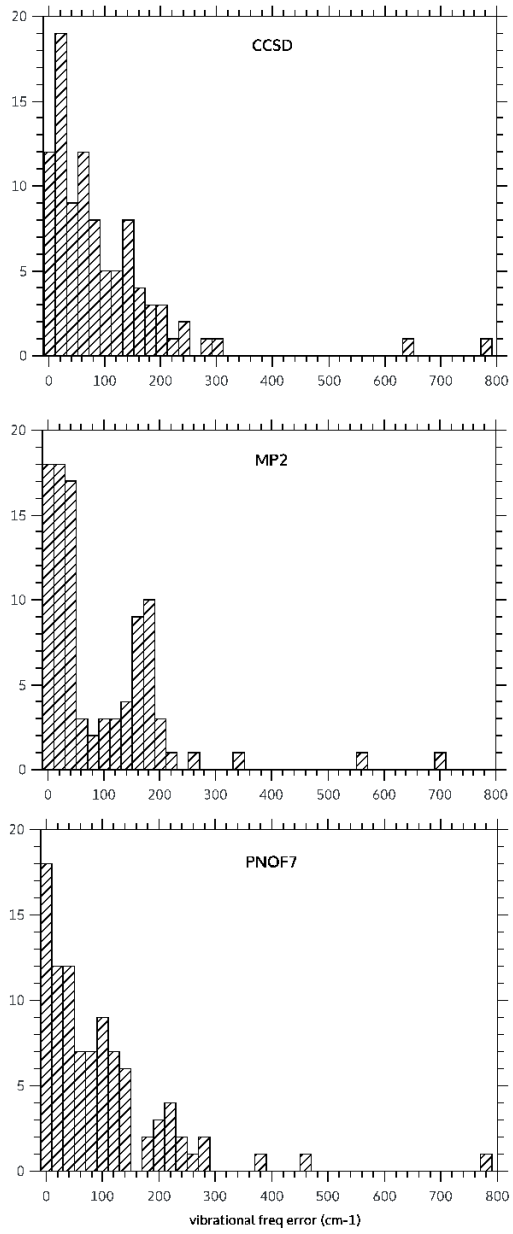

Figure 23 – Histograms with a bin of 20 cm^{-1} showing the distribution of errors with respect to experimental fundamentals obtained by using CCSD, MP2 and PNOF7 methods, with the cc-pVTZ basis set.

CHAPTER 6

Model systems

Simple correlated electron models are suitable for robust validation of approximate NOFs. In this section, we analyze the 1D Hubbard model with different number of sites, and hydrogen chains with different ring sizes, in order to test and improve the NOFAs available in the literature.

6.1 On the performance of NOFAs in 1D Hubbard model

6.1.1 Introduction

Recently the interest related to the Hubbard model has grown in electronic structure theory [89–93]. This system can be viewed as the simplest possible model of correlated fermions, since the compromise between kinetic energy, included via particles hopping, and Coulomb repulsion is included in the Hamiltonian. Thus, the Hubbard model exhibits magnetic ordering, metal-insulator transition, superconductivity, and Tomonaga-Luttinger liquid in 1D, among others, so it allows to study many properties in strongly correlated materials. In other words, this minimal model captures the basic nature of electron correlation, and offers full tunability in order to explore different correlation regimes. As such, the Hubbard model is an ideal candidate for calibration of approximate electronic structure methods.

Strongly correlated systems are challenging for theoretical methods, since the independent

electron picture fails to describe them. Variational wavefunction approaches such as Gutzwiller [181, 182] and Baeriswyl [183–185] have proven to be able to describe fermionic lattice models, and together with DMRG or Quantum Monte-Carlo methods, they are commonly employed to study the fundamental properties of strongly correlated lattice systems. An attempt to use another approach based on RDMFT is done here, in fact, appart from the good performance shown by variational 2RDM calculations [109, 186], NOFAs seem also to be suitable to give an accurate description of such systems [187, 188]. Therefore, the objective of the present chapter is to use the Hubbard model as a stringent validation tool for commonly used NOFAs. In particular, the one-dimensional Hubbard model with and without external potential is studied, focusing on energies, double occupancy, and natural ONs. The latter are an indicator of electron correlation [92], so together with the energy results they show how accurate the Hubbard model is being described. The chapter is organized as follows. In the next section we give a brief description of the Hubbard model, and we describe the properties that will be studied throughout the chapter. Results obtained by using a set of popular NOFAs are shown in Sec. 6.1.3, together with the exact results obtained from FCI calculations.

6.1.2 The Hubbard model

The Hubbard Hamiltonian is possibly the simplest prototype for modeling strongly correlated systems. This model has been largely used to benchmark electronic structure methods [89–93], but also to describe the electronic properties of many materials, e.g. metal-insulator transitions, charge- and spin-density waves in superlattices, etc. The 1D Hubbard model Hamiltonian reads as

$$H = -t \sum_{\langle \mu,\upsilon \rangle,\sigma} (c^\dagger_{\mu,\sigma} c_{\upsilon,\sigma} + c^\dagger_{\upsilon,\sigma} c_{\mu,\sigma}) + U \sum_{\mu} n_{\mu,\alpha} n_{\mu,\beta} + \sum_{\mu,\sigma} n_{\mu,\sigma} v_{\mu,\sigma} \tag{168}$$

where greek indexes μ and υ denote sites, $\langle \mu, \upsilon \rangle$ indicates only near-neighbors hopping, $t > 0$ is the hopping parameter, $\sigma = \alpha, \beta$, $n_{\mu,\sigma} = c^\dagger_{\mu,\sigma} c_{\mu,\sigma}$ where $c^\dagger_{\mu,\sigma}$ ($c_{\mu,\sigma}$) corresponds to fermionic creation(annihilation) operator, $v_{\mu,\sigma}$ is the on-site energy and U is the site interaction parameter. Hereafter, we will refer to as homogeneous Hubbard whenever $v_{\mu,\sigma} = 0$; $\forall \{\mu, \sigma\}$, whereas inhomogeneous Hubbard is used whenever non-zero external potential is present. Thus, for the Hubbard dimer it will be set $v_{S_A,\sigma} = -v_{S_B,\sigma}$ in Sec. 6.1.3.3, so that it gives rise to a nonzero potential Δv. An even more interesting external potential will be used to study inhomogeneous systems for the 10 sites model, namely the one-dimensional Aubry-André model [94] including

electron-electron repulsion

$$H = -t \sum_{\langle \mu,\upsilon \rangle,\sigma} (c^{\dagger}_{\mu,\sigma} c_{\upsilon,\sigma} + c^{\dagger}_{\upsilon,\sigma} c_{\mu,\sigma}) + U \sum_{\mu} n_{\mu,\alpha} n_{\mu,\beta} + \sum_{\mu,\sigma} n_{\mu,\sigma} V \cos(2\pi\alpha\mu + \delta), \tag{169}$$

where V is the modulation amplitude of the on-site potential, α determines the periodicity, and δ fixes the modulation phase. This model, which is intimately related with the Harper model, has been used to explore topological properties in 1D systems, among others.

The electron-electron repulsion is extremely local in the Hubbard model, and can be tunned by the parameter U. Although additional complexities can be included by setting variable parameters U_μ and t_μ [89], let us fix t and vary only the particle-particle interaction U in order to cover different correlation regimes, thus U/t will be used as a dimensionless measure for the relative contribution of both terms. In the limit $U/t \to 0$ the system can be described by mean-field theories, hence the Hartree-Fock approximation recovers the exact wavefunction for the symmetric Hubbard dimer if $U = 0$, however, as long as U/t gets larger the system is nevermore weak correlated and methods including electron correlation are needed to give an accurate description of the model.

A general solution for the Hubbard model requires a numerical treatment. We will restrict to half-filling cases throughout this chapter, so there is in average one particle per site in the model, such that corresponding distribution among the sites depends on the correlation regime and the number of sites of the Hubbard model. Overall, if the hopping parameter is larger than the on-site interaction the electrons tend to occupy doubly the sites, while at the $U/t \gg 1$ limit, also known as the strong correlation limit, electrons try to keep away one from each other by half-filling the sites, which corresponds to the Mott-Hubbard regime [37, 91]. This transition is quantified by the natural orbital occupancies of the system, n_i, which actually are an indicator of correlation [92]. Our analysis will focus on the latter, but also on E/t values and on the double occupancy of the sites dE/dU, which for a given pure state Ψ is defined as

$$\frac{dE}{dU} = \sum_{\mu} \langle \Psi | n_{\mu,\alpha} n_{\mu,\beta} | \Psi \rangle. \tag{170}$$

6.1.3 Results and discussion

The Hubbard model is here exploited in order to clarify the performance of commonly used NOFAs in many correlation regimes (specially in the strong correlation regime). The present chapter focuses on ground state E/t values, double occupancy (Eq. 170), and natural occupancies in comparison with the exact result; which are obtained from FCI calculations for a

range of U/t values in order to cover all correlation regimes in each case. To this purpose we have used a modified version of the code developed by Knowles and Handy [95,96]. 1RDM and 2RDM have been calculated from the FCI expansion coefficients using a homemade code DMN developed by E. Matito and F. Feixas [97]. The results here presented for all NOFAs have been computed using DoNOF code developed by M. Piris and co-workers. Note that double occupancy of sites has been numerically evaluated by using the five-point formula

$$\frac{dE}{dU} \approx \frac{E(U-2h) - 8E(U-h) + 8E(U+h) - E(U+2h)}{12h} \tag{171}$$

where the step size is set to $h = 0.001$ (the error within this approximation is of the order of h^4).

6.1.3.1 Exact results for homogeneous Hubbard model

In this section we discuss several properties of the homogeneous 2 sites, 4 sites square, and 6 sites hexagone Hubbard systems, which have been previously employed to study many electronic structure methods [89–93, 187, 189]. Energy values for the homogeneous 10 sites, 12 sites, and 14 sites are also included. Exact FCI E/t values for a range of U/t values corresponding to these systems are shown in Fig. (24).

There is a similar trend for the three curves corresponding to the graph in the top of Fig. (24): all of them show negative E/t values at the zero correlation point ($U = 0$) and converge asymptotically to $E/t = 0$ at the strong-correlation limit ($U/t \to \infty$). As expected the absolute energies are larger as the number of sites is increased. Interestingly, relative differencies are smaller in the case of 10, 12, and 14 sites systems, and the asymptotic limit is located at larger U/t values when more sites are added to the model.

In order to get a more reliable indicative of the energy, the derivative with respect to parameter U/t is also studied for the 2, 4, and 6 sites systems (Fig. 25), since physical interpretations can be obtained due to their conceptual simplicity. In fact, this is a measure of double occupancy of the sites according to Eq. (170). According to Fig. 25 the double occupancy is maximum in the weak correlation region, since the exact ground-state wave function is recovered by an independent particle model when there are no two-particle interactions. The population of the sites spreads out as the correlation increases, so for large U values the double occupancy tends to zero due to particle-particle repulsion. Neither the energy nor dE/dU show significant differences when the number of sites varies in the Hubbard model, but the study of the ONs displays another situation.

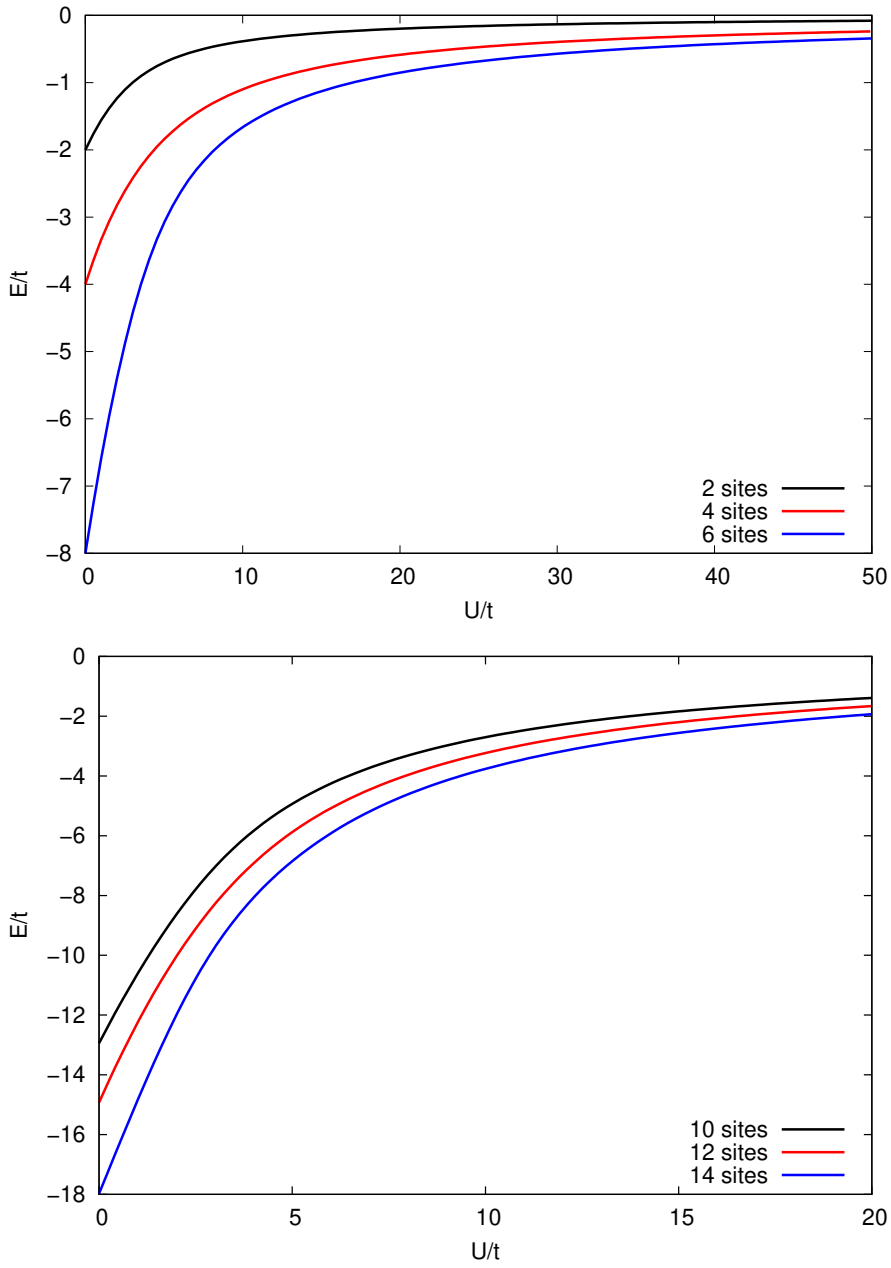

Figure 24 – Exact FCI E/t values for many U/t values for half-filled homogeneous 2, 4, 6, 10, 12, and 14 sites Hubbard systems.

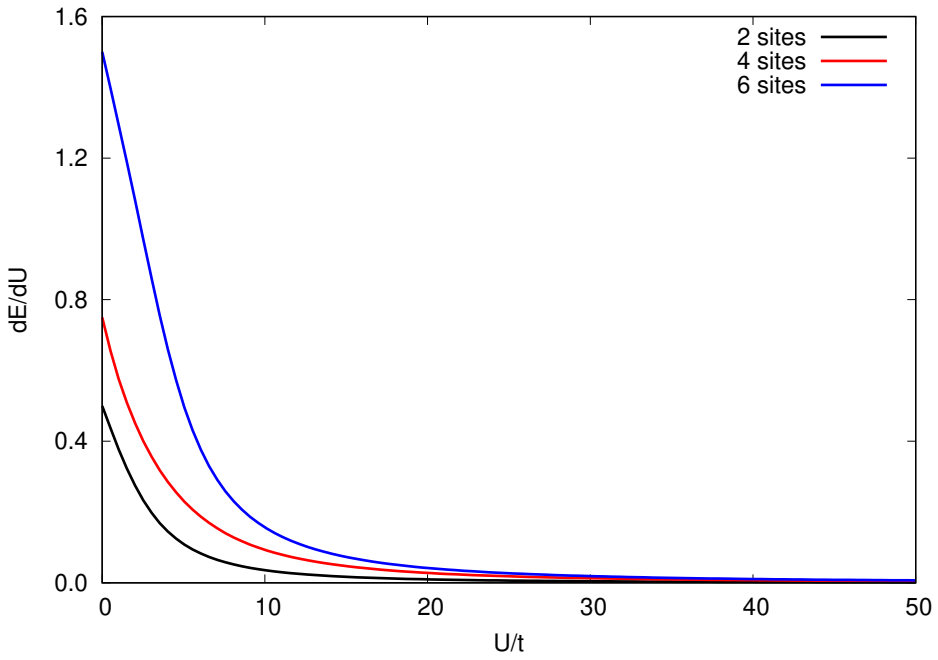

Figure 25 – Derivative of the energy with respect to parameter U/t for the homogeneous 2 sites, 4 sites square, and 6 sites hexagone Hubbard models.

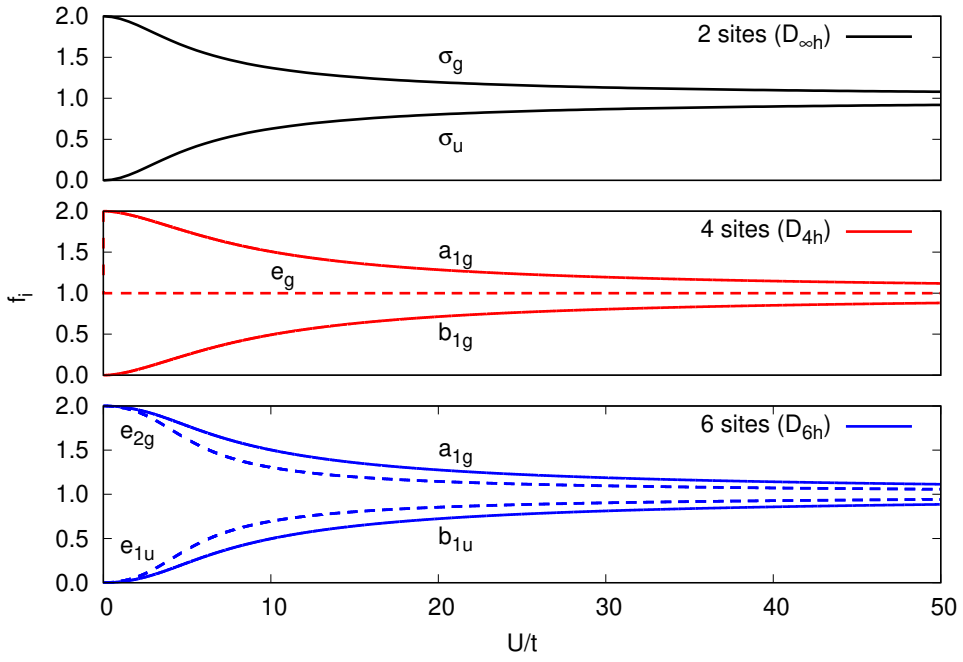

Figure 26 – Natural orbital occupancies (spins summed) in terms of U/t values for the homogeneous 2 sites, 4 sites square, and 6 sites hexagone Hubbard models. Solid lines are used for non-degenerate results, whereas dashed lines correspond to degenerate results. f stands for the ONs n in this plot.

The half-filled 2 sites Hubbard model is the simplest case that we have studied. It is known that when there is no correlation ($U = 0$) the exact wavefunction for the ground-state may be written as a single Slater determinant $|\Psi\rangle = |\sigma_g^2\rangle$ built using a σ_g orbital; labeled attending to $D_{\infty h}$ symmetry of the system. The σ_g orbital is defined as

$$\sigma_g = \frac{1}{\sqrt{2}}(S_A + S_B). \tag{172}$$

and is also known as the bonding orbital in quantum chemistry. Note that sites are labeled by S_X where X is replaced by a letter in alphabetic order.

Nevertheless, when correlation increases the single Slater determinant picture does not longer hold and the wavefunction may be written as $|\Psi\rangle = C_g|\sigma_g^2\rangle + C_u|\sigma_u^2\rangle$ where the expansion coefficients C_g and C_u are determined variationally, and the second Slater determinant is built using the σ_u orbital

$$\sigma_u = \frac{1}{\sqrt{2}}(S_A - S_B). \tag{173}$$

This orbital is also known as the antibonding orbital in quantum chemistry. The σ_g and σ_u orbitals form a basis which is adapted to the symmetry of $D_{\infty h}$ point group. These orbitals are also the NOs for the system since the 1RDM obtained from the wavefunction is already diagonal in this basis for the homogeneous 2 sites Hubbard model. Corresponding ONs are shown in the top of Fig. 26. Note that coefficients C_g and C_u are equalized in the strong-correlation limit ($U/t \to \infty$), so the occupancies of the NOs become equal to one (spins summed). In other words, the 1RDM is diagonal and equal to the identity matrix (this limit resembles the H_2 molecule in the dissociation limit for a minimal basis).

For the 4 sites square Hubbard model the orbitals adapted to the D_{4h} symmetry also correspond to the NOs, these are the non-degenerate

$$a_{1g} = \frac{1}{2}(S_A + S_B + S_C + S_D) \tag{174}$$

the 2-fold degenerate e_g orbitals

$$e_g(1) = \frac{1}{2}(S_A - S_B - S_C + S_D) \tag{175}$$

$$e_g(2) = \frac{1}{2}(S_A + S_B - S_C - S_D) \tag{176}$$

and the non-degenerate

$$b_{1g} = \frac{1}{2}(S_A - S_B + S_C - S_D) \tag{177}$$

According to the natural occupancies shown in the middle of Fig. 26, both e_g orbitals are half-occupied independently of the interaction strength U, whereas orbitals a_{1g} and b_{1g} play the role of the σ_g and σ_u orbitals in the 2 sites model. Regarding the orbitals adapted to the symmetry of the system in the case of the 6 sites hexagone Hubbard model, which also correspond to the exact NOs, these orbitals read as

$$a_{1g} = \frac{1}{\sqrt{6}}(S_A + S_B + S_C + S_D + S_E + S_F) \tag{178}$$

the 2-fold degenerate e_{2g} orbitals

$$e_{2g}(1) = \frac{1}{\sqrt{12}}(S_A + 2S_B + S_C - S_D - 2S_E - S_F) \tag{179}$$

$$e_{2g}(2) = \frac{1}{\sqrt{4}}(S_A - S_C - S_D + S_F) \tag{180}$$

the 2-fold degenerate e_{1u} orbitals

$$e_{1u}(1) = \frac{1}{\sqrt{4}}(S_A - S_C + S_D - S_F) \tag{181}$$

$$e_{1u}(2) = \frac{1}{\sqrt{12}}(S_A - 2S_B + S_C + S_D - 2S_E + S_F) \tag{182}$$

and the non-degenerate

$$b_{1u} = \frac{1}{\sqrt{6}}(S_A - S_B + S_C - S_D + S_E - S_F) \tag{183}$$

The plot in the bottom of Fig. 26 shows the exact NO occupancies. The behavior is similar to the one obtained for the 2 sites model; at the weak correlation limit the double occupancy of NOs is maximum, while all orbitals become half-occupied in the limit $U/t \to \infty$.

6.1.3.2 NOFA results for homogeneous Hubbard model

In this section, the Hubbard model is used as a stringent validation tool for commonly used NOFAs. Note that a spin-restricted formalism has been employed for all calculations in order to hold $\langle S^2 \rangle = 0$ and $\langle S_z \rangle = 0$. Here, we will use the adapted to symmetry basis set described in the previous section for each model, which is conceptually similar to a molecular-like basis set. Interestingly, the latter correspond to the NOs for the homogeneous 2 sites and 4 sites square systems, independently of the interaction strength U/t and the NOFA.

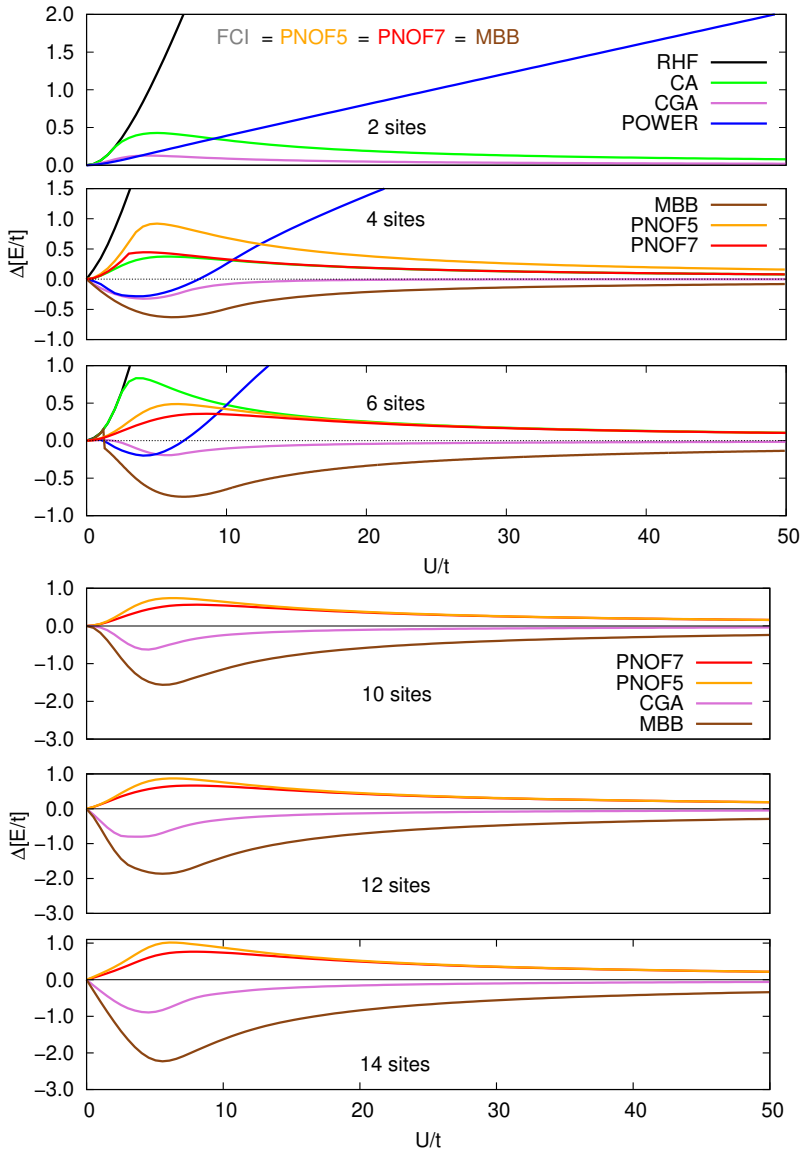

Figure 27 – Differences in E/t values with respect to exact FCI obtained for the 1D homogeneous Hubbard model by using many NOFAs.

Fig. 27 shows the differences obtained for E/t values with respect to FCI ($\Delta\,[E/t] = E^{NOFA}/t - E^{FCI}/t$) for a wide range of U/t values. As we observe from the top of Fig. 27 only MBB, PNOF5 and PNOF7(+) functionals reproduce the exact FCI energy for the Hubbard dimer (the result for MBB has been previously obtained [93]). Apart from MBB, PNOF5 and PNOF7(+); CA and CGA functionals show a good asymptotic behavior in the $U/t \to \infty$ limit. Conversely, neither restricted Hartree-Fock (RHF) nor the Power functional recover the exact energy or attain a good asymptotic behavior, though RHF shows a good performance at the weak correlation limit. (Results corresponding to some other NOFAs like the Goedecker and Umrigar [63], Marques and Lathiotakis [64], and Gritsenko, Pernal and Baerends [65] have not been included due to showing catastrophic performance even for the 2 sites case.) MBB and Power approximations are known to violate the N-representability P-, Q-, and G-conditions [20]; as some of us have recently shown [41], even for the two-electron case. E/t values corresponding to the Power functional differ from the ones reported by Kamil et al. (see Fig. 1 in reference [93]). The difference between Kamil's et al. energies and ours is due to the fact that we stick to a spin restricted formalism for our optimizations of the orbitals, so the σ_g and σ_u basis is not altered. Therefore, the orbitals for α and β electrons were the same. Of course, the usage of an unrestricted formalism improves the E/t values, as Kamil et al. shown, but the price that we have to pay using an unrestricted formalism is that $\langle S^2 \rangle \neq 0$ since a mixture between the singlet and triplet solutions may arise (also known as the lost of the exact nonmagnetic character). In order to conserve $\langle S^2 \rangle = 0$, we have to use a restricted formalism and expect that the accuracy of the NOFA produces the correct asymptotic behavior in the $U/t \to \infty$ limit (which is not the case of the Power functional as illustrated in the top of Fig. 27).

The robustness of well-behaved functionals has been tested beyond the dimer using a system with more degrees of freedom such as the half-filled 4 sites square Hubbard model. A similar problem, the H_4 molecule, has been recently studied in a NOFT context [98]. Contrary to what happened for the 2 sites homogeneous Hubbard model (where intra-pair nondynamic correlation effects were dominant), there is correlation between pairs in the 4 sites square Hubbard model. Therefore, a good functional for the 4 sites square homogeneous Hubbard model should have a good description of nondynamic intra-pair correlation effects but also a reasonable description of inter-pair correlation. Similar to the results obtained for the 2 sites Hubbard model, $E^{NOFA}/t - E^{FCI}/t$ values displayed in the left-middle of Fig. 27 obtained with RHF and Power present bad asymptotic curves, so they do not correspond to a solution of the problem. Conversely, all other NOFAs show proper behavior for small and large U/t

values. PNOF7(+) is in outstanding agreement with FCI for all correlation regimes, whereas CGA differs from the exact curve in the interval $0 < U/t < 10$. PNOF5, MBB, and CA yield qualitatively correct curves, but their corresponding energies are not as accurate as the ones obtained with CGA and PNOF7(+). It must be emphasized the importance of inter-pair correlation in order to describe properly this system, because the only difference between PNOF5 and PNOF7(+) is exclusively due to the addition of a term to account for inter-pair electron correlation.

The half-filled 6 sites hexagone Hubbard model presents an added complexity with respect to the 2 and 4 sites systems. This model has been previously used as a benchmarking, e.g. for testing new approaches based on coupled cluster methods like CCD0 in order to retrieve nondynamic correlation effects [90]. PNOF7(+) provides the most accurate total energies as illustrated in Fig. 27, followed closely by CGA. Both functionals yield energies slightly below the FCI energy beyond a certain U/t value, so even PNOF7(+), which is built imposing the analytic necessary N-representability conditions of the 2RDM [20, 40], is not stricly N-representable in constrast to PNOF5. CA, MBB, and PNOF5 show a correct behavior in the weak and strong correlation limits, however they yield poor results in the intermediate region.

Within the limitations imposed by the ED calculation, results for larger systems have been obtained, namely, the 10, 12, and 14 sites homogeneous Hubbard. Thus, results obtained for PNOF7(+), PNOF5, CGA, and MBB approximations are shown in the right hand plots of Fig. 27, whereas other NOFAs have been omitted due to present bad performance for tiny systems. Contrary to the errors shown for smaller systems, CGA yields larger errors going from 10 to 14 sites, as MBB, and both of them show energies below the exact one throughout all energy curve so the variational principle is strongly violated. PNOF approximations do not breakdown for large systems, and in spite of providing an error larger than CGA in absolute terms near the $U/t \approx 50$, they approach closely from above to the exact result for any correlation regime.

Let us focus now on the results obtained for the double occupancy in the case of the 2, 4, and 6 sites models. Since PNOF7(+) and CGA yield best energies, $dE^{NOFA}/dU - dE^{FCI}/dU$ differences obtained employing these approximations are plotted in Fig. 28. Results obtained by using RHF and PNOF5 are also included for comparison. Note that RHF gives a constant value for each model independently of the site interaction strength U. PNOF7(+) is the only functional able to go parallel to the exact dE/dU according to Fig. 28, whereas CGA shows large errors and discontinuities for the 2 and 4 sites systems at small U/t values, which is the region where it goes noticeably below the exact energies and, as it is shown below, CGA gives

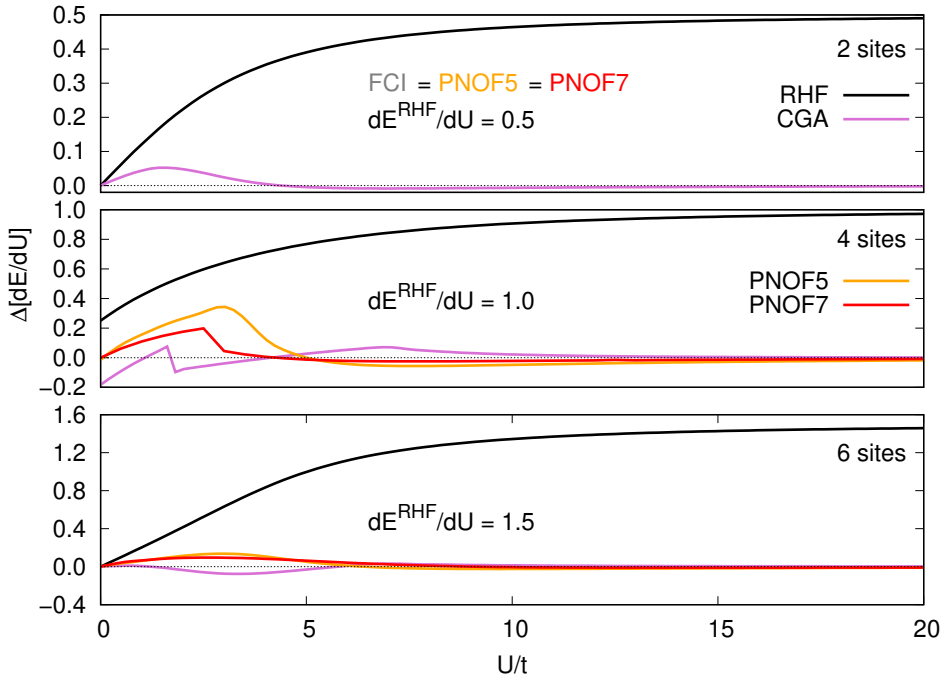

Figure 28 – Differences in dE/dU values with respect to exact FCI obtained for many NOFAs.

wrong pinned natural ONs. The independent-pair model PNOF5 fails significantly for systems beyond two particles, specially in the 4-sites case due to the missing inter-pair correlation. This functional shows a behavior similar to RHF for small U values, what can be associated with the result obtained for the natural ONs (see below).

NO occupancies obtained for FCI, CGA, PNOF5, and PNOF7(+) in the 4 sites square and 6 sites hexagone Hubbard systems are plotted in Fig. 29. Results corresponding to the Hubbard dimer have been omitted since MBB, CGA, PNOF5 and PNOF7(+) reproduce the exact occupancies. Regarding the result obtained for the 4 sites model, only PNOF7(+) is able to provide precise ONs for any interaction strength, in contrast to the rest of NOFAs, which show good asymptotic behavior in the $U/t \to \infty$ limit but tend to stick to $n_{a_{1g}} = 2.0$ (spins summed) occupancies in the weak correlation region related to the bad performance obtained for dE/dU in the same correlation region. CGA exhibit the largest occupancies pinned to 2.0 in the a_{1g} orbital but the changes of b_{1g} occupancy, so it shows a wrong break of the unitary occupation of the two-fold degenerate e_g orbitals that remain fixed in the exact solution. Pinned natural ONs are intimately related with the wrong description of the double occupancy. According to Eq. (170), a bad description of the latter is due to an incorrect 2RDM needed to evaluate

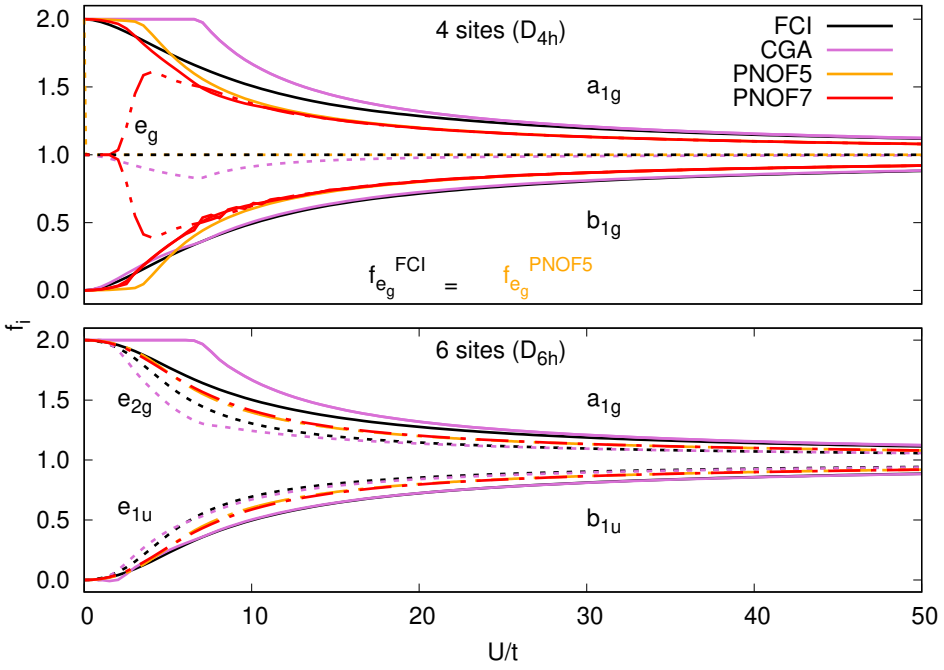

Figure 29 – Natural orbital occupancies (spins summed) obtained for FCI, CGA, PNOF5, and PNOF7(+), in the 4-sites square and 6-sites hexagone Hubbard systems. Solid lines are used for non-degenerate occupancies, whereas dotted and dashed-dotted lines correspond to degenerate occupancies. In this plot f stands for ON, i.e. n.

$\langle\Psi|n_{\mu,\uparrow}n_{\mu,\downarrow}|\Psi\rangle$ in the sites basis, so the double occupancy of the sites computed from first derivative of the energy also reflects the pitfalls in the 2RDM built from pinned to 2.0 ONs.
The situation is completely different for the 6 sites model, for which NOs corresponding to the ground state for both PNOF5 and PNOF7(+) depend on each approximation, whereas the NOs are still those adapted to the symmetry for the $\mathcal{JK}$-only NOFAs. Thus, PNOF NOs present 3-fold degeneracy and thereby are not related to D_{6h} point group symmetry, conversely, there is a double degeneracy of the occupations associated with the e_{2g} and e_{1u} orbitals for the rest of approximations. Similar to the results obtained for the 4 sites Hubbard model, CGA exhibits pinned occupancies at the weak correlation regime and thereby is not able to give an accurate description of the model. All of the NOFAs shown tend to unitary ONs in the strong correlation limit.
The 3-fold degeneracy can be explained considering that PNOFi $\{i = 5, 7\}$ functionals lead generally to localization of the molecular orbitals in the NO representation. Nevertheless, there is an equivalent canonical representation that can afford delocalized molecular orbitals adapted to the symmetry of the system upon diagonalization of the matrix of Lagrange multipliers (λ in Eq. 112) obtained from optimized NOs [100]. Thus, the NOs obtained by using the $\mathcal{JKL}$-only approximations, which are plotted on the right side of Fig. 30, transform into the symmetry-adapted orbitals shown on the left side of Fig. 30, so PNOFi $\{i = 5, 7\}$ functionals are able to retrieve the orbitals adapted to the symmetry of the system in the canonical orbital representation [100]. The 3-fold degeneracy is only a matter of the nature of PNOFi $\{i = 5, 7\}$ functionals but does not introduce any artifacts in the description of properties.

6.1.3.3 Inhomogeneous Hubbard model

MBB, PNOF5 and PNOF7(+) reproduce the exact results for the energy, double occupancy of sites, and NO occupancies in the homogeneous 2 sites Hubbard model. Nevertheless, the MBB functional does not really recover the exact expression of Löwdin-Shull [33, 54, 102, 190] for any 2-electron system (appart from some phases [102]), but PNOFi ($i = 5$ and 7) functionals do. In order to prove the deviation of MBB functional and that PNOFi ($i = 5$ and 7) actually recover the exact 2-electron functional, we include two additional tests for these approximations. Results obtained by using the CGA approximation are also included to test whether the accuracy of the method still holds. The tests proposed use a inhomogeneous 2 sites Hubbard model, so a non-zero on-site energy is set such that it gives rise to a potential difference

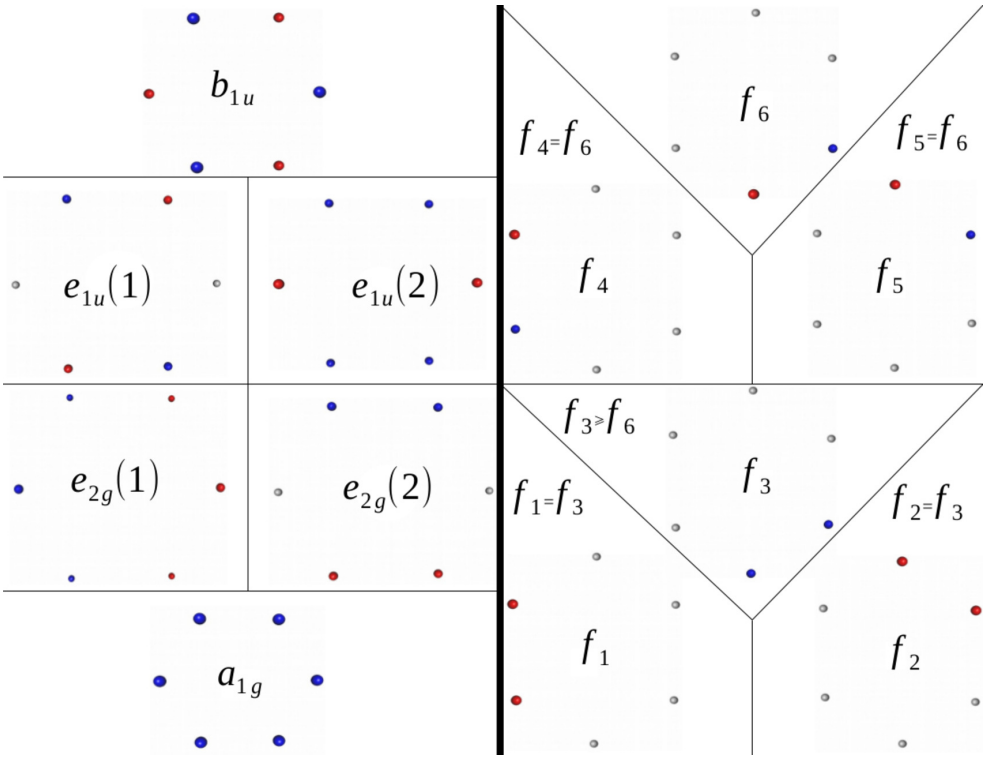

Figure 30 – Orbitals obtained by PNOF5 and PNOF7(+) for the 6-sites hexagone Hubbard model. Natural orbitals are shown on the right side, while symmetry adapted orbitals (obtained from diagonalization of matrix λ) are plotted on the left side.

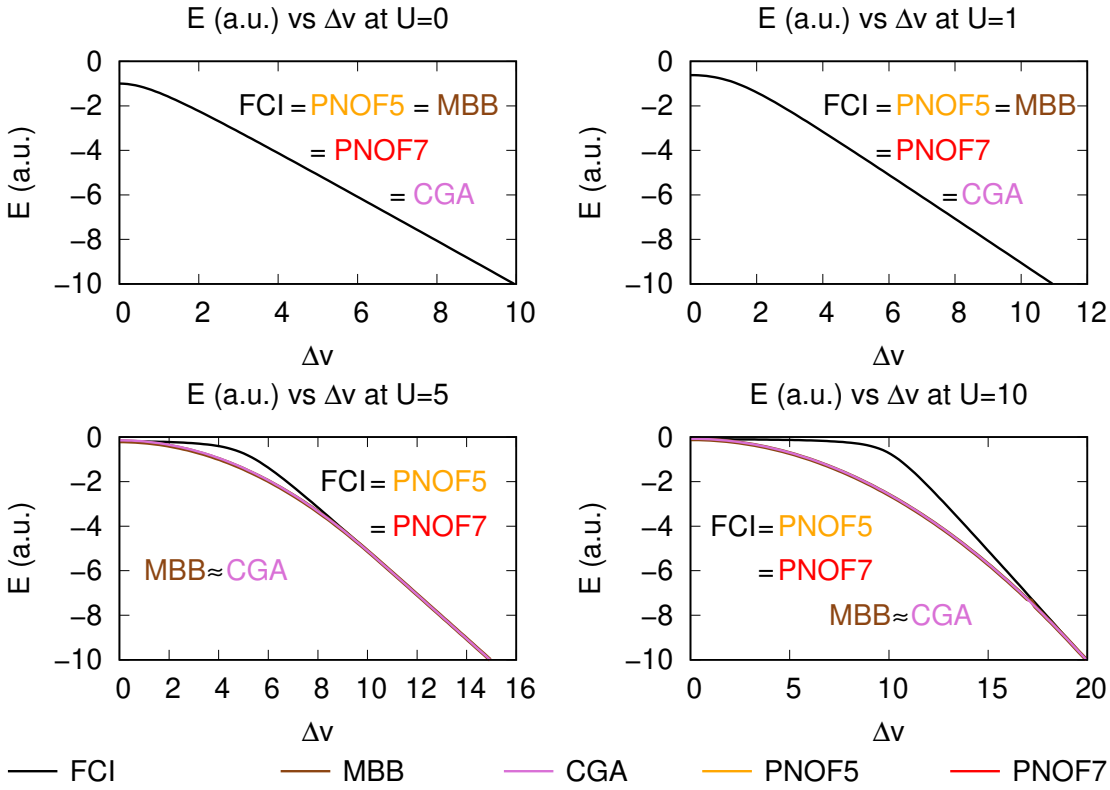

Figure 31 – Exact and approximate (obtained with MBB, CGA and PNOF approximations) energies for the inhomogeneous 2 sites Hubbard model for fixed values of U ($U = 0$, 1, 5 and 10) and fixed $t = 0.5$.

$\Delta v = v_{S_B} - v_{S_A} = 2v$. Since the system is nevermore symmetric the orbitals adapted to the symmetry are no longer the NOs, so the latter may arise from optimization of the energy functional $E\left[\{n_i\}, \phi_i(\boldsymbol{x})\right]$ for each NOFA. This model is being used also as benchmarking [91], e.g. for the widely use Bethe ansatz local density approximation (BALDA) developed by Capelle, K. and collaborators [191–195] (which fails recovering the exact results). Then, we have compared the exact results with the results obtained by using these NOFAs for the total energy and for the difference between site occupancies (i.e. $|\Delta n| = |n_{S_B} - n_{S_A}|$ where n_{S_X} is the occupancy of site X). Recall the differences between n referring to sites or molecular orbitals.

In Fig. 31 we have plotted for a fixed value of $t = 0.5$ and four values of U the exact energies and the energies obtained with MBB, CGA, PNOF5 and PNOF7(+). In general, the $\Delta v = 0$ limit recovers the homogeneous 2 sites Hubbard model where all functionals produce

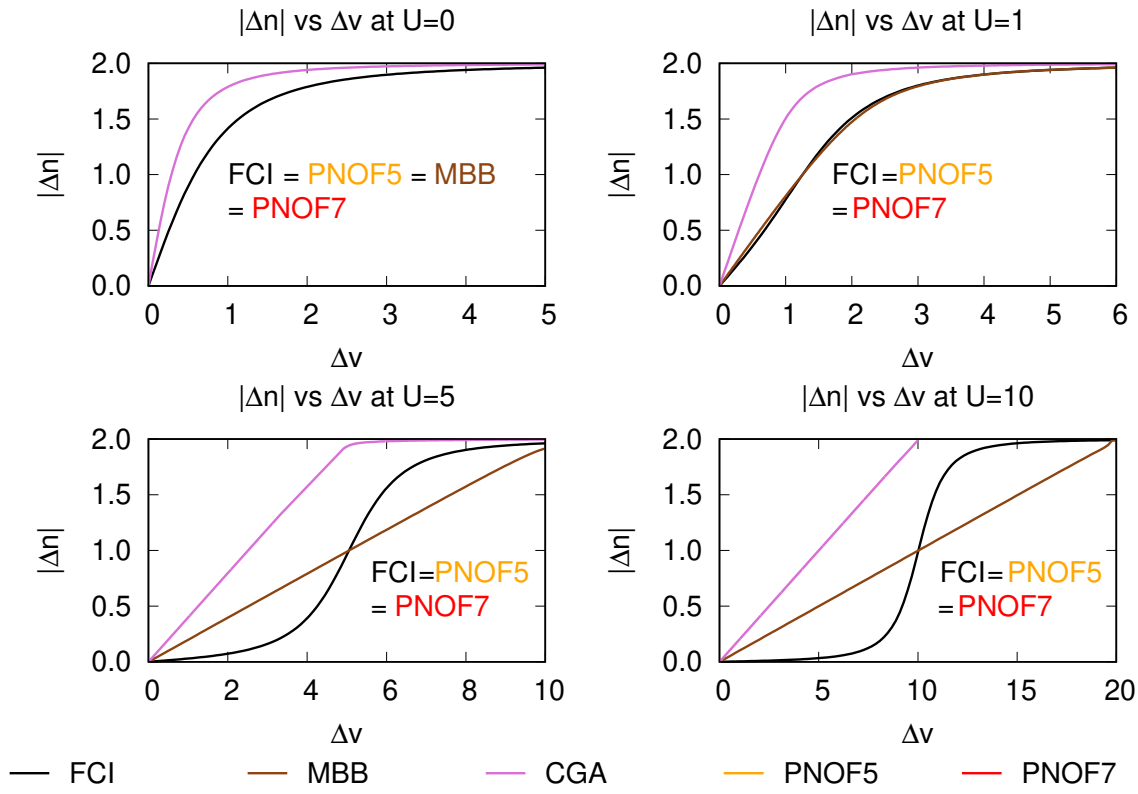

Figure 32 – Exact $|\Delta n|$ vs Δv and approximate values (obtained with MBB, CGA and PNOF approximations) for the inhomogeneous 2 sites Hubbard model for fixed values of U ($U = 0$, 1, 5 and 10) and fixed $t = 0.5$.

exact energies for any U as we observe in Fig. 31. For $U = 0$ the exact energy is given by $E = -\sqrt{(2t)^2 + (\Delta v)^2}$ where the RHF energy is exact since there are no electron-electron interactions for any Δv, hence MBB, CGA, PNOF5 and PNOF7(+) reproduce the exact Hartree-Fock energy. Nevertheless, once the on-site interaction is turned on, MBB and CGA do not longer produce exact results for the 2 sites inhomogeneous Hubbard model and only PNOF5 and PNOF7(+) yield exact energies.

Despite the energy obtained with MBB and CGA functionals for $U = 1$ (top right plot in Fig. 31 seems to be still exact, a property such as the $|\Delta n|$ reveals that MBB and CGA results are no longer exact (see Fig. 32). In Fig. 32 we have plotted $|\Delta n|$ for $t = 0.5$ and the same four values of U that we used in Fig 31. We observe from the $|\Delta n|$ test that MBB and CGA only yield exact results in the non-interaction limit ($U = 0$), even in the weak correlation region

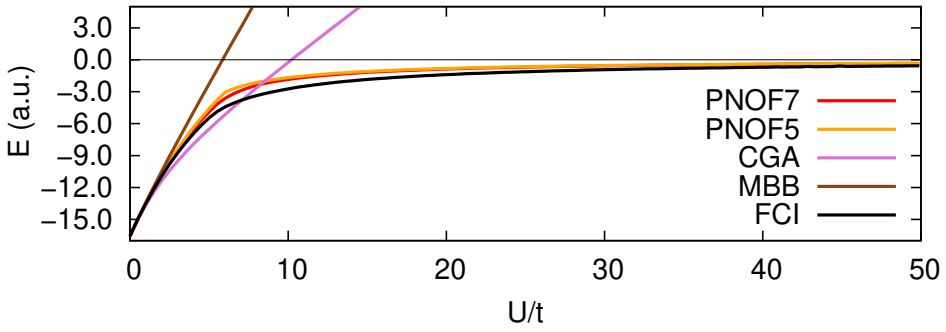

Figure 33 – Exact and approximate energies for the 10 sites Hubbard model including an Aubry-André on-site potential, for many U/t values.

($U = 1$) MBB and CGA $|\Delta n|$ values differ from the exact ones. A remarkable result is that PNOF5 and PNOF7(+) have proven to retrieve the exact functional of Löwdin-Shull. Thus, energies and properties, like for example $|\Delta n|$ vs Δv or the charge-transfer to Mott-insulator transitions (which happens around $\Delta v \approx U$), obtained with PNOF5 and PNOF7(+) in any correlation regime for the 2 sites inhomogeneous Hubbard model will be exact.

The on-site potential can be more interestingly modulated if a system with more sites is employed. Hence, we have used an oscillatory potential such as the introduced in the Aubry-André model [94] to carry out calculations on the 10 sites inhomogeneous Hubbard model. Note that the Hamiltonian of the system is now given by Eq. (169) with $\alpha = 1/10$, $V = 2.0$ and $\delta = -2\pi/10$. According to the results given in Fig. 33, and similar to the results obtained for the inhomogeneous Hubbard dimer, CGA and MBB approximations fail dramatically when studying inhomogeneous systems except in the weak correlation limit. PNOF5 and PNOF7(+) approximations not only show good asymptotic behavior, but they lie close to the exact curve for any correlation regime. Therefore, systems with spatial inhomogeneities are also well-described by PNOF approximations.

6.1.4 Conclusions

In this chapter the robustness of a set of NOFAs is put into test by using the homogeneous Hubbard model with 2, 4, 6, 10, 12, and 14 sites, and the inhomogeneous model which includes nonzero on-site potential for the Hubbard model with 2 and 10 sites. A simple comparison between the exact FCI calculations and approximate results for varying interaction strengths

U/t is carried out.

Both PNOF5 and PNOF7(+) reproduce the exact Löwdin-Shull functional for the 2 sites system, while the other NOFAs fail for one or another test. Consistently for all test cases studied in the homogeneous Hubbard model PNOF7(+) results are in outstanding agreement with FCI. Among $\mathcal{JK}$-only NOFAs only CGA is able to provide energies close to the exact ones, but fails significantly for ONs of the NOs, and yield a discontinuous curve for the double occupancy of the sites. The enhanced accuracy of CGA is in fact due to the inclusion of a proper particle-hole symmetry which is not the case for some other $\mathcal{JK}$-only NOFAs. Nevertheless, CGA violates many fundamental properties such as N-representability conditions or antisymmetry of the 2RDM [41]. Thus, CGA fails dramatically for the inhomogeneous Hubbard model, i.e when the on-site potential varies. PNOF7(+) presents particle-hole symmetry at the same time that the fundamental properties of the 2RDM are conserved, and thereby the inhomogeneous Hubbard is also well described.

In view of the results obtained for the Hubbard model with varying interaction strength, PNOF7(+) can describe not only weakly correlated systems, but also problems where strong correlation effects arise. This opens a new avenue where PNOF7(+) becomes a tool for studying many interesting applications which include confined fermions, disorder and critical behavior in optical lattices, effects of spatial inhomogeneity in strongly correlated systems, various critical phenomena in 1D chains, among others. Where up to now, appart from the well-established variational wavefunction methods of Gutzwiller and Baeriswyl, different perturbative expansions, or Quantum Monte-Carlo methods, the widely used BALDA approximation has lead, despite the pitfalls obtained with it even in the simple 2 sites nonsymmetric Hubbard model [91].

To conclude, the present study proves the importance of developing functionals that satisfy at least with the analytic necessary N-representability conditions of the 2RDM in order to obtain consistent results in systems with either weak or strong electronic correlation. Besides, concerning the improvement of PNOF7(+) over the independent-pair model PNOF5, it shows that a well-balanced inter-pair correlation is crucial to account properly for electron correlation effects.

6.2 Phase dilemma from the N-representability perspective

Any rigorous approach to 1RDM functional theory faces the phase dilemma, that is, having to deal with a large number of possible combinations of signs in terms of the electron-electron interaction energy. This problem was discovered by reducing a ground-state energy generated from an approximate N-particle wavefunction into a functional of Γ, known as the *top-down* method. Here, we show that the phase dilemma also appears in the *bottom-up* method. Approximations for $E[\Gamma]$ can be obtained essentially using two methods, namely, the *top-down* and *bottom-up* methods [30, 57]. The *top-down* method consists in the reduction of an N-particle ground-state energy generated from an approximate wavefunction into a functional of Γ, whereas, in the *bottom-up* method $E[\Gamma]$ is generated by progressive inclusion of N-representability conditions [20] on the reconstructed D $[\Gamma]$.

The use of the *top-down* method with a parametrization of coefficients in a configuration interaction (CI) expansions reveals a very serious bottleneck affecting any rigorous approach to $E[\Gamma]$, namely the phase dilemma that stems from the necessity to carry out minimization over a large number of possible combinations of CI coefficient signs [102]. As expected, the phase dilemma also appears when the *bottom-up* method is used, i.e., we have to deal with a large number of possible combinations of signs in terms of electron-electron interaction energy.

In the next section, we analyze how the phase dilemma arises when applying the N-representabilty conditions to the reconstructed D $[\Gamma]$. We demonstrate that a suitable choice of signs is essential to describe accurately the model systems for strong non-dynamic (static) electron correlation. This lead us to the PNOF7 with phases equal to -1 for the inter-pair energy terms containing the exchange-time-inversion integrals, which captures the electron correlation energy close to the exact diagonalization values.

6.2.1 Inter-pair correlation term in PNOF7

It is obvious that a possible election that favors decreasing of the energy (106) is to consider all the phase factors negative, i.e., $\Pi^{\Phi}_{qp} = -\Phi_q\Phi_p$. As stated above, we denote by PNOF7(+) the functional that considers +1 the phase factors of Π^{Φ}_{qp} for $q, p >$ N/2, whereas PNOF7(-) is employed to denote the NOFA (106) with these phases equal to -1. The latter is usually

referred to as PNOF7 as well.

Since we do not have an accurate functional like (101) that helps us to determine which is the best combination of signs for Π_{qp}^{Φ}, in the following sections, we analyze several examples with strong non-dynamic (static) electron correlation in order to make a proper phase choice after comparing with accurate exact diagonalization calculations.

6.2.2 Local inter-pair correlation

The performance of commonly used NOFAs for the 1D Hubbard model with periodic boundary conditions has been studied in the previous chapter, showing that the here presented PNOF7(+) is in good agreement with exact results for the Hubbard model at half-filling. Nevertheless, the amount of electron correlation recovered by PNOF7(+) for large systems is slightly less than for small systems. Since NOFT is a promising approach for large many-body systems, it is crucial to develop approximations that do not deteriorate as the size of the system increases. In the following, we show that a proper choice of inter-pair interaction signs avoids the cumulation of errors as the number of electron pairs present in the system gets larger.

For the sake of simplicity, we will employ the simplest form of the Hubbard model without external potentials as shown in Eq. (168), so hereafter the next Hamiltonian is considered

$$H = -t \sum_{\langle r,r'\rangle,\sigma} (a_{r,\sigma}^{\dagger} a_{r',\sigma} + a_{r',\sigma}^{\dagger} a_{r,\sigma}) + U \sum_{r} n_{r,\alpha} n_{r,\beta} \tag{184}$$

where $\langle r, r'\rangle$ indicates only near-neighbors hopping between the sites r and r'. $t > 0$ is the hopping parameter analogous to the kinetic energy, and U is the electron-electron on-site interaction parameter. $\sigma = \alpha, \beta$ stands for the spin. $a_{r,\sigma}^{\dagger}\,(a_{r,\sigma})$ is the creation (annihilation) operator, so $n_{r,\sigma} = a_{r,\sigma}^{\dagger} a_{r,\sigma}$ gives the number of electrons on site r with spin σ.

In Fig. 34 we show the differences in E values with respect to ED results ($\triangle E = E^{NOF} - E^{ED}$) obtained for the 8, 10, 12 and 14 sites systems for a range of U/t values in order to cover all correlation regimes. It is worth to mention that some of these systems were studied in the previous chapter. Exact results are computed using a modified version of the code developed by Knowles and Handy [95,96], whereas results here presented for all NOF approximations have been computed using DoNOF code developed by M. Piris and coworkers. First, we observe that energies obtained by using the independent-pair model PNOF5 underestimate systematically correlation effects for all U/t values independently of the number of sites of the system. Thereby the interactions between electron pairs must be considered in an electron pairing scheme such as PNOF to get an accurate description of the Hubbard model.

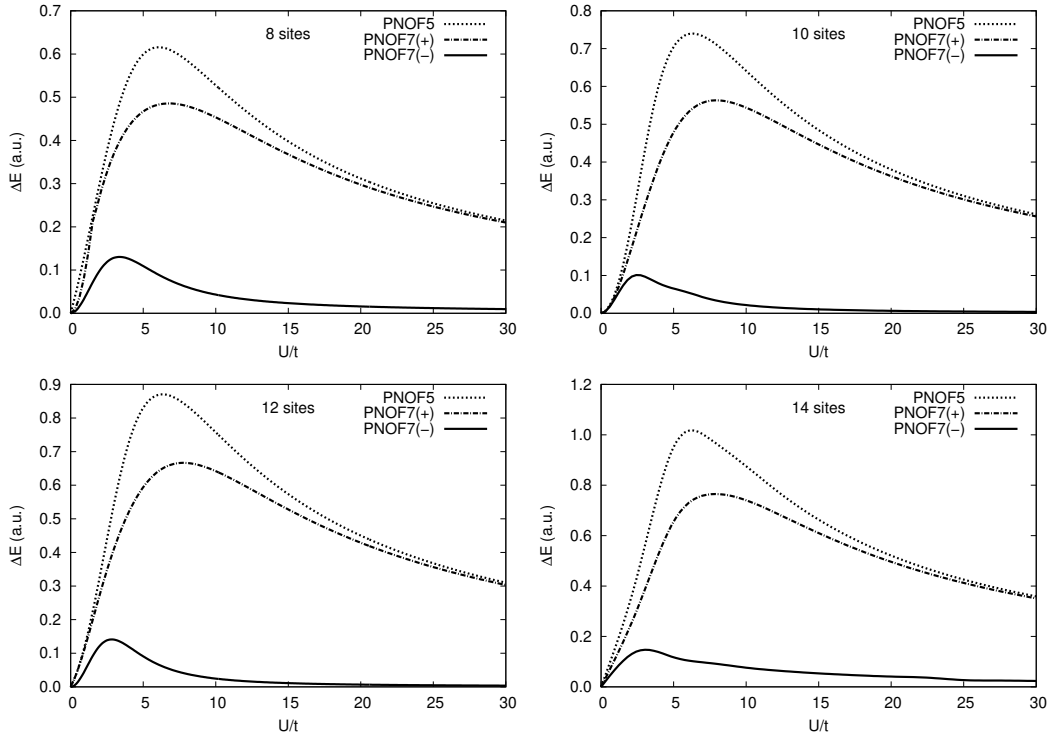

Figure 34 – Differences in E values with respect to exact results vs. U/t values for the 8, 10, 12, and 14 sites homogeneous 1D Hubbard model at half-filling with periodic boundary conditions; obtained by using PNOF7(+), PNOF5, and PNOF7(-).

Considering nonzero inter-pair interactions by introducing the Π_{qp}^{Φ} term given in eq. (106), the amount of electron correlation recovered in the region $0 < U/t < 10$ is larger, but the behavior for large U/t values is rather similar to neglecting inter-pair interactions if PNOF7(+) is used. As illustrated in Fig. 34, this issue can be properly solved simply by considering the proper choice of the sign functions for Π_{qp}^{Φ}. Thus, PNOF7(-) improves significantly the performance of PNOF7(+) not only for any correlation regime, but also for any size of the system. While PNOF7(+) produces larger errors as one increases the number of sites, the accuracy of PNOF7(-) is independent of this issue. In the region $U/t \gg 1$, when the on-site electronic repulsion gets larger, the PNOF7(-) curve attaches to the exact curve giving an outstanding description of the asymptotic behavior. Hence, this approximation is able to reproduce the antiferromagnetic nature of the model in this region, in contrast to other approaches based on electron-pair states, such as AP1roG [3], which fail to describe the weak orbital-pair correlations arising from singly occupied states in the strong correlation limit.

6.2.3 Revisiting PNOF7(+) results for 1D Hubbard model

In view of the improvement obtained for PNOF7(-), which outperforms its predecessor PNOF7(+) as shown above, it is worth to come back to the study carried out in the previous chapter in order to include PNOF7(-). In Fig. 35, we show the energies obtained for the 1D Hubbard model by using many NOFAs. Note that PNOF7 stands now for the negative sign in the inter-pair interactions, i.e. PNOF7(-). The relative error with respect to exact energies obtained by using PNOF7(-) is about one order smaller than any other NOFA. Besides, PNOF7(-) is more stable for varying U/t, and thus it is more appropiate in order to study processes that involve many correlation regimes, such as breaking bond processes.

Let us focus on the double occupancy in the case of two, four, and six sites Hubbard model. PNOF7(-) is the only functional able to go parallel to the exact dE/dU according to Fig. 36. Therefore, the proper selection of the phase for the inter-pair correlation amends any issue related with pinned occupancies, as it is illustrated in Fig. 37.

In contrast with the results shown in Fig. 29, PNOF7(-) yields the exact occupancies for any correlation regime in the four sites Hubbard model. In fact, the occupancies of e_g orbitals remain fixed to 1.0, while there is a occupation transference from the a_{1g} orbital to the b_{1g} one as U/t increases. For the six site hexagon, no significant changes appear for PNOF7 when we modify the phase of inter-pair interactions. According to Figs. 35, 36, and 37, the proper selection of phases amends not only the PNOF7 energies, but also its corresponding NOs and

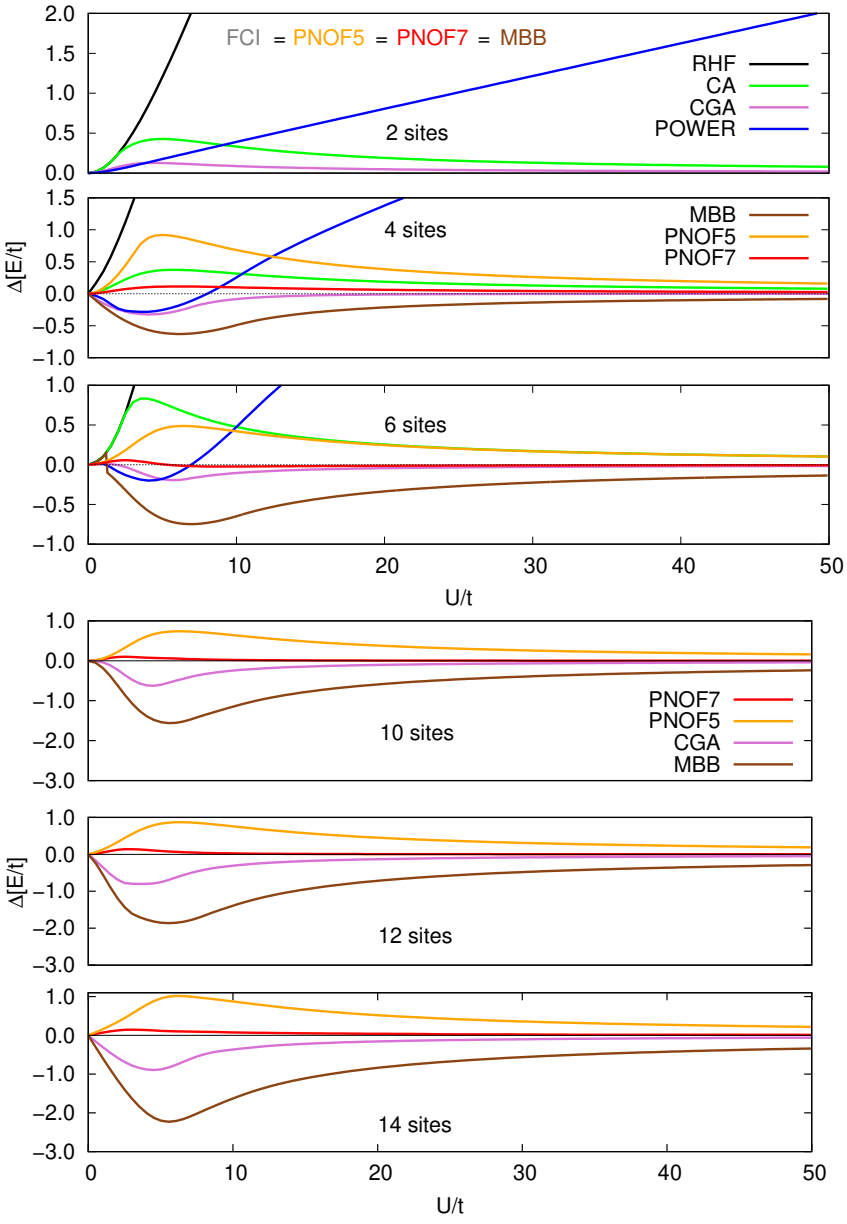

Figure 35 – Differences in E/t values with respect to exact FCI obtained for the 1D homogeneous Hubbard model by using many NOFAs. PNOF7 refers here to PNOF7(-).

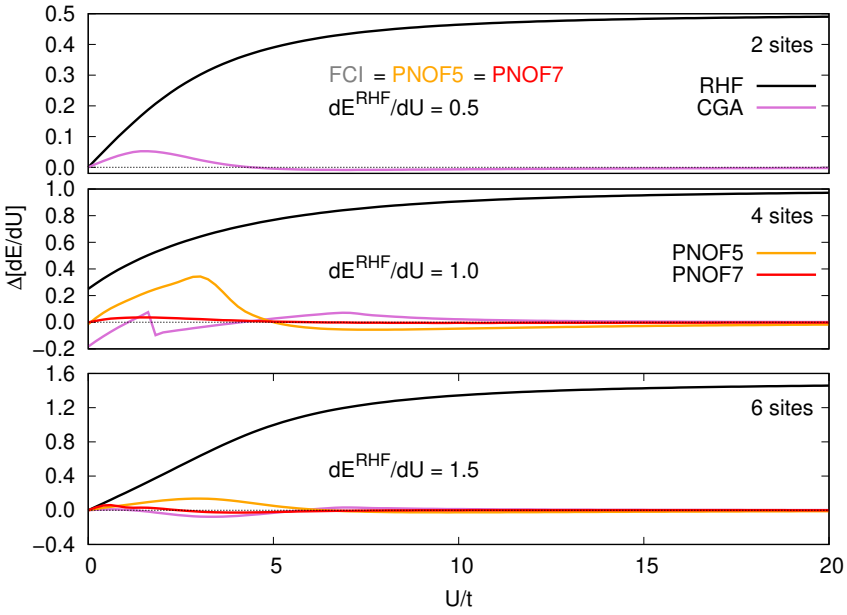

Figure 36 – Differences in dE/dU values with respect to exact FCI obtained for many NOFAs. PNOF7 stands here for PNOF7(-).

ONs.

6.2.4 Hydrogen rings

In accordance with the results shown in chapter 6.1, and results showed in Figs. 35-37, PNOF7(-) is the best approximation within NOFT to study systems described by the Hubbard model. Within the limitations of the Hubbard model, the lack of long-range inter-electron interactions may be one of the most important. Therefore, in the following we focus on a model system for the strong static electron correlation in order to examine if the conclusion obtained from the previous section still holds in presence of long-range interaction effects.

Let us consider a periodic chain of hydrogen atoms and vary the number of atoms as done in the Hubbard model with the sites. We consider the non-relativistic many-electron Hamiltonian to describe these systems, i.e.

$$\begin{aligned} H &= H_{nuc} + \sum_{\sigma} \sum_{ij} h_{ij} c^{\dagger}_{i\sigma} c_{j\sigma} \\ &+ \frac{1}{2} \sum_{\sigma\tau} \sum_{ijkl} < ij|kl > c^{\dagger}_{i\sigma} c^{\dagger}_{j\tau} c_{k\tau} c_{l\sigma}, \end{aligned} \tag{185}$$

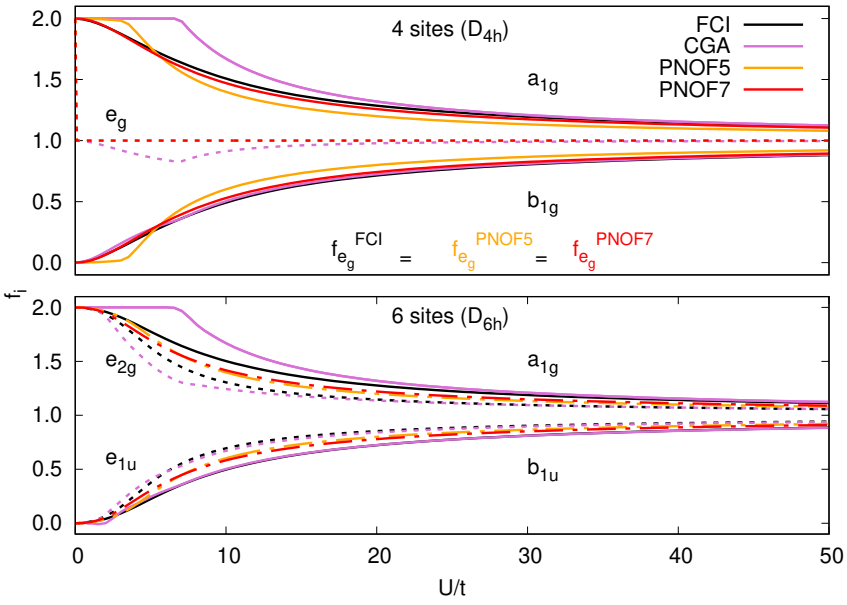

Figure 37 – Natural orbital occupancies (spins summed) obtained for FCI, CGA, PNOF5, and PNOF7(-), referred to as just PNOF7, in the 4-sites square and 6-sites hexagone Hubbard systems. Solid lines are used for non-degenerate occupancies, whereas dotted and dashed-dotted lines correspond to degenerate occupancies. In this plot f stands for ON, i.e. n.

Figure 38 – 2D polygon distribution of hydrogen atoms for 2, 4 and 16 atoms. Near-neighbor distance is fixed to $R_{H-H} = 2.0$ Å for all the cases.

where the first term accounts for the inter-nuclear repulsion, the second term includes both the kinetic energy and the nuclear repulsion, and the last term introduces Coulombic repulsion between electrons. Note that in Eq. (185) indices i, j, k, and l run over spatial orbitals, whereas τ and σ run over spin functions. This model may be the simplest example of strong electronic correlation in low dimensions, since a multireference method is required to get an accurate description for $R_{H-H} = 2.0$ Å or larger bond distances due to the strong correlation near the equilibrium geometry and in the limit of dissociation [103]. The employed systems are illustrated in Fig. 38 for the chains of 2, 4, and 16 hydrogen atoms.

In Fig. 39 we show the relative energies obtained by using PNOF7(-) and PNOF7(+) with respect to exact diagonalization (ED), increasing the chain of hydrogen atoms from 2 to 16 at an internuclear distance of $R_{H-H} = 2.0$ Å. We use minimal basis in all the calculations. According to Fig. 39, the results obtained employing PNOF7(+) show the same drawbacks already displayed for the Hubbard model. The relative errors shown by this approximation get larger as the size of the chain increases, so PNOF7(+) is not expected to give an accurate description of the electron correlation in the presence of many inter-pair interactions. In contrast, when we choose all the sign functions negative for the inter-pair electron correlation in eq. (106), the relative errors with respect to exact diagonalization results do not increase with the number of hydrogens, as shown in Fig. 39. Note that the accurate energy (101) is recovered for the two-electron system by using either PNOF7(+) or PNOF7(-), so there is no error for this system. The largest error obtained by using PNOF7(-) is below 0.007 hartree, so the latter is notably superior to PNOF7(+), and does not present any issue with the size of the system. According to Fig. 40, the relative errors shown by PNOF5 get larger as the size of the chain increases, so PNOF5 is not expected to give an accurate description of the electron correlation in the presence of many inter-pair interactions. The poor performance obtained by the

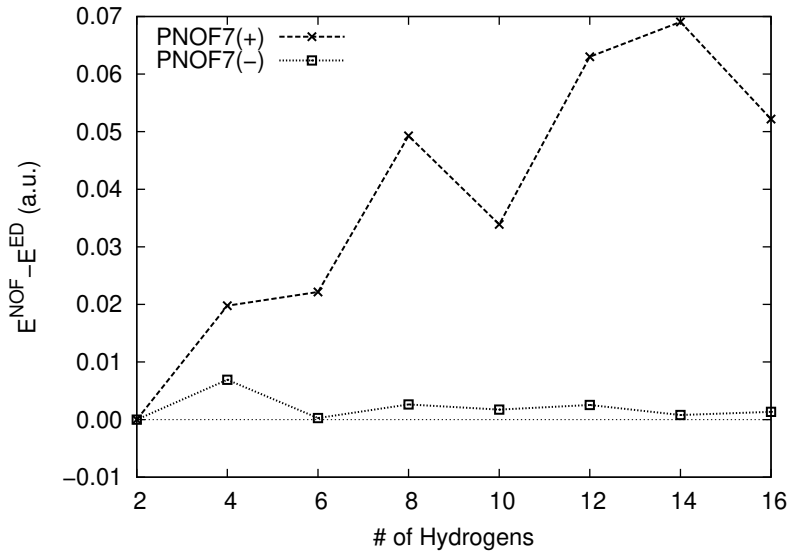

Figure 39 – Relative differences with respect to ED energies obtained by using PNOF7(+) and PNOF7(-) for the periodic chain of hydrogens at $R_{H-H} = 2.0$ Å with varying size. Calculations are performed using minimal basis.

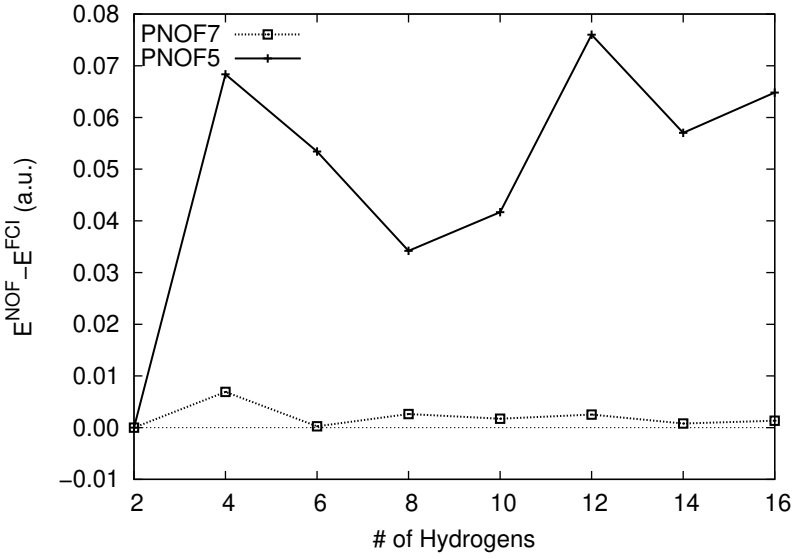

Figure 40 – Relative differences with respect to ED energies obtained by using PNOF5 and PNOF7(-) (referred to as just PNOF7) for hydrogen rings at $R_{H-H} = 2.0$ Å with varying size. Calculations are performed using minimal basis.

independent-pair model PNOF5 comparing to PNOF7(-) demonstrates that fully correlated methods are indeed needed to describe properly 1D hydrogen chains.

6.2.5 Closing remarks

In this chapter, we have presented a novel approach to tackle the phase dilema in the context of NOFT. The *bottom-up* method employed by Piris to develop approximate ensemble N-representable functionals does not require the use of the wavefunction and makes use of ensemble N-representability conditions to get an explicit form of the functional. Nevertheless, there is still an indeterminacy with respect to the pahse of the interaction between electrons pairs with opposite spins. We have shown that this indefiniteness must be studied carefully, as it dramatically affects the performance of our approach.

For this purpose we select model systems for electron correlation, such as the 1D Hubbard model with periodic boundary conditions and molecular hydrogen rings. Despite of their simplicity, the Hubbard model and the chain of hydrogen atoms (located at $R_{H-H} = 2.0$ Å) present strong non-dynamic correlation effects, and can be viewed as benchmarking systems to test multireference electronic structure methods. It has been demonstrated that the PNOF7 approach presented here captures the physics that appears in strongly correlated systems. After an adequate choice of sign factors for the inter-pair interactions, the so-called PNOF7 approximation gives a quasi-exact description of non-dynamic correlation effects appearing in these systems, even in the region of strong correlation.

According to the results shown throughout the chapter, the proper selection of phases amends the behavior of the functional when applying to large systems. Thus, the performance of PNOF7(-) (or just PNOF7), does not deteriorate with the size of the system, so the latter could be used to study strongly correlated systems beyond small molecules, e.g. periodic polymers or heavy-element-containing molecules.

CHAPTER 7

Strongly correlated electrons

7.1 1D

1D many-electron systems remain a non-trivial problem for electronic structure methods. DFT in its conventional local or semilocal approximations is not able to provide a correct description of correlated insulators [91], CI methods cannot deal with too large systems, and CCSD(T) shows instabilities at large interatomic distances in 1D chains of hydrogen (H) atoms [1]. The DMRG algorithm [104] provides exact results in 1D systems, so it is employed as benchmark for our calculations.

The electronic wavefunction is taken as a linear combination of geminal functions to have a non-factorial scaling. In this context, variational Monte Carlo calculations using a Jastrow-antisymmetrized geminal power wavefunction has recently been used [105] to successfully investigate periodic 1D H chains. Another approach based on geminal expansions is AP1roG. The optimized orbital version of AP1roG (OO-AP1roG) has proven [2] to be a reliable method for strongly correlated 1D systems, such as the 1D Hubbard model with periodic boundary conditions (PBC), as well as for metallic and molecular H rings. Nevertheless, it has recently been shown [3] that contributions from singly occupied states are important in the strong correlation limit, so OO-AP1roG needs to include open-shell configurations to accurately describe the $U/t \to \infty$ limit in the 1D Hubbard model and the dissociation limit in H chains.

From the outset NOFT correctly handles the multiconfigurational character inherent in strongly

Table 22 – Equilibrium distances (R_e) and dissociation energies (D_e) for the symmetric dissociation of linear H_{50} using the STO-6G basis set. RHF, MP2, PBE, OO-AP1roG, and DMRG data from [2].

	RHF	MP2	PBE	OO-AP1roG	PNOF7	DMRG
R_e (Å)	0.940	0.955	0.971	0.966	0.976	0.970
D_e (eV)	199.0	144.1	146.6	82.2	86.9	89.7

correlated systems. The electron pairing approach came to the NOFT with the proposal of PNOF5 [56]. The latter is closely related to geminal approaches, since it corresponds to an APSG [57]. PNOF5 draws a system of N electrons as independent electron pairs providing a good description of the intra-pair electron correlation, but lacks the correlation between pairs. Consequently, a bad description of the strong correlation limit is obtained [47]. To introduce inter-pair electron correlation effects in singlet states, PNOF7 was proposed [45, 47] (see Eq. 106).

In PNOF7 the particle-hole symmetry is explicitly considered through Φ_p in the $\mathcal{L}$-term (see Eq. 106). This resembles the original formulation of Bardeen, Cooper and Schrieffer (BCS) [106], which uses these types of interactions for all orbitals. The BCS method is one of the best mean-field approaches to the Hubbard model with attractive interactions [10], but underestimates the correlation effects in systems with repulsive Hamiltonians [107]. For the latter, recent studies [47, 99, 196] suggest that PNOF7 could correctly recover the strong correlation limit. In this chapter, we provide an extensive study of H chains composed of 50 atoms and the 1D Hubbard model in many filling situations, sizes, and correlation regimes.

7.1.1 Long molecules

First, we show the ability of PNOF7 to describe bond-breaking processes by using a linear H chain composed of 50 atoms. The latter is the simplest prototype of strong correlation in 1D, and a challenging test [1] for non-dynamic correlation. All calculations are carried out using the STO-6G minimal basis [6].

Fig. 41 shows the energies obtained for symmetric stretching of linear H_{50} by using PNOF7, together with reference DMRG results and other well-established electronic structure methods, namely, restricted Hartree-Fock (RHF), second-order Möller-Plesset pertubation theory (MP2),

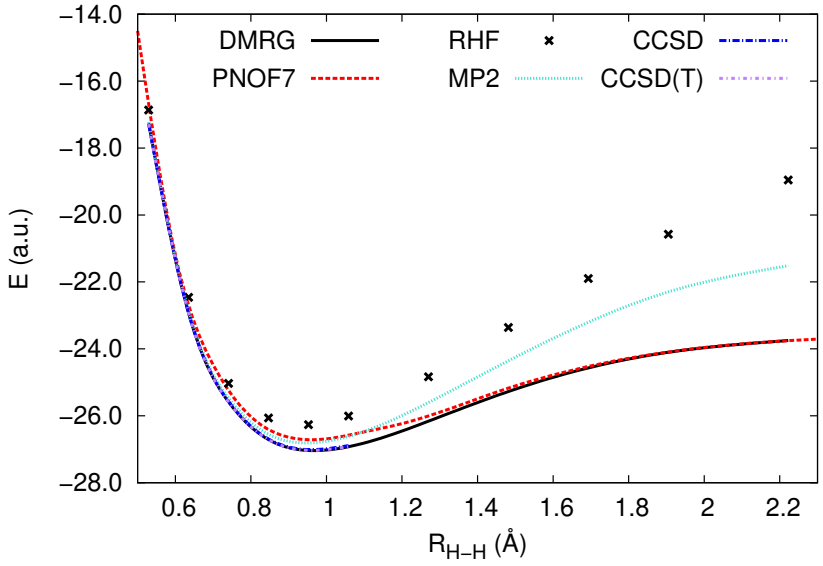

Figure 41 – Symmetric dissociation of linear H_{50} using the STO-6G basis set. RHF, MP2, CCSD, CCSD(T), and DMRG data from [1].

CCSD, and CCSD(T). There is an outstanding agreement between PNOF7 and DMRG along the dissociation curve, specially at large bond distances (insulating phase) as well as at short H-H distances (metallic phase). At the equilibrium distance, PNOF7 underestimates slightly the correlation, however an inspection of spectroscopic constants (see table 22) shows that PNOF7 agrees with DMRG better than standard methods such as RHF, MP2, or the Perdew-Burke-Ernzerhof (PBE) density functional. These methods fail dramatically at the dissociation limit [2] since the occupancies become strongly fractional at intermediate and long H-H distances, a behavior that PNOF7 (see Fig. 42) and OO-AP1roG (see Fig. 4 in Ref. [2]) correctly reproduce. Non-integer occupations also make CCSD and CCSD(T) not convergent [1], so the latter can be exclusively employed in the equilibrium region. Note that OO-AP1roG underestimates the equilibrium distance (R_e) and dissociation energy (D_e), whereas PNOF7 underestimates D_e and yields slightly large R_e.

Fig. 43 shows the energies obtained for the asymmetric dissociation of linear H_{50}. It should be noted that the energy decreases monotonically from the reference state composed of equidistant H atoms to the set of independent H_2 molecules. In the asymmetric stretching, we alternate the bond-stretching, so that half of the bonds remain fixed, while the other half is stretched. In the dissociation limit, we have 25 near-independent H_2 molecules. Similar to symmetric

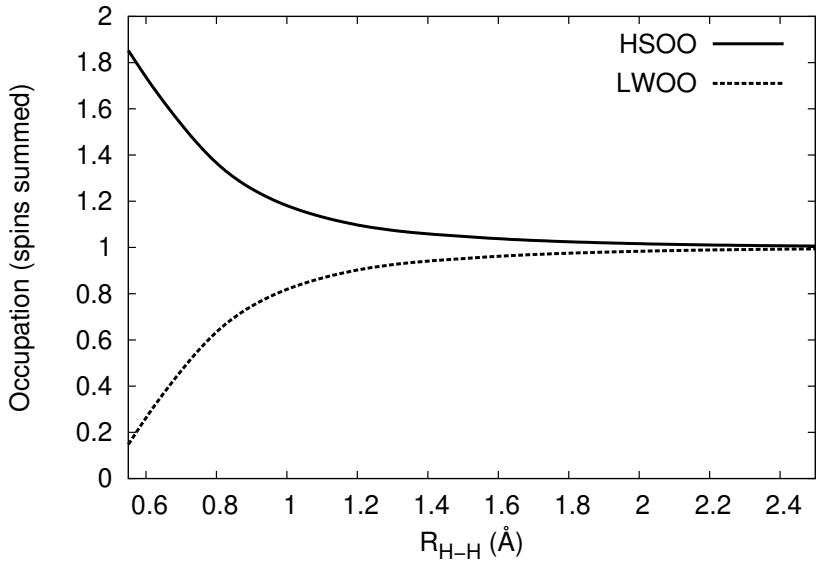

Figure 42 – ONs of the highest strongly occupied NO (HSOO) and the lowest weakly occupied NO (LWOO) for the symmetric dissociation of linear H_{50} at the PNOF7/STO-6G level of theory.

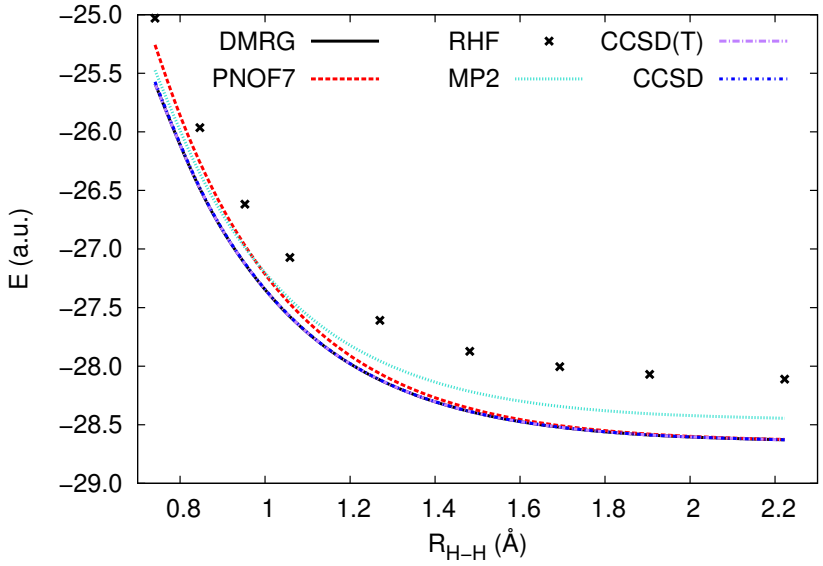

Figure 43 – Asymmetric dissociation of linear H_{50} using the STO-6G basis set. RHF, MP2, CCSD, CCSD(T), and DMRG data from [1].

dissociation, PNOF7 agrees with DMRG over large bond distances, whereas there are slight differences at shorter bonds.

The results obtained for H_{50} chains prove that numerical accuracy of PNOF7 is comparable to that of the DMRG in many different correlation regimes. This study includes the PNOF7 in the list of highly correlated methods to study any system related to linear H chains [111].

7.1.2 1D Hubbard model

In a minimal basis set, there is only one band in 1D H systems, therefore, as long as long-range interactions are negligible, the problem resembles the 1D Hubbard model. We will employ the Hubbard Hamiltonian described by Eq. (184), in which $\mathbf{r}$ has only one component in order to have a 1D system. Let us restrict to the repulsive Hubbard model, hence U is always positive. U/t is used as a dimensionless measure for the relative contribution of both terms, therefore, at $U/t \to 0$ (metallic state) the mean-field theories work well due to the lack of two-electron interactions, whereas at $U/t \to +\infty$ (insulating state) strong correlations play the dominant role keeping electrons away from each other.

In Fig. 44, we report the PNOF7 energy differences with respect to the exact results for the 1D Hubbard model at half-filling. The number of sites varies from 14 to 122 in small and intermediate correlation regimes. For comparison, OO-AP1roG results [3] have been included. The data sets used in this figure can be found in Table 23. Note that OO-AP1roG deteriorates for large systems (some errors fall out of Fig. 44), as well as for large U/t values. Conversely, PNOF7 is able to hold its accuracy with respect to exact results when the system size increases. Similar to the results obtained for the H chains, for a given system, PNOF7 converges to the exact results in the strong correlation limit.

Since the particle-hole symmetry is explicitly introduced into the functional 106, PNOF7 is expected to be appropriate for the half-filling case. Now we test the performance of PNOF7 away from half-filling where the particle-hole symmetry is broken, so that inhomogeneous phases can appear [108]. The energy per site for the 1D Hubbard model is shown in table 24. We focus on the strong correlation limit, i.e., large U/t values, which is particularly problematic for geminal-based theories like OO-AP1roG [3]. For reference, we use the variational 2RDM (v2RDM) with P, Q and G N-representability constraints values and quasi-exact results of the variational Matrix Product State (vMPS) algorithm taken from Ref. [7].

Table 24 shows that PNOF7 remains close to vMPS for $N = 16$ in 20 sites chain, whereas it lacks correlation energy for $N = 12$. In the case of 50 sites, PNOF7 produces accurate energies and it

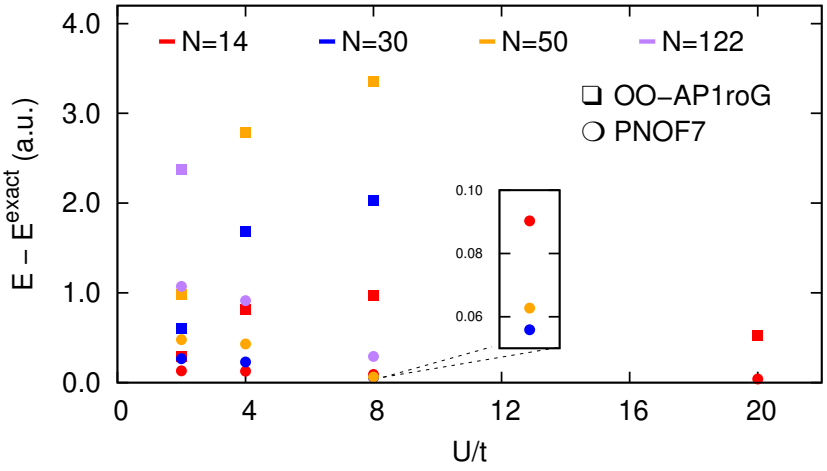

Figure 44 – Energies (a.u.) for the 1D Hubbard model at half-filling with PBC. OO-AP1roG and exact data from [2,3]. For U/t = 20, only the result for N = 14 is reported.

Table 23 – Energies (a.u.) for the 1D Hubbard model at half-filling with periodic boundary conditions. OO-AP1roG, RHF, and exact data from Ref. [2,3].

N_{sites}	U/t	RHF	OO-AP1roG	PNOF7	EXACT
14	2	-10.9758	-11.6627	-11.8230	-11.9543
	4	-3.9758	-7.2701	-7.9610	-8.0883
	8	10.0242	-3.6471	-4.5228	-4.6131
	20	52.0242	-1.4132	-1.8932	-1.9340
30	2	-23.2671	-24.7779	-25.1161	-25.3835
	4	-8.2671	-15.5495	-17.0035	-17.2335
	8	21.7329	-7.8152	-9.78283	-9.8387
50	2	-38.7039	-41.2570	-41.7650	-42.2443
	4	-13.7039	-25.9154	-28.2696	-28.6993
	8	36.2961	-13.0253	-16.3215	-16.3842
122	2	-94.3524	-100.6497	-101.9499	-103.0211
	4	-33.3524	-63.2336	-69.0861	-70.0003
	8	88.6476	-31.7817	-39.6698	-39.9619

Table 24 – Energy per site (a.u.) for 1D Hubbard model away from half-filling at $U/t \to 100$. Reference vMPS, v2RDM, and exact data from [7]. N_{sites} and N stands for the number of sites and electrons, respectively.

N_{sites}	N	PNOF7	vMPS	v2RDM	Exact*
20	12	-0.6025	-1.0312	-1.2177	-1.0008
	16	-0.3820	-0.4951	-0.7860	-0.4639
50	20	-0.9081	-	-1.2191	-1.0008
	40	-0.4444	-	-0.7862	-0.4671

*Exact results correspond to $U/t \to \infty$.

approaches the exact result. Consequently, PNOF7 turns out to be particularly accurate from a certain amount of electrons, from which the strong correlation limit is described successfully. It is worth noting that PNOF7 is more accurate than v2RDM when only two-particle conditions are applied. It has recently been emphasized [109,110] that three-particle conditions are needed in v2RDM to accurately describe the strong correlation limit of the Hubbard model.

7.1.3 Closing remarks

With the present chapter, a step forward has been taken in the development of efficient methods for strong correlation. With a mean-field scaling, the PNOF7 approximation compares with state-of-the-art methods for describing strongly correlated electrons, e.g. DRMG, quantum Monte Carlo or complete active space configuration interaction methods, and overcomes the problems shown by similar approaches in the strong correlation limit. The present chapter will have a significant impact on the development of new materials in which large unit cells are required.

7.2 2D

7.2.1 Introduction

The Hubbard model defined on 2D lattices with repulsive interactions constitutes a powerful tool to understand the physics of 2D materials. For instance, the 2D Hubbard model has been recently employed to describe experimental observations in graphene nanoribbons [112], as well as to study the phase diagram of high-T_c cuprate superconductors [113]. A general solution for the 2D Hubbard model remains unknown, although several approaches have proven to be accurate for specific cases, namely the auxiliary-field quantum Monte Carlo (AFQMC) method at half-filling [10], the density matrix embedding theory (DMET) [114] in the noninteracting and atomic limits, and the density matrix renormalization group (DMRG) algorithm [115] if a sufficient number of retained renormalized basis states is considered [5]. The latter is probably the most efficient method to study 1D systems, however, the DMRG performance is less accurate in 2D due to its 1D topology [104].

A recent benchmarking [108] shows the performance of well-established methods in quantum chemistry in the context of 2D fermionic systems. Many of these methods, such as CCSD(T), the gold-standard in quantum chemistry, dramatically fail at strong correlation regimes. Variational methods based on RDM emerge as promising alternatives for studying strongly correlated materials [188]. The variational second-order RDM (v2RDM) method has demonstrated to accurately describe the 2D Hubbard model at half-filling [4] and away from half-filling [5] if three-particle constraints are imposed. Unfortunately, this implies a slow computational scaling of $\mathcal{O}\left(M^9\right)$, M being the dimension of the single-particle space.

Favorable computational efficiency can be achieved using one-particle theories such as DFT or 1RDM functional theory (1RDMFT) [33]. 1RDMFT describes correctly metal insulator transitions [187] and strongly correlated electrons in 1D [34, 47, 99, 196]. The goal of this chapter is then to investigate the ability of 1RDMFT to deal with correlated electrons in 2D systems. Recently [197], a formulation for the 1RDMFT on a lattice has been published, based on the exact solution of the two-site problem. We demonstrate that a more general and fundamental formulation of 1RDMFT is equally valid to deal with lattice models, without any loss of generality.

In this chapter, we provide an extensive study of 2D systems using the PNOF7 [45, 47] formulation for spin-multiplets, which is reviewed in section 7.2.2. In section 7.2.3, we employ the 2D

Hubbard model varying the relative contribution between the hopping (t) and electron-electron on-site interaction (U) parameters, as well as the filling, for different system sizes that reach up to 12x12 square lattices. Here, our results are compared to state-of-the-art methods for the study of strong correlation, such as DMRG, v2RDM, AFQMC, and ED.

The lack of long-range inter-electronic interactions may be the most important limitation of the Hubbard model. In fact, it has been recently [111] emphasized that the properties of hydrogen chains can strongly differ from those obtained by means of the 1D Hubbard model. Accordingly, in section 7.2.4 we focus on 2D lattices of hydrogen atoms to model the strong electron correlation in the presence of long-range interaction effects. The symmetric dissociation of 2D hydrogen lattices is studied.

7.2.2 NOF for multiplets

Let us consider a non-relativistic Hamiltonian free of spin coordinates, hence the ground state with total spin S is a multiplet, i.e., a mixed quantum state (ensemble) that allows all possible S_z values. Next, we briefly describe how we do the reconstruction of D to achieve the PNOF7 for spin-multiplets. A more detailed description can be found in Ref. [69].

First, we consider $\mathrm{N_I}$ single electrons and $\mathrm{N_{II}}$ paired electrons, so that $\mathrm{N_I} + \mathrm{N_{II}} = \mathrm{N}$. We also assume that all spins corresponding to $\mathrm{N_{II}}$ electrons are coupled as a singlet, thence the $\mathrm{N_I}$ electrons determine the spin S of the system. We focus on the mixed state of highest multiplicity: $2S + 1 = \mathrm{N_I} + 1$, $S = \mathrm{N_I}/2$ ($<\hat{S}^2> = \mathrm{N_I}/2\,(\mathrm{N_I}/2 + 1)$). For this ensemble of pure states $\{|SM\rangle\}$, the expected value of $\hat{S}_z$ is zero, namely,

$$<\hat{S}_z> = \frac{1}{\mathrm{N_I} + 1} \sum_{M=-\mathrm{N_I}/2}^{\mathrm{N_I}/2} M = 0 \tag{186}$$

Consequently, we can adopt the spin-restricted theory in which a single set of orbitals is used for α and β spins. All spatial orbitals will be then double occupied in the ensemble, so that occupancies for particles with α and β spins are equal: $n_p^\alpha = n_p^\beta = n_p$.

In turn, we divide the orbital space Ω into two subspaces: $\Omega = \Omega_\mathrm{I} \oplus \Omega_\mathrm{II}$. Ω_II is composed of $\mathrm{N_{II}}/2$ mutually disjoint subspaces Ω_g. Each subspace $\Omega_g \in \Omega_\mathrm{II}$ contains one orbital g below the level $\mathrm{N_{II}}/2$, and N_g orbitals above it. In this chapter, N_g is equal to a fixed number corresponding to the maximum value allowed by the basis set used in calculations. Taking into account the spin, the total occupancy for a given subspace Ω_g is 2, which is reflected in additional sum rule,

namely,

$$\sum_{p\in\Omega_g} n_p = 1,\ \Omega_g \in \Omega_{\rm II} \tag{187}$$

It follows that

$$2\sum_{p\in\Omega_{\rm II}} n_p = 2\sum_{g=1}^{{\rm N_{II}}/2}\sum_{p\in\Omega_g} n_p = {\rm N_{II}} \tag{188}$$

Similarly, $\Omega_{\rm I}$ is composed of $\rm N_I$ mutually disjoint subspaces Ω_g, but in contrast to $\Omega_{\rm II}$, each subspace $\Omega_g \in \Omega_{\rm I}$ contains only one orbital g with $2n_g = 1$. It is worth noting that each orbital is completely occupied individually, but we do not know whether the electron has α or β spin: $n_g^\alpha = n_g^\beta = n_g = 1/2$. It follows that

$$2\sum_{p\in\Omega_{\rm I}} n_p = 2\sum_{g={\rm N_{II}}/2+1}^{{\rm N_{II}}/2+{\rm N_I}} n_g = {\rm N_I}, \tag{189}$$

so taking into account eq. (188), the trace of the 1RDM is verified equal to the number of electrons:

$$2\sum_{p\in\Omega} n_p = 2\sum_{p\in\Omega_{\rm II}} n_p + 2\sum_{p\in\Omega_{\rm I}} n_p = {\rm N_{II}} + {\rm N_I} = {\rm N} \tag{190}$$

To guarantee the existence of an N-electron system compatible with the functional (75), we must observe the N-representability conditions [20] on the reconstructed 2RDM [31]. Assuming real spatial orbitals, the employment of necessary N-representability conditions leads to PNOF7 for multiplets:

$$E = \sum_{g=1}^{{\rm N_{II}}/2} E_g + \sum_{g={\rm N_{II}}/2+1}^{{\rm N_{II}}/2+{\rm N_I}} \mathcal{H}_{gg} + \sum_{f\neq g=1}^{{\rm N_{II}}/2+{\rm N_I}} E_{fg} \tag{191}$$

$$E_g = 2\sum_{p\in\Omega_g} n_p\mathcal{H}_{pp} + \sum_{q,p\in\Omega_g} \Pi_{qp}\mathcal{K}_{pq},\ \Omega_g \in \Omega_{\rm II} \tag{192}$$

$$\Pi_{qp} = \begin{cases} \sqrt{n_q n_p}\,, & q = p \text{ or } q, p > \frac{N_{\rm II}}{2} \\ -\sqrt{n_q n_p}\,, & q = g \text{ or } p = g \end{cases} \tag{193}$$

$$E_{fg} = \sum_{p\in\Omega_f}\sum_{q\in\Omega_g} \left[n_q n_p\left(2\mathcal{J}_{pq} - \mathcal{K}_{pq}\right) - \Phi_q\Phi_p\mathcal{K}_{pq}\right] \tag{194}$$

where $\Phi_p = \sqrt{n_p(1-n_p)}$. $\mathcal{J}_{pq}$ and $\mathcal{K}_{pq}$ refer to the usual Coulomb and exchange integrals $\langle pq|pq\rangle$ and $\langle pq|qp\rangle$, respectively. It should be noted that E_g reduces to a NOF obtained from ground-state singlet wavefunction (see Eq. 101), so it describes accurately two-electron systems [153]. In the last term of eq. (191), E_{fg} correlates the motion of electrons with parallel and opposite spins belonging to different subspaces ($\Omega_f \neq \Omega_g$).

7.2.3 2D Hubbard model

Along this section we restrict to the 2D model, so each vector $\mathbf{r}$ in the Hubbbard Hamiltonian (see Eq. 184) has two components. In the noninteracting limit ($U = 0$), the Hartree-Fock 2RDM provides the exact solution for the tight-binding Hamiltonian, whereas for nonzero electron-electron on-site interactions ($U \neq 0$) a correlated approximation for the 2RDM must be given.

In the following, we test the performance of PNOF7 against some of the benchmarks used in Refs. [108, 113]. The results obtained by means of the v2RDM methods with two-particle constraints (PQG), and $T1$ and $T2'$ N-representability conditions (PQGT') are also included. We study the Hubbard model on 2D square lattices for different sizes, filling situations (or densities), and spin multiplicities.

7.2.3.1 Half-filling

Let us set the number of electrons to be equal to the number of sites, therefore, we have a half-filled lattice. There is one electron per site, that is, half the maximum possible number (two electrons per site).

In Fig. 45, we show the PNOF7, PQG, and PGQT' energy differences with respect to ED for the 4x4 square lattice Hubbard model at half-filling. Fig. 45 reveals that PNOF7 is in good agreement with the ED results and perform similar to PQGT'. The latter reproduces accurately the ED results, but at the expense of an unfavorable scaling of $\mathcal{O}\left(M^9\right)$. The scaling can be reduced to $\mathcal{O}\left(M^6\right)$ if only two-particle constraints are applied, but this deteriorates the performance for large U/t as shown by the PQG results.

It is interesting to look at the 1RDM in the site basis, denoted hereafter as γ. Since PNOF7 contains particle-hole symmetry, γ is completely symmetric (i.e. $\gamma_{ij} = \gamma_{ji}$). All sites are equivalent, so we have just to look at the elements involving one site and its neighbours. At half-filling the average occupation of each site is one for any value of U/t, i.e. $\gamma_{11} = 1.0$. On the contrary, off-diagonal elements vary depending on the correlation regime. As shown in Fig. 46, the largest value is obtained for nearest-neighbours, so that γ_{12} is maximum at $U/t = 0$, and it decreases monotonically to zero at the strong correlation limit. The latter is intimately related with electron delocalization, which is inversely proportional to U/t. There is another nonvanishing off-diagonal element that shows a similar dependence on electron correlation. As expected, these values are four-fold degenerate due to the 2D nature of the system with periodic

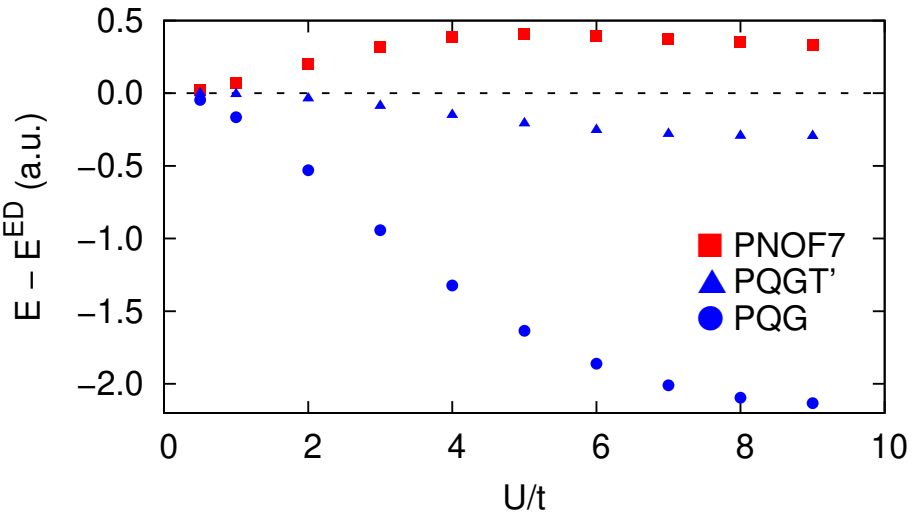

Figure 45 – PNOF7, PQG, and PGQT' energy differences with respect to ED for the 4x4 square lattice Hubbard model at half-filling. ED, PQG, and PQGT' data from Ref. [4].

boundary conditions in both directions.

At half-filling the Hubbard Hamiltonian has particle-hole symmetry and the AFQMC method turns out to be numerically exact [10], so it can be used as benchmark in larger systems. In Table 25, we show the absolute energies corresponding to the 8x8=64, 10x10=100, and 12x12=144 sites 2D Hubbard model. It should be noted that the conclusions obtained in Ref. [47] for the 1D Hubbard model hold in two-dimensions: (1) results obtained by using PNOF7 are comparable to exact results for a wide range of U/t values, and (2) the performance of PNOF7 does not deteriorate with the increasing size of the system. According to Table 25, PNOF7 recovers approximately 98% of the total energy for $U/t = 2$, whereas for $U/t = 8$, 96% of the total energy is retrieved. It is worth noting that the mean absolute error per site (MAES) does not change significantly going from 64 to 144 sites.

In Table 26, we report the PNOF7 electron detachment energies (EDE) for the 10x10 square lattice by varying U/t. The EDEs are computed as the energy difference between doublet- and singlet-spin states ($E^{S=1/2} - E^{S=0}$), so that an electron is removed to produce $S = 1/2$. We observe that EDEs are negative since in our model Hamiltonian (**??**) we do not consider an on-site attractive potential that represents the effects of an external field on the electrons. EDE increase in absolute value as the on-site electron-electron repulsion increases for a given t, since overall electron repulsion is reduced by removing an electron. Accordingly, the localization of

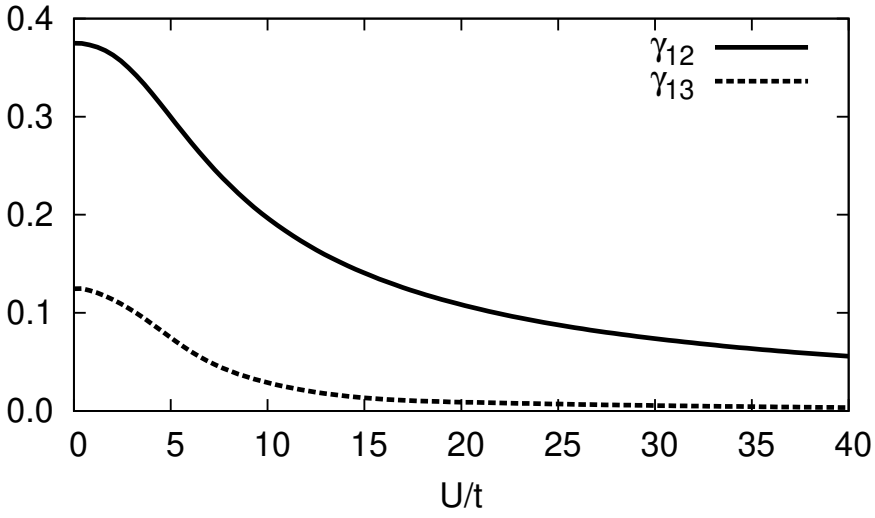

Figure 46 – PNOF7 1RDM in the site basis at half-filling for the 4x4 square lattice Hubbard model.

electrons that takes place at half-filling with large U/t values favors the removal of an electron.

7.2.3.2 Away from half-filling

In Eq. (191), the last term of PNOF7 correlates the motion of electrons belonging to different subspaces by introducing explicitly the particle-hole symmetry through $\Phi_p = \sqrt{n_p(1-n_p)}$. Consequently, PNOF7 is expected to be particularly accurate at half-filling since the Hubbard model exhibits particle-hole symmetry in this case. Let us now break the particle-hole symmetry of the system in order to test the performance of PNOF7 away from the half-filling. Breaking this symmetry strongly affects the nature of the system, since it deformates its Fermi surface and, therefore, the corresponding electronic interactions turn out to be less localized [104].
Results corresponding to the 4x4=16 sites Hubbard model including 14 and 16 electrons are shown in Fig. 47. Exact results corresponding to ED, as well as approximate energies from v2RDM with PQGT' constraints, are taken from Ref. [5]. PNOF7 retains its accuracy for any filling as U/t increases, while v2RDM fails away from half-filling in the intermediate and strong correlation regimes. The maximum error shown by PNOF7 ($\Delta E \sim 2.5\%$) corresponds to $U/t = 4$, wherein the two points, N=14 and N=16, are on top of each other. Note that PNOF7 approaches the exact result for large U/t values.

Table 25 – PNOF7 and exact energies (in a.u.) from AFQMC calculations [10] for the Hubbard model defined on 8x8, 10x10, and 12x12 square lattices at half-filling varying U/t. Mean absolute error per site (MAES) is shown for the three systems.

U/t	8x8		10x10		12x12	
	Exact	PNOF7	Exact	PNOF7	Exact	PNOF7
2	-74.47	-73.37	-116.91	-115.19	-168.75	-166.17
4	-55.05	-53.27	-86.12	-83.32	-123.95	-120.20
6	-42.16	-40.53	-64.80	-63.39	-94.66	-91.24
8	-33.68	-32.26	-52.54	-50.48	-75.54	-72.53
MAES	0.02		0.02		0.03	

Table 26 – PNOF7 electron detachment energies (EDE), in a.u., for the 10x10 square lattice Hubbard model at half-filling.

U/t	2	4	6	8
EDE	-0.48	-1.06	-1.61	-1.88

In Fig. 48, we show the PNOF7 and PQGT' energy differences with respect to DMRG for the 6x6 square lattice Hubbard model at different correlation regimes and fillings, including N = 30, 34, and 36 electrons. DMRG and PQGT' values are taken from Ref. [5]. Although the largest deviations with respect to DMRG are obtained for the lowest density, corresponding to 30 electrons in 36 sites, the PNOF7 agreement with DMRG is below 1 a.u. for all U/t values reported.

At low densities (N=34 or N=30) PNOF7 reaches the strong correlation limit at smaller U/t values, as expected. In contrast, v2RDM cannot recover the large amount of correlation energy at partial-filling, although it does correctly in 1D [**?**, 110, 116]. Such dependence on dimensionality does not appear with PNOF7. We must recall that the N-representability conditions are imposed in the construction of the functional [45, 47], whereas in the v2RDM methods these constraints are imposed in the minimization of the energy functional by means of semidefinite programming techniques. The latter may become numerically unstable if all the states are nearly degenerate [4], something that is observed in strongly correlated systems. The advantages of imposing N-representability constraints on the construction of the functional rather

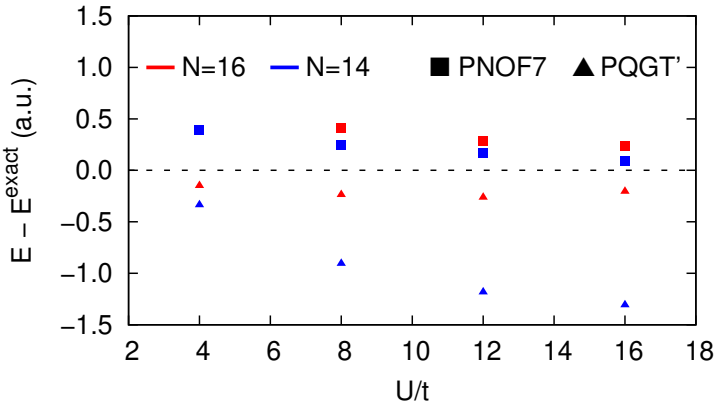

Figure 47 – PNOF7 and PQGT' energies with respect to ED for the 4x4 square lattice Hubbard model with 14 and 16 electrons. ED and PQGT' data from [5].

than the minimization process have already been emphasized [**?**] for pure N-representability conditions of the 1RDM. In addition, we have not observed particular difficulties to converge PNOF7 away from half-filling, in contrast to many other numerical methods in which convergence errors arise due to the lack of particle-hole symmetry [108].

To obtain a more reliable indication of the energy, its derivative with respect to the parameter U was also studied, namely,

$$\frac{dE}{dU} = \sum_{\boldsymbol{r}} \langle \hat{n}_{\boldsymbol{r},\alpha} \hat{n}_{\boldsymbol{r},\beta} \rangle \tag{195}$$

According to Eq. (195), dE/dU yields the double occupancy of the sites. This magnitude is very sensitive to the NOF used in the Hubbard model as our previous study on 1D systems demonstrated [99]. Several functionals other than PNOF7 produced discontinuous curves for double occupancy of the sites. In this chapter, the double occupancy is numerically evaluated by using the formula

$$\frac{dE}{dU} \approx \frac{E(U-2h) - 8E(U-h) + 8E(U+h) - E(U+2h)}{12h} \tag{196}$$

where the step size h is set to 10^{-3}.

In Fig. 49, we report the double occupancy of sites as a function of U/t for the 6x6 square lattice Hubbard model with 30 and 36 electrons. As expected, the double occupancy is maximum in the weak correlation region, since there are no two-particle interactions. The population of the sites spreads out as the correlation increases, so for large U/t values the double occupancy decreases due to the electron-electron on-site interaction. As we can see in Fig. 49, PNOF7

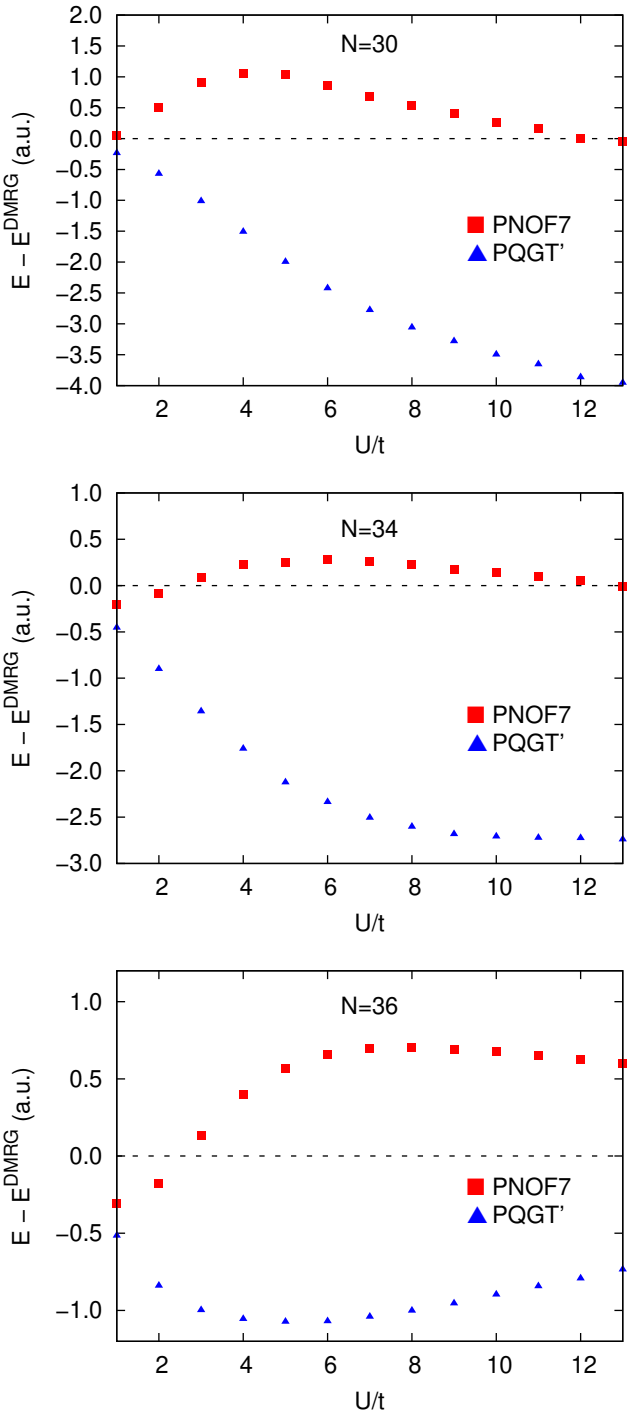

Figure 48 – PNOF7 and PQGT' energy differences with respect to DMRG for the 6x6 square lattice Hubbard model with 30, 34, and 36 electrons. DMRG and PQGT' data from [5].

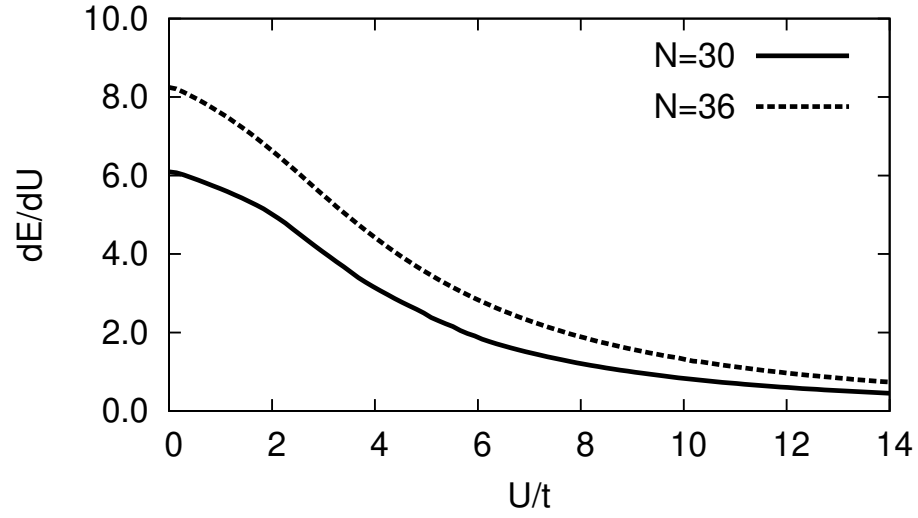

Figure 49 – Double occupancy as a function of U/t for the 6x6 square lattice Hubbard model with 30 and 36 electrons.

Table 27 – PNOF7 electron detachment energies, in a.u., for the 6x6 square lattice Hubbard model with 30 and 36 electrons.

U/t	1	6	10	14
N=36	-0.35	-1.70	-2.27	-2.62
N=30	0.46	-1.01	-1.42	-1.61

produces smooth double occupancy without discontinuities for the 2D Hubbard model. Our method shows qualitatively good trend for increasing U/t regardless of the filling. Note that at partial-filling the strong correlation limit is reached for smaller U/t values than at half-filling. Consequently, the intermediate correlation region, for which the maximum error is usually obtained, is placed at smaller U/t values in the aforementioned results.

In Table 27, we report PNOF7 EDE for the 6x6 square lattice with 30 and 36 electrons by varying U/t. Table 27 reveals that the EDE can take positive and negative values at low densities, in contrast to the half-filling ($N = 36$). In fact, at large correlation regimes EDE are negative, whereas they become positive in presence of weak correlation effects and low filling, as is the case for $U/t \sim 1$ and $N/N_s = 30/36 = 0.833$ (where N_s represents the number of sites). Note from Table 27 that the EDE increase in absolute value together with the amount

of correlation, as it has been observed for the 10x10 lattice at half-filling (see Table 26).

7.2.4 2D hydrogen lattice

We have already proven the ability of PNOF7 to describe the symmetric and asymmetric dissociation of a 1D hydrogen chain with 50 atoms, wherein the PNOF7 energies compared remarkably well with those obtained at the DMRG level of theory along the dissociation curves. The addition of a spatial dimension increases the amount of interactions and makes the bond-breaking process more complex, so new and diverse strong correlations can emerge. This section is dedicated to the study of 2D hydrogen square lattices.

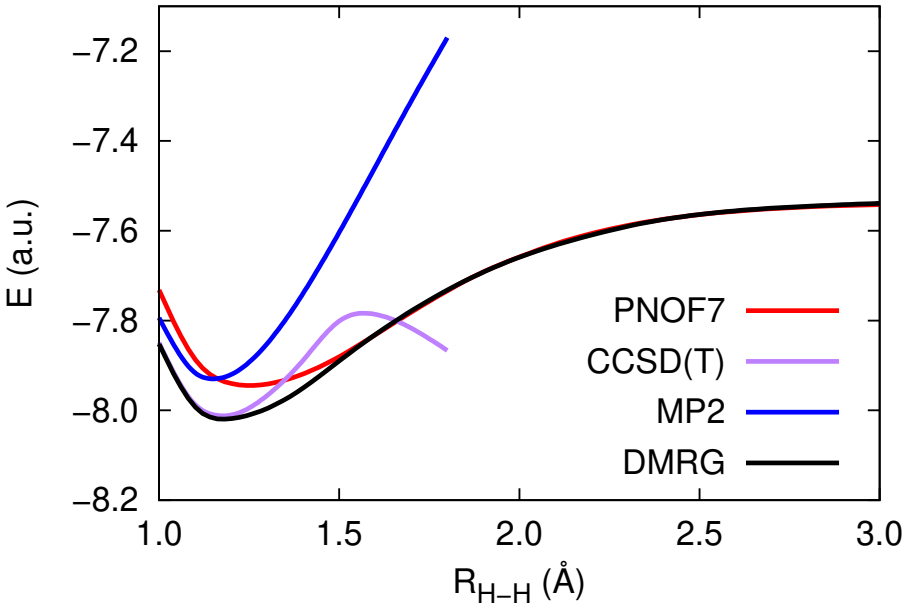

Figure 50 – Total energies for the symmetric dissociation of the 4x4 hydrogen square lattice, in a.u., using PNOF7, CCSD(T), MP2 and DMRG methods with the STO-6G basis set [6].

In Fig. 50, we show the energies obtained along the symmetric dissociation of the 4x4 hydrogen square lattice by using second-order Møller–Plesset perturbation theory (MP2), PNOF7, CCSD(T) and DMRG methods with the STO-6G basis set [6]. The streching of bonds has been done symmetrically in the two dimensions. CCSD(T) and MP2 calculations have been carried out by using the PSI4 electronic structure package [117], while the interface to CHEMPS2 by S. Wouters et al. [118] has been employed for DMRG calculations. DMRG is employed as ref-

erence for our calculations. In fact, despite the limitations of tensor network state algorithms beyond 1D, the latter are still very efficient to simulate short-range interactions dominated systems [104], such as those encountered in the minimal basis approach.

As expected, the single-reference methods MP2 and CCSD(T) fail in multireference scenarios, where we observe large deviations of the ONs from 0 and 1. CCSD(T) breaks down at $R_{H-H} >$ 1.5Å, and does not even converge for long bond lengths $R_{H-H} > 1.9$Å, as previously observed in 1D hydrogen chains [1]. For its part, MP2 provides reasonable energies slightly above CCSD(T) around the equilibrium distance, but yields too high energies over long distances, so it cannot describe the bond-breaking process either.

On the contrary, PNOF7 produces a qualitatively correct dissociation curve. PNOF7 performs similar to MP2 around the equilibrium region (see Ref. [46]), and it approaches reference DMRG results as the bond distance increases. It is worth noting the agreement at $R_{H-H} \geq 1.5$ Å, and specially at the dissociation limit. PNOF7 does not show convergence issues at any bond distance, so it can be easily employed to describe bond-breaking processes in presence of strong correlation effects, regardless of the dimensionality of the system. If more accuracy is required around the equilibrium region, we can employ a recent [45, 46] method proposed to add the missing dynamic correlation to PNOF's, denoted as NOF-MP2. For the equilibrium point obtained in Fig. 50; $R_{H-H} = 1.18$ Å, NOF-MP2 reduces the error obtained by PNOF7 in $0.04\, a.u.$, i.e. half of the total difference between DMRG and PNOF7.

Table 28 – PNOF7 electron detachment energies (EDE), in a.u., for the chain (1D) and square lattice (2D) composed of 16 hydrogen atoms with STO-6G basis set [6].

R (Å)	0.6	0.8	1.0	1.4	2.0	3.0	4.0
1D	0.03	0.16	0.21	0.29	0.37	0.45	0.47
2D	0.02	0.12	0.14	0.21	0.33	0.44	0.47

In Table 28, we report the EDE along the dissociation curve of the 4x4 hydrogen square lattice obtained as the energy difference $E^{S=1/2} - E^{S=0}$. In contrast to the results obtained for the Hubbard model, the EDE are positive along the whole dissociation curve so can be interpreted as ionization energies. EDE take larger values as non-dynamic correlation increases at large bond distances. These results leave us the following conclusions: (1) long-range non-dynamic correlation effects are crucial for the study of different spin multiplicities and they must be carefully introduced in the Hubbard model by additional terms in the Hamiltonian, and (2)

EDE show the same trend regardless the dimensionality of the system, so EDE for 1D or 2D system with 16 electrons are comparable as shown in Table 28.

7.2.5 Closing remarks

In the present chapter, it was proved that PNOF7 is an efficient method to describe strongly correlated electrons in two dimensions with a mean-field computational scaling. Two models were extensively investigated, namely the Hubbard model and the square lattice of hydrogens. We studied the singlet ground-state, as well as the doublet mixed quantum state that is obtained by extracting an electron from the system.

It was shown that the performance of the present RDM functional approximation is comparable to that of the state-of-the-art numerical methods such as AFQMC or DMRG for the Hubbard model defined on 2D square lattices. This agreement was confirmed for many filling situations and sizes up to 144 electrons, from weak to strong correlation. Unlike other RDM methods, PNOF7 showed no dependence on dimensionality, and we obtained the same accuracy in two dimensions as that achieved in one dimension. An outstanding feature is that the performance of PNOF7 does not deteriorate with the increasing size of the system. The reliability of our energies was verified by calculations of the double occupancy of sites that are known to be sensitive to the functional used in the Hubbard model. No difficulties were observed in converging PNOF7 away from half-filling. It was corroborated that the localization of the electrons that takes place at large U/t values favors the removal of an electron.

In the case of the hydrogen lattice, PNOF7 showed good convergence properties for any bond distance. The results obtained are close to the DMRG reference values throughout the symmetric dissociation curve and especially at the dissociation limit. It was observed that the calculated electron detachment energies (ionization energies) increase with the bond distance. It can be concluded that the hydrogen lattice model can be employed to describe bond-breaking processes in presence of strong correlation effects, regardless of the dimensionality of the system.

CHAPTER 8

Molecular electric moments calculated by using NOFT

8.1 Introduction

The interpretation and understanding of intermolecular forces, particularly those relating to long-range electrostatic interactions, require knowledge of the electrostatic moments [67, 68]. The electric moments are essential to provide simple ways to figure out the electric field behaviour of complex molecules. These electrical properties provide also information about the molecular symmetry since the electric moments depend on the geometry and charge distribution of the molecule.

It has long recognized the role of electrostatic interactions in a wide range of biological phenomena [198]. The electrostatic energy is frequently the ruling contribution to molecular interactions in large biological systems, hence it is extremely important to describe properly the electrostatic potentials around these molecules. In order to improve the current treatment of the electrostatics for biomolecular simulations, which are traditionally modeled using a set of atom-centered point charges, the knowledge of higher multipole moments is required to include the effects of non-spherical charge distributions on intermolecular electrostatic interactions.

In principle, one can experimentally find the components of the electric field at each point, but it turns into a formidable task for large molecular systems. There are several techniques to

determine experimentally the dipole moments [199, 200], but it is still very difficult to obtain precise experimental values of higher multipole moments such as quadrupole or octupole moments [67, 119, 120], independently of the experimental conditions. Theoretical calculations are therefore essential but challenging for quantum chemistry methods. The accurate calculation of these properties is highly dependent on the method employed [201], either regarding approximate density functionals [202] or methods based on wavefunctions [123, 124]. Consequently, calculating the multipole moments is a way to assess any electronic structure method.

In this chapter we employ PNOF6 [44], since it has proved a more balanced treatment of both dynamic and non-dynamic electron correlations than its predecessors [60,61,166,167,203]. In view of the results obtained for the equilibrium geometries, PNOF7 and PNOF5 are not expected to compete with PNOF6 for the molecular electrostatic moments. Thereby, neither PNOF7 nor PNOF5 are considered in the present chapter. PNOF6 is applied, in its extended version, to the determination of molecular dipole and quadrupole moments of selected spin-compensated molecules, namely, H_2, HF, BH, HCl, H_2O, H_2CO, C_2H_2, C_2H_4, C_2H_6, C_6H_6, CH_3CCH, CH_3F, HCCF, ClF, CO, CO_2, O_3, N_2, NH_3, and PH_3. Moreover, the octupole moment of CH_4, a molecule without dipole and quadrupole moments is also studied. The Gaussian basis set of Sadlej [121,122], which has been specially developed to compute accurately molecular electric properties, is employed to perform all calculations.

We compare the obtained PNOF6 results with the experimental values reported in the literature [119,123,124,129–131,136], as well as with the theoretically computed values of Bundgen et al. who used the multi-reference single and double excitation configuration interaction (MRSD-CI) method, and the coupled-cluster single and doubles (CCSD) values calculated by us. Recall that the CCSD values for one-electron properties differ from full-CI results in only 2% if no multiconfigurational character is observed [133], so they can be considered as benchmark calculations. To our knowledge, this is the first NOF study of higher multipole moments such as quadrupole and octupole moments.

This chapter is organized as follows. We start in section 8.2 with the basic concepts and notations related electric multipole moments. The section 8.3 is dedicated to present our results and those obtained by using CCSD and MRSD-CI methods. Here, we discuss the outcomes obtained for the dipole, quadrupole and octupole principal moments, in separate sections. The performance of PNOF6 is established by carrying out a statistical analysis of the mean absolute errors (MAE) with respect to the experimental marks.

8.2 Dipole, Quadrupole and Octupole Moments

The potential of the electric field at any point outside a distribution of charges is simply related to the electric multipole moments. As any distribution function, the essential features of the charge distribution can be characterized by its moments, thereby for an uncharged molecule the first (dipole), second (quadrupole) and third (octupole) electric moments are the most important terms in the multipole expansion, therefore, are usually sufficient to characterize its interaction with an external field. The components of the symmetric dipole, quadrupole, and octupole moments were defined by Buckingham [67, 68] as

$$\mu_\alpha = -\frac{1}{2}\int \rho(\mathbf{r}) r_\alpha dV + \sum_{i=1}^{NUC} Z_i R_{i\alpha} \tag{197}$$

$$\Theta_{\alpha\beta} = -\frac{1}{2}\int \rho(\mathbf{r})(3r_\alpha r_\beta - \delta_{\alpha\beta} r^2)dV + \frac{1}{2}\sum_{i=1}^{NUC} Z_i(3R_{i\alpha}R_{i\beta} - \delta_{\alpha\beta}R_i^2) \tag{198}$$

$$\begin{aligned}\Omega_{\alpha\beta\gamma} = &-\frac{5}{2}\int \rho(\mathbf{r})\, r_\alpha r_\beta r_\gamma dV + \frac{1}{2}\int \rho(\mathbf{r}) r^2 \left(r_\alpha\delta_{\beta\gamma} + r_\beta\delta_{\alpha\gamma} + r_\gamma\delta_{\alpha\beta}\right) dV \\ &+ \frac{5}{2}\sum_{i=1}^{NUC} Z_i\, R_{i\alpha}R_{i\beta}R_{i\gamma} - \frac{1}{2}\sum_{i=1}^{NUC} Z_i R_i^2 \left(R_{i\alpha}\delta_{\beta\gamma} + R_{i\beta}\delta_{\alpha\gamma} + R_{i\gamma}\delta_{\alpha\beta}\right)\end{aligned} \tag{199}$$

where the Greek subscripts denote the Cartesian directions x, y and z. Note that the nuclear contribution is taken into account separately from the electronic contribution, which arises from the negative charge distribution over all the space. The formulas (198) and (199) define symmetric tensors in all subscripts. Moreover, equation (198) defines a traceless tensor for the quadrupole moment, namely, $\Theta_{xx} + \Theta_{yy} + \Theta_{zz} = 0$, similarly, equation (199) leads to $\Omega_{xxz} + \Omega_{yyz} + \Omega_{zzz} = 0$ for octupole tensor, and respective permutations between the subscripts x, y and z.

8.2.1 Computational details

In this section we explain how to program the electric dipole, quadrupole, and octupole moments in DoNOF.

For the nuclear contribution the point-charge approximation has been considered, so the term is simply given by the product of nuclear coordinates and their corresponding Coulombic charges. The situation is much more difficult in the case of the negative charge. This is given by the

electronic density, which in NOFT can be computed from the multiplication between the square of the module of NOs and their corresponding ONs, i.e

$$\rho_{NO}\left(\mathbf{r}\right)=\sum_{i}n_{i}|\phi_{i}|^{2}. \tag{200}$$

Thus, in the basis of NOs the electric dipole moment is computed by (along this section, assume we have a pure state ψ_0)

$$\overrightarrow{\mu_{e}}=\langle\rho\cdot(x,y,z)\rangle=\langle\psi_{0}|-\sum_{p}\mathbf{r}_{p}|\psi_{0}\rangle=-2\sum_{p}n_{p}\langle\phi_{p}|\mathbf{r}_{p}|\phi_{p}\rangle, \tag{201}$$

where a factor 2 comes from considering a singlet state system. In practice, we work in the Atomic Orbital (AO) basis, so after expanding the NOs in AOs, $\phi_p=\sum_k C_{kp}\chi_k^{AO}$, the expression of the dipole moment is

$$\overrightarrow{\mu_{e}}=-2\sum_{p}n_{p}\sum_{k,l}C_{kp}C_{pl}^{*}\langle\chi_{l}^{AO}|\mathbf{r}_{p}|\chi_{k}^{AO}\rangle, \tag{202}$$

where the set of integrals $\langle\chi_k^{AO}|\mathbf{r}_p|\chi_l^{AO}\rangle$, known as 1^{st}-order moment integrals, has been directly read from the GAMESS program [126,127]. Note that the first summation runs over the spatial NO basis, whereas indices k and l run over the basis of AOs.

The procedure is completely analogous for higher multipole moments, so only the last expressions of quadrupole and octupole moments are reported in the next lines.

In the case of quadrupole moment, the traceless formula introduced by Buckingham leads to the expression

$$\Theta_{i,j}=-\sum_{k}\sum_{l,t}n_{k}C_{lk}C_{kt}^{*}\left[3\langle\chi_{t}^{AO}|r_{i}r_{j}|\chi_{l}^{AO}\rangle-\langle\chi_{t}^{AO}|\mathbf{r}_{i}^{2}\delta_{ij}|\chi_{l}^{AO}\rangle\right], \tag{203}$$

where the factor 2 is compesated with a fraction $\frac{1}{2}$ that is implicit in the definition of the quadrupole moment. For instance, two relevant cases are

$$\Theta_{x,x}=-\sum_{k}\sum_{l,t}n_{k}C_{lk}C_{kt}^{*}\left[2\langle\chi_{t}^{AO}|r_{x}r_{x}|\chi_{l}^{AO}\rangle-\langle\chi_{t}^{AO}|r_{y}r_{y}|\chi_{l}^{AO}\rangle-\langle\chi_{t}^{AO}|r_{z}r_{z}|\chi_{l}^{AO}\rangle\right],$$

and

$$\Theta_{x,y}=-\sum_{k}\sum_{l,t}n_{k}C_{lk}C_{kt}^{*}\left[3\langle\chi_{t}^{AO}|r_{x}r_{y}|\chi_{l}^{AO}\rangle\right].$$

For the octupole moment, the formula leads to the next expression for programming:

$$\Omega_{i,j,k} = -\sum_{m}\sum_{l,t} n_m C_{lm} C^*_{mt} \left[5\langle\chi_t^{AO}|r_i r_j r_k|\chi_l^{AO}\rangle - \langle\chi_t^{AO}|\mathbf{r}_i^2\left(r_{i\alpha}\delta_{\beta\gamma} + r_{i\beta}\delta_{\alpha\gamma} + r_{i\gamma}\delta_{\alpha\beta}\right)|\chi_l^{AO}\rangle\right] \tag{204}$$

Note that the factor 2 arising from doubly occupancies is removed again. In this case the relevant cases are three:

$$\Omega_{x,x,x} = -\sum_{m}\sum_{l,t} n_m C_{lm} C^*_{mt} \left[2\langle\chi_t^{AO}|r_x r_x r_x|\chi_l^{AO}\rangle - 3\langle\chi_t^{AO}|\left(r_x r_y r_y + r_x r_z r_z\right)|\chi_l^{AO}\rangle\right],$$

$$\Omega_{x,x,y} = -\sum_{m}\sum_{l,t} n_m C_{lm} C^*_{mt} \left[4\langle\chi_t^{AO}|r_x r_x r_y|\chi_l^{AO}\rangle - \langle\chi_t^{AO}|\left(r_y r_y r_y + r_y r_z r_z\right)|\chi_l^{AO}\rangle\right],$$

and

$$\Omega_{x,y,z} = -\sum_{m}\sum_{l,t} n_m C_{lm} C^*_{mt} \left[5\langle\chi_t^{AO}|r_x r_y r_z|\chi_l^{AO}\rangle\right].$$

Recall that both quadrupole and octupole tensors are symmetric in all suffixes.

8.3 Results and discussion

In the following sections, we show the PNOF6(N_c) results obtained for the dipole, quadrupole, and octupole moments with respect to the center of mass.

The chosen basis set is known to be an important factor in the calculation of molecular electric properties. We used the Gaussian basis set of Sadlej [121,122], which is a correlation-consistent valence triple-ζ basis set augmented with additional basis functions selected specifically for the correlated calculation of electric properties. Thus, it contains sufficient diffuse and polarization functions in order to give an accurate description of the outer-valence region. It has been shown [204,205] that the Sadlej basis set has effectively the same accuracy as the aug-cc-pVTZ basis set.

Since the number N_c of usually weakly-occupied orbitals is related to the description of the electron pairs, we begin studying the H_2 molecule, where there are not inter-pair correlation effects. This molecule has zero dipole moment, hence the calculated quadrupole moment values for different N_c values are shown in Table 29.

Table 29 – Θ_{zz} component of H_2 quadrupole moment, in atomic units, obtained by employing PNOF6(N_c) and CCSD with the Sadlej-pVTZ basis set at the experimental equilibrium geometry [8], together with the experimental value [9].

PNOF6(1)	PNOF6(3)	PNOF6(5)	PNOF6(17)	CCSD	EXP.
0.3697	0.4030	0.3965	0.3935	0.3935	0.39 ± 0.01

As expected, the best description of the electron pair is obtained when the number of usually weakly-occupied orbitals is maximum, in fact, the calculated quadrupole moment converges to the CCSD value, which is the full CI result for this molecule. In the present chapter, we will carry out all PNOF6(N_c) calculations by using the maximum N_c value allowed by the Sadlej basis set for each molecule. In our calculations, we have set to one the occupancies of the core orbitals. Consequently, the maximum possible value of N_c is given by the number of basis functions above the Fermi level, divided by the number of the considered strongly occupied orbitals.

For comparison, we have included the available experimental data, and the calculated Hartree-Fock (HF) and CCSD values using the GAMESS program [126, 127]. The experimental equilibrium geometries [8, 123–125] have been used to carry out all calculations. The performance of theoretically obtained results is established by carrying out a statistical analysis of the mean absolute errors (MAE) with respect to the experimental data. Atomic units (a.u.) are used throughout.

8.3.1 Dipole moment

In this chapter, the dipoles are aligned along the principal symmetry axis of the studied molecules, set on z direction. Table 30 shows the independent component μ_z of the dipole moments obtained at the HF, PNOF6(N_c), and CCSD levels of theory.

Overall, the inclusion of electron correlation effects through, both PNOF6(N_c) and CCSD, improves significantly the performance of the HF method. PNOF6(N_c) and CCSD afford MAEs with respect to experimental data of 0.0309 a.u. and 0.0177 a.u., respectively. It is worth noting the agreement between PNOF6(N_c) and CCSD results, as well as with the experimental data. Note that the aug-cc-pVTZ basis set of Dunning [87] was used for the BH molecule since there is no Sadlej-pVTZ basis set available for Boron. In this case, the PNOF6(38) result is very

Table 30 – μ_z component of molecular dipole moments in atomic units (ea_0) computed with the Sadlej-pVTZ basis set at the experimental equilibrium geometries [8]. N_c is the number of weakly-occupied orbitals employed in PNOF6(N_c) for each molecule.

Molecule	HF	PNOF6	(N_c)	CCSD	EXP.
HF	0.7565	0.7223	7	0.6994	0.7089 [123]
BH*	0.6854	0.5395	38	0.5551	0.4997 [123]
H_2O	0.7808	0.7458	9	0.7225	0.7268 [123]
H_2CO	1.1134	0.9872	10	0.9084	0.9175 [123]
HCl	0.4746	0.4598	8	0.4416	0.4301 [123]
HCCF	0.3535	0.3189	9	0.2733	0.2872 [119]
NH_3	0.6372	0.6153	12	0.5943	0.5789 [124]
PH_3	0.2780	0.2755	13	0.2340	0.2258 [128]
O_3	0.3033	0.1370	7	0.2276	0.2099 [129]
ClF	0.4453	0.3226	6	0.3451	0.3462 [130]
CH_3F	0.7706	0.7283	10	0.6919	0.7312 [131]
CH_3CCH	0.3203	0.3141	12	0.2866	0.3070 [132]
CO	−0.0987	0.0414	9	0.0725	0.0481 [123]
MAE	0.0843	0.0309		0.0177	

*Calculations performed with the aug-cc-pVTZ basis set.

close to the Full-CI/aug-cc-pVTZ value obtained by Halkier et al. [133], 0.5433 a.u., showing a result as good as the CCSD one.

The electronic structure and bonding situation of carbon monoxide is of special interest for modern electronic structure methods. The dipole moment of CO, extensively studied in Refs. [205–207], is very small (0.0481 a.u.) and ends at the carbon atom, although carbon is less electronegative than oxygen. The result shown in Table 30 is representative, while HF gives the wrong direction for the CO dipole moment, PNOF6(9) corrects the sign, giving a result that is in excellent agreement with the experimental value. Remarkably, the result obtained at CCSD level is 34% away from the experimental value, so that it is necessary to include third order triplet excitations in the cluster theory in order to obtain a reasonable value, such as the one reported by Maroulis [207] at the CCSD(T) level, 0.0492 a.u.. Accordingly, the relevant electron correlation for CO is well accounted by the PNOF6(9) method.

Regarding the values obtained for HF, H_2O, H_2CO, HCl, NH_3, and ClF, PNOF6(N_c) competes with Coupled Cluster, providing values that differ from experimental data in less than a 7%. In the case of HCCF and PH_3, PNOF6(N_c) seems to lack relevant dynamic electron correlation and thereby the obtained dipole moments are not as accurate as the CCSD ones. Conversely, our values are in excellent agreement with experimental data in the case of the methyls CH_3F and CH_3CCH, often attached to large organic molecules, giving dipole moments with errors of 0.4% and 2% respectively, with respect to experimental values.

A special case is ozone, which is a molecule with strong multiconfigurational character. The PNOF6(7) dipole moves into the right direction from the HF value, but overestimates the effects of the electron correlation. Taking into account the good CCSD result for O_3, which is not valid for higher electric moments, it seems that the dynamic electron correlation compensates for the lack of non-dynamical in this method, and could improve our numerical value of the dipole.

8.3.2 Quadrupole moment

Tables 31 and 32 list the molecular quadrupole moments obtained at the HF, CCSD, MRSD-CI and PNOF6(N_c) levels of theory, along with the experimental values taken from Refs. [9, 119, 123, 124, 128–131, 134–136]. Inspection of these Tables shows that PNOF6(N_c) quadrupole moments agree satisfactorily with the experimental data, whereas the discrepancies are consistent with those observed using the CCSD and MRSD-CI methods in most cases.

In the case of linear molecules (H_2, HF, BH, HCl, HCCF, ClF, CO, C_2H_2, CO_2 and N_2), NH_3

Table 31 – Θ_{zz} component of the quadrupole moments, in atomic units, computed with the Sadlej-pVTZ basis set at the experimental equilibrium geometries [8] for molecules with linear, C_{3v}, D_{6h}, and D_{3d} symmetry. N_c is the number of weakly-occupied orbitals employed in PNOF6(N_c) for each molecule.

Molecule	HF	PNOF6	(N_c)	CCSD	EXP.
H_2	0.4381	0.3935	17	0.3935	0.39 ± 0.01 [9]
HF	1.7422	1.6939	7	1.7156	1.75 ± 0.02 [124]
BH*	2.6772	2.3706	38	2.3388	2.3293† [133]
HCl	2.8572	2.7753	8	2.7233	2.78 ± 0.09 [123]
HCCF	3.3530	3.2482	9	2.9335	2.94 ± 0.10 [119]
CO	1.5366	1.4562	9	1.4889	1.44 ± 0.30 [124]
N_2	0.9397	1.0530	9	1.1712	1.09 ± 0.07 [124]
NH_3	2.1258	2.1080	12	2.1661	2.45 ± 0.30 [123]
PH_3	1.7217	1.6507	13	1.5695	1.56 ± 0.70 [128]
ClF	0.9413	1.1122	6	1.0514	1.14 ± 0.05 [130]
CH_3F	0.3482	0.3269	10	0.3002	0.30 ± 0.02 [131]
C_2H_2	5.3655	5.1531	12	4.6850	4.71 ± 0.14 [134]
C_2H_6	0.6329	0.6275	13	0.6234	0.59 ± 0.07 [135]
C_6H_6	6.6418	6.3571	12	5.6653	6.30 ± 0.27 [136]
CH_3CCH	4.2913	4.1146	12	3.6939	3.58 ± 0.01 [8]
CO_2	3.8087	3.6012	8	3.1966	3.19 ± 0.13 [124]
MAE	0.2646	0.1517		0.0902	

*Calculations performed with the aug-cc-pVTZ basis set.

† Full CI calculation reported by Halkier et al. [133]

Table 32 – Θ_{zz} and Θ_{xx} components of molecular quadrupole moments, in atomic units, computed using the Sadlej-pVTZ basis set at the experimental equilibrium geometries [8]. N_c is the number of weakly-occupied orbitals employed in PNOF6(N_c) for each molecule.

Molecule	HF	PNOF6	(N_c)	MRSD-CI	EXP.
H_2O (xx)	1.7966	1.7808	9	1.8050	1.86 ± 0.02 [123]
H_2O (zz)	0.0981	0.0869	9	0.0950	0.10 ± 0.02 [123]
H_2CO (xx)	0.1019	0.0516	10	0.1100	0.04 ± 0.12 [137]
H_2CO (zz)	0.0921	0.1255	10	0.2230	0.20 ± 0.15 [137]
C_2H_4 (xx)	2.7819	2.5892	13	2.3700	2.45 ± 0.12 [123]
C_2H_4 (zz)	1.4942	1.3266	13	1.1700	1.49 ± 0.11 [123]
O_3 (xx)	1.1175	1.2426	7	1.2830	1.03 ± 0.12 [129]
O_3 (zz)	-0.2387	0.3606	7	0.1680	0.52 ± 0.08 [129]
MAE	0.1772	0.1066		0.1448	

and PH_3, belonging to the C_{3v} point symmetry group, the D_{6h} C_6H_6 molecule, and the trigonal planar C_2H_6, which has D_{3d} symmetry, the relation $\Theta_{xx} = \Theta_{yy} = -\frac{1}{2}\Theta_{zz}$ holds for quadrupole moment tensor, so Θ_{zz} alone is sufficient to determine completely the quadrupole moment. Setting the main axis of symmetry in the z direction of the coordinate system, the results for these molecules are reported in Table 31. From the latter, one can observe that PNOF6(N_c) yields a MAE of 0.15 a.u., hence considering the added complexity of the quadrupole moment, the performance of PNOF6(N_c) is within a reasonable accuracy.

Taking into account the experimental uncertainty, PNOF6(N_c) results agree with the experimental data for H_2, HCl, CO, N_2, PH_3, ClF, CH_3F, C_2H_6, and C_6H_6. The value obtained for H_2 reproduces the experimental one with high precision. It is also worth noting the excellent agreement with the experiment obtained for the quadrupole moment of Benzene, which is of great interest for many fields of chemistry and biology [136, 208]. Indeed, the quadrupole moment of Benzene plays an important role in determining the crystal structures and molecular recognition in biological systems because it is the key to the intermolecular interactions between π-systems.

For HCCF, NH_3, C_2H_2, and CO_2, the quadrupole moments fall out of the experimental error intervals, however, in the case of HCCF, C_2H_2, and CO_2 the mean relative percentage error

is below 11%, whereas the results obtained for NH_3 is only 0.05 a.u. away from the higher limit of the experimental uncertainty. For CH_3CCH the PNOF6(12) result deviates from the experimental value in a 13%, ergo more dynamic correlation is clearly necessary to improve this result, an effect not observed for the dipole moment of this molecule.

For the hydrogen fluoride, the HF result is the closest to the experimental value, however, the PNOF6(7) result is in outstanding agreement with the full-CI/aug-cc-pVTZ value of 1.6958 a.u. [133]. For the Boron monohydride, the experimental quadrupole moment is not available, so we use the full-CI/aug-cc-pVTZ calculation reported by Halkier et al. [133], 2.3293 a.u., in order to carry out the comparison. The agreement between PNOF6(38) and full-CI is good, according to the relative percentage error obtained below 1.7%.

Table 32 shows the Θ_{zz} and Θ_{xx} components obtained for H_2O, H_2CO, C_2H_4, and O_3. In this chapter, we use the traceless quadrupole moment, hence two components are sufficient to determine completely this magnitude. On the other hand, MRSD-CI values are significantly better than CCSD calculations when many components of the quadrupole tensor are studied [123], thereby MRSD-CI is used as benchmark theoretical method in Table 32.

According to the results reported in Table 32, PNOF6(N_c) performs better than the MRSD-CI method for this selected set of molecules. For H_2O and H_2CO, the PNOF6(N_c) values fall into the experimental error interval, which is specially broad for H_2CO. In the case of the C_2H_4 molecule, the longitudinal component Θ_{zz} obtained with PNOF6(13) is near the limit of the experimental error interval, as well as the Θ_{xx} component. Finally, we have the results obtained for O_3, which is a stringent test for quadrupole calculations due to its two-configurational character [129,138]. One can observe that Ozone is well described by PNOF6(7) comparing to the results obtained by using HF and MRSD-CI methods.

8.3.3 Octupole moment

The octupole moment is particularly interesting in the case of methane. It is the first non-zero term in the multipole expansion of the electrostatic interaction for methane molecule, so it is crucial in order to describe properly its interactions with external fields. Actually, the octupole-octupole interaction is the main long-range orientation dependent interaction in methane. Moreover, the complex charge distribution of methane, which has long been studied in the literature [125,139,140], is mainly dependent on its octupole moment, thus, the octupole moment is essential to characterize the charge distribution of tetrahedral molecules.

For tetrahedral molecules the octupole moment is simply given by one component, namely $\Omega =$

Ω_{xyz}. Employing PNOF6(14) with the Sadlej-pVTZ basis set at the experimental equilibrium geometry [125], the result obtained for CH_4 is $\Omega_{xyz} = 2.1142\,a.u.$, whereas the experimental mark reported in Ref. [120] is $\Omega_{xyz} = 2.95 \pm 0.17\,a.u.$ Although the PNOF6(14) result falls out of the experimental interval error, this value is reasonable taking into account the discrepancies between experimental marks obtained by different experimental techniques [120]. Besides, comparing to theoretical calculations, the PNOF6(14) value is very close to the result obtained by using CCSD, $\Omega_{xyz} = 2.1255\,a.u.$. Consequently, we can conclude that PNOF6(14) describes properly the octupole moment of methane.

8.4 Conclusions

The PNOF6 method, in its extended version, has been assessed by comparing the molecular electric moments with the experimental data as well as with CCSD and MRSD-CI theoretical values. The dipole, quadrupole and octupole moments for a selected set of well-characterized 21 molecules have been calculated at the experimental equilibrium geometries using the triple-ζ Gaussian basis set with polarization functions developed by Sadlej. Our results show that PNOF6(N_c) is able to predict electric properties as accurate as high-level electronic structure methods such as CCSD or MRSD-CI, therefore the functional computes quite accurately the charge distribution of molecular systems. To our knowledge, this is the first NOF study of higher multipole moments such as quadrupole and octupole moments.

For PNOF6(N_c) dipole moments, the obtained MAE with respect to experimental data is $0.0309\,a.u.$, being consistent with the theoretical benchmark calculations. Remarkable is the result obtained by PNOF6(9) for Carbon monoxide, for which, HF gives a wrong direction of the dipole and CCSD overestimates it severely, whereas PNOF6(9) corrects the sign, giving a result that is in excellent agreement with the experimental mark.

The high performance of PNOF6(N_c) in computing electric quadrupole moments has been shown by most of the studied molecules, for which the computed values fall into the experimental interval error. It has been shown that the method is capable of providing the different components of the quadrupole moment tensor. The PNOF6(N_c) MAE with respect to the experiment is $0.1291\,a.u.$, which is very close to the corresponding MAEs of $0.0902\,a.u.$ and $0.1448\,a.u.$ obtained by using the well-established CCSD and MRSD-CI methods, respectively. In particular, the results obtained for the ozone molecule with a marked multiconfigurational

character, show that the method is able to treat properly non-dynamic and dynamic electron correlations.

Finally, the study of the octupole moment was focused here on methane, due to its important role in the description of the long-range electrostatic interactions for this molecule. The PNOF6(14) result is in excellent agreement with the value provided by the CCSD method.

CHAPTER 9

Conclusions

The exact N-electron energy for atomic and molecular systems can be expressed as a known, linear functional of the 2RDM. Direct determination of approximate 2RDMs without the N-particle wavefunction is possible enforcing N-representability conditions of the 2RDM, but the latter is computationally expensive if high accuracy is required. Despite the popularity of approximate density functionals for the energy, there are still important limitations regarding the description of strong correlation by using DFT approaches. NOFT presents as a compromise between both approaches, that is, developing a functional theory of the 1RDM could improve the accuracy of approximate density functionals with a mean-field computational scaling far below from $\mathcal{O}\left(M^9\right)$ or $\mathcal{O}\left(M^{12}\right)$ (M being the dimension of the single-particle space), as is the case of imposing two- and three-particle positivity conditions of the 2RDM.

We began this thesis with the basics of RDMs, paying special attention to the properties of 1 and 2 RDMs. The use of reduced quantities leads us to the N-representability problem, i.e., the need to ensure that a given RDM (or electron density in DFT) corresponds to an N-particle wavefunction. We showed that ensemble and pure N-representability conditions of the 1RDM are already known, although only the former are of practical use. On the contrary, ensemble N-representability conditions of the 2RDM are much more complicated, so, in practice, we limit to those that are expressible in terms of two- and three-particle operators. The latter are necessary but not sufficient conditions to obtain an N-representable 2RDM.

The seminal paper of Löwdin [24], followed by the work of Gilbert [13], Levy [25], Valone [26],

and Donelly and Parr [27] laid the foundations of a functional theory of the 1RDM. The latter is correctly referred to as NOFT, since the diagonal representation of the 1RDM is usually employed. We showed that NOFT is in practice an approximate one-particle theory where the 2RDM continues to play a dominant role. In fact, the typical approach is to employ the well-known 2RDM functional but using solely a reconstruction of the 2RDM in terms of the ONs. This particular reconstruction leads us to different NOFAs. Despite reviewing many NOFAs employed in the literature, we focused on PNOF theory, since only the latter enforce N-representability constraints on the reconstructed 2RDMs. In this context, we remarked the importance of electron-pairing constraints, employed in the PNOFi (i=$\overline{5,7}$) approximations. These restrictions allow us to exploit the knowledge of the quasi-exact two-electron NOFA, and trivialize the recently discovered pure N-representability conditions of the 1RDM. In this scenario, the proposal of the independent-pair model PNOF5 come up naturally. PNOF5 is the first pure N-representable NOFA introducing electron correlation, since it corresponds to an antisymmetrized product of strongly orthogonal geminals. On top of PNOF5, two attempts to introduce correlation between pairs of electrons were introduced, namely, PNOF6 and PNOF7. The methodology used along this thesis included the Euler equations, that is, the procedure for the minimization of the energy. There is no a Fockian in NOFT, so this problem does not reduce to a pseudo-eigenvalue equation as it happens in single-reference approaches. We described the iterative diagonalization method developed by Piris and Ugalde [55] to optimize the ONs and NOs, separately. We ended this section with a list of new capabilities implemented in the DoNOF program package. In fact, all calculations related with NOFAs were carried out by using DoNOF, a code mainly owned by Prof. Mario Piris and extensively developed along this thesis.

The main objective of this thesis was the development and applications of NOFAs, in order to establish them as an electronic structure method able to compete with standard wavefunction and DFT approaches.

So far the scientific context of this thesis. In view of the results obtained along chapters 5 through 8, the next question arise: What could be concluded in relation with the objectives proposed and with the development and applications achieved? Let us examine by chapters the accomplishments of the objectives, and finish with an overall conclusion of the thesis.

Our development started with the study of the geomerty optimization procedure. The latter is indeed the most popular task after single-point energy calculations. We demonstrated that analytic energy gradients are efficiently computed at one-shot similar to the case of HF, so

the machinery used to obtain HF gradients was employed to calculate energy gradients of NOFAs. Our test showed the accuracy of PNOFi (i=$\overline{5,7}$) equilibrium geometries, comparable to those obtained at the CCSD level of theory. The theory needed to obtain second-order derivatives in NOFT was derived, as well as the coupled-perturbed equations to compute the linear response of the NOs and ONs to an external or internal perturbation. In contrast with previous derivations [84, 177], we did not assume the existence of a Fockian, and we provided an expression valid for any NOFA even if the basis set presents explicit dependence on the perturbation. Unfortunately, the analytic calculation of the Hessian is much more computational demanding than first-order derivatives. Therefore, we employed a numerical differentiation of the latter to obtain harmonic vibrational frequencies. The results obtained for PNOF7 overcomed MP2 and CCSD for a selected set of small molecules. This opens up the possibility of using PNOF7 to study thermodynamical properties daily employed in chemistry, such as free energy or enthalpy differences.

The next chapter of this thesis was devoted to model systems. Simple correlated electron models are suitable for robust validation of NOFAs, so goals and limitations of the usually employed NOFAs are revealed. In the first part, we analyzed the 1D Hubbard model with and without on-site external potentials. Interestingly, some of the approximations built following heuristic arguments produced reasonable energies from weak to strong correlation regimes. Nevertheless, the inspection of the double occupancy and ONs revealed that the latter give accurate energies for the wrong reasons, since their corresponding 1 and 2 RDMs are dramatically inaccurate, in comparison with FCI calculations. On the contrary, PNOF5 and PNOF7 yielded consistent results regardless of the nature of the problem. We concluded that N-representability conditions of the 2RDM are essential in the development of NOFAs, contrary to what it has been largely believed, since the N-representability of the 1RDM is uniquely considered in many approaches. In the second part of this chapter, we exploited model systems to shine some light into the phase dilemma appeared in the development of the PNOF7 approximation. In fact, the two-particle N-representability constraints do not determine the phase of the inter-pair correlation term in the context of the *bottom-up* method employed by Piris to develop NOFAs. Our study showed this phase to be crucial in the description of model systems such as the 1D Hubbard model and hydrogen chains. Therefore, an adequate choice of this phase made PNOF7 an accurate method for these systems, independently of the correlation regime and the increasing size of the system.

In view of the accurate results obtained by the improved PNOF7 approximation, we worked on

many applications to prove PNOF7 as an efficient method for strongly correlated electrons in low dimensions by means of a minimal basis approach. In 1D, PNOF7 described accurately the symmetric and asymmetric dissociation of a long molecule such as the H_{50}, which exhibits a varying nature of chemical bonding and multireference correlation. Regarding the 1D Hubbard model, PNOF7 accurately described the system even if particle-hole symmetry is broken away from half-filling. In the case of 2D, the problem becomes much more difficult and even a general solution for the simple Hubbard model is still missing. We showed the ability of PNOF7 to describe strong correlation effects in these 2D systems by comparing our results with ED, DMRG, v2RDM (including PQG and PQGT') and AFQMC. The study of singlet and doublet spin- multiplicities revealed an interesting feature: electron detachment energies increase with the bond distance for 2D hydrogen square lattices, whereas they are negative and take larger absolute values increasing U/t in the 2D Hubbard model at half-filling. Beyond the energy, smooth double occupancy of sites was obtained by using PNOF7 regardless of the filling, so it is concluded that the reconstructed 2RDM is qualitatively correct.

Our last work focused on the molecular electric moments. Despite being a method that retrieves less correlation energy than the independent-pair model PNOF5 or PNOF7, PNOF6 showed to describe dipole, quadrupole and octupole moments at the level of CCSD and MRSD-CI (whenever static correlation is important) for a wide variety of molecular systems. Therefore, charge distributions of molecular systems, electrostatic interactions, and response to external fields are expected to be accurately described by this method.

To conclude, in this thesis the robustness of NOFT was put into test from both the theoretical and practical viewpoints. We claimed for a NOF practice in which the already known energy functional of the 2RDM $E[D]$ is employed together with the reconstruction $D[\Gamma]$. The PNOF approximations served us as a practical tool to show that NOFAs already compete with standard electronic structure methods, and we developed all machinery to prove it, as was the case of analytic derivative methods and model Hamiltonians. According to this development, the NOFT is not only a promising method of quantum chemistry, but also an emerging method for the condensed matter physics. Therefore, we recommend its use in problems wherein single-reference approaches fail, and in which *apriori* knowledge of the system is rather poor. In fact, although for very specific situations other methods yield more accurate results, PNOF is a *black-box* method for electron correlation that produces qualitatively reliable results in any situation.

There is without doubt room for improvement and fresh perspectives. Firstly, a free open-

source code should be available in order to facilitate the access to a more broad community. In this vein, we are making DoNOF public and free relatively soon, so that it serves to encourage new people to this field. Secondly, the numerical algorithms related with the procedure for the minimization of the energy need to be optimized in order to make NOFT as fast as HF. Finally, regarding the NOFAs, we focused on PNOFi (i=$\overline{5,7}$) because they care about the N-representability of the 2RDM, something that we proved to be of crucial importance for any NOFA. However, different reconstructions $D\left[\Gamma\right]$ must be explored to improve the description of the dynamic correlation and thereby squeeze the potentiality of NOFT. For instance, try different cumulant approximations, assume dependence on more indices, or whatever one can imagine according to the rules of quantum mechanics.

References

[1] J. Hachman, W. Cardoen, and G. K.-L. Chan, "Multireference correlation in long molecules with the quadratic scaling density matrix renormalization group," *J. Chem. Phys.*, vol. 125, no. 144101, 2006.

[2] K. Boguslawski, P. W. Ayers, P. Bultinck, S. D. Baerdemacker, and D. V. Neck, "Efficient description of strongly correlated electrons with mean-field cost," *Phys. Rev. B*, vol. 89, p. 201106(R), 2014.

[3] K. Boguslawski, P. Tecmer, and Ö. Legeza, "Analysis of two-orbital correlations in wave functions restricted to electron-pair states," *Phys. Rev. B*, vol. 96, no. 155126, 2016.

[4] J. S. Anderson, M. Nakata, R. Igarashi, K. Fujisawa, and M. Yamashita, "The second-order reduced density matrix method and the two-dimensional hubbard model," *Comp. Theor. Chem.*, vol. 1003, pp. 22 – 27, 2013.

[5] B. Verstichel, W. Poelmans, S. De Baerdemacker, S. Wouters, and D. Van Neck, "Variational optimization of the 2DM: Approaching three-index accuracy using extended cluster constraints," *Eur. Phys. J. B*, vol. 87, no. 3, p. 59, 2014.

[6] B. P. Pritchard, D. Altarawy, B. Didier, T. D. Gibson, and T. L. Windus, "A New Basis Set Exchange: An Open, Up-to-date Resource for the Molecular Sciences Community," 2019 (in preparation).

[7] B. Verstichel, H. van Aggelen, W. Poelmans, S. Wouters, and D. V. Neck, "Extensive v2dm study of the one-dimensional hubbard model for large lattice sizes: Exploiting translational invariance and parity," *Comput. Theor. Chem.*, vol. 1003, pp. 12 – 21, 2013.

[8] R. D. Johnson III, ed., *NIST Computational Chemistry Comparison and Benchmark Database*, vol. 17b. 2015.

[9] R. H. Orcutt, "Influence of Molecular Quadrupole Moments on the Second Virial Coefficient," *J. Chem. Phys.*, vol. 39, p. 605, 1963.

[10] M. Qin, H. Shi, and S. Zhang, "Benchmark study of the two-dimensional hubbard model with auxiliary-field quantum monte carlo method," *Phys. Rev. B*, vol. 94, p. 085103, 2016.

[11] M. Piris, "Natural Orbital Functional Theory," in *Reduced-Density-Matrix Mechanics: with applications to many-electron atoms and molecules* (D. A. Mazziotti, ed.), ch. 14, pp. 387–427, Hoboken, New Jersey, USA: John Wiley and Sons, 2007.

[12] A. J. Coleman, "Structure of Fermion Density Matrices," *Rev. Mod. Phys.*, vol. 35, p. 668, 1963.

[13] T. L. Gilbert, "Hohenberg-Kohn theorem for nonlocal external potentials," *Phys. Rev. B*, vol. 12, p. 2111, 1975.

[14] M. Altunbulak and A. Klyachko, "The Pauli Principle Revisited," *Communications in Mathematical Physics*, vol. 282, no. 2, pp. 287–322, 2008.

[15] A. Klyachko, "Quantum marginal problem and N-representability," *Journal of Physics: Conference Series*, vol. 36, pp. 72–86, 2006.

[16] I. Theophilou, N. N. Lathiotakis, M. A. L. Marques, and N. Helbig, "Generalized Pauli constraints in reduced density matrix functional theory," *J. Chem. Phys.*, vol. 142, p. 154108, 2015.

[17] C. Schilling and R. Schilling, "Diverging Exchange Force and Form of the Exact Density Matrix Functional," *Phys. Rev. Lett.*, vol. 122, no. 1, pp. 013001–7, 2019.

[18] C. L. Benavides-Riveros and M. A. L. Marques, "Static correlated functionals for reduced density matrix functional theory," *Eur. Phys. J. B*, vol. 91, p. 133, 2018.

[19] A. E. DePrince III, "Variational optimization of the two-electron reduced-density matrix under pure-state N-representability conditions," *J. Chem. Phys.*, vol. 145, p. 164109, 2016.

[20] D. A. Mazziotti, "Structure of fermionic density matrices: complete n-representability conditions," *Phys. Rev. Lett.*, vol. 108, p. 263002, 2012.

[21] J. Fosso-Tande, T.-S. Nguyen, G. Gidofalvi, and A. E. DePrince III, "Large-scale variational two-electron reduced-density-matrix-driven complete active space self-consistent field methods," *J. Chem. Theory Comput.*, vol. 12, no. 5, pp. 2260–2271, 2016.

[22] R. M. Erdahl, "Representability," *Int. J. Quantum Chem.*, vol. 13, no. 6, pp. 697–718, 1978.

[23] Z. Zhao, B. J. Braams, M. Fukuda, M. L. Overton, and J. K. Percus, "The reduced density matrix method for electronic structure calculations and the role of three-index representability conditions," *J. Chem. Phys.*, vol. 120, no. 5, pp. 2095–2104, 2004.

[24] P.-O. Löwdin, "Quantum theory of many-particle systems. i. physical interpretations by means of density matrices, natural spin-orbitals, and convergence problems in the method of configurational interaction," *Phys. Rev.*, vol. 97, p. 1474, 1955.

[25] M. Levy, "Universal variational functionals of electron densities, first-order density matrices, and natural spin-orbitals and solution of the v-representability problem," *Proc. Natl. Acad. Sci. USA*, vol. 76, p. 6062, 1979.

[26] S. M. Valone, "Consequences of extending 1-matrix energy functionals from pure–state representable to all ensemble representable 1 matrices," *J. Chem. Phys.*, vol. 73, p. 1344, 1980.

[27] R. A. Donnelly and R. G. Parr, "Elementary properties of an energy functional of the first-order reduced density matrix," *J. Chem. Phys.*, vol. 69, p. 4431, 1978.

[28] M. Rosina, "Transition amplitudes as ground state variational parameters," in *Reduced Density Operators with Application to Physical and Chemical Systems* (A. J. Coleman and R. M. Erdahl, eds.), p. 369, Queens University, Kingston, Ontario: Queens Papers in Pure and Applied Mathematics No. 11, 1967.

[29] R. A. Donnelly, "On fundamental difference between energy functionals based on first- and second-order density matrices," *J. Chem. Phys.*, vol. 71, no. 7, pp. 2874–2879, 1979.

[30] E. V. Ludeña, F. J. Torres, and C. Costa, "Functional n-representability in 2-matrix, 1-matrix, and density functional theories," *J. Math. Phys.*, vol. 4, p. 391, 2013.

[31] M. Piris, "The role of the n-representability in one-particle functional theories," in *Many-body approaches at different scales: a tribute to N. H. March on the occasion of his 90th*

birthday (G. G. N. Angilella and C. Amovilli, eds.), ch. 22, pp. 283–300, New York: Springer, 2018.

[32] M. Piris and J. M. Ugalde, "Perspective on natural orbital functional theory," *Int. J. Quantum Chem.*, vol. 114, pp. 1169–1175, 2014), (and references therein.

[33] K. Pernal and K. J. H. Giesbertz, "Reduced Density Matrix Functional Theory (RDMFT) and Linear Response Time-Dependent RDMFT (TD-RDMFT)," *Top Curr. Chem.*, vol. 368, pp. 125–184, 2016), (and references therein.

[34] I. Mitxelena, M. Piris, and J. M. Ugalde, "Advances in approximate natural orbital functional theory," Advances in Quantum Chemistry, Academic Press, 2019.

[35] A. M. K. Müller, "Explicit approximate expression between reduced two- and one-particle density matrices," *Phys. Lett.*, vol. 105A, p. 446, 1984.

[36] M. A. Buijse, *Thesis: Electron Correlation. Fermi and Coulomb holes, dynamical and nondynamical correlation.* PhD thesis, Vrije Universiteit, Amsterdam, The Netherlands, 1991.

[37] S. Sharma, J. K. Dewhurst, N. N. Lathiotakis, and E. K. U. Gross, "Reduced density matrix functional for many-electron systems," *Phys. Rev. B*, vol. 78, p. 201103, 2008.

[38] G. Csányi and T. A. Arias, "Tensor product expansions for correlation in quantum many-body systems," *Phys. Rev. B*, vol. 61, p. 7348, 2000.

[39] G. Csányi, S. Goedecker, and T. A. Arias, "Improved tensor-product expansions for the two-particle density matrix," *Phys. Rev. A*, vol. 65, p. 032510, 2002.

[40] J. M. Herbert and J. E. Harriman, "N-representability and variational stability in natural orbital functional theory," *J. Chem. Phys.*, vol. 118, p. 10835, 2003.

[41] M. Rodríguez-Mayorga, E. Ramos-Cordoba, M. Via-Nadal, M. Piris, and E. Matito, "Comprehensive benchmarking of density matrix functional approximations," *Phys. Chem. Chem. Phys.*, vol. 19, p. 24029, 2017.

[42] M. Piris, "A generalized self-consistent-field procedure in the improved BCS theory," *J. Math. Chem.*, vol. 25, pp. 47–54, 1999.

[43] M. Piris, "A natural orbital functional based on an explicit approach of the two-electron cumulant," *Int. J. Quantum Chem.*, vol. 113, pp. 620–630, 2013.

[44] M. Piris, "Interacting pairs in natural orbital functional theory," *J. Chem. Phys.*, vol. 141, p. 44107, 2014.

[45] M. Piris, "Global Method for Electron Correlation," *Phys. Rev. Lett.*, vol. 119, pp. 063002–5, 2017.

[46] M. Piris, "Dynamic electron-correlation energy in the natural-orbital-functional second-order-Møller-Plesset method from the orbital-invariant perturbation theory," *Phys. Rev. A*, vol. 98, pp. 022504–6, 2018.

[47] I. Mitxelena, M. Rodríguez-Mayorga, and M. Piris, "Phase Dilemma in Natural Orbital Functional Theory from the N-representability Perspective," *Eur. Phys. J. B*, vol. 91, p. 109, 2018.

[48] W. Kutzelnigg and D. Mukherjee, "Cumulant expansion of the reduced density matrices," *J. Chem. Phys.*, vol. 110, no. 6, pp. 2800–2809, 1999.

[49] D. A. Mazziotti, "Cumulants and the contracted schrödinger equation," in *Many-Electron Densities and Reduced Density Matrices*, pp. 139–163, Springer, 2000.

[50] M. Piris, J. M. Matxain, X. Lopez, and J. M. Ugalde, "Spin conserving natural orbital functional theory," *J. Chem. Phys.*, vol. 131, p. 021102, 2009.

[51] M. Piris, J. M. Matxain, X. Lopez, and J. M. Ugalde, "Communication: The role of the positivity N-representability conditions in natural orbital functional theory," *J. Chem. Phys.*, vol. 133, p. 111101, 2010.

[52] R. van Meer, O. V. Gritsenko, and E. J. Baerends, "A non-jkl density matrix functional for intergeminal correlation between closed-shell geminals from analysis of natural orbital configuration interaction expansions," *J. Chem. Phys.*, vol. 148, no. 10, p. 104102, 2018.

[53] J. W. Hollett and P.-F. Loos, "Capturing static and dynamic correlation with ΔNO-MP2 and ΔNO-CCSD," *arXiv:1908:09914v1*, 2019.

[54] P.-O. Löwdin and H. Shull, "Natural orbitals in the quantum theory of two-electron systems," *Phys. Rev.*, vol. 101, pp. 1730–1739, 1956.

[55] M. Piris and J. M. Ugalde, "Iterative Diagonalization for Orbital Optimization in Natural Orbital Functional Theory," *J. Comput. Chem.*, vol. 30, pp. 2078–2086, 2009.

[56] M. Piris, X. Lopez, F. Ruipérez, J. M. Matxain, and J. M. Ugalde, "A natural orbital functional for multiconfigurational states.," *J. Chem. Phys.*, vol. 134, p. 164102, 2011.

[57] M. Piris, J. M. Matxain, and X. Lopez, "The intrapair electron correlation in natural orbital functional theory," *J. Chem. Phys.*, vol. 139, no. 23, pp. 234109–9, 2013.

[58] K. Pernal, "The equivalence of the Piris Natural Orbital Functional 5 (PNOF5) and the antisymmetrized product of strongly orthogonal geminal theory," *Comput. Theor. Chem.*, vol. 1003, pp. 127–129, 2013.

[59] I. Mitxelena and M. Piris, "Molecular electric moments calculated by using natural orbital functional theory," *J. Chem. Phys.*, vol. 144, p. 204108, 2016.

[60] J. Cioslowski, M. Piris, and E. Matito, "Robust Validation Of Approximate 1-Matrix Functionals With Few-Electron Harmonium Atoms," *J. Chem. Phys.*, vol. 143, p. 214101, 2015.

[61] E. Ramos-Cordoba, X. Lopez, M. Piris, and E. Matito, "H4: A challenging system for natural orbital functional approximations," *J. Chem. Phys.*, vol. 143, p. 164112, 2015.

[62] I. Mitxelena and M. Piris, "Analytic gradients for natural orbital functional theory," *J. Chem. Phys.*, vol. 146, p. 014102, 2017.

[63] S. Goedecker and C. J. Umrigar, "Natural orbital functional for the many-electron problem," *Phys. Rev. Lett.*, vol. 81, p. 866, 1998.

[64] M. A. L. Marques and N. N. Lathiotakis, "Empirical functionals for reduced-density-matrix-functional theory," *Phys. Rev. A*, vol. 77, p. 032509, 2008.

[65] O. Gritsenko, K. Pernal, and E. J. Baerends, "An improved density matrix functional by physically motivated repulsive corrections.," *J. Chem. Phys.*, vol. 122, no. 20, p. 204102, 2005.

[66] D.C. Liu and J. Nocedal, "On the Limited Memory Method for Large Scale Optimization," *Math. Program.*, vol. 45, pp. 503–528, 1989.

[67] A. D. Buckingham, "Direct method of measuring molecular quadrupole moments," *J. Chem. Phys.*, vol. 30, p. 1580, 1959.

[68] A. D. Buckingham, "Permanent and induced molecular moments and long-range intermolecular forces," *Adv. Chem. Phys.*, vol. 12, pp. 107–142, 1967.

[69] M. Piris, "Natural Orbital Functional Theory for Multiplets," *Phys. Rev. A*, vol. 100, p. 032508, 2019.

[70] P. Pulay and H. F. Schaefer, *Direct Use of the Gradient for Investigating Molecular Energy Surfaces*, pp. 153–185. Boston, MA: Springer US, 1977.

[71] N. C. Handy and H. F. Schaefer, "On the evaluation of analytic energy derivatives for correlated wave functions," *J. Chem. Phys.*, vol. 81, no. 11, p. 5031, 1984.

[72] Y. Osamura, Y. Yamaguchi, and H. F. Schaefer, "Analytic configuration interaction (CI) gradient techniques for potential energy hypersurfaces. A method for open-shell molecular wave functions," *J. Chem. Phys.*, vol. 75, p. 2919, 1981.

[73] A. Y. Sokolov, J. J. Wilke, A. C. Simmonett, and H. F. Schaefer, "Analytic gradients for density cumulant functional theory: The DCFT-06 model," *J. Chem. Phys.*, vol. 137, no. 5, 2012.

[74] J. A. Pople, R. Krishnan, H. B. Schlegel, and J. S. Binkley, "Derivative studies in hartree-fock and møller-plesset theories," *Int. J. Quantum Chem. Symp.*, vol. 13, pp. 225–241, 1979.

[75] J. Gauss and J. F. Stanton, "Analytic gradients for the couples-cluster singles, doubles, and triples (CCSDT) model," *J. Chem. Phys.*, vol. 116, pp. 1773–1782, 2002.

[76] M. Dupuis and H. F. King, "Molecular symmetry. II. Gradient of electronic energy with respect to nuclear coordinates," *J. Chem. Phys.*, vol. 68, p. 3998, 1978.

[77] H. Horn, H. Weiss, M. Häser, M. Ehrig, and R. Ahlrichs, "Prescreening of 2-Electron Integral Derivatives in Scf Gradient and Hessian Calculations," *J. Comput. Chem.*, vol. 12, pp. 1058–1064, 1991.

[78] K. L. Bak, J. Gauss, P. Jørgensen, J. Olsen, T. Helgaker, and J. F. Stanton, "The accurate determination of molecular equilibrium structures," *J. Chem. Phys.*, vol. 114, pp. 6548–6556, 2001.

[79] I. Papai, A. St-Amant, J. Ushio, and D. Salahub, "Calculation of equilibrium geometries and harmonic frequencies by the LCGTO–MCP–local spin density method," *Int. J. Quantum Chem.*, vol. 38, pp. 29–39, 1990.

[80] M. J. Frisch, M. Head-Gordon, and J. A. Pople, "A direct mp2 gradient method," *Chem. Phys. Lett.*, vol. 166, no. 3, pp. 275 – 280, 1990.

[81] J. Russel Thomas, J. DeLeeuw Bradley, George Vacek, T. Daniel Crawford, "The balance between theoretical method and basis set quality: A systematic study of equilibrium geometries, dipole moments, harmonic vibrational frequencies, and infrared intensities," *J. Chem. Phys.*, vol. 99, no. 1992, p. 403, 1993.

[82] M. W. Wong, "Vibrational frequency prediction using density functional theory," *Chem. Phys. Lett.*, vol. 256, pp. 391–399, 1996.

[83] Y. Yamaguchi and H. F. Schaefer, *Analytic Derivative Methods in Molecular Electronic Structure Theory : A New Dimension to Quantum Chemistry and its Applications to Spectroscopy*. John Wiley and Sons, LTD, 2011.

[84] K. Pernal and E. J. Baerends, "Coupled-perturbed density-matrix functional theory equations. application to static polarizabilities," *J. Chem. Phys.*, vol. 685, p. 014102, 2006.

[85] D. Bykov, T. Petrenko, R. Izsák, S. Kossmann, U. Becker, E. Valeev, and F. Neese, "Efficient implementation of the analytic second derivatives of hartree-fock and hybrid dft energies: a detailed analysis of different approximations," *Mol. Phys.*, vol. 113, pp. 1961–1977, 2015.

[86] J. W. Ochterski, "Vibrational Analysis in Gaussian The short answer," *Help@ Gaussian. Com*, pp. 1–10, 1999.

[87] T. H. Dunning Jr., "Gaussian basis sets for use in correlated molecular calculations. I. The atoms boron through neon and hydrogen," *J. Chem. Phys.*, vol. 90, pp. 1007–1023, 1989.

[88] M. L. Laury, M. J. Carlson, and A. K. Wilson, "Vibrational Frequency Scale Factors for Density Functional Theory and the Polarization Consistent Basis Sets," *J. Comput. Chem.*, vol. 33, pp. 2380–2387, 2012.

[89] M. F. Silva, N. A. Lima, A. L. Malvezzi, and K. Capelle, "Effects of nanoscale spatial inhomogeneity in strongly correlated systems," *Phys. Rev. B*, vol. 71, no. 12, pp. 1–5, 2005.

[90] I. W. Bulik, T. M. Henderson, and G. E. Scuseria, "Can Single-Reference Coupled Cluster Theory Describe Static Correlation?," *J. Chem. Theory Comput.*, pp. 3171–3179, 2015.

[91] D. J. Carrascal, J. Ferrer, J. C. Smith, and K. Burke, "The Hubbard Dimer: A density functional case study of a many-body problem," *J. Phys.: Condens. Matter*, vol. 27, no. 39, p. 393001, 2015.

[92] S. Di Sabatino, J. A. Berger, L. Reining, P. Romaniello, and S. D. Sabatino, "Reduced density-matrix functional theory: Correlation and spectroscopy," *J. Chem. Phys.*, vol. 143, no. 143, p. 24108, 2015.

[93] E. Kamil, R. Schade, T. Pruschke, and P. E. Blöchl, "Reduced density-matrix functionals applied to the Hubbard dimer," *Phys, Rev. B*, vol. 93, p. 085141, 2016.

[94] H. Z. Shen, X. X. Yi, and C. H. Oh, "Dynamical signature of the edge state in the 1d aubry–andré model," *J. Phys. B: Atomic, Molecular and Optical Physics*, vol. 47, no. 8, p. 085501, 2014.

[95] P. J. Knowles and N. C. Handy, "A new determinant-based full configuration interaction method," *Chem. Phys. Lett.*, vol. 111, no. 4, pp. 315–321, 1984.

[96] P. J. Knowles and N. C. Handy, "A determinant based full configuration interaction program," *Comput. Phys. Commun.*, vol. 54, p. 75, 1989.

[97] E. Matito and F. Feixas, "DMn program," 2009. University of Girona (Spain) and University of Szczecin (Poland).

[98] E. Ramos-Cordoba, X. Lopez, M. Piris, and E. Matito, "H_4: A challenging system for natural orbital functional approximations," *J. Chem. Phys.*, vol. 143, no. 16, p. 164112, 2015.

[99] I. Mitxelena, M. Piris, and M. A. R. Mayorga, "On the performance of Natural Orbital Functional Approximations in Hubbard model," *J. Phys. Condens. Matter*, vol. 29, p. 425602, 2017.

[100] M. Piris, J. M. Matxain, X. Lopez, and J. M. Ugalde, "The one-electron picture in the Piris natural orbital functional 5 (PNOF5)," *Theor. Chem. Acc.*, vol. 132, p. 1298, 2013.

[101] M. Piris, "A New Approach for the Two-Electron Cumulant in Natural Orbital," *Int. J. Quantum Chem.*, vol. 106, pp. 1093–1104, 2006.

[102] K. Pernal and J. Cioslowski, "Phase dilemma in density matrix functional theory," *J. Chem. Phys.*, vol. 120, p. 5987, 2004.

[103] A. V. Sinitskiy, L. Greenman, and D. A. Mazziotti, "Strong correlation in hydrogen chains and lattices using the variational two-electron reduced density matrix method," *J. Chem. Phys.*, vol. 133, p. 014104, 2010.

[104] G. Ehlers, J. Sólyom, O. Legeza, and R. M. Noack, "Entanglement structure of the hubbard model in momentum space," *Phys. Rev. B*, vol. 92, p. 235116, 2015.

[105] L. Stella, C. Attaccalite, S. Sorella, and A. Rubio, "Strong electronic correlation in the hydrogen chain: A variational monte carlo study," *Phys. Rev. B*, vol. 84, p. 245117, 2011.

[106] J. Bardeen, L. N. Cooper, and J. R. Schrieffer, "Theory of Superconductivity," *Phys. Rev.*, vol. 108, no. 5, pp. 1175–1204, 1957.

[107] T. Tsuchimochi and G. E. Scuseria, "Strong correlations via constrained-pairing mean-field theory," *J. Chem. Phys.*, vol. 131, no. 12, p. 121102, 2009.

[108] J. P. F. and LeBlanc, A. E. Antipov, F. Becca, I. W. Bulik, G. K.-L. Chan, C.-M. Chung, Y. Deng, M. Ferrero, T. M. Henderson, C. A. Jiménez-Hoyos, E. Kozik, X.-W. Liu, A. J. Millis, N. V. Prokof'ev, M. Qin, G. E. Scuseria, H. Shi, B. V. Svistunov, L. F. Tocchio, I. S. Tupitsyn, S. R. White, S. Zhang, B.-X. Zheng, Z. Zhu, and E. Gull, "Solutions of the Two-Dimensional Hubbard Model: Benchmarks and Results from a Wide Range of Numerical Algorithms," *Phys. Rev. X*, vol. 5, no. 4, pp. 1–28, 2015.

[109] N. C. Rubin and D. A. Mazziotti, "Comparison of one-dimensional and quasi-one-dimensional Hubbard models from the variational two-electron reduced- density-matrix method," *Theor. Chem. Acc.*, vol. 133, p. 1492, 2014.

[110] B. Verstichel, H. van Aggelen, W. Poelmans, and D. Van Neck, "Variational two-particle density matrix calculation for the hubbard model below half filling using spin-adapted lifting conditions," *Phys. Rev. Lett.*, vol. 108, p. 213001, 2012.

[111] M. Motta, D. M. Ceperley, G. K.-L. Chan, J. A. Gomez, E. Gull, S. Guo, C. A. Jiménez-Hoyos, T. N. Lan, J. Li, F. Ma, A. J. Millis, N. V. Prokof'ev, U. Ray, G. E. Scuseria, S. Sorella, E. M. Stoudenmire, Q. Sun, I. S. Tupitsyn, S. R. White, D. Zgid, and S. Zhang, "Towards the solution of the many-electron problem in real materials: Equation of state of the hydrogen chain with state-of-the-art many-body methods," *Phys. Rev. X*, vol. 7, p. 031059, 2017.

[112] L. Jingcheng, S. Sanz, M. Corso, D. Jang Choi, D. Peña, T. Frederiksen, and J. Ignacio Pascual, "Single spin localization and manipulation in graphene open-shell nanostructures," *Nat. Commun*, vol. 10, no. 200, 2019.

[113] B.-X. Zheng, C.-M. Chung, P. Corboz, G. Ehlers, M.-P. Qin, R. M. Noack, H. Shi, S. R. White, S. Zhang, and G. K.-L. Chan, "Stripe order in the underdoped region of the two-dimensional hubbard model," *Science*, vol. 358, no. 6367, pp. 1155–1160, 2017.

[114] B.-X. Zheng and G. K.-L. Chan, "Ground-state phase diagram of the square lattice hubbard model from density matrix embedding theory," *Phys. Rev. B*, vol. 93, p. 035126, 2016.

[115] S. Raghu, S. A. Kivelson, and D. J. Scalapino, "Superconductivity in the repulsive hubbard model: An asymptotically exact weak-coupling solution," *Phys. Rev. B*, vol. 81, p. 224505, 2010.

[116] N. C. Rubin and D. A. Mazziotti, "Strong electron correlation in materials from pair-interacting model hamiltonians," *J. Phys. Chem. C*, vol. 119, no. 26, pp. 14706–14713, 2015.

[117] R. M. Parrish, L. A. Burns, D. G. A. Smith, A. C. Simmonett, A. E. DePrince, E. G. Hohenstein, U. Bozkaya, A. Y. Sokolov, R. Di Remigio, R. M. Richard, J. F. Gonthier, A. M. James, H. R. McAlexander, A. Kumar, M. Saitow, X. Wang, B. P. Pritchard, P. Verma, H. F. Schaefer, K. Patkowski, R. A. King, E. F. Valeev, F. A. Evangelista, J. M. Turney, T. D. Crawford, and C. D. Sherrill, "Psi4 1.1: An open-source electronic structure program emphasizing automation, advanced libraries, and interoperability," *J. Chem. Theory Comput.*, vol. 13, no. 7, pp. 3185–3197, 2017.

[118] S. Wouters, W. Poelmans, P. W. Ayers, and D. V. Neck, "Chemps2: A free open-source spin-adapted implementation of the density matrix renormalization group for ab initio quantum chemistry," *Comput. Phys. Commun.*, vol. 185, no. 6, pp. 1501 – 1514, 2014.

[119] W. H. Flygare and R. C. Benson, "The molecular zeeman effect in diamagnetic molecules and the determination of molecular magnetic moments (g values), magnetic susceptibilities, and molecular quadrupole moments," *Mol. Phys.*, vol. 20, p. 225, 1971.

[120] E. R. Cohen and G. Birnbaum, "Far infrared collisioninduced absorption in gaseous methane. ii. determination of the octupole and hexadecapole moments," *J. Chem. Phys.*, vol. 62, pp. 3807–3812, 1975.

[121] A. Sadlej, "Medium-size polarized basis sets for high-level correlated calculations of molecular electric properties," *Collect. Czech. Chem. Commun.*, vol. 53, p. 1995, 1988.

[122] A. Sadlej *Theor. Chim. Acta*, vol. 79, pp. 123–140, 1991.

[123] P. Bundgen, F. Grein and A. J. Thakkar, "Dipole and quadrupole moments of small molecules. An ab initio study using perturbatively corrected, multi-reference, configuration interaction wave functions," *J. Mol. Struct*, vol. 334, pp. 7–13, 1994.

[124] J. M. Junquera-Hernández, J. Sánchez-Marín, and D. Maynau, "Molecular electric quadrupole moments calculated with matrix dressed SDCI," *Chem. Phys. Lett.*, vol. 359, pp. 343–348, 2002.

[125] E. Hirota, "Anharmonic potential function and equilibrium structure of methane," *J. Mol. Struct.*, vol. 77, pp. 213–221, 1979.

[126] M. W. Schmidt, K. K. Baldridge, J. A. Boatz, S. T. Elbert, M. S. Gordon, J. H. Jensen, S. Koseki, N. Matsunaga, K. A. Nguyen, S. U. Shyjun, M. Dupuis, and J. A. Montgomery, "General Atomic and Molecular Electronic Structure System," *J. Comput. Chem.*, vol. 14, pp. 1347–1363, 1993.

[127] M. S. Gordon and M. W. Schmidt, *Theory and Applications of Computational Chemistry.* Elsevier, 2005.

[128] S. Hofinger and M. Wendland, "Method/Basis Set Dependence of the Traceless Quadrupole Moment Calculation for N2, CO2, SO2, HCl, CO, NH3, PH3, HF, and H2O," *Int. J. Quantum Chem.*, vol. 86, pp. 199–217, 2002.

[129] G. Maroulis, "Accurate electric dipole and quadrupole moment, dipole polarizability, and first and second hyperpolarizability of ozone from coupled cluster calculations," *J. Chem. Phys.*, vol. 101, pp. 4949–4955, 1994.

[130] B. Fabricant and J. S. Muenter, "Molecular beam Zeeman effect and dipole moment sign of ClF," *J. Chem. Phys.*, vol. 66, pp. 5274–5277, 1977.

[131] A. J. Russel and M. A. Spackman, "An ab initio study of vibrational corrections to the electric properties of the fluoromethanes: CH3F, CH2F2, CHF3 and CF4," *Mol. Phys.*, vol. 98, pp. 633–642, 2000.

[132] A. Arapiraca and J. Mohallem, "DFT vibrationally averaged isotopic dipole moments of propane, propyne and water isotopologues," *Chem. Phys. Lett.*, vol. 609, pp. 123–128, 2014.

[133] A. Halkier, H. Larsen, J. Olsen, P. Jørgensen and J. Gauss, "Full configuration interaction benchmark calculations of first-order one-electron properties of BH and HF," *J. Chem. Phys.*, vol. 110, pp. 734–740, 1999.

[134] D. J. Gearhart, J. F. Harrison, K. L. C. Hunt, "Molecular Quadrupole Moments of HCCH, FCCF, and ClCCCl," *Int. J. Quantum Chem.*, vol. 95, pp. 697–705, 2003.

[135] E. S. G. Luca, N. Russo and M. Toscano, "Molecular quadrupole moments, second moments, and diamagnetic susceptibilities evaluated using the generalized gradient approximation in the framework of Gaussian density functional method," *J. Chem. Phys.*, vol. 105, pp. 3206–3210, 1996.

[136] G. L. Heard and R. J. Boyd, "Density functional theory studies of the quadrupole moments of benzene and naphthalene," *Chem. Phys. Lett.*, vol. 277, pp. 252–256, 1997.

[137] S. G. Kukolich, "Molecular Beam Measurement of the Magnetic Susceptibility Anisotropies and Molecular Quadrupole Moment in H2CO," *J. Chem. Phys.*, vol. 54, pp. 8–11, 1971.

[138] J. D. Watts and R. J. Bartlett, "Coupled-cluster calculations of structure and vibrational frequencies of ozone: Are triple excitations enough?," *J. Chem. Phys.*, vol. 108, no. 6, pp. 2511–2514, 1998.

[139] J. P. Coe, D. J. Taylor, and M. J. Paterson, "Monte Carlo configuration interaction applied to multipole moments, ionisation energies and electron affinities.," *J. Comput. Chem.*, vol. 34, p. 1083, 2013.

[140] H. N. W. Lekkerkerker, P. Coulon and R. Luyckx, "Dispersion Forces in Méthane," *J. Chem. Soc., Faraday Trans.*, vol. 73, no. 2, pp. 1328–1334, 1977.

[141] C. Garrod and J. K. Percus, "Reduction of the n-particle variational problem," *J. Math. Phys.*, vol. 5, pp. 1756–1776, 1964.

[142] A. J. Coleman, "Structure of Fermion Density Matrices," *Rev. Mod. Phys.*, vol. 35, pp. 668–687, 1963.

[143] F. Colonna and A. Savin, "Correlation energies for some two- and four-electron systems along the adiabatic connection in density functional theory," *J. Chem. Phys.*, vol. 110, no. 6, pp. 2828–2835, 1999.

[144] A. J. Cohen and P. Mori-Sánchez, "Landscape of an exact energy functional," *Phys. Rev. A*, vol. 93, p. 042511, 2016.

[145] S. M. Valone, "Density and one-matrix functionals generated by constrained-search theory," *Phys. Rev. B*, vol. 44, pp. 1509–1522, 1991.

[146] P. Mori-Sánchez and A. J. Cohen, "Exact density functional obtained via the levy constrained search," *J. Phys. Chem. Lett.*, vol. 9, no. 17, pp. 4910–4914, 2018.

[147] P. W. Ayers and S. Liu, "Necessary and sufficient conditions for the N-representability of density functionals," *Phys. Rev. A*, vol. 75, p. 022514, 2007.

[148] O. V. Gritsenko and K. Pernal, "Approximating one-matrix functionals without generalized pauli constraints," *Phys. Rev. A*, vol. 100, p. 012509, 2019.

[149] U. C. Goedecker S., "Natural Orbital Functional Theory," in *Many-Electron Densities and Reduced Density Matrices. Mathematical and Computational Chemistry* (C. J., ed.), ch. 8, pp. 165–181, Boston, MA: Springer, 2000.

[150] J. M. Matxain, M. Piris, F. Ruipérez, X. Lopez, and J. M. Ugalde, "Homolytic molecular dissociation in natural orbital functional theory.," *Phys. Chem. Chem. Phys.*, vol. 13, pp. 20129–20135, 2011.

[151] F. Ruipérez, M. Piris, J. M. Ugalde, and J. M. Matxain, "The natural orbital functional theory of the bonding in Cr(2), Mo(2) and W(2).," *Phys. Chem. Chem. Phys.*, vol. 15, no. 6, pp. 2055–2062, 2013.

[152] M. Piris, J. Matxain, and X. Lopez, "The intrapair electron correlation in natural orbital functional theory," *J. Chem. Phys.*, vol. 139, no. 23, pp. 234109–234109, 2013.

[153] M. Piris, "The Electron Pairing Approach in Natural Orbital Functional Theory," in *Theoretical and Quantum Chemistry at the Dawn of the 21st Century* (T. Chakraborty and R. Carbó-Dorca, eds.), ch. 22, pp. 593–620, New Jersey: Apple Academic Press, 2018.

[154] S. Bratoz, "Le calcul non empirique des constantes de force et des dérivées du moment dipolaire," *Colloq. Int. C.N.R.S.*, vol. 82, pp. 287–301, 1958.

[155] V. Bakken, T. Helgaker, W. Klopper, and K. Ruud, "The calculation of molecular geometrical properties in the Hellmann—Feynman approximation," *Mol. Phys.*, vol. 96, pp. 653–671, 1999.

[156] H. Huber, "Geometry optimization in ab initio scf calculations. Floating orbital geometry optimization applying the Hellmann-Feynman force," *Chem. Phys. Lett.*, vol. 62, pp. 95–99, 1979.

[157] R. Vianna, R. Custodio, H. Chacham, and J. R. Mohallem, "Reliable Hellmann-Feynman Forces for Nuclei- Centered," *Int. J. Quantum Chem. Symp.*, vol. 26, pp. 311–318, 1992.

[158] M. Piris, "Analytic gradients in the improved BCS method," *J. Math. Chem.*, vol. 23, pp. 399–404, 1998.

[159] H. Hellmann, "Einführung in die Quantenchemie," *Angewandte Chemie*, vol. 54, p. 156, 1937.

[160] R. P. Feynman, "Forces in molecules," *Phys. Rev.*, vol. 56, pp. 340–343, 1939.

[161] P. Pulay, "Ab initio calculation of force constants and equilibrium geometries," *Mol. Phys.*, vol. 21, pp. 329–339, 1971.

[162] M. Piris and N. H. March, "Is the Hartree-Fock prediction that the chemical potential μ of non-relativistic neutral atoms is equal to minus the ionization potential I sensitive to electron correlation?," *Phys. Chem. Liq.*, vol. 53, no. 6, pp. 696–705, 2015.

[163] R. Schutski, C. A. Jiménez-Hoyos, and G. E. Scuseria, "Analytic energy gradient for the projected Hartree-Fock method," *J. Chem. Phys.*, vol. 140, no. 20, 2014.

[164] R. Fletcher, "Function minimization by conjugate gradients," *Comput. J.*, vol. 7, pp. 149–154, 1964.

[165] M. Piris, "Interpair electron correlation by second-order perturbative corrections to PNOF5," *J. Chem. Phys.*, vol. 139, no. 6, p. 064111, 2013.

[166] M. Piris, X. Lopez, and J. M. Ugalde, "The Bond Order of C 2 from an Strictly N-Representable Natural Orbital Energy Functional Perspective," *Chemistry - A European Journal*, vol. 22, 2016.

[167] X. Lopez, M. Piris, F. Ruipérez, and J. M. Ugalde, "Performance of PNOF6 for Hydrogen Abstraction Reactions," *J. Phys. Chem. A*, vol. 119, no. 27, pp. 6981–6988, 2015.

[168] M. Piris and P. Otto, "Natural orbital functional for correlation in polymers," *Int. J. Quantum Chem.*, vol. 102, pp. 90–97, 2005.

[169] S. Sharma, J. K. Dewhurst, S. Shallcross, and E. K. U. Gross, "Spectral density and metal-insulator phase transition in mott insulators within reduced density matrix functional theory," *Phys. Rev. Lett.*, vol. 110, no. 11, pp. 116403–5, 2013.

[170] Y. Shinohara, S. Sharma, S. Shallcross, N. N. Lathiotakis, and E. K. U. Gross, "Spectrum for Nonmagnetic Mott Insulators from Power Functional within Reduced Density Matrix Functional Theory," *J. Chem. Theory Comp.*, vol. 11, no. 10, pp. 4895–4899, 2015.

[171] A. F. Izmaylov and G. E. Scuseria, "Efficient evaluation of analytic vibrational frequencies in Hartree-Fock and density functional theory for periodic nonconducting systems," *J. Chem. Phys.*, vol. 127, no. 14, p. 144106, 2007.

[172] A. J. Valentine and D. A. Mazziotti, "Analytical nuclear derivatives for the parametric two-electron reduced density matrix method," *Chem. Phys. Lett.*, vol. 685, pp. 300 – 304, 2017.

[173] D. A. Mazziotti, "Variational two-electron reduced-density-matrix theory," in *Reduced-Density-Matrix Mechanics: with applications to many-electron atoms and molecules* (D. A. Mazziotti, ed.), ch. 3, pp. 21–59, Hoboken, New Jersey, USA: John Wiley and Sons, 1 ed., 2007.

[174] D. A. Mazziotti, "Enhanced constraints for accurate lower bounds on many-electron quantum energies from variational two-electron reduced density matrix theory," *Phys. Rev. Lett.*, vol. 117, p. 153001, 2016.

[175] A. W. Schlimgen, C. W. Heaps, and D. A. Mazziotti, "Entangled electrons foil synthesis of elusive low-valent vanadium oxo complex," *J. Phys. Chem. Lett.*, vol. 7, no. 4, pp. 627–631, 2016.

[176] A. R. McIsaac and D. A. Mazziotti, "Ligand non-innocence and strong correlation in manganese superoxide dismutase mimics," *Phys. Chem. Chem. Phys.*, vol. 19, pp. 4656–4660, 2017.

[177] K. J. H. Giesbertz, O. V. Gritsenko, and E. J. Baerends, "Response Calculations with an Independent Particle System with an Exact One-Particle Density Matrix," *Phys. Rev. Lett.*, vol. 105, p. 013002, 2010.

[178] R. van Meer, O. V. Gritsenko, and E. J. Baerends, "Excitation energies with linear response density matrix functional theory along the dissociation coordinate of an electron-pair bond in N-electron systems," *J. Chem. Phys.*, vol. 140, p. 024101, 2014.

[179] W. H. Miller, N. C. Handy, and J. E. Adams, "Reaction path Hamiltonian for polyatomic molecules," *J. Chem. Phys.*, vol. 72, p. 99, 1980.

[180] V. Szalay, "Eckart-Sayvetz conditions revisited," *J. Chem. Phys.*, vol. 140, no. 23, p. 234107, 2014.

[181] M. C. Gutzwiller, "Effect of correlation on the ferromagnetism of transition metals," *Phys. Rev. Lett.*, vol. 10, pp. 159–162, Mar 1963.

[182] M. C. Gutzwiller, "Correlation of electrons in a narrow s band," *Phys. Rev.*, vol. 137, pp. A1726–A1735, Mar 1965.

[183] D. Baeriswyl, "Variational scheme for the mott transition," *Found. Phys.*, vol. 30, no. 12, pp. 2033–2048, 2000.

[184] M. Dzierzawa, D. Baeriswyl, and M. Martelo, "Variational wave-functions for the mott-hubbard transition," *Helv. Phys. Acta*, vol. 70, pp. 124–140, 1997.

[185] D. Baeriswyl in *Nonlinearity in Condensed Matter* (A. R. Bishop, D. K. Campbell, P. Kumar, and S. E. Trullinger, eds.), Springer-Verlag, 1986.

[186] J. R. Hammond and D. A. Mazziotti, "Variational reduced-density-matrix calculation of the one-dimensional Hubbard model," no. 062505, pp. 1–6, 2006.

[187] Y. Shinohara, S. Sharma, J. K. Dewhurst, S. Shallcross, N. N. Lathiotakis, and E. K. U. Gross, "Doping induced metal-insulator phase transition in NiO—a reduced density matrix functional theory perspective," *New J. Phys.*, vol. 17, no. 9, p. 093038, 2015.

[188] K. Pernal, "Turning reduced density matrix theory into a practical tool for studying the Mott transition," *New J. Phys.*, vol. 17, p. 111001, 2015.

[189] A. Akande and S. Sanvito, "Electric field response of strongly correlated one-dimensional metals: A Bethe ansatz density functional theory study," *Phys. Rev. B*, vol. 82, p. 245114, 2010.

[190] J. Cioslowski and K. Pernal, "Unoccupied natural orbitals in two-electron coulombic systems," *Chem. Phys. Lett.*, vol. 430, no. 1, pp. 188–190, 2006.

[191] N. A. Lima, L. N. Oliveira, and K. Capelle, "Density-functional study of the mott gap in the hubbard model," *EPL (Europhysics Letters)*, vol. 60, no. 4, p. 601, 2002.

[192] N. A. Lima, M. F. Silva, L. N. Oliveira, and K. Capelle, "Density functionals not based on the electron gas: local-density approximation for a luttinger liquid," *Phys. Rev. Lett.*, vol. 90, p. 146402, 2003.

[193] K. Capelle, N. Lima, M. Silva, and L. Oliveira, vol. 14. Springer Netherlands, 2003.

[194] G. Xianlong, M. Polini, M. P. Tosi, V. L. Campo, and K. Capelle, "Bethe ansatz density-functional theory of ultracold repulsive fermions in one-dimensional optical lattices," *Phys. Rev. B*, vol. 73, p. 165120, 2006.

[195] V. V. França, D. Vieira, and K. Capelle, "Simple parameterization for the ground-state energy of the infinite hubbard chain incorporating mott physics, spin-dependent phenomena and spatial inhomogeneity," *New J. Phys.*, vol. 14, no. 7, p. 073021, 2012.

[196] I. Mitxelena, M. Piris, and M. Rodríguez-Mayorga, "Corrigendum: "on the performance of natural orbital functional approximations in the hubbard model" [j. phys.: Condens. matter 29 (2017) 425602]," *J. Phys. Condens. Matter*, vol. 30, p. 089501, 2018.

[197] M. Saubanère and G. M. Pastor, "Density-matrix functional study of the hubbard model on one- and two-dimensional bipartite lattices," *Phys. Rev. B*, vol. 84, p. 035111, 2011.

[198] B. Honig and a. Nicholls, "Classical electrostatics in biology and chemistry.," *Science*, vol. 268, no. 5214, pp. 1144–1149, 1995.

[199] W. Gordy and R. L. Cook, *Microwave Molecular Spectra*. Wiley, New York, 1984.

[200] A. L. McClellan, *Tables of Experimental Dipole Moments*, vol. 3. Rahara, El Cerrito, CA, 1989.

[201] R. Glaser, Z. Wu, and M. Lewis, "A higher level ab initio quantum-mechanical study of the quadrupole moment tensor components of carbon dioxide," *J. Mol. Struct.*, vol. 556, pp. 131–141, 2000.

[202] A. J. Cohen and Y. Tantirungrotechai *Chem. Phys. Lett.*, vol. 299, pp. 465–472, 1999.

[203] M. Piris and N. H. March, "Low-Lying Isomers Of Free-Space Halogen Clusters With Tetrahedral And Octahedral Symmetry In Relation To Stable Molecules Such As SF6," *J. Phys. Chem. A*, vol. 119, no. 40, pp. 10190–10194, 2015.

[204] A. L. Hickey and C. N. Rowley, "Benchmarking Quantum Chemical Methods for the Calculation of Molecular Dipole Moments and Polarizabilities," *J. Phys. Chem. A*, vol. 118, pp. 3678–3687, 2014.

[205] K. L. Bak, J. Gauss, T. Helgaker, P. Jørgensen, and J. Olsen, "The accuracy of molecular dipole moments in standard electronic structure calculations," *Chem. Phys. Lett.*, vol. 319, no. 5-6, pp. 563–568, 2000.

[206] G. Frenking, C. Loschen, A. Krapp, S. Fau and S. H. Strauss, "Electronic Structure of CO - An Exercise in Modern Chemical Bonding Theory," *J. Comput. Chem.*, vol. 28, pp. 117–126, 2006.

[207] G. Maroulis, "On the Electric Multipole Moments of Carbon Monoxide," *Z. Naturforsch*, vol. 47a, pp. 480–484, 1992.

[208] K. Shimizu, M. F. C. Gomes, A. A. H. Padua, L. P. N. Rebelo, and J. N. C. Lopes, "On the role of the dipole and quadrupole moments of aromatic compounds in the solvation by ionic liquids," *J. Phys. Chem. B*, vol. 113, no. 29, pp. 9894–9900, 2009.